The development of peptide-based inhibitors for Tau aggregation as a potential therapeutic for Alzheimer's disease

Lancaster University

Thesis submitted in partial fulfilment of the requirements for the degree of Doctor of Philosophy

Anthony George Athanasios Aggidis
BSc (Hons), MSc

April 2019

Declaration

The author declares that this thesis has not previously been submitted for award

of a higher degree to this or any university, and that the contents, except where

otherwise stated, are the authors's own work.

Signed:

Date:

Abstract

There are currently approximately 50 million individuals worldwide with dementia resulting in predicted global societal costs of up to US $1 trillion. Approximately 60-70% of these individuals have Alzheimer's disease, which results in a chronic and insidious decline in memory. One of the main proteins that misfolds in this disease is Tau protein, which aggregates into toxic oligomers and neurofibrillary tangles. It is these aggregates, which cause damage to the brain resulting in dementia. As a result, it is imperative to be able to prevent or suppress the pathogenic aggregation of this protein, so the onset of dementia is halted or delayed, improving quality of life. Certain amino acid sequences in Tau such as VQIINK and VQIVYK play important roles in aggregation. Targeting these sequences can potentially prevent aggregation. This project aims to produce effective peptide inhibitors based on the human Tau peptide sequences VQIINK and VQIVYK, to specifically target pathogenic Tau aggregation. Using molecular docking softrware '*ICM-Pro*' the potential binding locations of a variety of peptide candidates were computationally investigated to determine which will be most successful in a laboratory setting. Recombinant TauΔ1-250 was incubated in the prescence of heparin and subsequently aggregated to display highly ordered parallel, in-register β-strand structures; including fibrils and paired helical filaments presenting the characteristic twist under transmission electron microscope. This aggregation was achieved using of 20μM Tau at pH 7.4 in the presence of 20mM Tris buffer, 1mM DTT, 5μM Heparin, and 15uM ThT and incubated at 37 °C for 48 hours. The first generation of peptides AG01, AG02, AG02, AG02R4, AG02R5, AGR502, AG02PR5, AG02R6, AG02R9, AG02TAT, AG02ΔI, AG02ΔV inhibited approximately 50% of Tau aggregation determined by Thioflavin-T (ThT) fluorescence assay. The next generation, AG03 was slightly more effective, however when retroinverted (RI-AG03) inhibited over 90% of Tau aggregation, confirmed by Thioflavin-T fluorescence assay, transmission electron microscopy, circular dichroism and Congo red birefringence. RI-

AG03 was determined to be stable in cells at therapeutic concentrations. After determining stability of RI-AG03 using SDS-PAGE, thermal circular dichroism and mass spectrometry, it was tested *in vivo* in rough eye *Drosophila* model. Results suggested that RI-AG03 partially rescued the rough eye phenotype in this model. This research demonstrates that retro-inverted peptide RI-AG03 is a potent inhibitor of Tau aggregation and can be further developed as a novel therapeutic for Tauopathies like Alzhimer's Disease.

Key words: ALZHEIMER, TAUOPATHY, TAU, PHOSPHORYLATION, PROTEIN, AGGREGATION, SECONDARY, STRUCTURE, β-SHEET, INHIBIT, THIOFLAVIN, FLUORESCENCE, TEM, DOCKING, DROSOPHILA.

Dedication

I dedicate this thesis to honour my mother and father who have always encouraged me to be the very best version of myself that I can be and who never doubted my abilities. They have always thoroughly supported me throughout my life in all my endevours, even at the drop of the hat no matter the circumstances, for which I am so grateful. Their steadfastness has been an unmovable rock behind me, their examples have taught me to work hard for the things I aspire to achieve, and their wisdom has taught me priceless lessons of life. I would not have been able to reach this point without you and I humbly thank you both so much.

Acknowledgements

Outputs

1. **Patent application:**
   a. Aggidis, A. and Allsop, D., 2018, *Compositions for Binding to Tau Proteins*, PE959458GB.

2. **Successful funding applications:**

   a. Alzheimer's Research UK - Small Grant application, lead applicant (£4,670).

   b. Alzheimer's Society Project Grant 2019(a), named applicant (£101,110.78).

3. **Additional research:**
   a. Development of High-Throughput Synchrotron Radiation Circular Dichroism for Rapid Screening of Amyloid Inhibitors, SM17645-2, 2018.
   b. Quantifying the effects of polyphenols in Greek olive oil which bind to Aβ and Tau, 2018.

4. **Publications:**
   a. Allsop, D., Aggidis, A., et al., 2018, Untangled - peptide-based inhibitors of tau aggregation as a potential treatment for Alzheimer's Disease, Journal of Prevention of Alzheimer's Disease, 5;S15-S16.
   b. Allsop, D., Aggidis, A., et al., 2017, A novel approach to the therapy of Alzheimer's disease based on peptide nanoliposome inhibitors of Aβ and tau aggregation, Journal of Prevention of Alzheimer's Disease, 4(4);385-386.

5. **Presentations:**
   a. Aggidis, A., 2018, Presented PhD research to industry, including Eli Lilly and MAC Clinical Research for continued colaboration.
   b. Aggidis, A., 2018, Presented PhD research to the research groups of Dr. Amritpal Mudher and Professor Sumeet Mahajan at Southampton University.
   c. Aggidis, A., 2018 Presented research to executive officer of Sir John Fisher Foundation.
   d. Aggidis, A., 2018 Presented to Prof. Magda Tsolaki at Artistotle University of Thessaloniki.
   e. Aggidis, A., 2017 Presented research to layman trustees of Sir John Fisher Foundation.
   f. Aggidis, A., 2016-18 Presented at the Faculty of Health and Medicine Symposiums at Lancaster University.

6. **Collaborations:**
   a. Collaborated with the Tokyo Metropolitan Institute of Medical Science (Japan) to synthesise Tau proteins at Lancaster University, 2016.
   b. Networked with a Dr. Shreyasi Chatterjee at the ARUK, 2017 conference and initiated a collaboration with Southampton University where I was invited for two months in 2018 to their instution by Dr. Amritpal Mudher, to test my Tau aggregation inhibitor *in vivo* using their rough-eye *Drosophila melanogaster* model.
   c. In 2017 a series of confrence calls were arranged with Dr Andrew Orry from Molsoft LLC (USA), to troubleshoot their ICM-Pro software which resulted in an improved insight for their own software design regarding peptide docking.

7. **Conferences:**
   a. SynaNET 2018, Lisbon
   b. ARUK 2017, Aberdeen
   c. ARUK 2016, Manchester

Contents

List of Figures

X

4.13	QMEAN4 values. **A:** 6QJH.pdb heparin-induced 2N4R Tau snake filament = -2.30, **B:** 6QJM.pdb heparin-induced 2N4R Tau twisted filament = -1.14, **C:** 6QJP.pdb heparin-induced 2N4R Tau jagged filament = -1.67. All structures scored satisfactory global quality. Structures from Zhang et al. (2019).	98
4.14	ICM-Pro display of PDB 5o3lusing theicmPocketFinderfunction, **A:**Six binding pockets were predicted and displayed in blue, red, cyan, green, orange and purple,**B:**Raw data describing the compactness of the binding pockets which are calculated based on the**Volume**of the pocket;**Area**of the pocket;**Hyrdophobicity**signifying pocket surfaces in contact with hydrophobic protein residues;**Buriedness**suggesting how open (> 0.5) or closed (1.0) pockets were; **DLID**is the druggabilityof the pocket (>0.5); **Nonsphericity**representing pocket sphericity (1.0 isspherical).	99
4.15	**Figure 4.15**: ICM-Pro display of PDB 5o3l with computationally docked compounds at their highest energy binding sites Tau$_{306-378}$; **A:** Sodium Heparin; **B:** ThT; **C:** DTT; **D:** Raw data describing the docked compounds. ICM score of < -32 suggests a strong bind; H bond Score denotes hydrogen bond energy; Hydrophobicity denotes hydrophobic energy to expose a surface to water; Van der Waals denotes strong van der Waals interaction energy (< 0); Eintl denotes strong ligand internal conformation energy (< 0); Dsolv denotes desolvation of exposed hydrogen bond donors and acceptors; SolEl denotes solvation electrostatics energy change upon binding; mfScore denotes potential of average force score. **E:** Superimposed image of **A-C** with highlighted binding pockets. Compounds in the Tau aggregation mix maximally bind to different binding pockets in PDB 5o3l. DTT binds to the green pocket, ThT binds to the red pocket and Heparin binds to the blue pocket. Circled in black is the theoretical binding site for the peptide inhibitor.	100
4.16	Optimal docking areas for PDB 5o3l PHF on A: top of PHF, including V306, Q307, I308, V309 and F378; B: bottom of PHF including V306, I308 and F378. C: Average optimal docking area values for PDB 5o3l PHF for A and B.	102
4.17	VQIVYK bound to complementary VQIVYK sequence (cyan) on the PDB 5o3l PFF structure. **A:** bound in parallel and shifted to the top of the protofilament, **B:** bound in anti-parallel to the bottom of the protofilament. Experiment was run with maximum effort.	104

6.4	The relatively rapid life cycle of *Drosophila* at 25 ˚C takes ~10 days. Development is split into several stages including embro, larva, pupa and adult (adapted from Ong et al. 2014).	177
6.2	15% SDS PAGE gelsofAG03 (100µM) and RI-AG03 (100µM) treated with and without equimolar Trypsin concentration for 24-hours at 37˚C.AG03 has no signal in the presence of Trypsin whereas RI-AG03 has a strong signal in the presence of Tyrpsin. Digests were conducted in triplicate and densitometric analysis suggested a 19% reduction in signal after equimolar incubation of RI-AG03 with Trypsin for 24-hours at 37˚C.	180
6.3	HEK-293 cells. **A:** Cellular uptake of FAM-RI-AG03(15µM) by HEK-293 cells over 24-hours. Almost no peptide is visible in the medium, suggesting that majorityof the peptide was taken up into the cells. **B:** Varying concentrations ofRI-AG03were co-incubated withHEK-293cellsand cytotoxicity was analysed using an LDH cytotoxicity kit. Toxicity begins to increase at 40µM.	181
6.4	RP-UPHPLC MS data for RI-AG03 at time zero (top) and after 8 days incubation at 25˚ and heated to 55˚Cfor one hour (bottom). **A:** UV Chromatogram, 254 nm at **B:** MS 3.7min retention **C:** MS with maximum entropy deconvolutionisotopic cluster peaks using Dalton units. This demonstratesthat RI-AG03 remains unchanged over 8 days and heating.	182-184
6.5	RP-UPHPLC MS data for RI-AG03 **A:** Demonstrated RI-AG03 exists as three separate species, **B:** Outlines the charge states for the three species. Species 1 ($C_{104}H_{189}N_{49}O_{22}$) has monoisotopic mass of 2476.5, RI-AG03 species 2 ($C_{98}H_{177}H_{45}O_{21}$) has a monoisotopic mass of 2320.4 (-156.1), RI-AG03 species 3 ($C_{92}H_{165}N_{41}O_{22}$) has a monoisotopic mass of 2164.3 (-156.1).	185
6.6	Thermal CD spectroscopy data demonstratingthat temperature does not induce RI-AG03 (20µM) to adopt a specific secondary structure.	186
6.7	Shows experimental pilot data of Drosophila over-expressing Tau in the eye (GMR-hTau) and healthy Drosophila (GMR-GAL4) treated with RI-AG03 (40µM). Tau expression causes toxicity resulting in morphological changes in the eye shape and width at the middle of the eye. Notice the increased size of the eye when the Tau fly is treated with RI-AG03. Error bar = 100µm.	188

List of Tables

Table	Description	Page
1.1	2N4R Tau phosphorylation sites from AD and control brains summarised by the Hanger group, Muckle group and Kuret group (Adapted from Kings College London, 2019). Residues highlighted in yellow have no currently identified associated kinase. Kinases involved in Tau phosphorylation are grouped into 3 classes: proline-directed protein kinases (blue), non-proline-directed kinases (black) and tyrosine kinases (red) (Morris et al., 2015; Funk et al., 2014). Abbreviations: 5' adenosine monophosphate-activated protein kinase (AMPK), Brain-specific kinase 1/2 (BRSK1/2), Calcium-calmodulin kinase II, Cyclin-dependent kinase-5 (cdk5), Casein kinase 1 (CK1), Casein kinase 2 (CK2), Cyclic AMP-dependent protein kinase (PKA), Dual-specificity tyrosine-phosphorylation regulated kinase 1A (DYRK1A), Glycogen synthase kinase-3 (GSK-3), Microtubule affinity-regulating kinase (MARK), Mitogen and stress activated protein kinase-1 (MSK1), p42/p44 mitogen-activated protein kinases (ERKs1/2), p38 mitogen-activated kinase (p38MAPK), Protein kinase C (PKC), Protein kinase N (PKN), Prostate-derived sterile 20-like kinase 1 alpha/beta (PSK1/TAOK2), Prostate-derived sterile 20-like kinase 2 (PSK2/TAOK1), 90 kDa Ribosomal S6 kinase (RSK1/2), Stress-activated protein kinase (SAPK) Tau-tubulin kinase 1/2 (TTBK1/2).	19-20
1.2	Four classes of Tau isoform aggregation and respective diseases they are found in. Class I is characterised by aggregation of all six isoforms. Class II and Class II are characterised by aggregation of Tau isoforms containing four and three repeat domains. Class IV is characterised by the aggregation of Taylacking exons 2 and 3 (Adapted from Sergeant et al., 2008).	30
1.2	Current pipeline treatments in clinical development for Tauopathies associated with AD. 20 are active, 2 are completed, 3 are terminated (ClinicalTrials.gov, 2019, Alzform, 2019 and Medina, 2018).	35-37

2.1	List of peptide inhibitor designs customly synthesised for research in this thesis. Underlined sequence corresponds to Tau binding region. Peptide inhibitors were custom made by Peptide Synthetics (Fareham, UK) with >90% purity and Severn Biotech (Kidderminster, UK) with >95% purity; determined by HPLC-MS. Peptide HPLC-MS data can be found in **Appendix D-V.**	45
3.2	Bloomington fly media recipe per litre (Bloomington Drosophila Stock Centre, 2019).	70
4.1	Average aggregation propensity value VQXVYK where X is consecutively replaced with every amino acid. **A:** aggregatory residues, **B:** non-aggregatory residue Note the replacement of isoleucine massively reduces the aggregation propensity. Residues coloured red, blue and black are hydrophobic, hydrophilic or neutral, respectively.	86
4.2	Average aggregation propensity value VQIxYK where x is consecutively replaced with every amino acid. **A:** aggregatory residues, **B:** non-aggregatory residues. Note the replacement of valine massively reduces the aggregation propensity. Residues coloured red, blue and black are hydrophobic, hydrophilic or neutral, respectively.	86-87
4.3	Triplicate average of computationally calculated values describing self-association properties of AG02ΔI and AG02ΔV. **ICM score** of < -32 suggests a strong bind; **Natom** denotes the number of atoms in the docked ligand; **Nflex** denotes the number of rotatable torsions; **Hbond** denotes hydrogen bond energy; **Hphob** denotes hydrophobic energy to expose a surface to water; **VwInt** denotes strong van der Waals interaction energy (< 0); **Eintl** denotes strong ligand internal conformation energy (< 0); **Dsolv** denotes desolvation of exposed hydrogen bond donors and acceptors; **SolEl** denotes solvation electrostatics energy change upon binding; **mfScore** denotes potential of average force score; **dTSc** denotes loss of entropy via rotatable side-chains.	94
4.4	Summary table of the average computationally calculated values describing the docked compounds to Tau306-378, as seen in **Figure 4.17-4.19**. **A**: peptides bound to the top of the PHF, **B**: peptides bound to the bottom of the PHF. **ICM score** of < -32 suggests a strong bind; **H bond Score** denotes hydrogen bond	107

List of Abbreviations

- AD - Alzheimer's Disease

- ADAMS - Disintegrin and metalloproteinases

- AMPK - 5' adenosine monophosphate-activated protein kinase

- APP - Amyloid precursor protein

- Aβ - Amyloid-β

- BACE1 - B-secretase 1

- BRSK1/2 - Brain-specific kinase 1/2

- CaMKII - Calcium-calmodulin kinase II

- CD - Circular Dichroism

- CDK5 - Cyclin-dependent kinase 5

- cdk5 - Cyclin-dependent kinase-5

- CK1 - Casein kinase 1

- CK2 - Casein kinase 2

- CPP - Cell penetrating peptide

- DTT - Dithiothreitol

- DYRK1A - Dual-specificity tyrosine-phosphorylation regulated kinase 1A

- ERKs1/2 - p42/p44 mitogen-activated protein kinases

- F - Filial
- FTDP-17 - Frontotemporal dementia and parkinsonism linked to chromosome

- GAL4 - Yeast transcription factor

- GMR - Glass multiple reporter

- GSK-3 - Glycogen synthase kinase-3

- GSK-3β - Glycogen synthase kinase 3β

- GTO - Granular Tau oligomer

- HSPG – heparan sulphate proteoglycan

- ht23 - Human Tau 36.8 kDa

- ht24 - Human Tau 39.7 kDa

- ht34 - Human Tau 42.8 kDa

- ht37 - Human Tau 40 kDa

- ht39 - Human Tau 42.9 kDa
- ht40 - Human Tau 45.9 kDa
- ICM – internal coordinates mechanics
- K18 - Recombinant Tau 13.8kDa (4 repeat domain only)
- LDH - lactose dehydrogenase
- mAb - Monoclonal antibody
- MAP - Microtubule associated protein
- MARK - Microtubule affinity-regulating kinase
- MSK1 - Mitogen and stress activated protein kinase-1
- NDMA - N-methyl-D-aspartate
- NFT - Neurofibrillary tangle
- P3 - Peptide 3
- p38MAPK - p38 mitogen-activated kinase
- PHF - Paired helical filament
- PKA - Cyclic AMP-dependent protein kinase
- PKC - Protein kinase C
- PKN - Protein kinase N
- PP - Protein phosphatase
- PSK1/TAOK2 - Prostate-derived sterile 20-like kinase 1 alpha/beta
- PSK2/TAOK1 - Prostate-derived sterile 20-like kinase 2
- R1/2/3/4- Repeat domains
- RSK1/2 - 90 kDa Ribosomal S6 kinase
- SAPK - Stress-activated protein kinase
- SEM - Scanning electron microscope
- SH3 - src Homology-3
- TAT - Trans-Activator of Transcription
- TEM - Transmission electron microscope
- ThT - Thioflavin-T
- TTBK1/2 - Tau-tubulin kinase 1/2
- UAS – Upstream activating sequence

1.INTRODUCTION TO ALZHEIMER'S DISEASE

1.1 DEMENTIA BACKGROUND

The syndrome Dementia is an umbrella of brain diseases that originate from different and often multi-causal pathogenesis resulting in a reduction of cognitive ability. Professor Joshua Thornhill IV (2012), defined dementia as a chronic, insidious and acquired decline in memory with impairment of at least one other cognitive function: aphasia (communication/language), apraxia (motor execution/visuospatial), agnosia (recognition/judgement) and executive function (synthesis). This significantly impairs intellectual functioning thus interfering with everyday activities and relationships due to lost problem-solving capabilities and emotional control/personality changes.

Currently there are approximately 50 million individuals with dementia worldwide of which the most common variation is Alzheimer's disease (AD) which accounts for around 60-70% of dementia cases (World Health Organisation, 2015). Other causes of dementia include vascular dementia, dementia with Lewy bodies, fronto-temporal dementia, Creutzfeldt-Jakob disease, Korsakoff's syndrome, HIV, and mild cognitive impairment (Alzheimer's Society, 2015). More than one kind of dementia can occur in the same patient such as AD and vascular dementia; this is known as mixed dementia.

1.2 ALZHEIMER'S DISEASE

AD is a progressive neurodegenerative disease first discovered by Alois Alzheimer (Möller and Graeber, 1998). Povova et al., (2015) stated that the aetiology of AD is still unknown, however three main risk factor groups are identified: vascular, genetic and behavioural. Li et al., (2015), suggested that most AD cases have sporadic origins and highlighted distinct established risk factors including old age, female gender, vascular disease, cranial trauma or injury, family history of dementia and genetic factors. Distinct

controllable risk factors mentioned by Smith et al., (2014) are believed to cause >50% of sporadic or late onset AD cases and include:

- Age

- Apolipoprotein e4 gene

- Family history

- Mild cognitive impairment

- Cardiovascular disease

- Obesity

- Diabetes

- Sedentary lifestyle

- Smoking

- High blood pressure

- Depression

- Low levels of education and socioeconomic status

- Traumatic Brain Injury

Excluding ~5-10% instances of early onset familial AD due to genetic mutations in Amyloid precursor protein, Presenilin-1 and Presenilin-2, it is believed that the disease develops due to multiple factors as opposed to a single cause (Villegas-Llerena et al., 2016; Alzheimer's Association, 2015).

1.2.1 **DIAGNOSIS**

There is currently no simple clear-cut test to diagnose AD however criteria and guidelines for diagnosing the disease were proposed in 2011 by the National Institute on Aging and the Alzheimer's Association (Jack et al., 2011). Typically, a medical screen is initially conducted by obtaining the patients' medical and family history which includes information on any psychiatric and cognitive or behavioural changes. For further insight this information could be drawn from people close to the patient. According to Reuben (2013), this process usually identifies >90% of individuals with dementia, however, this again is not a proper diagnosis. Several hours' long mental status tests can be performed with a clinician of which, the following three are the state of the art: 1) Three item recall test, 2) Mini-cog test (3 item recall plus clock drawing), 3) Mini Mental State Examination.

Unfortunately to date there is no simple, inexpensive and accurate blood test to clinically indicate AD however research is currently underway in three main biomarker categories: those for CSF accumulation of Amyloid-β (Aβ)/phosphorylated Tau/total Tau and those showing neuron damage/degeneration (Dubois et al., 2014; Alzheimer's Association, 2015). PET imaging

In diagnosis it is important to highlight which of the three stages proposed by the 2011 criteria and guidelines of AD the patient is at in order to enable the most appropriate course of treatment. The three stages of AD include:

1. Preclinical AD

    i. It is difficult to diagnose these patients as they are pre-symptomatic i.e. show no signs of memory loss however insidious changes in brain biochemistry can be detected through biomarker testing and brain imaging (Alzheimer's Association, 2015). This suggests that these changes may begin at least 20 years prior to symptomatic development (Villemagne et al., 2013).

2. Mild cognitive impairment due to AD

    i. Patients have noticeably mild symptoms and however are still able to perform everyday tasks. A study by Roberts et al. (2008), indicated that 10-20% of individuals aged >65 have mild cognitive impairment and 15% of individuals whom contact their physicians due to their symptoms progress to develop dementia each year (Alzheimer's Association, 2015).

3. Dementia due to AD

    i. Symptoms of memory loss, thinking and behavioural changes are much more pronounced which as a result impair ability to perform everyday tasks.

1.2.2 GLOBAL BURDEN

Prince et al., (2013) predicted that the world population of individuals suffering from dementia would increase to approximately 115 million by 2050 however the World Health Organisation, (2015) report this figure to be 135.5 million; suggesting by 2050 there could be potentially ~69-95 million individuals with Alzheimer's (World Health Organisation, 2015; Povova et al., 2015). The number of individuals with dementia may double every 20 years (Blennow et al., 2006). This may be linked to the growing incidences of diabetes globally (Aggidis et al, 2015). Alzheimer's Disease International, (2015) released a report stating that the global societal cost of dementia has increased by 35% since 2010 and they estimated that dementia costs would increase from US $818 billion to US $1 trillion by 2018. This figure approximately equates to Apple which is the current largest market valued company in the world at US $1 trillion (Shubbar and Smith, 2019). If total costs of global dementia care were likened to a country it would be ranked 18 in the largest economies in the world and by 2030 global costs are predicted to reach over $2 trillion as seen in **Figure 1**.1 (Alzheimer's Disease International, 2015). On a smaller scale of appreciation, currently the average cost per person in the UK to manage dementia annually is £32,250 (Alzheimer's Society, 2014). This rise in dementia costs can be attributed to more people being diagnosed with dementia due to increased life expectancy or enhanced awareness/screening methods. Associated demetia costs per person may also be a contributing factor (Wimo et al., 2017).
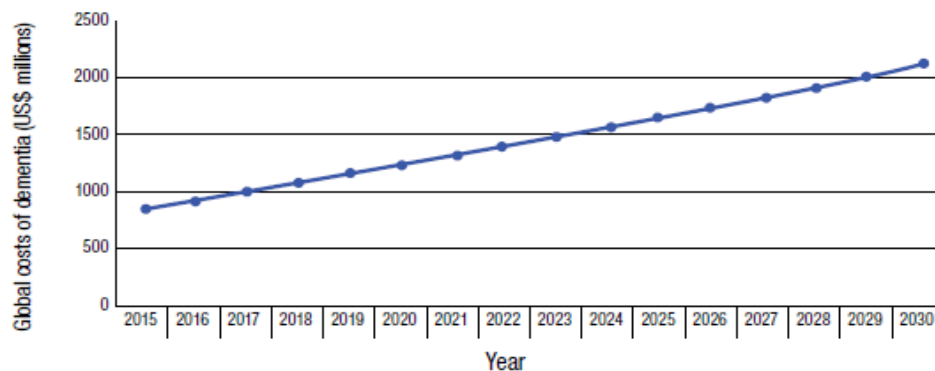
Figure 1.1: Predicted global costs of dementia worldwide from 2015-2030 (Alzheimer's disease International, 2015).

1.3 **AMYLOID BACKGROUND**

The International Society for Amyloidosis, (2018), recognises 36 species of human amyloid (including Tau protein) where they define 'amyloid' as extracellular proteins that misfold into insoluble non-branching fibrils through a series of changes. These fibrils are approximately 10 nm in diameter and subsequently deposit within tissues and the extracellular space of organs (Goedert and Spillantini, 2017 and Sipe et al., 2016). Biopsy amyloid deposits present as amorphous under light microscope however under high magnification electron microscopy small non-branching amyloid fibrils can be seen. Congo red dye is the current gold standard for detecting amyloid in tissue as it binds to amyloid and displays a characteristic apple green birefringence when viewed under polarized lens (International Society for Amyloidosis, 2018). Birefringence is discussed further in **Section 6.1.1**. β-strands are stretches of polypeptides (~3-10 amino acids) which laterally connect to other adjacent β-strands via backbone hydrogen bond interactions, resulting in a β-sheet. β-Sheets are a common secondary structure motif and are particularly present in misfolded insoluble proteins, which are discussed further in **Sections 1.3.1 and 1.4.4**. From a structural perspective, amyloids are defined as fibrils having a backbone consisting of β-sheets in a cross β-sheet arrangement (where a set of β-sheets are aligned in parallel to the fibril axis and their β-strands are aligned perpendicular to the fibril axis giving rise to a pattern of repeating side chains), with meridional and equatorial x-ray diffraction reflections of ~4.7 Å parallel to the fibril axis, and 8-12 Å perpendicular to the axis, respectively. (Sunde et al., 1997; Serpel et al., 1999; Mandelkow et al., 2007).

1.3.1 PROTEIN MISFOLDING

Protein synthesis generates long polypeptide chains without secondary structure. These proteins then, via intermediates, follow specific folding pathways following an energy landscape mechanism, resulting in stable 3D structures. These specific folds, based on the protein amino acid sequence and the surrounding environment, give rise to different individual biological functions. There are however some fully functional unordered proteins, such as Tau, which have an increased likelihood of aggregating. These folding pathways are said to follow an energy landscape and are depicted as a funnel-like mechanism. Unfolded proteins at the top of the funnel systematically adopt random folding conformations to stablise their structure via hydrophobic and electrostatic interactions, intramolecular hydrogen bonds and Van der Waals forces (Pace et al., 2014). This process continues until the proteins reach their lowest free energy, adopting their thermodynamically favourable native fold at the bottom of the funnel. Alternatively, proteins may encounter off-pathway kinetic traps within the funnel which result in misfolded proteins. These misfolded intermediates may be recovered via Chaperone proteins which can reverse the off-pathway fold. Chaperone proteins achieve this by inhibiting intermolecular interactions and reducing free energy barriers, enabling the misfolded protein to adopt a different conformation (Adamcik and Mezzenga, 2018). Contrary to native proteins where hydrophobic interactions occur within the folded protein, misfolded proteins typically display exposed hydrophobic amino acid residues to their solvent. If misfolded proteins are too far from their native folding pathway they can interact with other misfolded proteins through hydrophobic interactions and aggregate (Chiti et al., 2017).

1.3.2 **AMYLOID & ALZHEIMER'S DISEASE**

AD is a proteopathy manifested through the production Aβ protein and hyperphosphorylated Tau protein which misfold (adopting high β-sheet content) and aggregate into their respective fibrils. Aβ is produced through the processing of Amyloid precursor protein (APP) which is normally processed by α-secretase and γ-secretase. However, in the amyloidogenic pathway, β-secretase and γ-secretase cleave APP, resulting in the formation of Aβ (Hardy and Allsop, 1991). Tau protein is found naturally in the brain however in AD it becomes hyperphosphorylated and misfolds (discussed further in **Section 1.4).** Aggregation of these proteins causes neurotoxicity and as a result the destruction of basal forebrain cholinergic neurones which are necessary for innervating regions such as the hippocampus and the cortex (Zheng et al., 2002). Monomeric Aβ and Tau initiate a nucleation process to form semi-soluble oligomers and protofibrils with β-sheet structure (Cohen et al., 2013, Hardy and Allsop, 1991, Ballatore et al., 2007). They then aggregate to form insoluble Aβ1–40 or Aβ1–42 amyloid fibrils and Tau fibrils which deposit in the brain as extracellular amyloid plaques and hyper-phosphorylated intraneuronal neurofibrillary tangles (NFTs), respectively, as seen in **Figure 1.2** (Kaffy et al., 2016). Interestingly the most neurotoxic form of Aβ and Tau is believed to be small aggregates known as oligomers. These oligomers are responsible for neurodegeneration, particularly of neuronal synapses, and fibrils have been demonstrated to cause damaging redox activity and promote nucleation of oligomers (Mayes et al., 2014). These aggregation and deposition processes of Aβ and Tau are known as amyloidopathies and Tauopathies, respectively, and sometimes together along with α-synuclein cause AD upon accumulation in the brain (Kumar et al., 2014). Soluble α-synuclein is believed to normally play a role in neurotransmitter release through interaction with vesicle fusion complexes. In pathogenic conditions α-synuclein is mainly associated with Parkinson's disease and for unknown reasons it misfolds and aggregates to form Lewy Body's which are insoluble,

spherical inclusion bodies. With relation to AD, α-synuclein has shown to be able to bind to microtubules, induce aggregation of Tau and potentially be mediated by GSK3β (Twohig and Nielsen, 2019).
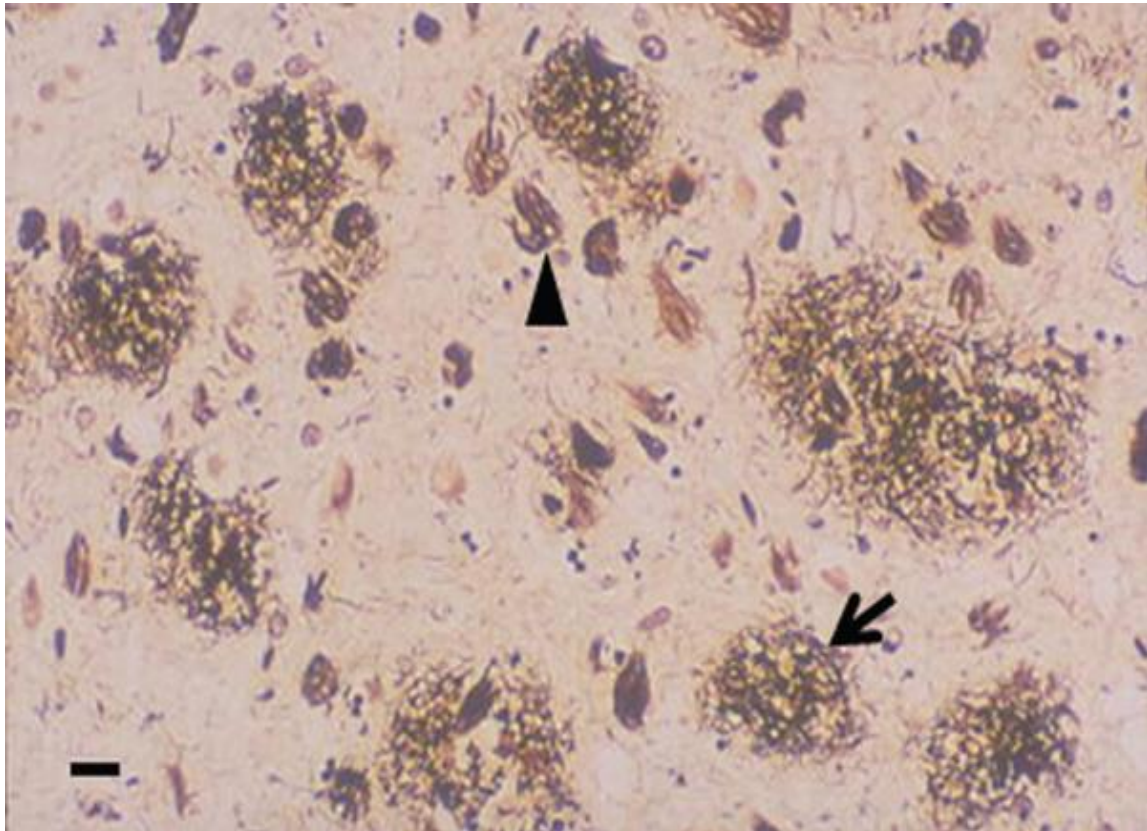
Figure 1.2: Senile plaques (arrow) and neurofibrillary tangles (arrowhead). Image courtesy of Professor D.M.A. Mann from University of Manchester, U.K. (Allsop and Mayes, 2014).

Moreira et al., (2007) suggested that these toxic proteins result in massive destruction of neurones and synapses, particularly of the hippocampus and cortex. Aβ and Tau are recognised by the Internatinoal Society of Amyloidosis as amyloid fibril proteins (Benson et al., 2018). Tau fibrils are classified as amyloid proteins and play an intrinsic pathological role in neurodegenerative diseases (Sipe et. al., 2016).

Amyloid hypothesis was first coined by Hardy and Allsop (1991), who suggested that extracellular Aβ deposition was the central event which led to the aetiology of AD; and has been the mainstream concept for the last two decades. However, following a vast series of terminated clinical trials, many Aβ targeting

drugs have been withdrawn or become inactive (72%), as seen in **Appendix A**. As a result, researchers have begun to investigate other avenues for treatment, such as inflammation and particularly Tau protein. There is conflicting research correlating deposition of amyloid with loss of cognition; whereas hyper-phosphorylated Tau NFT's and neuronal destruction are more closely linked to memory deficits (Giacobini and Gold, 2013). As a result, targeting Tau pathology may be more clinically suitable as opposed to other strategies. This is supported by the fact that over 200 candidate treatment compounds have failed in the attempt to treat AD; and these have mainly targeted Aβ or the cholinergic system, with very little focus applied to targeting Tau (Becker and Greig, 2012). Giacobini and Gold, (2013) discovered that amyloid toxicity may be Tau-dependent which would suggest that targeting Tau as a monotherapy could be therapeutically effective, regarding Aβ toxicity, but not entirely. This suggests that Aβ is not the only cause for cognitive impairment in AD patients and that having more than one target, such as Tau, is more effective than anti-Aβ monotherapy (Gong and Iqbal, 2008). The argument to support Tau as a target is backed up by many primary research sources such as those suggesting that NFT load and number of neurones, but not amyloid load can independently predict the cognitive status of patients (Giannakopoulos et al., 2003; Gold et al., 2001). This is further supported by Pievani et al., (2011) who using functional MRI and EEG, discovered that hyper-phosphorylated Tau pathology is linked closely to AD related memory deficits, whereas Aβ deposition better correlates with functional network disruption rather than cognition (Pievani et al., 2011). Functional connectivity is defined as the co-activation time series of different brain regions; therefore, functional network disruptions result in a delay to these time series (Giza et al., 2018). This is supported by the study of Desikan et al. (2012), who identified that longitudinal clinical decline associated with CSF Aβ in 107 clinically normal older individuals only occurred in the presence of increased CSF phosphorylated Tau levels. They suggested that 50% of individuals aged over 90 who had high amyloid neuropathology did not have clinical dementia accompanying it. Tansgenic mice models are also in agreement with these findings such as Leroy et al. (2012), who using APP/PSEN1

mice identified that by eliminating Tau resulted in improvements in memory deficits and synaptic loss. Similar results were also seen by Roberson et al. (2007), who stated that all cognitive deficits were prevented when they crossed APP transgenic mice with Tau knockout mice. 3xTg-AD mice contain three mutations including human APP, PS1 and Tau transgenes. Oddo et al., 2003 demonstrated that intraneuronal Aβ preceeded accumulation of somatodendritic Tau. It was then demonstrated via immunotherapy that removal of this Aβ later resulted in removal of Tau also, on the condition that the Tau was not aggregated (Oddo et al., 2004). Oddo (2008), identified that proteasome function is inhibited by Aβ oligomers which may prevent degradation of excess Tau (LaFerla and Green, 2012). This evidence clearly shows a close relationship between Aβ and Tau. Jack et al., (2013) used Pittsburgh compound B (radioactive analogue of thioflavin-T) positron emission tomography to image Aβ and discovered variation in cognitive impairment amongst individuals with high amyloid load. Villemagne et al., (2013) stated that Aβ aggregation needs to reach a certain threshold (~19 years) to be possibly detected with current technology in AD patients. These suggest that targeting Tau would be a wise decision, and wiser still to devise a therapeutic approach which would also combat Aβ aggregation that is known to have an involvement in the neuropathology of AD and suggested to be downstream ot Tau pathology (LaFerla and Green, 2012).

1.4 TAU BACKGROUND

Tau protein is a neuronal microtubule associated protein which is naturally found mainly in neurones of the central nervous system. Tau proteins bind to microtubules through the 4 repeat domains (**Figure 1.3**) and supresses microtubule shortening thereby stabilising axon structural integrity. This process lowers the critical concentration of tubulin polymerization to promote microtubule assembly and supports intracellular transport between the cell body and nerve terminals (Kadavath et al., 2015). Microtubules are located throughout the cytoplasm and are formed through the polymerisation of α-tubulin and β-tubulin dimers. Microtubules are involved in maintaining cell structure, cellular process (e.g. intracellular trafficking), cell division and cell morphogenesis.
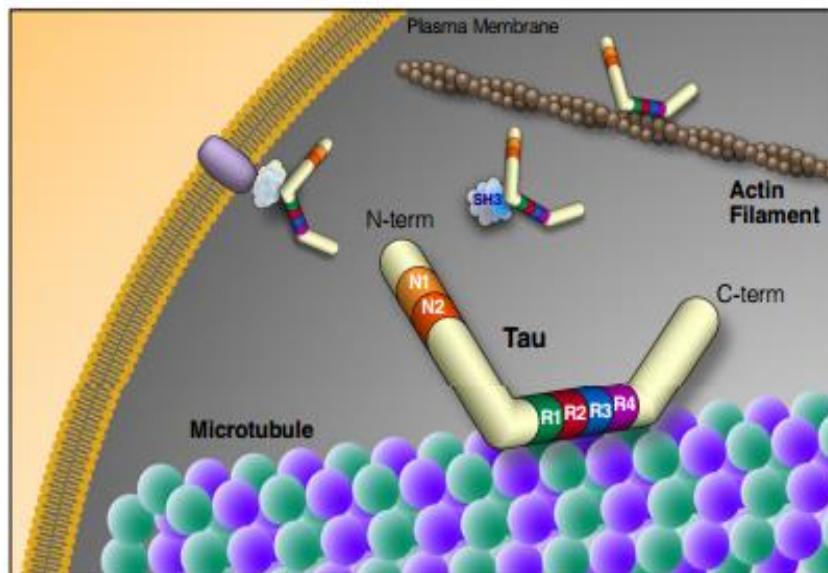
Figure 1.3: Illustrates the structure and function of Tau including phosphorylation by the kinase catalytic domain of Src protein (Morris et al., 2011). Tau binds to microtubules through its four repeat domains. The proline rich region of Tau can bind to the src Homology-3 (SH3) domain of Fyn, resulting in phosphorylation (Frame, 2001).

Tau exists as six isoforms which derive from alternative splicing of the *microtubule-associated protein Tau*

(MAPT) gene consisting of 16 exons. This gene is located at position 17q21 which is over 100kb on the

long arm of chromosome 17 and transcribes into a Tau primary transcript (Buée, et al., 2000). The Tau

primary transcript comprises 13 exons as 4A, 6 and 8 are not transcribed in humans. Exons 2, 3 and 10 are

adult brain specific and alternative splicing of these in the central nervous system results in six mRNAs

which are translated into the six Tau isoforms as seen in **Figure 1.4** with constitutive exons: 1, 4, 5, 7, 9,

11, 12 and 13 (Buée, et al., 2000). Exons 9, 10, 11 and 12 are each responsible for encoding a microtubule

binding motif whereby each of these are imperfect copies of an 18 amino acid repeat which are separated

by 13-14 amino acid inter-repeat sequences (Lee and Leugers, 2012). The presence or absence of exon 10

determines whether a Tau isoform has four or three repeats, respectively, as seen highlighted in the panel

on the right-hand side of **Figure 1.4**. It is these repeat regions, specifically residues 306-378 which form

the core of Tau fibrils (Fitzpatrick et al., 2017 and von Bergen et al., 2006). Goedert and Jakes (1990),
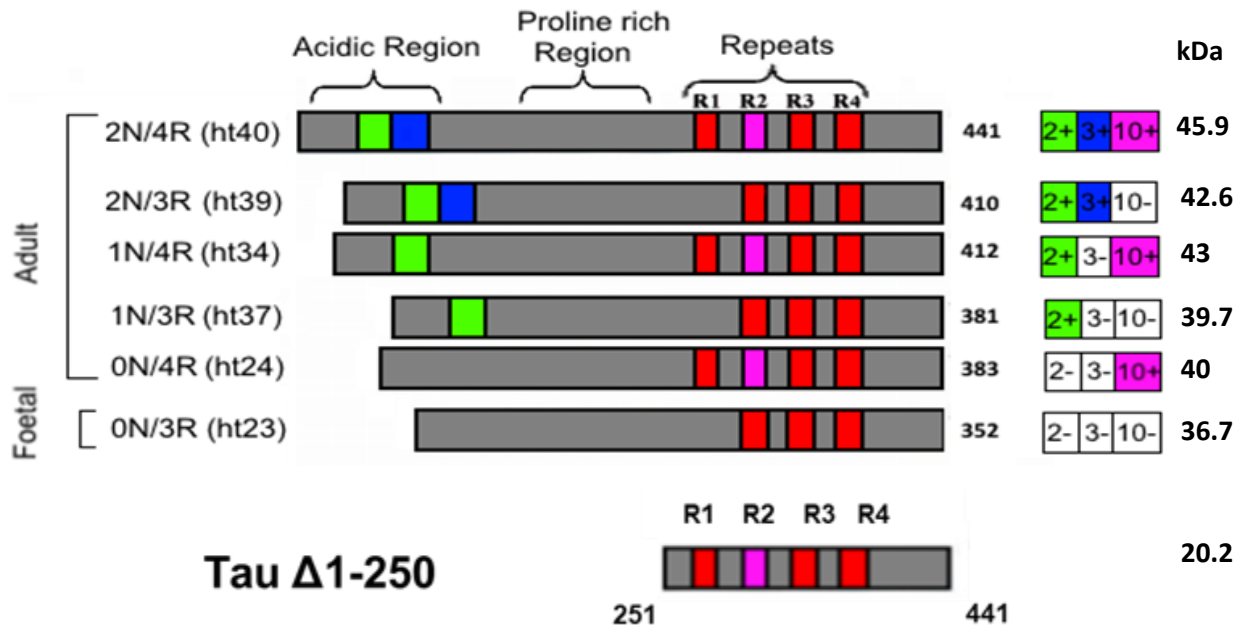
Figure 1.4: Schematic of the six human CNS Tau isoforms and two constructs (adapted from Buée, et al., 2000 and Johnson and Stoothoff, 2004) – From N terminal (left) to C terminal (right): including ht40, ht39, ht34, ht37, ht24 and ht23 R1–4 indicates the four microtubule-binding domains encoded by exons 9–12. Tau Δ1-250 (20.2 kDa) is a recombinant construct used in this research (discussed in **Section 3.2)**.

suggested that there are similar quantities of 3R and 4R Tau expressed in the cerebral cortex of adults. In addition to the six isoforms of Tau, there also exists 'Big Tau' expressed in the peripheral nervous system, which includes an additional exon at the N-terminal (Goedert et al., 1992 and Couchie et al., 1992).

The two main domains of Tau isoforms are the N terminal projection and the microtubule binding repeat domains (R1-R4) as seen in **Figure 1.5** which are also both largely hydrophilic making it a highly water-soluble protein. The second half of the N terminal domain is acidic due to high proportion of Glutamic Acid and Aspartic Acid. This is followed by a Proline-rich region (P1 and P2) between residues 150-240 whereby prolines are mainly preceded by either Serine or Threonine phosphorylation sites. Six PXXP motifs exist within P1 and P2 which allow proteins comprising SH3 domains to bind (Mandelkow and Mandelkow, 2012). Next comes the repeat domains (R1-R4) which is also forms the basic part of the protein and then the C-terminal tail (Kolarova et al., 2012). This suggests that Tau is a dipole protein as each domain possesses opposing charges to the other. The N terminal defines the intermolecular spacing between plasma membranes and bundled microtubules as well behaving as mediator between their interactions (Ganguly et al., 2015). It projects out from the microtubule surface to interact with other cytoskeletal elements including the neuronal plasma membrane and mitochondria; whereas the repeat domain binds to microtubules (Kolarova et al., 2012).

N-terminal

| | | | | | 50 |
MAEPRQEFEV MEDHAGTYGL GDRKDQGGYT MHQDQEGDTD AGLKESPLQT

N1   N2   100

PTEDGSEEPG SETSDAKSTP TAEDVTAPLV DEGAPGKQAA AQPHTEIPEG

150

TTAEEAGIGD TPSLEDEAAG HVTQARMVSK SKDGTGSDDK KAKGADGKTK

P1   200

IATPRGAAPP GQKGQANATR IPAKTPPAPK TPPSSGEPPK SGDRSGYSSP

P2   250

GSPGTPGSRS RTPSLPTPPT REPKKVAVVR TPPKSPSSAK SRLQTAPVPM

R1 ^{275}VQIINK^{280} R2   300

PDLKNVKSKI GSTENLKHQP GGGKVQIINK KLDLSNVQSK CGSKDNIKHV

^{306}VQIVYK^{311} R3   350

PGGGSVQIVY KPVDLSKVTS KCGSLGNIHH KPGGGQVEVK SEKLDFKDRV

R4   400

QSKIGSLDNI THVPGGGNKK IETHKLTFRE NAKAKTDHGA EIVYKSPVVS

C-terminal

GDTSPRHLSN VSSTGSIDMV DSPQLATLAD EVSASLAKQG L

X = Basic AA (+)
X = Polar uncharged AA (hydrophilic)
X = Nonpolar AA (hydrophobic)
X = Acidic AA (−)

Figure 1.5: Schematic of the amino acid sequence for 2N4R Tau: N1 and N2 encoded by exons 2 and 3 represent the polypeptide sequences; P1 and P2 represent the proline-rich regions; R1–4 encoded by exons 9-12 represent the microtubule-binding domains; ^{275}VQIINK^{280} (R2) and ^{306}VQIVYK^{311} (R3) are critical region sequences with β-structure (Kolarova et al., 2012).

1.4.1 TAU PHOSPHORYLATION

Tau is regulated by several post-translational modifications including oxidation (oxidation of cysteine residues results in disulphide cross-bridges), methylation (addition of methyl groups), glycation (addition of carbohydrate to lysines), acetylation (addition of acetyl groups to lysines) and phosphorylation (addition of phosphate groups). Phosphorylation is the most abundant and involves attaching negatively charged phospates to the side chains of serine, threonine and tyrosine, of which are 85 potential sites in Tau (Medina et al., 2016; Arendt et al., 2016). KXGS motifs in Tau (residues 244-370) are key phosphorylation sites and are closely involved in both physiological functions and pathological dysfunctions of Tau through their participation in microtubule assembly and paired helical filament (PHF) aggregation, respectively. Kamat et al. (2016), suggested that Aβ promotes the production of reactive oxygen species and oxidative stress mediated hyperphophorylation of Tau, as seen in **Figure 1.6**. Behl, (2012) demonstrated the relationship that oxidative stress levels increased with age. It is also important to note that Aβ levels also increase with age. Reactive oxygen species are chemically reactive molecules which cause oxidative stress upon breaching oxidant defences, resulting in damage to cells, including
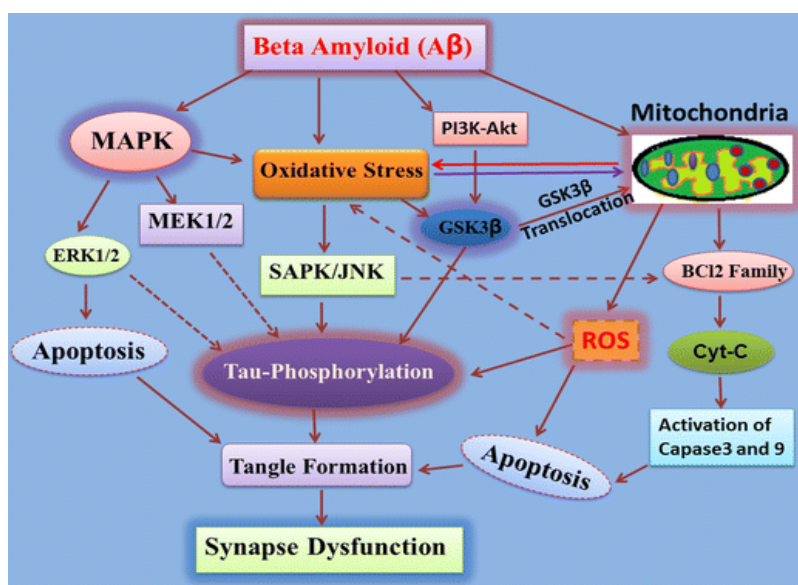
Figure 1.6: Synaptic dysfunction because of Aβ causing MAPK and mitochondrial oxidative stress mediated Tau hyper-phosphorylation (Kamat et al., 2016).

cellular lipids, DNA, RNA and proteins; contributing to ageing (Sayre et al., 2001). The reduction of molecular oxygen O_2 results in the formation of superoxide ($O_2 + e^- \rightarrow \cdot O_2^-$) which is the precursor of most reactive oxygen species (Turrens, 2003). Superoxide then reacts to produces hydrogen peroxide ($2H^+ + \cdot O_2^- + \cdot O_2^- \rightarrow H_2O_2 + O_2$). Hydrogen peroxide is then reduced to water ($H_2O_2 + H_2O_2 \rightarrow H_2O + H_2O + O_2$) or partially reduced to hydroxyl radical ($H_2O_2 \rightarrow HO \cdot + \cdot OH$) (Kissova et al., 2006). In AD the brain is excessively phosphorylated to the extent of around 3x that of the normal brain (Funk et al., 2014). Phosphorylation of Ser-262 (localised within a KXGS motif of the first repeat domain, as seen in **Figure 1.7**) is believed to be the initiator of the phosphorylation cascade resulting in Tau hyper-phosphorylation. Mutation of either Ser-262 or Ser-356 into alanine is reported to rescue Tau microtubule assembly properties and reduce toxicity in wild type phosphorylated brain extracts (Yu et al., 2012). These motifs are essential for microtubule interactions and aggregation.
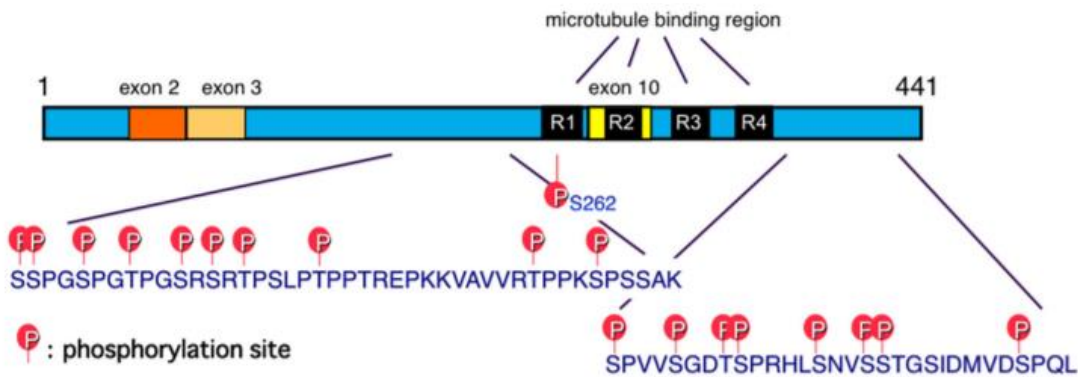
Figure 1.7: Schematic illustration of the main phosphorylation sites identified in Tau441 PHF from AD brains (Kametani and Hasegawa, 2018).

A list of phosphorylation sites identified in 2N4R Tau are summarised by the Hanger group, Muckle group and Kuret group in **Table 1.1** (Morris et al., 2015 and Funk et al., 2014). Cytosolic Tau is usually maintained in an equilibrium through kinases and phosphatases which phosphorylate and dephosphorylate Tau, respectively (Kolarova et al., 2012). When protein kinases phosphorylate proteins, the newly covalently bound phosphate group changes the proteins structural conformation, resulting in activation, deactivation or altered protein function. Hyper-phosphorylation of Tau reduces its binding affinity to tubulin resulting in the disassembly of microtubules which interferes with axonal flow and the sequestering of Tau (Giacobini and Gold, 2013 and Pooler et al., 2012).

2N4R Tau Phosphorylation sites			
Residue number	Alzheimer PHF-Tau	Control brain Tau	Protein Kinases
Y18	✓		Fyn, Syk
S46	✓	✓	GSK-3, ERKs1/2, p38MAPK, SAPK2a, SAPk2b, SAPK3, CK1
S68	✓		N/A
T69	✓		GSK-3, ERKs1/2, p38MAPK
T71	✓		BRSK1/2
S113	✓		CK1
T123	✓		PSK1/TAOK2
T149	✓		GSK-3, CK1, LRRK2, PSK2/TAOK1
T153	✓		cdk5, GSK-3, ERKs1/2, SAPK, SAPK2a, SAPK2b, SAPK3, SAPK4, LRRK2
T175	✓		GSK-3, JNK, ERKs1/2, p38MAPK, SAPK, SAPK2a, SAPK2b, SAPK3, LRRK2, PSK2/TAOK1
T181	✓	✓	cdk5, GSK-3, JNK, ERKs1/2, p38MAPK, SAPK, SAPK2a, SAPK2b, SAPK3, SAPK4, LRRK2
S184	✓		GSK-3, SAPK2a, SAPK2b, SAPK3, CK1, PSK1/TAOK2, PSK2/TAOK1
S185	✓		p38MAPK, PSK1/TAOK2, PSK2/TAOK1
S191	✓		PSK1/TAOK2, PSK2/TAOK1
Y197	✓		Met
S198	✓	✓	GSK-3, CK1, PKA, PSK1/TAOK2, TTBK1/2
S199	✓	✓	cdk5, GSK-3, ERKs1/2, CK2, PKA, PSK2/TAOK1, TTBK1/2
S202	✓	✓	cdk5, DYRK1A, GSK-3, JNK, ERKs1/2, p38MAPK, SAPK, SAPK2a, SAPK2b, SAPK3, SAPK4, PKA, TTBK1/2
T205	✓	✓	cdk5, GSK-3, JNK, ERKs1/2, p38MAPK, SAPK, SAPK2a, SAPK2b, SAPK3, SAPK4, PKA, LRRK2, PSK1/TAOK2, PSK2/TAOK1
S208	✓		AMPK, CK1, TTBK1/2
S210	✓		GSK-3, CK1, PKA, LRRK2, TTBK1/2
T212	✓	✓	cdk5, DYRK1A, GSK-3, JNK, ERKs1/2, p38MAPK, SAPK, SAPK2a, SAPK2b, SAPK3, SAPK4, CaMKII, CK1, PKA, LRRK2, p70S6 kinase, PSK1/TAOK2
S214	✓		cdk5, GSK-3, SRPK2, AMPK, CaMKII, CK1, PKA, MSK1, p70S6 kinase, PKB/AKT, PKC, PKN, PSK1/TAOK2, PSK2/TAOK1, RSK1/2, SGK1
T217	✓	✓	GSK-3, JNK, ERKs1/2, p38MAPK, SAPK, SAPK2a, SAPK2b, SAPK3, SAPK4, LRRK2, PKA
T231	✓	✓	cdk5, GSK-3, JNK, ERKs1/2, p38MAPK, SAPK, SAPK3, SAPK4, AMPK, PKA, LRRK2

19

S235	✓	✓	cdk5, GSK-3, JNK, ERKs1/2, p38MAPK, SAPK, SAPK2a, SAPK2b, SAPK3, SAPK4, AMPK, PKA, Phosphorylase kinase,
S237	✓		GSK-3, CK1, LRRK2, Phosphorylase kinase, PSK1/TAOK2, PSK2/TAOK1
S238	✓		CK1, PSK2/TAOK1
S258	✓		GSK-3, AMPK, CK1, PKA, LRRK2, PKC, PKN, PSK1/TAOK2, PSK2/TAOK1
S262	✓		GSK-3, phosphorylase kinase, AMPK, BRSK, CaMKII, CK1, PKA, LRRK2, MARK, MSk1, p45/41, p70S6 kinase, PKC, PSK1/TAOK2, PSK2/TAOK1, Rho kinase
S289	✓		GSK-3, AMPK, CK1, PSK1/TAOK2, PSK2/TAOK1
S356	✓		GSK-3, JNK, ERKs1/2, ps38MAPK, SAPK, SAPK2a, SAPK2b, SAPK3, SAPK4, AMPK, CaMKII, CK1, PKA, LRRK2, MARK, Phosphorylase kinase, PSK1/TAOK2, PSK2/TAOK1,
Y394	✓		c-Abl, LRRK2
S396	✓	✓	GSK-3, JNK, ERKs1/2, p38MAPK, SAPK, SAPK2a, SAPK2b, SAPK3, SAPK4, CK1, CK2, PKA,
S400	✓	✓	GSK-3, AMPK, CK2, PSK1/TAOK2, PSK2/TAOK1
T403	✓		AMPK, LRRK2, PSK1/TAOK2, PSK2/TAOK1
S404	✓	✓	cdk5, DYRK1A, GSK-3, ERKs1/2, p38MAPK, CK1, CK2
S409	✓		cdk5, GSK-3, p38MAPK, SAPK3, SAPK4, PKA, p35/41, PSK1/TAOK2, PSK2/TAOK1, Rho kinase
S412	✓	✓	CK1, CK2, PKA, PSK2/TAOK1
S413	✓	✓	GSK-3, CK1, CK2, PKA, PSK1/TAOK2, PSK2/TAOK1
T414	✓	✓	CK1, CK2, PSK1/TAOK2, PSK2/TAOK1
S416	✓	✓	CaMKII, CK1, CK2, PKA, PSK1/TAOK2, PSK2/TAOK1
S422	✓		JNK, ERKs1/2, p38MAPK, CaMKII, PSK1/TAOK2, PSK2/TAOK1, TTBK1/2
T427	✓		PSK1/TAOK2, PSK2/TAOK1
S433	✓		CK1, PSK1/TAOK2, PSK2/TAOK1
S435	✓		CK1, PKA, LLRK2, PSK1/TAOK2, PSK2/TAOK1

Table 1.1: 2N4R Tau phosphorylation sites from AD and control brains summarised by the Hanger group, Muckle group and Kuret group (Adapted from Kings College London, 2019). Residues highlighted in yellow have no currently identified associated kinase. Kinases involved in Tau phosphorylation are grouped into 3 classes: proline-directed protein kinases (blue), non-proline-directed kinases (black) and tyrosine kinases (red) (Morris et al., 2015; Funk et al., 2014). Abbreviations: 5' adenosine monophosphate-activated protein kinase (AMPK), Brain-specific kinase 1/2 (BRSK1/2), Calcium-calmodulin kinase II, Cyclin-dependent kinase-5 (cdk5), Casein kinase 1 (CK1), Casein kinase 2 (CK2), Cyclic AMP-dependent protein kinase (PKA), Dual-specificity tyrosine-phosphorylation regulated kinase 1A (DYRK1A), Glycogen synthase kinase-3 (GSK-3), Microtubule affinity-regulating kinase (MARK), Mitogen and stress activated protein kinase-1 (MSK1), p42/p44 mitogen-activated protein kinases (ERKs1/2), p38 mitogen-activated kinase (p38MAPK), Protein kinase C (PKC), Protein kinase N (PKN), Prostate-derived sterile 20-like kinase 1 alpha/beta (PSK1/TAOK2), Prostate-derived sterile 20-like kinase 2 (PSK2/TAOK1), 90 kDa Ribosomal S6 kinase (RSK1/2), Stress-activated protein kinase (SAPK) Tau-tubulin kinase 1/2 (TTBK1/2).

1.4.2 **TAU AGGREGATION**

Following hyperphophorylation, specifically T231, S396, S422 and S404 which promote filament formation of Tau (Cown and Muder, 2013; Alonso et al., 2004; Gamblin et al., 2003; Jackson et al., 2002). Increased concentrations of cytosolic and sequestered Tau begin to misfold, inducing a polymerisation cascade which assembles filaments through the repeat binding regions and some sequences in the C-terminus, whereas the rest of the N-terminus forms a fuzzy coat around the core amino acids 306-378 (Fitzpatrick et al., 2017). This aggregation cascade begins with Tau monomers which aggregate to form soluble dimers and larger oligomers. As aggregation increases these oligomers become increasingly insoluble and form off pathway oligomers or protofibrils which subsequently form mature fibrils and ultimately aggregate into NFTs of PHFs, as seen in **Figure 1.8**. Tau morphology and secondary structural transition are discussed in **Sections 1.4.2 and 1.4.3**, respectively. Tau aggregation without mutation, is a result of the suppression of phosphatases and/or the activation of Tau protein kinases (involving a loss of microtubule binding ability) and exposure to poly-anions (e.g. heparan sulphate) which bind Tau and promote the likelihood of Tau proteins interacting together and aggregating (Boutajangout et al., 2011). Contrarily, Arendt et al (2003), suggested that formation of hyper-phosphorylated Tau is a reversible phenomenon observed during hibernation. In addition to phosphorylation; glycation, acetylation and truncation have also been observed to promote aggregation of Tau (Funk et al., 2014). Two important nucleating sequences within the repeat domain are [275]VQIINK[280] and [306]VQIVYK[311]; located at the beginning of R2 and R3, respectively (Mukrasch et al., 2005). R3 is present in all Tau isoforms, consistent with their shared ability to all form PHFs; R2 is only found in ht40, ht34 and ht24. The interaction of VQIINK and VQIVYK is believed to produce the twisted PHF-like filament morphology (Von Bergen et al., 2000).
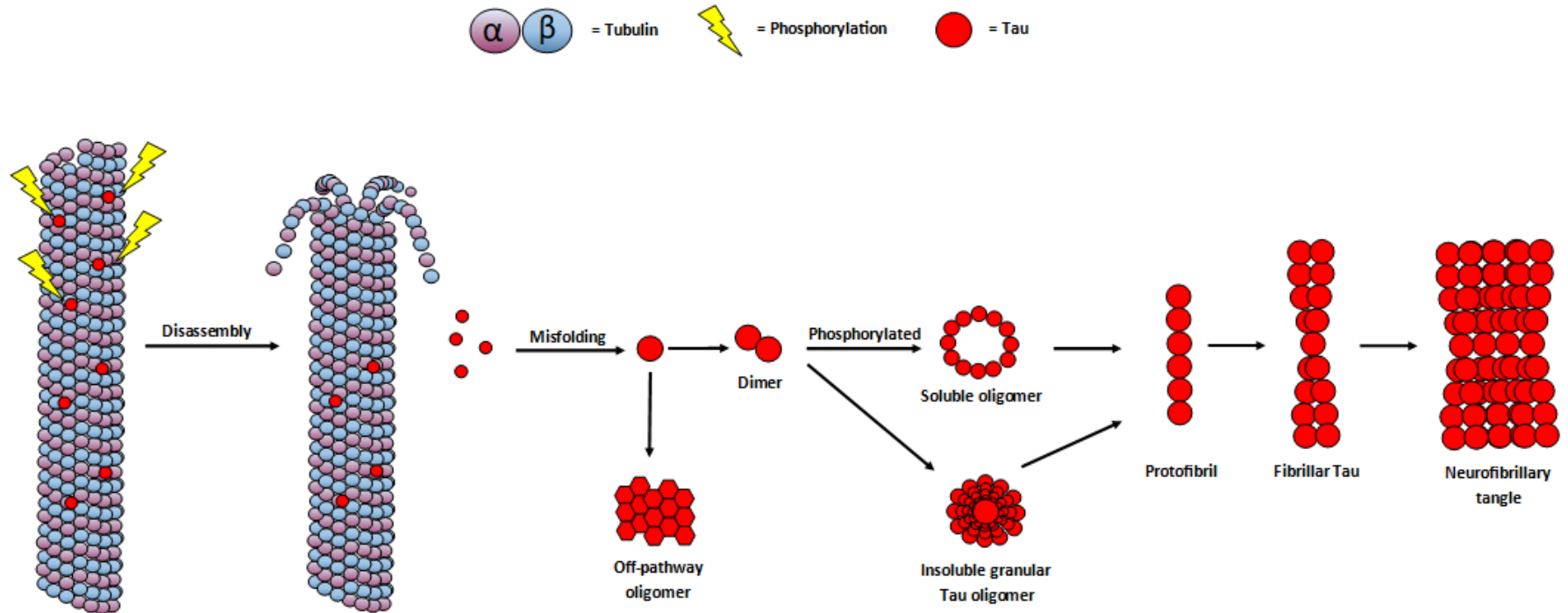
Figure 1.8: Schematic illustration of the Tau disassembly from microtubules and its aggregation cascade. Phosphorylation causes unordered Tau to transition into beta sheet structures and disassemble from microtubules. Monomeric Tau misfolds and forms off-pathway oligomers or dimers. Dimers form phosphorylated soluble oligomers and non-phosphorylated insoluble granular Tau oligomers. Oligomers form protofibrils, then fibrils and NFTs.

1.4.3 TAU MORPHOLOGY

Tau straight filaments are ~10nm wide and PHFs typically have an average width of 10-20nm, average length of 530nm, and a half periodicity of 80nm (Pollanen and Bergeron, 2000, Sadqi et. al., 2002, Xu et. al., 2010, Morozova et. al., 2013). PHFs should look appear as two fibrils twisted around each other with the cross over repeats around 75-80nm and a varying width between 10-22nm; suggesting a single strand has a diameter of 10nm (Crowther and Wischik, 1985). PHFs from brains, recombinant proteins and different length Tau have similar dimensions when viewed under electron microscope as seen in **Figure 1.9A+C**. This suggests that most of the protein comprising ~70% of residues (1-240 and 379-441) that makes up the fuzzy coat, offers little to the morphology due to their natively unordered structure as seen in **Figure 1.9B** (Drechsel et al., 2017 and Barghorn et al., 2004).
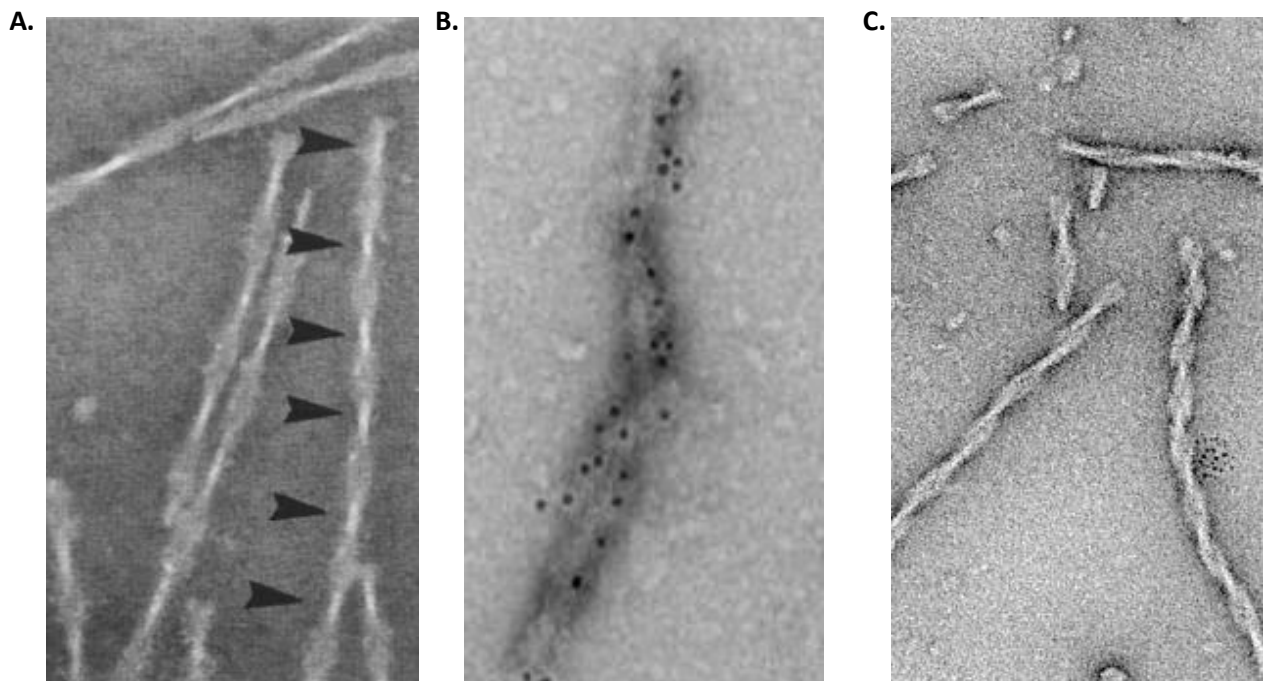
Figure 1.9: Negative stained electron micrographs of PHFs. **A:** AD brain PFHs with arrowheads pointing to crossover repeats of ~80nm (Mandelkow and Mandelkow., 2012). **B:** AD brain PHFs immunogold labelled using PHF1 (epitope S396/404) to emphasise the fuzzy coating (Rissman et al., 2012). **C:** K18ΔK280 Recombinant Tau PHFs (Madelkow and Mandelkow, 2012).

As PHFs accumulate, they form NFTs. The separate maturation states of NFTs are 0, 1, 2 and 3 which correspond to healthy cells, pretangles, classic NFTs and ghost tangles, respectively (Uematsu et al., 2017). These stages can be summarised by **Figure 1.10**. Ghost tangles are extracellular and are formed from the death of neurons which previously hosted intracellular NFT's.
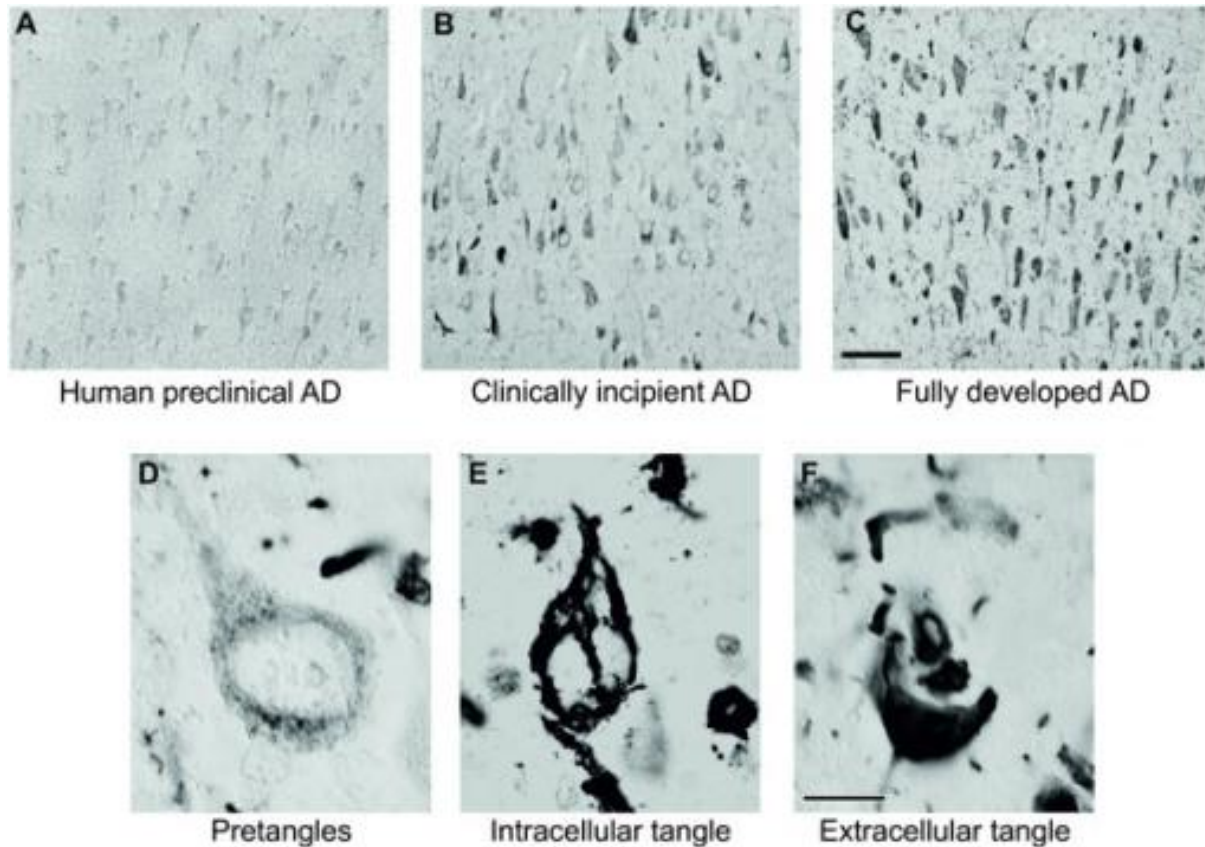
Figure 1.10: Monoclonal antibody DC8E8 immunostaining of **A:** human preclinical AD, **B:** clinically incipient AD, **C:** fully developed AD. Hippocampal immunostaining of **D:** pretangles, **E:** intracellular tangle, **F:** extracellular tangle. Scale bar: **A-C** 100 μm; **D-F** 10 μm (Kontsekova et al., 2014).

1.4.4 TAU SECONDARY STRUCTURE

Native Tau has a very low secondary structure content of α-helix and ß-strands and so has an unordered secondary structure as determined by Circular Dichroism (CD). Pathogenic aggregation of Tau is manifested as a structural transition from unordered to β-sheet structure around some some hexapeptide motifs of the repeat domain which form the core of PHF's and can be summarised as a nucleation elongation reaction. These core β-sheet sequences (residues 306-378) identically stack in register and in parallel to one another to form protofilaments, and then mate anti-parallell to one other. (Fitzpatrick et al., 2017). as seen in **Figure 1.11.**
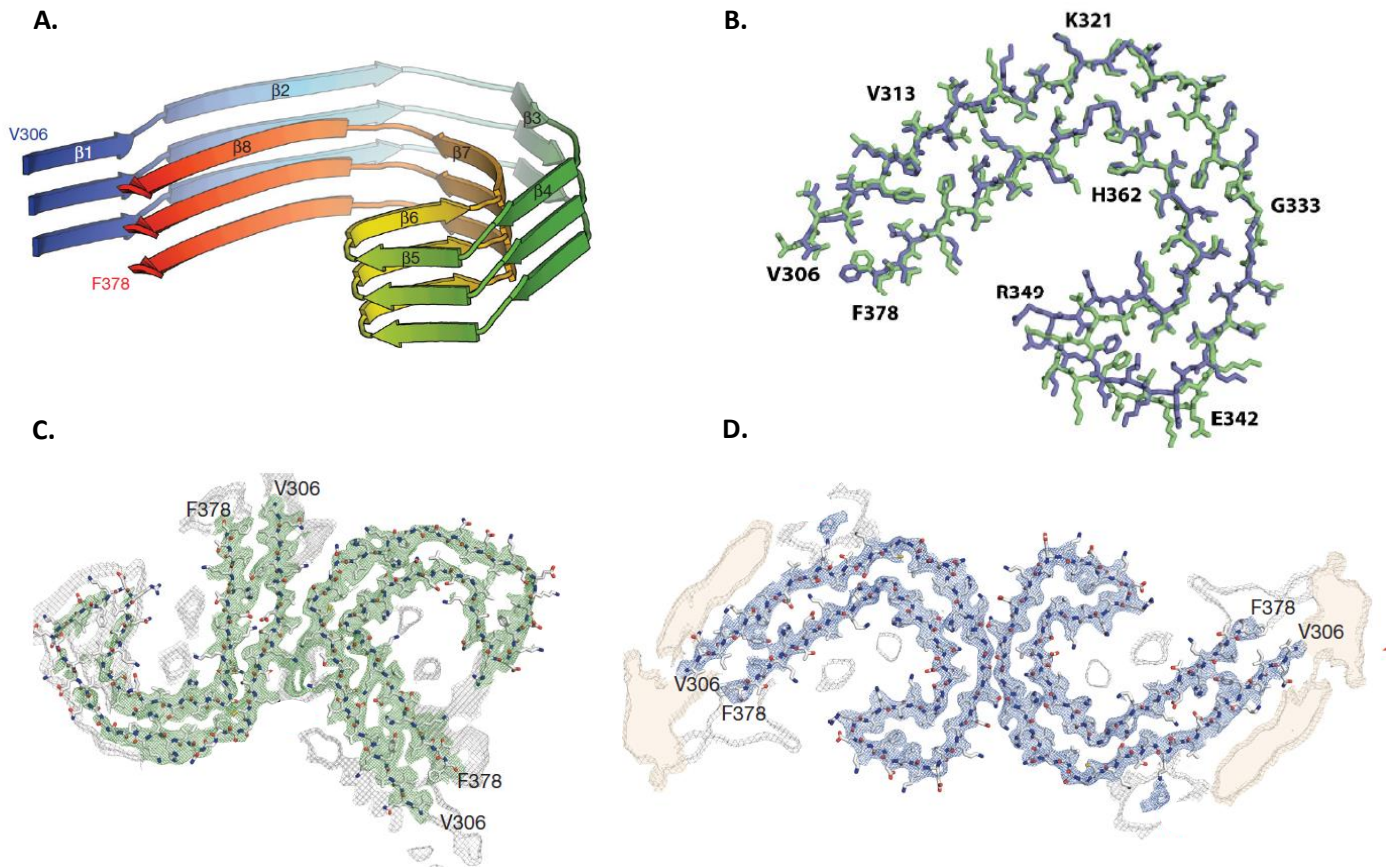
Figure 1.11: Tau PHF protofilament core comprising two microtubule-binding repeats; R3-R4, demonsrating in register and in parallel β-sheet stacking. **A**: Rendered secondary structure view of the protofilament core, **B**: Demonstrates backbone atoms similarity between SF (green) and PHF (blue) protofilament cores **C**: Cross-section of the SF cryo-EM structure **D**: Cross-section of the PHF cryo-EM structure (Fitzpatrick et al., 2017).

Using X-ray microcrystallography, Sawaya et al., (2007) suggested that the VQIVYK hexapeptide forms a Class 1 steric zipper, in which β-strands are stacked into parallel, antifacial β-sheets which stack face to face with sheet edges facing up. This can be visualised by **Figure 1.12** which also demonstrates the symmetry relationship between sheet mates by a 180° rotation about the arrow. This relationship allows side chains to interlock between the side chains of their sheet mate and when viewing these protofilaments down the fibril axis, the interlocking side chains resemble teeth from a zipper and so are dubbed steric zippers (Eisenberg and Sawaya, 2017, Sawaya et al., 2007). The term '*unordered*' will be used instead of '*random coil*' throughout this thesis as native monomeric Tau does not have a random structure and neither is it a coil. It has a structure, but it does not follow a well-defined secondary structure motif like α-helix or β-sheet. Turns also have less defined bond angles and so are also unordered.
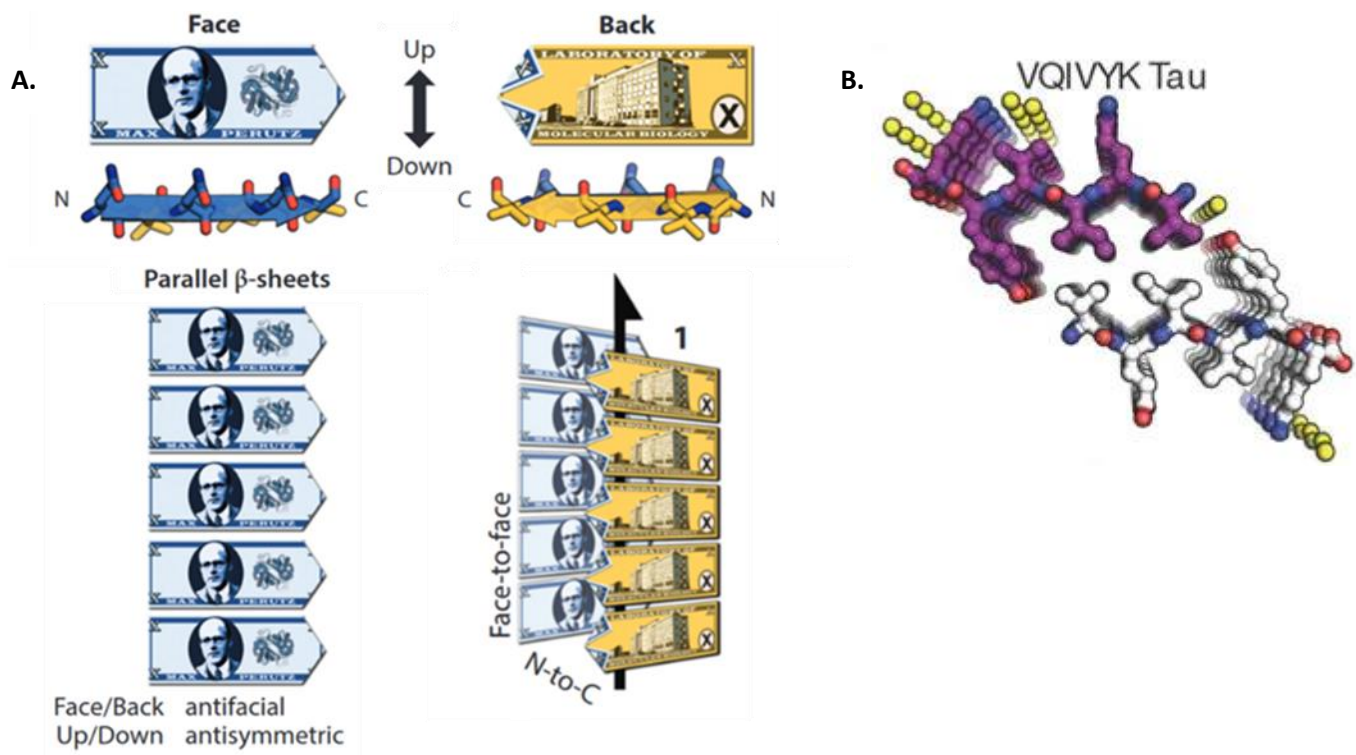
Figure 1.12: **A:** Illustrative example of a Class 1 steric zipper amyloid spine. β-strands have an N and C terminus, front/back faces and up/down edges. Arrow indicates symmetry axes demonstrating that the sheets are related by a 180° rotation. Adaptaed from (Eisenberg and Sawaya, 2017). **B:** Example of VQIVYK peptides forming a face to face class 1 steric zipper (Sawaya et al., 2007).

1.4.5 **TAU TOXICITY & PROPAGATION**

There is some dispute as to which species of Tau are toxic (Eisenberg and Sawaya, 2017). Bakota and Brandt, (2016) stated that it is still currently unclear whether it is Tau oligomers or higher aggregates which are most toxic. They also suggested that higher aggregates such as PHFs or NFTs may be a self defence mechanism whereby cells store toxic misfolded Tau monomers and oligomers in a more inert form. As a result, approaches to disassemble higher aggregates may exacerbate cognitive impairment. It is difficult to conceive however that a neuron can function effectively when it contains tangles occupying most of the cytoplasm which inevitably result as ghost tangles which demonstrate cell death. It is generally appreciated that soluble Tau oligomers are most toxic, however, there is some evidence to suggest that not all oligomers are toxic and that it remains unknown which size oligomers are responsible for toxicity and what conformation and phosphorylation state are they in (Cowan and Mudher, 2013). For example, there is currently evidence of monomeric Tau and granular Tau oligomers (GTOs) forming PHFs, however no evidence suggesting that small soluble oligomers can form GTOs (Maeda et al., 2007). It is not yet understood if GTOs are a neuroprotective strategy although Cowan et al. (2015), illustrated in a Drosophila model of tauopathy that GTOs are not phosphorylated and are not toxic, suggesting they could be an alternative aggregation pathway to PHFs (Cowan et al., 2015). GTOs are not completely understood with regards to potential toxicity because although insoluble, they are too small to sediment in current assays and do not enter PAGE resolving gels (Maeda et al., 2007). On the other hand, soluble Tau oligomers are highly phosphorylated and believed to be toxic (Maeda et al., 2018; Cowen et al., 2015). There is a lot of evidence in both Drosophila and mouse models suggesting that neurodegeneration occurs without the presence of NFTs (Mudher et al., 2004; Wittman et al., 2001; Andorfer et al., 2005). Using inducible mouse models Eckermann et al. (2007) and Spires et al. (2006), expressed full length Tau-ΔK280 or P301L, respectively. Expression was switched off after NFTs had formed but cell loss was stabilised despite the

presence of NFTs, suggesting aggregates smaller than NFTs cause degeneration but larger insoluble aggregates are less toxic, suggesting NFT formation is neuroprotective.

Tau propagation has been demonstrated to intracellularly spread in a "prion-like" manner. Prion stands for "proteinaceous infectious particle" (Prusiner, 1982). It achieves this by infiltrating healthy neurones and promoting pathogenic misfolding of stable Tau and inducing aggregation through templated seeding, without being infectious to other humans (Frost et al., 2009; Goedert and Spillantini, 2017, Mudher et al., 2017). The initial transformation from healthy monomeric Tau into aberrant Tau is still not properly characterised (Mudher et al., 2017). Clavaguera et al. (2009), suggested that oligodendrocytes and nerve cell processes are the main areas of filament induction. However, oligomers have also been demonstrated to induce NFT pathology in various mouse models (Hu et al., 2016; Wu et al., 2013, Lasagna-Reeves et al., 2012). Approximately 90% of extracellular Tau is free Tau. Mechanisms by which Tau has been suggested to potentially leave its host cell and infiltrate its recipient cell include exocytosis and heparan sulphate proteoglycan (HSPG), Amyloid precursor protein (APP) or non-receptor-mediated endocytosis/macropinocytosis, diffusion, in ectosomes or exosomes and through nanotubes (Dujardin et al., 2014; Wang et al., 2017; Simon et al., 2012). Exact mechanisms how free Tau enters the synaptic cleft remains unknown, but this species is believed to be mainly un-phosphorylated (Mohammed et al., 2017). It is believed that Tau transported in vesicles is phosphorylated and so pathogenic, however the mechanism how it is chaperoned via vesicles, how it exits its vesicle and then how it enters its recipient cell remains unclear (Mudher et al., 2017; Jackson et al., 2002).

1.4.6 **OTHER TAUOPATHIES**

A list of Tauopathies and their Tau isoforms identified with are summarised by **Table 1.2**. The most prevalent Tauopathies include, progressive supranuclear palsy (PSP), Argyrophilic grain disease (AGD), Corticobasal degeneration (CBD), Pick's disease (PiD), Frontotemporal dementia and parkinsonism linked to chromosome 17 (FTDP-17), Post-encephalitic parkinsonism, Parkinsonism-dementia complex (PDC) Guam, Guadeloupean parkinsonism, Dementia pugalistica and Down's syndrome (Williams, 2006). Other diseases with Tau neuropathology not summarised in **Table 1.2** include aging-related Tau astrogliopathy, Hallevorden–Spatz disease, Creutzfeldt-Jakob disease, Gerstmann-Straussler-Scheinker disease, Lewy body disease, Meningioangiomatosis, Post-encephalitic Parkinsonism, Prion protein cerebral amyloid angiopathy, Progressive subcortical gliosis, Subacute sclerosing panencephalitis and Tuberous Sclerosis (Castellani and Perry, 2019). There are two Tau mutations in FTDP-17 which increase aggregation propensity of Tau; ΔK280 and P301L (Mandelkow et al., 2007). Aside from NFTs, other large non-fibrillar Tau aggregates include Pick bodies and Argyrophilic grains. Most Tauopathies are associated with 4R-Tau pathology except PiD which predominantly has 3R-Tau and AD which has both 3R and 4R-Tau inclusions (Mudher et al., 2017 and Buee and Delacourte, 1999). According to Grinberg et al. (2013), acetylated Tau is found in a all Tauopathies except AGD, which is characterised by neuropil grains, NFTs and oligodendroglial coiled bodies; suggesting it to be a distinct Tauopathy. Tau filament morphologies vary between diseases, despite deriving from the same Tau isoforms (Goedert and Spillantini, 2017). For example, PiD straight filaments, PSP twisted filaments and CBD twisted ribbons have diameters of 15-18nm, 13-14nm and 15-25nm, respectively (Taniguchi-Watanabe et al., 2016).

Class I
Aggregation of six Tau isoforms

Exon 2   Exon 3   Exon 10

Alzheimer's disease
Amyotrophic lateral sclerosis
Cerebral aging (over 75 years)
Chronic traumatic encephalopathy
Dementia pugalistica
Diffuse neurofilament tangles with calcification
Down's syndrome
Familial British dementia
FTDP-17
Guadeloupean Parkinsonism
Niemann-Pick disease type C
Parkinsonism–dementia complex of Guam
Post-encephalitic parkinsonism
Primary age-related Tauopathy

Class II
Aggregation of 4R Tau

Argyrophilic grain disease
Corticobasal degeneration
FTDP-17
Globular glial Tauopathy
Supranuclear palsy

Class III
Aggregation of 3R Tau

FTDP-17
Pick's disease

Class IV
Aggregation of Tau lacking exons 2 and 3

Myotonic dystrophy

Table 1.2: Four classes of Tau isoform aggregation and respective diseases they are found in. Class I is characterised by aggregation of all six isoforms. Class II and Class II are characterised by aggregation of Tau isoforms containing four and three repeat domains. Class IV is characterised by the aggregation of Tay lacking exons 2 and 3 (Adapted from Sergeant et al., 2008).

1.5   CURRENT THERAPEAUTIC STRATEGIES

The only approved drugs for the treatment of AD by the FDA modulate neurotransmission and only provide symptomatic treatment as opposed to altering the disease course. These include acetylcholinesterase inhibitors and an 1.5.2 N-methyl-D-aspartate (NMDA) receptor antagonist. Anand et al., (2014) summarised the potential therapeutic strategies for AD in **Appendix B**.

1.5.1   ACETYLCHOLINESTERASE INHIBITORS

Cholinergic hypothesis originated from research which demonstrated that cholinergic neurones located through the low to the high areas of the brain involved in memory are selectively lost in early AD; thereby effecting short term memory by diminishing nerve cell communication. This theory suggests that levels of choline acetyltransferase and pyruvate dehydrogenase complex decrease, and as they are responsible for the synthesis of acetylcholine, results in the decrease of cholinergic transmission (Kuca et al., 2016).

Preganglionic fibers secrete acetylcholine and bind either postganglionic muscarinic or nicotinic receptors which innervate skeletal muscle and peripheral tissues, respectively. Upon acetylcholine stimulation, muscarinic receptors form G coupled-protein receptor complexes to open ion channels, whereas nicotinic receptors use ligand gated ion channels which open directly upon stimulation. Diminished cholinergic transmission causes impairment of muscarinic receptor function, especially M1 receptors found abundantly in the brain (Pákáski and Kálmán, 2008). On top of this impairment of muscarinic receptors, nicotinic receptor numbers are diminished, (especially subtypes α7 and α4β2) due to the high affinity of toxic Aβ to these receptors (Okada et al., 2013). This exacerbates the reduction in cholinergic transmission. This decrease in cholinergic transmission is associated with a reduction in cognitive function and so it can be postulated that amyloid and cholinergic theories may well be intertwined cascades. **Figure 1.13** demonstrates how acetycholine is broken down in the synaptic cleft by acetylcholinesterase. As a result, drugs which inhibit the decomposition of acetylcholine or activate central M1 muscarinic and

nicotinic receptors have beneficial effects for dementia patients (Kuca et al., 2016). However, there are currently no M1 muscarinic receptor agonists for AD on the market, despite keen interest from the pharmaceutical industry. This is because although they are effective at improving cognition, however in high doses they have negative side effects which halted further clinical trials (Greig et al., 2013).

Current drugs are mainly acetylcholinesterase inhibitors and include Donepezil (Acricept), Galantamine (Reminyl) and Rivastigmine (Exelon). The downside to these drugs is that they are only for symptomatic treatment and can only delay cognitive decline for 6-12 months in roughly 50% of patients with AD (Blennow et al., 2006). They also have side effects such as nausea, vomiting, loss of appetite and diarrhoea being the mains ones and muscle cramps fatigue, dizziness and insomnia being the others. Gastrointestinal side effects can be controlled by beginning treatment with low doses and consuming with food to delay absorption (Blennow et al., 2006).
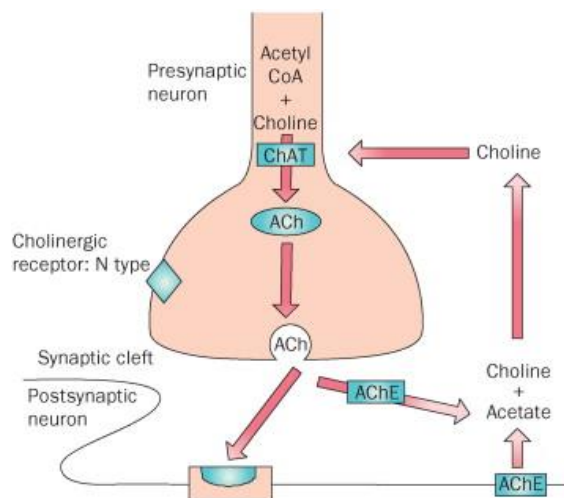
Figure 1.13: Mechanism of the cholinergic system (Scarpini et al., 2003). Choline acetyltransferase catalyses Acetyl CoA + Choline to form Acetylcholine which enters the synaptic cleft, binds to receptors and is degraded back into Acetate and Choline.

1.5.2 **NMDA RECEPTOR ANTAGONIST**

Memantine is a non-competitive, voltage dependent NMDA receptor antagonist which effects glutamatergic transmission dysfunction, as seen in **Figure 1.14**. It is currently the only drug used in advanced AD, however its effect is modest. In normal, resting physiological brain conditions NMDA receptor channels are blocked by Mg^{2+} ions which are revealed upon a glutamate synaptic signal. When this signal occurs, the post-synaptic membrane depolarises, allowing Ca^{2+} to enter the post-synaptic neurone (Parsons et al., 2013). Glutamate and its interactions with NMDA receptor are involved in learning and memory, however in abnormal circumstances such as in AD, excess glutamate reduces NMDA receptor function which is fatal to nerve cells. In AD, glutamate and amyloid cause continuous membrane depolarisation which removes Mg^{2+} from NMDA channels and therefore allow Ca^{2+} to continuously flow into the post-synaptic neurone resulting in constant stimulation at rest. This excess stimulation of NMDA receptors causes excitotoxicity. NMDA receptor activation along with Aβ toxicity alters the function of the synapse which is associated with the inhibition of protein phosphatase and hyper-phosphorylation of Tau. Mediation of oxidative stress and production of reactive oxygen species through NMDA receptor activation may be one of the main causes for Tau hyper-phosphorylation and synapse dysfunction (Kamat et al., 2016). This excess in glutamate also causes impairment of mitochondrial functions by activating the permeability transition pores, increases release of cytochrome c (due to reductions in cytochrome c oxidase) and reduces ATP levels along with the simultaneous production of reactive oxygen species.

Memantine prevents synapse dysfunction from excess stimulation of glutamate to NMDA receptors through non-competitive binding with a stronger affinity and voltage dependency than Mg^{2+} ions (Parsons et al., 2013). Memantine restores deficits in cognition and also seems to reduce levels of insoluble and soluble Aβ in triple-transgenic mice with AD like pathology and protect against associated synaptic deterioration (Martinez-Coria et al., 2010). Ultimately the mechanisms by which Memantine links to its

clinical efficacy in AD are still not yet fully understood. Li et al., (2004) discovered using a hippocampal slice culture model that memantine may also influence PP2A as it reversed Tau hyper-phosphorylation induced by okadaic acid. So perhaps Memantine has pleiotropic mechanisms of action against AD.
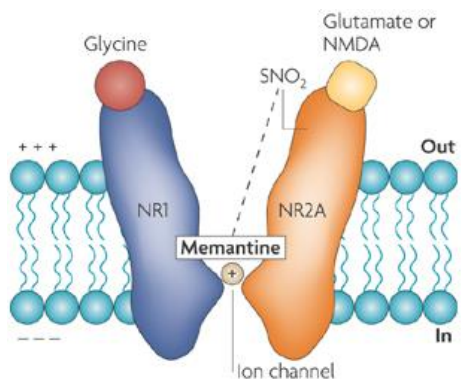
Figure 1.14: Memantine mechanism of action on NMDA receptors (Lipton, 2007).

1.6   TAU RELATED PIPELINE TREATMENTS

Over 70% of Aβ targeting drugs have been terminated or become inactive, as seen in **Appendix A**. Following these developments and research suggesting that Tau pathology correlates more closely with clinical symptoms of AD than Aβ does, Tau targeting drugs has become a new focus. **Table 1.3** summarises the compounds targeting Tau that have been taken forward into clinical trials. The only current Tau aggregation inhibitor in clinical trials is LMTM (TauRx Therapeutics) and the only peptide in clinical trials is the NAPVSIPQ (NAP) peptide (Allon Therapeutics Inc. / Paladin Labs Inc.). LMTM and NAP are discussed in **Sections 1.6.1.2** and **1.6.1.3**, respectively.

	Drug	Company	Mechanism of Action	Indication	Clinical Phase	Clinical Trial Identifier	Status
1	ACI-35	Janssen/AC Immune	Active Immunotherapy	Mild-Moderate AD	Phase 1	ISRCTN13033912	Completed
2	LMTM (TRx0237)	TauRx Therapeutics	Aggregation Inhibitor	Mild-Moderate AD	Phase 3	NCT03539380	Active
3	AADvac-1	Axon Neuroscience SE	Active Immunotherapy	Mild AD	Phase 2	NCT02579252	Active
4	Davunetide (NAP)	Allon Therapeutics Inc. / Paladin Labs Inc.	Peptide MT stabilizer	Tauopathy	Phase 2	NCT01056965	Completed
5	Epothilone D (BMS-241027)	Bristol-Myers Squibb	MT stabilizer	Mild AD	Phase 1	NCT01492374	Terminated
6	Methylene Blue (Rember, TRx0014)	TauRx Therapeutics	Aggregation Inhibitor	Mild-Moderate AD	Phase 2	NCT00684944	Terminated
7	Tideglusib (NP031112)	Zeltia Group	GSK-3β Inhibitor	Mild-Moderate AD	Phase 2	NCT00948259	Terminated
8	BIIB076 (NI-105)	Biogen	Passive Immunotherapy	AD	Phase 1	NCT03056729	Active
9	BIIB080 (IONIS-MAPTRx)	Ionis Pharmaceuticals, Inc.	RNA-based	Mild AD	Phase 1	NCT03186989	Active

10	**BIIB092 (BMS-986168)**	Biogen / Bristol-Myers Squibb	Passive Immunotherapy	Early AD	Phase 2	NCT03352557	Active
11	**C2N 8E12 (ABBV-8E12)**	AbbVie	Passive Immunotherapy	Early AD	Phase 2	NCT03712787	Active
12	**JNJ-63733657**	Janssen	Passive Immunotherapy	Mild AD	Phase 1	NCT03375697	Active
13	**LY3303560**	Eli Lilly	Passive Immunotherapy	Early AD	Phase 2	NCT03518073	Active
14	**RG7345 (RO6926496)**	Hoffmann-La Roche	Passive Immunotherapy	AD	Phase 1	NCT02281786	Terminated
15	**RO7105705**	AC Immune/ Genentech Inc.	Passive Immunotherapy	Prodromal or Mild-AD	Phase 2	NCT03289143	Active
16	**Abeotaxane (TPI 287)**	Cortice Biosciences	MT Stabiliser	AD or Tauopathies	Phase 1	NCT01966666	Active
17	**UCB0107**	UCB Biopharma S.P.R.L.	Passive Immunotherapy	AD	Phase 1	NCT03605082	Active
18	**CCT020312**	Academic	PERK Activator	Progressive Supranuclear Palsy	Phase 1	N/A	Active
19	**Nilotinib (Tasigna)**	Georgetown University	c-Abl inhibitor	AD + Parkinsons	Phase 2	NCT02954978	Active
20	**AZP2006**	AlzProtect	Autophagy Stimulator	AD or Tauopathies	Phase 1	N/A	Active

21	MK-8719	Alectos Therapeutics	O-GlcNAcase inhibitor	Progressive Supranuclear Palsy	Phase 1	N/A	Active
22	Salsalate	Adam Boxer	Acetylation inhibitor	Mild-Moderate AD	Phase 1	NCT02422485	Active
23	Saracatinib (AZD-0530)	AstraZeneca	Fyn inhibitor	AD	Phase 2	NCT01864655	Active
24	ASN120290 (ASN-156)	O-GlcNAcase inhibitor	O-GlcNAcase inhibitor	Progressive Supranuclear Palsy	Phase 1	N/A	Active
25	IVIg	Baxalta now part of Shire	Active immunotherapy	AD	Phase 3	NCT01300728	Active

Table 1.3: Current pipeline treatments in clinical development for Tauopathies associated with AD. 19 are active, 2 are completed, 4 are terminated (ClinicalTrials.gov, 2019, Alzform, 2019a and Medina, 2018)

1.6.1 IMMUNOTHERAPY

Immunotherapy is one of the most promising approaches to treat AD and the past 10 years has seen a lot of emphasis on preventing the aggregation of Aβ in the brain (Kuca et al., 2016). Active immunotherapy involves inducing a humoral immune response whilst passive immunotherapy involves administering monoclonal antibodies, as summarised by **Figure 1.15**. The preferred method although expensive is passive immunotherapy as active immunotherapy could potentially induce Tau pathology as seen in transgenic mice studies (Clavaguera et al., 2014). Chronic administration however may lead to the formation of anti anti-bodies which could neautralise the therapy. Lovestone et al., (2015) and Agadjanyan et al., (2015) suggested that immunotherapy aimed at targeting Tau pathology will have greater therapeutic impact as Tau neurofibrillary tangles correlate very strongly with cognitive deterioration in AD patients. Clearance of Aβ plaques did not appear to stop progression of AD and Aβ immunotherapy approaches do not affect tangle pathology (Holmes et al., 2008). Boche et al., (2010) and Serrano-Pozo et al., (2010) mentioned that only plaque associated Tau had been reduced with application of Aβ immunotherapy. Oddo et al., (2004) used the 3XTg mouse model for Aβ targeted immunotherapy and discovered a reduction in early Tau pathology but not in hyper-phosphorylated or aggregated Tau, suggesting an appropriate focus on oligomeric Tau.
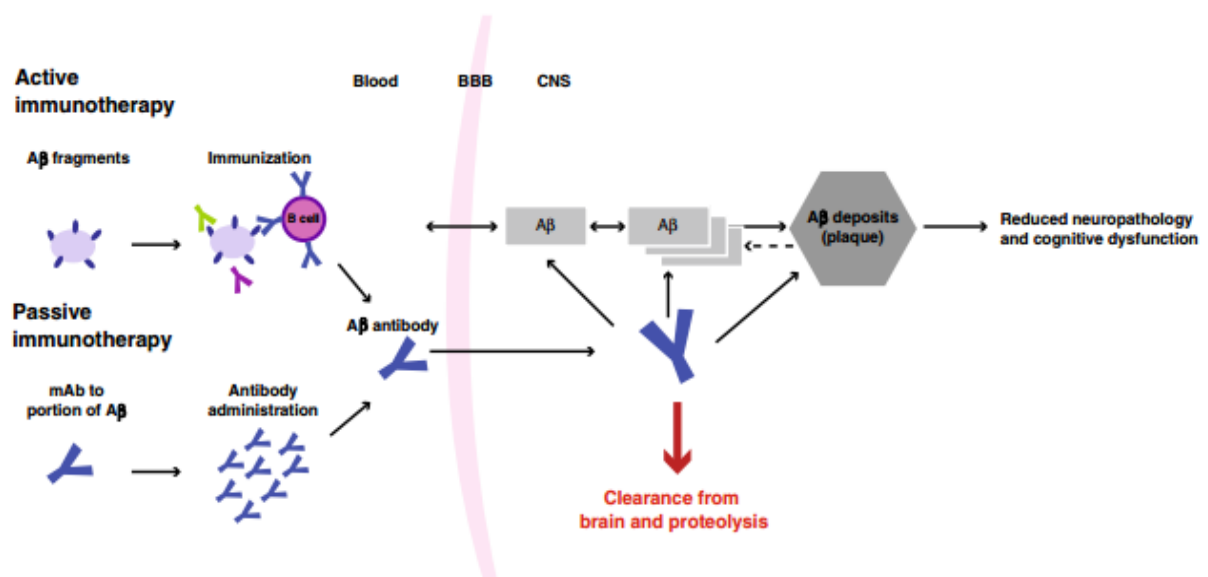
Figure 1.15: Schematic of active and passive immunotherapy approaches to clearing Aβ (Winblad et al., 2014). mAb, monoclonal antibody; BBB, blood–brain barrier; CNS, central nervous system.

Goyal et al. (2017), summarised the physiochemical influences for BBB permeability to include molecular weight, charge, lipid solubility, molecule size and surface activity. Positively charged small molecules which are <600 Da and form <8 hydrogen bonds can cross the blood brain barrier (BBB) via lipid mediated diffusion; however, these properties are absent in most drugs (Partridge 2012). The BBB consists of brain capillary endothelial cells and tight junctions which restrict the transport of molecules in order to protect the brain. As a result, the development of therapeutic antibodies for neurodegenerative diseases are limited by their poor BBB permeability and in fact, 95% of molecules for drug development stumble upon this hurdle (Dong, 2018). Georgieva et al. (2014) summarised mechanisms of molecular transport across the BBB in **Figure 1.16.** Drugs can be enhanced through reengineering to utilise endogenous transport systems such as carrier mediated transport and receptor mediated transcytosis. (Partridge, 2012). BBB transport mechanisms described for peptides include: 1) passive diffusion – mainly associated with lipophilic peptides, 2) carrier-mediated transcytosis - associated with transporters at the endothelial surface, 3) receptor mediated transcytosis – associated with a specific receptor and 4) adsorptive-mediated transcytosis - associated with non-specific positively charged peptides (Dong, 2018).
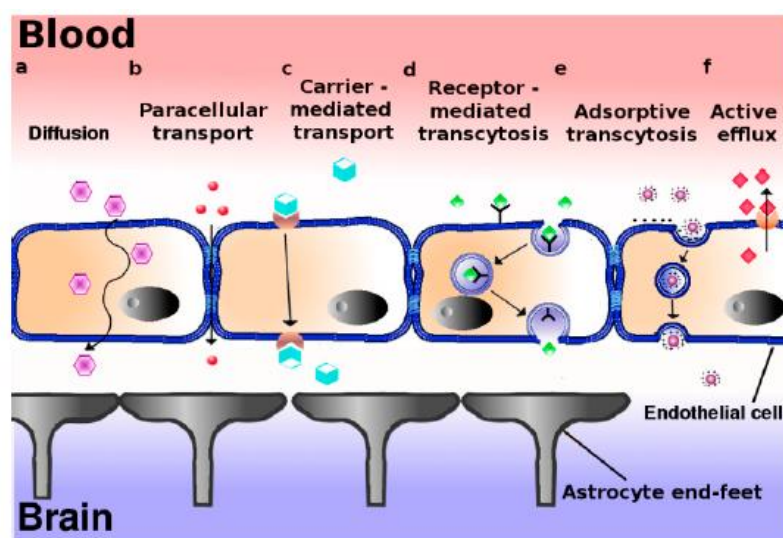
Figure 1.16: Schematic of mechanisms by which molecules can cross the BBB include: (a) diffusion, which is non-saturable and driven by a concentration gradient often involving hydrophobic molecules (b) paracellular transport, involving soluble molecules (c) carrier-mediated transport, e.g. gluocse (d) receptor mediated transcytosis, e.g.insulin transporter (e) adsorptive transcytosis, involving non specific positively charged amino acids and (f) active efflux, involving proton pump efflux transporters (Georgieva et al., 2014).

Current pipeline anti-Tau active immunotherapies include AADVac-1 (Axon Neuroscience SE), ACI-35 (Janssen/AC Immune) and IVIg (Baxalta now part of Shire). Current pipeline anti-Tau passive immunotherapries include BMS-986168 (Biogen/Bristol-Myers Squibb), ABBV-8E12 (AbbVie), RO7105705 (AC Immune/Genentech Inc.), UCB0107 (UCB Biopharma S.P.R.L.), NI-105 (Biogen), JNJ-63733657 (Janssen) and LY3303560 (Eli Lilly).

AADvac-1 (Axon Neuroscience SE) is an immune-stimulant phospho-tau specific vaccine which is liposome based containing synthetic Tau peptides from amino acids 294-305 and coupled to the carrier metalloprotein 'keyhole limpet hemocyanin' with an aluminium hydroxide adjuvant to promote a humoral immune response and stimulate antibody production (Kontsekova et al., 2014). This drug has demonstrated safety, immunogenicity and a preference for hyperphosphorylated truncated Tau than healthy Tau (Novak et al., 2017; Zilka et al., 2006. This drug is currently in a phase II safety and efficacy trial for patients with mild to moderate Alzheimer's disease.ACI-35 (Janssen/AC Immune) is an immune-stimulant phospho-tau specific vaccine which is liposome based containing 16 copies of synthetic Tau fragments phosphorylated at residues S396 and S404 anchored to the lipid bilayer with a monophosphoryl lipid A adjuvant (Bakota and Brandt, 2016 and Hickman et al., 2011). As a result, autoimmune B or T cell response to normal Tau is voided. This drug completed a phase Ib randomized, double blind, placebo controlled clinical trial to evaluate safety, immunogenicity and tolerability for mild to moderate, however results have not yet been published (Medina et al., 2018; AC Immune, 2015). Theunis et al., (2013) reported that this drug is safe and active based on a mouse tauopathy model. It is suggested this drug creates an extracellular sink to remove all extracellular Tau present in the CSF and tau leaked from neurones. By removing extracellular tau this may inhibit the propagation of Tau from one neurone to another (Yanamandra et al., 2013). It is also suggested based on brain slices that the monoclonal anti-tau antibodies can be taken up by cells (Gu et al., 2013).

IVIg (Baxalta now part of Shire) is a polyclonal serum of IgG derived from human plasma and believed to contain Tau specific antibodies targeting recombinant Tau residues 155-421 (Krestova et al., 2017).

When tested in a phase III, randomised, double blind, placebo controlled clinical trial, it demonstrated good tolerability with low doses over 18 months, however failed to demonstrate improvements in cognition or function for participants with mild-moderate AD (Relkin et al., 2017).

ABBV-8E12 (AbbVie) is an IgG4 monoclonal antibody targeting N-terminal Tau amino acid residues 25-30 with the aim of inhibiting seeding by clearing extracellular Tau (West et al., 2017). Safety and tolerablility was demonstrated when administered as 50mg/kg injections. RO7105705 (AC Immune/Genentech Inc.) is is an IgG4 monoclonal antibody also targeted at the N-terminus of extracellular Tau without discrimination between species of Tau in healthy and disease brains. BMS-986168 (Biogen/Bristol-Myers Squibb) is an IgG4 monoclonal antibody and again targets the N-terminus of Tau but with the aim of interacting with N-terminal fragments of Tau to reduce their involvement in secondary Aβ pathology (Novak et al., 2018).

UCB0107 (UCB Biopharma S.P.R.L.) is a monoclonal antibody targeteting N-terminal Tau amino acid residues 235-246 in the second proline rich region with the aim of inhibiting seeding by interfering with cell to cell propagation of Tau; previously demonstrated in cell and mouse models. Alzforum (2019b), stated that according to Courade, other antibodies targeting phosphorylated S202/T205 in the Tau N-terminus only partially inhibited seeding due to heterogeneity between seed phosphorylation states. This further highlights the importance of not only targeting pathogenic phoshorylated Tau, but also different variants of pathogenic Tau which have different phosphorylation profiles. UCB0107 however has demonstrated almost 100% inhibition at 300 nM, performing equally effectively in Tau isolated from PSP and frontotemporal dementia.

NI-105 (Biogen) is an IgG1 monoclonal antibody classified as a pan-Tau antibody which can interact with monomeric and fibrillar Tau species without discrimination for healthy and disease Tau (Czerkovicz et al., 2018). JNJ-63733657 (Janssen) has an undisclosed targeting region however presumably the mid region of Tau and aims to eliminate Tau seeds (Novak et al., 2018). LY3303560 (Eli Lilly) is a monoclonal IgG1 antibody derived from the MC1 antibody which targets amino acid

residues 313-322 entailing the VQIVYK sequence and residues 7-9 in the third repeat domain and the

N-terminus, respectively (Novak et al., 2018; Jicha et al., 1997). According to Riazul et al. (2017) it

priorises selectivity of aggregated Tau rather than monomeric Tau.

1.6.2 TAU AGGREGATION INHIBITORS

TRx0237 (LMTM) - TauRx Therapeautics

The first generation of Tau aggregation inhibitors taken forward by TauRx Therapeautics was

Methylene blue ("Rember") and was claimed to block Tau aggregation based on a phase 2 clinical trial

which compared oral 30, 60 and 100 mg. Rember was reported to demonstrate benefits in mild-

moderate AD and cognition for the two lower doses. It was claimed that the 100 mg dose did not work

due to interactions with gelatine in the capsule wall. Rember exists in an equilibrium of reduced and

oxidised forms. TRx0237 (leucomethylthioninium) is a stabilised and reduced version of Rember

(methylthioninium) which has improved bio-availability and tolerability. This compound is also

uncharged colorless, unlike Rember which is a blue dye. Braddeley et al. (2015), demonstrated that

LMTM had increased uptake into red blood cells in vitro and in vivo. They also demonstrated that food

interfered with absorption of Rember, but not TRx0237 and that Rember was ionised at intestinal pH,

but TRx0237 was not. Phase 3 clincal trial NCT00515333 demonstrated that TRx0237 failed to slow

cognitive decline in mild-moderate AD patients (ClinicalTrials.gov, 2008). A beneit was claimed for a

small sub-group not on other AD drugs, however controversially the statistical analysis of the research

was flawed as the sub-group was compared with the placebo group which included individuals on

other AD drugs (Alzforum 2016; Gauthier et al., 2016). Crowe et al., (2013) reported that in 1996

methylene blue elicited oxidation when incubated *in vitro* with Tau which may involve oxidation of

cysteines to disulphides in the microtubule binding region. When incubated with 4R Tau this oxidation

inhibited fibrilisation through intramolecular bonding of the two cysteine residues in 4R Tau. However,

when 3R Tau is oxidised it promoted intermolecular bonding to form dimers capable of fibrilisation as

3R Tau has only 1 cysteine residue. Zweckstetter, (2013) mentioned that according to his research the

metabolites of methylene blue; azure A and azure B, modify cysteine residues to sulphenic, sulphinic and sulphonic acids Zweckstetter, (2013) confirming methylene blue induced oxidation of cysteine residues. Daebel et al., (2012) used NMR spectroscopy to show that cysteine residues upon oxidation cause conformational changes in the Tau second hexapeptide. Methylene blue has pleiotropic properties which allows various therapeutic uses such as in non-neurodegenerative disorders such as methemoglobinemia where it accelerates enzymatic reduction of methemoglobin. As a result, it should not be exclusively considered as a Tau based therapy (Bakota and Brandt, 2016).

1.6.3 **MICROTUBULE PEPTIDE STABILISERS**

NAP (Davunetide)

This intranasal neuropeptide therapy entails a sequence of eight amino acids (NAPVSIPQ) derived from the Activity-dependent neuroprotective protein (ADNP) which is essential for brain formation, cognitive function and regulates RNA transcription and splicing (Gozes et al., 2014). Deficiencies in ADNP leads to Tauopathies and administration of NAP to AD mice represented an increase in ADNP (Fernandez-Montesinos et al., 2010). NAP protects microtubules by enhancing Tau-microtubule interaction 20-fold. It achieves this through its ADNP association motif 'SIP' that binds to microtubule end protein1/3 (EB) which then interacts with microtubule growing ends and Tau (Ivashko-Pachima et al., 2017; Sayas et al., 2015; Oz et al., 2014). NAP has also demonstrated to stimulate neurite growth and synapse formation (Ivashko-Pachima et al., 2017). Matsuoka et al., (2008) discovered that NAP reduces Tau hyper-phosphorylation and stabilises microtubules. It was shown to reduce Tau hyper-phosphorylation in mice over expressing α-synuclein for a Parkinsons disease model as well as improve their behavioural deficits (Magen et al., 2014). There definitely is a link as phase II clinical trials in patients with mild cognitive impairment showed improved cognition and the drug also proved to be safe and well tolerated (Morimoto et al., 2013). Bakota and Brandt (2016), reported that existing evidence for a direct relation between NAP and Tau remains weak and so further research is required. They also suggested the drug to have pleiotropic effects as intranasal administration lowered levels of

Aβ1-40 and 1-42 and Tau hyperphosphorylation in triple transgenic AD mice (expressing the APP_{swe}, $TauP_{301L}$, and $PS1_{M146V}$ transgenes) and protected against oxidative stress and zinc intoxication (Matsouka et al., 2007; Gozes et al., 2005; Divinski et al., 2006, respectively). Zinc intoxication results in the breakdown of microtubules, however NAP protects microtubules by promoting reorganisation (Gozes et al., 2005). Matsouka et al. (2008), explained using a "pure" Tauopathy mouse model that mice treated with NAP over 6 months performed better in the Morris water maze. However, NAP failed to show efficacy in a clinical trial for progressive supranuclear palsy which is a pure Tauopathy. It may be possible that this drug is valid for AD but not all Tauopathies (Giacobini, and Gold, 2013; Oz et al., 2012).

2. AIMS AND OBJECTIVES

Aggregation of Tau protein plays important roles in neurodegenerative diseases such as AD. The two following sequences are essential for Tau aggregation: [275]VQIINK[280] and [306]VQIVYK[311] which are found in R3 and R4 Tau isoforms, respectively. This project aims to develop effective peptide-based inhibitors against these specifically stated binding sequences to prevent Tau from pathogenically aggregating. This project aims to demonstrate this by:

1) *In silico* investigations of potential binding sequences and binding locations using two aggregation hot spot prediction softwares Aggrescan/Camsol and docking software Molsoft ICM-Pro, respectively.

2) *In vitro* investigations of the peptides listed in **Table 2.1** in their ability to inhibit Tau aggregation. Lead peptide was N-methylated or retro-inverted to improve peptide stability. Peptide N- and C-termini were acetylated and amidated, respectively, to mimic native protein and improve activity.

Peptide ID	Sequence	Purity %
AG01	Ac - R G <u>V Q I I N K</u> G R - NH$_2$	>90
AG02	Ac - R G <u>V Q I V Y K</u> G R - NH$_2$	>90
AG02R4	Ac - R R G <u>V Q I V Y K</u> G R R - NH$_2$	>90
AG02R5	Ac - R G <u>V Q I V Y K</u> G R R R R - NH$_2$	>90
AGR502	Ac - R R R R G <u>V Q I V Y K</u> G R -N H$_2$	>90
AG02PR5	Ac - R G <u>V Q I V Y K</u> P G R R R R - NH$_2$	>90
AG02R6	Ac - R R R G <u>V Q I V Y K</u> G R R R - NH$_2$	>90
AG02R9	Ac - R G <u>V Q I V Y K</u> G R R R R R R R R - NH$_2$	>90
AG02TAT	Ac - R G <u>V Q I V Y K</u> G R Y G R K K R R Q R R R - NH$_2$	>90
AG02ΔI	Ac - R G <u>V Q K(Ac) V Y K</u> G R - NH$_2$	>90
AG02ΔV	Ac - R G <u>V Q I K(Ac) Y K</u> G R - NH$_2$	>90
AG03	Ac - R G <u>V Q I K(Ac) Y K</u> P G R R R R R R R R - NH$_2$	>95
AG03-Cys	Ac - R G <u>V Q I K(Ac) Y K</u> P G R R R R R R R R C - OH	>95
Scramble AG03	Ac – R G Q P K I K(Ac) Y V G R R R R R R R R - NH$_2$	>95
AG03M	Ac - R G <u>V(m) Q I(m) K(Ac) Y(m) K P(m)</u> G R R R R R R R R - NH$_2$	>95
RI-AG03	Ac - r r r r r r r r G <u>p k y k(ac) i q v</u> G r - NH$_2$	>95
FAM-RI-AG03	Ac - k(FAM) r r r r r r r r G <u>p k y k(ac) i q v</u> G r - NH$_2$	>95
Poly-R	R R R R R R R R R - NH$_2$	>95
TAT	Ac - Y G R K K R R Q R R R - NH$_2$	>95

Table 2.1 List of peptide inhibitor designs customly synthesised for research in this thesis. Underlined sequence corresponds to Tau binding region. Peptide inhibitors were custom made by Peptide Synthetics (Fareham, UK) with >90% purity and Severn Biotech (Kidderminster, UK) with >95% purity; determined by HPLC-MS. Peptide HPLC-MS data can be found in **Appendix D-V.**

3) *In vitro* experiment to investigate effectiveness of the lead peptide when attached to liposomes.

4) *In vitro* experiments to investigate peptide stability of the lead peptide for suitability as a drug candidate *in vivo* using N-methylation (AG03M [Ac-RGV(m)QI(m)K(Ac)Y(m)KP(m)GRRRRRRRR-NH2]) and retro-inversion and (RI-AG03 [Ac-rrrrrrrrGpkyk(ac)iqvGr-NH2]) to stabilise the peptide. These experiments include testing against enzymatic degregation and temperature stability.

5) *In vitro* experiments to investigate toxicity and cell penetration of the retro-inverted lead peptide candidate (RI-AG03 [Ac-rrrrrrrrGpkyk(ac)iqvGr-NH2]) for suitability as a drug candidate *in vivo* using HEK-293 cell lines.

6) *In vivo* experiments to investigate the effects of feeding the lead peptide candidate (RI-AG03 [Ac-rrrrrrrrGpkyk(ac)iqvGr-NH2]) to a rough-eye *Drosophila* model of Tauopathy by observing any improvements in eye phenotype. These flies express full length Human Tau$_{441}$ soley in the eyes.

3. MATERIALS AND METHODS

3.1 DESIGNING PEPTIDE INHIBITORS

3.1.1 AGGRESCAN AND CAMSOL INTRINSIC

Two web-based softwares were utilised to predict potential aggregation prone sequences of full length Tau_{441}:

1. **AGGRESCAN :** http://bioinf.uab.es/aggrescan (Conchillo-Solé et al., 2007).

2. **CamSol Intrinsic :** http://www-mvsoftware.ch.cam.ac.uk (Sormanni et al., 2015 and Sormanni et al., 2017).

In FASTA format the full length Tau_{441} sequence was inputted:

"**MAEPRQEFEV MEDHAGTYGL GDRKDQGGYT MHQDQEGDTD AGLKESPLQT PTEDGSEEPG SETSDAKSTP TAEDVTAPLV DEGAPGKQAA AQPHTEIPEG TTAEEAGIGD TPSLEDEAAG HVTQARMVSK SKDGTGSDDK KAKGADGKTK IATPRGAAPP GQKGQANATR IPAKTPPAPK TPPSSGEPPK SGDRSGYSSP GSPGTPGSRS RTPSLPTPPT REPKKVAVVR TPPKSPSSAK SRLQTAPVPM PDLKNVKSKI GSTENLKHQP GGGKVQIINK KLDLSNVQSK CGSKDNIKHV PGGGSVQIVY KPVDLSKVTS KCGSLGNIHH KPGGGQVEVK SEKLDFKDRV QSKIGSLDNI THVPGGGNKK IETHKLTFRE NAKAKTDHGA EIVYKSPVVS GDTSPRHLSN VSSTGSIDMV DSPQLATLAD EVSASLAKQG L**"

AGGRESCAN service was run using Mandrake Linux 9.0 on a Pentium 4 1300 MHz (willamette) with 1GB RDRAM, using experimental data derived from de Groot et al. (2006), AGGRESCAN calculated the aggregation propensity value for each amino acid residue (a3v), highlighted regions above the precalculated threshold and the regions predicted to be potential aggregation "hot spots". NH_3^+ and COO^- were added to the N and C terminus of each peptide sequence, respectively, to quantify charge effects. The a3v average (a4v) was calculated using sliding windows (5 for < 75 residues, 7 for < 175 residues, 9 for < 300 residues, and 11 for > 300 residues) and compared with 57 amyloidogenic proteins with experimentally known "hot spot" locations. Peptide aggregation profiles were defined

as the a4v. The sum of a4v and average of a3v, divided by the sequence (a4vSS and a3vSA, respectively) were calculated. "Hot spots" were defined as regions (excluding regions containing proline) with ≥ 5 continuous residues with an a4v greater than the "hot spot" threshold. The average a4v from each "hot spot" was calculated (a4vAHS). The area of the aggregation profile greater than the hot spot threshold (AAT), the total area and the area greater than the hot spot threshold of each hot spot, were integrated using the trapezoidal rule. The normalised a4vSS value across up to 100 residues was finally calculated and is termed the Na4vSS. Results were generated in both tabulated and graphical formats for the entire sequence (Conchillo-Solé et al., 2007).

CamSol calculated and scored the intrinsic solubility profile of Tau and for regions within the amino acid sequence whereby scores >1 denoted high solubility and scores <-1 denoted poor solubility (Sormanni et al., 2015). High solubility and poor solubility were colour coded blue and red, respectively. The CamSol method employs four specific steps: calulating the residue intrinsic solubility profile, calculating structural correction, identifying suitable mutation sites, screening possible variants for the most soluble version. The equations employed to calculate the intrinsic solubility profiles are **Equations 1**, **2** and **3** (Pavlou and Reichert, 2004; Leader et al., 2008; Goodman, 2013). The equations employed to calculate the structurally corrected solubility profiles are **Equations 4**, **5**, **6**, **7**, **8** (Carter, 2011; Winter et al., 1994; Sidhu, 2000; Hoogenboom, 2005; Bradbury et al., 2011). The equation employed to calculate the solubility score is **Equation 9** (Lee et al., 2013)**.** These equations are discussed in detail by Sormanni et al. (2015).

Calculation of the intrinsic solubility profiles:

$\boldsymbol{Equation}$ **1**: $\quad s_i = a_H p_i^H + a_H p_i^C + a_H p_i^a + a_H p_i^\beta$

In **Equation 1**, "s_i" denotes the solubility score. To calculate the solubility score, each residue (denoted as "i") is assessed for: hydrophobicity (p_i^H), charge at neutral pH (p_i^C), α-helix propensity (p_i^a), and β-strand propensity (p_i^β) using the linear combination parameters denoted as "a" which are documented as 0.598, 0.318, 5.77, and -4.807, respectively (Sormanni et al., 2015).

Equation 2: $\quad S^i = \frac{1}{7}\left(\sum_{j=i-3}^{i+3} s_j\right) + a_{pat}I_i^{pat} + a_{gk}I_i^{gk}$

In **Equation 2**, the solubility score is smoothed over a window of seven residues to compensate for the effect of neighbouring residues, corrected to compensate for potential patterns of hydrophilic/hydrophobic patterns (I_i^{pat}) and acknowledges same sign charge influences (I_i^{gk}). The structurally corrected solubility score is denoted as "S^i" (Sormanni et al., 2015).

Equation 2a: $\quad I_i^{gk} = \sum_{j=-5}^{5} e^{-\frac{j^4}{200}} C_{i+j}$

Equation 2a calculates the I_i^{gk} which takes into consideration the relative distance of charged amino acids along the sequence where C_{i+j} denotes the charge of amino acid $i+j$ (Sormanni et al., 2015).

Calculation of the structurally corrected solubility profiles:

Equation 3: $\quad S_i^{surf} = w_i^E\left(\tilde{S}_i^{int} + \sum_{j\notin[i-3,i+3]} w_j^D w_j^E \tilde{S}_j^{int}\right)$

Equation 3 calculates the structurally corrected solubility propensity score of residue "i" (S_i^{surf}). This value applies the intrinsic solubility profile of residue "i" ($\tilde{S}_i^{int}$) to the protein surface. The $\tilde{S}_i^{int}$ is smoothed over by applying the sum to all amino acids within 8 Å of residue "i" which are not next together in the sequence as these amino acids are already considered by the $\tilde{S}_i^{int}$. This equation also takes into consideration the exposure weight (w_i^E) denoting the exposure of residue "j" to the solvent and the smoothing weight (w_j^D) which are defined in **Equations 3a and 3b**, respectively. $\tilde{S}_i^{int}$ and $\tilde{S}_j^{int}$ are calculated using using **Equation 7** and a modified version of this equation, respectively (Sormanni et al., 2015).

Equation 3a: $\quad w_j^D = max\left(1 - \frac{d_{ij}}{r_A}, 0\right)$

Equation 3a calculates the smoothing weight. d_{ij} denotes the distance between residues "i" and "j", suggesting that closer residues have a greater contribution to local surface aggregation propensity than distant residues do. The patch radius (r_A) is defined as 8 Å, consistent with the smoothing window of seven residues used to calculate the intrinsic solubility profile in **Equation 2** (Sormanni et al., 2015).

Equation 3b: $w_j^E = \dfrac{\vartheta(x_j - 0.05)}{1 + e^{-a(x_j-b)}}$

Equation 3b calculates the exposure of residue "*j*" to the solvent. The relative exposure of residue "*j*" is denoted as x_j which is the solvent accessible surface area of residue "*j*" divided by the solvent accessible surface area of residue "*j*" in a Gly-Xxx-Gly peptide. Heaviside step function "ϑ" (positive and negative argument values are 1 and 0, respectively) is used as a correction to exclude residues with < 5% solvent exposure. "a" and "b" are parameters set at -10 and 0.3, respectively to assign residues not exposed to the solvent a value of 0, that they be excluded from subsequent algorithms (Sormanni et al., 2015).

Equation 4: $\tilde{S}_i = \dfrac{1}{\sum_{j=i-3}^{i+3} \tilde{x}_j} \left(\sum_{j=i-3}^{i+3} \tilde{x}_j S_j \right) + a_{pat} I_i^{pat} + a_{gk} \tilde{I}_i^{gk}$

Equation 4 employs a weighted average of the smoothing window of seven residues using the relative exposures of residue "*j*" ($\tilde{x}_j$) linearly rescaled (in the range of [0.25, 1] to prevent division by zero.

Equation 4a: $\tilde{I}_i^{gk} = \sum_j w_j^D \left(d_{ij}, 2r_A \right) w_j^E \left(x_j^C \right) C_j$

In **Equation 4a,** $\tilde{I}_i^{gk}$ is similar as in **Equation 2a** except that the gatekeeping effect of charges from the same sign are now calculated three-dimensionally ($\tilde{I}_i^{gk}$). x_j^C denotes the relative exposure of the charged atom in residue "*j*".

Calculation of CamSol solubility score:

Equation 5: $S_P = \dfrac{1}{N} \sum_{i=1}^{N} \begin{cases} Si & if\ S_i < -0.7\ or\ S_i > 0.7 \\ 0 & otherwise \end{cases}$

Equation 5 calculates the overall solubility score (S_P) from the intrinsic solubility profile and the number of amino acids in the protein sequence (N). Scores of ~-1 or less are poorly soluble whereas scores of ~1 or greater are considered more soluble. ±0.7 thresholds are used for sensitivity to single mutations (Sormanni et al., 2015).

3.1.2 QUALITATIVE MODEL ENERGY ANALYSIS (QMEAN)

5o3l PHF and 5o3t SF PDB cryo-EM structures depict the cores a paired helical filament and straight filament in Alzheimer's disease, respectively, from Fitzpatrick et al. (2017). These structures were acquired using resolution method FSC 0.143 CUT-OFF, reconstruction software Relion, a FEI Titan Krios microscope with a Gatan K2 Quamtum (4k x 4k) detector and have a resolution of 3.4 Å (Protein Data Bank in Europe, 2017). 6QJH, 6QJM, 6QJP PDB from Zhang et al. (2019) are cryo-EM structures depicting different heparin induced 2N4R Tau conformations and are and acquired using resolution method FSC 0.143 CUT-OFF, reconstruction software Relion, a FEI Polaria 300 microscope with a FEI Falcon III (4k x 4k) detector and have a resolution of 3.3 Å (Protein Data Bank in Europe, 2019).

PDB structures were loaded onto SWISS-MODEL QMEAN to determine the global and local quality estimates of these structures by relating their structural features to similar sized experimental stuctures (Benkert et al., 2011). Before docking experiments are conducted it is advised to test the quality of the PDB structure in case there are errors such as incomplete data. QMEAN combined several statistical potentials and agreement terms in a linear manner (Benkert et al., 2008; Benkert et al., 2009). Benkert et al. (2011), described that the QMEAN methodology analyses secondary structure dependent long range ineractions, local back-bone geometry, residue burial status and two agreement terms for secondary structure and solvent accessibility. Prediction of secondary structure and solvent accessibility is achieved by PSIPRED amd ACCpro, respectively; which are calculated by DSSP (Jones, 1999; Cheng et al., 2005; Kabsch and Sander, 1983). Evaluation of experimental structures are determined by the QMEAN4 score; structures scoring less than -4 are deemed low quality and structures scoring less than -5 are generally rejected for further computational experimentation. QMEANDisCo, enhances accuracy of local quality estimations by analysing consistency of atomic distances.

3.1.3 BUILDING AND DOCKING INHIBITORS USING (ICM)-PRO SOFTWARE

PDB structures were loaded onto Molsoft ICM-Pro (*version 3.8-7*) graphical user interface (GUI) and converted from PDB format into an internal coordinate mechanics (ICM) object (for compatability with the ICM-Pro docking software). Water was kept tight and His, Pro, Asn, Gln and Cys side chains were optimised (because crystallographers are unable to see the correct orientation) to correct their orientation and the H-bond network. Docking probes were prepared on the outer chains and assigned to a specific directory. Standard ICM-dock three-dimensional grid potential maps (potential binding site regions) were calculated with 0.5 Å grid spacing (Totrov and Abagyan, 1997; Neves et al., 2012). The Merck molecular force field (MMFF94) assigned ligand atom types and charges (Lam et al., 2019; Halgren, 1996).

Peptides were initially contructed as .txt files containing sequence codes e.g:

#line 1: "*ml AG03*"

#line 2: *"se 0 ace arg gly val gln ile lys tyr lys pro gly arg arg arg arg arg arg arg conh2"*

#line 3: *"modres 6/nz NC(=O)C".*

Line 1 command establishes the name of the peptide sequence "*AG03*". Line 2 command writes the code for peptide sequence: "*Ac-RGVQIKYKPGRRRRRRRR-NH2*". Line 2 command writes the code to acetylate lys at position 6 in the sequence. The .txt file was saved as AG03.txt into the same directory as the docking probe files. Using Windows command prompt the directory containing all the docking files was navigated to using the "*cd*" command. To virtually generate the peptide sequence for use in docking experiments; "AG03.txt" was converted into "AG03.se" using the following command: "*copy AG03.txt AG03.se*". To run the docking experiment the following command was inserted: *"c:\Program Files\Molsoft LLC\ICM-Pro\icmconsole64.exe" "c:\Program Files\Molsoft LLC\ICM-Pro_dockScan" 5o3l input=AG03.se effort=10. -S confs=5"*. This command docked the ligand (AG03.se) onto the receptor (5o3l PHF) using 'peptide docking mode' (forcefield) with maximum sampling effort factor (10) and

recorded top 5 poses with highest binding affinity. This docking setup applied flexible ring sampling (2) and biased probability Monte Carlo to randomly select independent subspaces according to predefined continuous probability distribution. Each random subspace was followed by local minimisations in torsion angle space (Abagyan and Totrov, 1994). Once the simulation completed, the experiment hit lists were fetched using the Molsoft ICM-Pro GUI. Chemicals were downloaded from PubChem and docked onto structure using "*small molecule mode*" forcefield. ICM scores of -32 are considered strong binds depending on the properties of the receptor, such as pocket exposure or presence of metal ions may produce scores higher than-32. Lower hydrogen bond and hydrophobic scores indicate stronger binding and hydrophobic energy exposing a surface to water, respectively. Lower Van der Waals scores also indicate a better binding (Molsoft, 2019). Convergence of simulations were monitored closely by running multiple identical simulations and comparing the results. If top poses weren't the same or similar, the results were deemed random.

3.1.4 OPTIMAL DOCKING AREA (ODA) IN ICM-PRO

ICM object format 5o3l PHF was loaded onto Molsoft ICM-Pro (*version 3.8-7*) GUI. ODA was performed on chains B and J of with maximum sampling effort factor (10) to analyse surfaces for favourable energy change once buried as a protein-protein complex. The lower the ODA value was, the more likely the residue is predicted to be involved in protein-protein interactions on protein surfaces (red); whereas high values indicated an unlikely propbability (blue). It calculates atomic solvation parameters derived from experimental research to generate optimal surface patches which have the lowest docking desolvation energy values (Fernandez-Reico et al., 2005).

3.1.5 ICM POCKET FINDER IN ICM-PRO

This function was utilised to identify binding pockets on Tau; if they matched with the binding locations of compounds in the *in vitro* Tau aggregation mix (consisting of TauΔ1-250, inhibitor, heparin, ThT and dithiothreitol) and if there was any competition for these binding pockets. The main

objective was to predict that the inhibitor did not directly compete for binding sites on Tau with heparin (this prediction was later confirmed in **Section 6.2.2**).

ICM object format of structure was loaded onto Molsoft ICM-Pro (*version 3.8-7*) GUI. ICMPocketFinder was performed on the entire protein structure with maximum sampling effort factor (10). Based on the protein structure alone, ICMPocketFinder identifies potential ligand binding pockets based on physical interaction by predicting the position and size of ligand binding pockets found in the structure's cavities and clefts through a series of calculations. Calculated binding pockets denote continuous regions of space where the receptor has significantly favorable van der Waals interaction. Factors calculated include the volume of the pocket; area of the pocket; buriedness of the pocket signifying how open (>0.5) or closed (1.0) the pocket is; hydrophobicity of the pocket signifying the percentage of pocket surfaces which make contact with hydrophobic residues; compactness of the pocket and nonsphericity of the pocket signifying pocket sphericity (1.0 is spherical) which is calculated using the radius $(3/4 \text{ Volume} / \pi)^{1/3}$. Buriedness is calculated by measuring the pocket solvent accessible surface area (PSASA) using a probe radius of 1.4 and then measuring the PSASA covered by its shell. The fraction buried is determined as a ratio of the PSASA covered by its shell to the PSASA. Drug-Like-Density (DLID) is an additional algorithm employed to calculate the drugability of a pocket; values >0.5 are considered druggable (drug-like molecules meaning those with molecular weight < 500 with moderate lipophilicity. These predictions are calculated using a transformation of the Lennard-Jones potential through convolution with a specific sized Gaussian kernel, a binding potential grid map and equipotential surface construction along the maps (Abagyan and Kufareva, 2009; Sheridan et al., 2010; Kufareva et al., 2011; Molsoft, 2019).

3.2 RECOMBINANT EXPRESSION

Expression plasmid pRK-172 containing genes for human TauΔ1-250 and ampicillin resistance (kindly donated by Professor M. Hasegawa; Tokyo Metropolitan Institute of Medical Science, Tokyo, Japan) was transformed into *E. coli* BL21(DE3) chemically competent cells (Agilent Technologies) for recombinant expression. Methodology based on Hasegawa and Smith, (1998). Taniguchi-Watanabe et al. (2016), constructed the deletion mutant using PCR using 4R1N in pRK172 as a template. They cloned TauΔ1-250 cDNA into *Nde*I and *Eco*RI restriction sites of bacterial expression vector pRK-172 and verified construct by DNA sequencing. Taniguchi-Watanabe et al. (2016) received 4R1N in pRK-172 from Dr. Michel Goedert; University of Cambridge, Cambridge, UK (Goedert and Jakes, 1990).

3.2.1 CONFIRMATION OF CONSTRUCT

A DNA digest was performed using 2µL of 100ng µL plasmid, 2µL digest buffer 15µL with and without 0.5µL *Nde*I and 0.5µL *Eco*RI (New England Biolabs). An uncut sample without enzymes was also prepared using 16µL water. Samples were mixed via gentle agitation, spun for 5 seconds on a desktop centrifuge and incubated for 1 hour at 37°C. A 0.4% agarose gel was prepared by dissolving 0.4g agarose in 40 mL Tris acetate EDTA (TAE) buffer, heated for 1 minute in a microwave and then added 3µL SYBR Safe DNA gel stain (Invitrogen, UK). The 0.4% gel solution was poured into a gel cast, ensuring no bubbles were present and left to set over 10 minutes at 4°C. 2.5µL FAST DNA ladder (New England Biolabs) was pipetted into the first well. For each sample, 4µL of 6x sample buffer was mixed with 20µL sample and 16µL of each sample was loaded into subsequent wells. Agarose electrophoresis was run at 75V for 60 minutes and imaged under UV light using the Chemidoc™ XRS+ System and Image Lab 4™ software. A plasmid vector map was prepared using SnapGene® software and the base pairs of the Tau plasmid and vector calculated from the plasmid vector map were compared to the weight of the bands in the agarose gel.

3.2.2 PLASMID CONSTRUCT AGAROSE GEL ELECTROPHORESIS

Using the genetic sequences of TauΔ1-250 and pRK172 empty vector, a plasmid vector map was prepared using SnapGene, as seen in **Figure 3.1**. To confirm the codons for the TauΔ1-250 sequence were correct, they were translated into their amino acids as seen in **Figure 3.2** and matched to the known Tau amino acid sequence. The TauΔ1-250 insert and empty vector were calculated to be 579bp and 2538bp, respectively. Plasmid digest (20 μL mix) was performed using 2 μL 100 ng plasmid, 2 μL 10x Digest buffer, 0.5 μL *Nde*I and 0.5 μL *Eco*RI enzymes at 37°C for 1 hour. A 1.5% agarose gel was prepared using SYBR-Safe. To prepare samples; 4uL of 6x sample buffer was added to 20 uL sample. 2.5 μL FAST DNA ladder (New England Biolabs) was used as a reference. Electrophoresis was performed at 76 V for 1 hour.
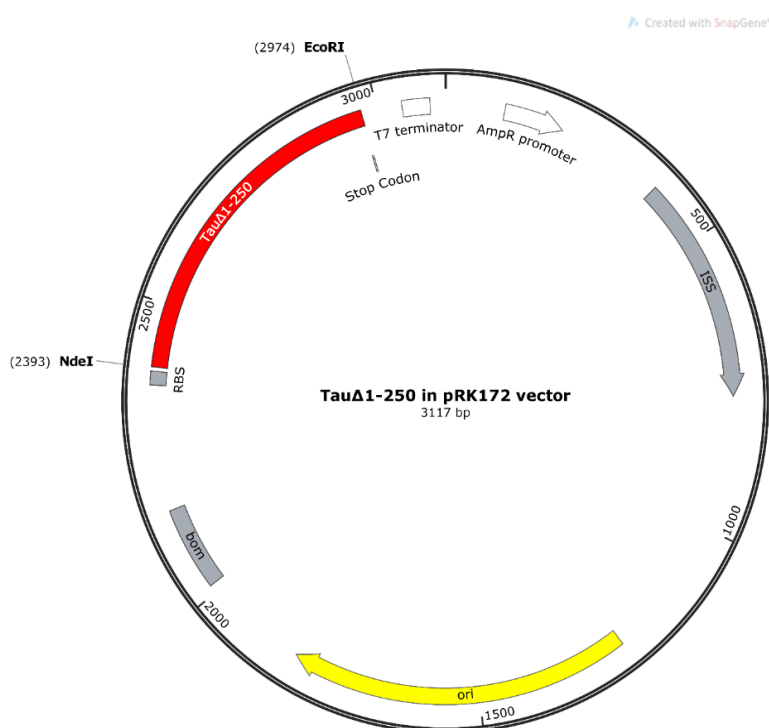
Figure 3.1: Plasmid map of pRK172 expression vector containing the of TauΔ1-250 DNA of interest, driven by the T7 promoter

```
TTC  TTG  AAG  ACG  AAA  GGG  CCT  CGT  GAT  ACG  CCT  ATT  TTT  ATA  GGT  TAT  TGT  CAT  GAT  AAT
 F    L    K    T    K    G    P    R    D    T    P    I    F    I    G    Y    C    H    D    N      20

AAT  GGT  TTC  TTA  GAC  GTC  AGG  TGG  CAC  TTT  TCG  GGG  AAA  TGT  GCG  CGG  AAC  CCC  TAT  TTG
 N    G    F    L    D    V    R    W    H    F    S    G    K    C    A    R    N    P    Y    L      40

TTT  ATT  TTT  CTA  AAT  ACA  TTC  AAA  TAT  GTA  TCC  GCT  CAT  GAG  ACA  ATA  ACC  CTG  ATA  AAT
 F    I    F    L    N    T    F    K    Y    V    S    A    H    E    T    I    T    L    I    N      60

GCT  TCA  ATA  ATA  TTG  AAA  AAG  GAA  GAG  TAT  GAG  TAT  TCA  ACA  TTT  CCG  TGT  CGC  CCT  TAT
 A    S    I    I    L    K    K    E    E    Y    E    Y    S    T    F    P    C    R    P    Y      80

TCC  CTT  TTT  TGC  GGC  ATT  TTG  CCT  TCC  TGT  TTT  TGC  TCA  CCC  AGA  AAC  GCT  GGT  GAA  AGT
 S    L    F    C    G    I    L    P    S    C    F    C    S    P    R    N    A    G    E    S      100

AAA  AGA  TGC  TGA  AGA  TCA  GTT  GGG  TGC  ACG  AGT  GGG  TTA  CAT  CGA  ACT  GGA  TCT  CAA  CAG
 K    R    C    *    R    S    V    G    C    T    S    G    L    H    R    T    G    S    Q    Q      120

CGG  TAA  GAT  CCT  TGA  GAG  TTT  TCG  AAA  AGA  AGA  ACG  TTT  TCC  AAT  GAT  GAG  CAC  TTT  TAA
 R    *    D    P    *    E    F    S    K    R    R    T    F    S    N    D    E    H    F    *      140

AGT  TCT  GCT  ATG  TGG  CGC  GGT  ATT  ATC  CCG  TGT  TGA  CGC  CGG  GCA  AGA  GCA  ACT  CGG  TCG
 S    S    A    M    W    R    G    I    I    P    C    *    R    R    A    R    A    T    R    S      160

CCG  ACT  ACA  CTA  TTC  TCA  GAA  TGA  CTT  GGT  TGA  GTA  CTC  ACC  AGT  CAC  AGA  AAA  GCA  TCT
 P    T    T    L    F    S    E    *    L    G    *    V    L    T    S    H    R    K    A    S      180

TAC  GGA  TGG  CAT  GAC  AGT  AAG  AGA  ATT  ATG  CAG  TGC  TGC  CAT  AAC  CAT  GAG  TGA  TAA  CAC
 Y    G    W    H    D    S    K    R    I    M    Q    C    C    H    N    H    E    *    *    H      200

TGC  GGC  CAA  CTT  ACT  TCT  GAC  AAC  GAT  CGG  AGG  ACC  GAA  GGA  GCT  AAC  CGC  TTT  TTT  GCA
 C    G    Q    L    T    S    D    N    D    R    R    T    E    G    A    N    R    F    F    A      220

CAA  CAT  GGG  GGA  TCA  TGT  AAC  TCG  CCT  TGA  TCG  TTG  GGA  ACC  GGA  GCT  GAA  TGA  AGC  CAT
 Q    H    G    G    S    C    N    S    P    *    S    L    G    T    G    A    E    *    S    H      240

ACC  AAA  CGA  CGA  GCG  TGA  CAC  CAC  GAT  GCC  TGC  AGC  AAT  GGC  AAC  AAC  GTT  GCG  CAA  ACT
 T    K    R    R    A    *    H    H    D    A    C    S    N    G    N    N    V    A    Q    T      260

ATT  AAC  TGG  CGA  ACT  ACT  TAC  TCT  AGC  TTC  CCG  GCA  ACA  ATT  AAT  AGA  CTG  GAT  GGA  GGC
 I    N    W    R    T    T    Y    S    S    F    P    A    T    I    N    R    L    D    G    G      280

GGA  TAA  AGT  TGC  AGG  ACC  ACT  TCT  GCG  CTC  GGC  CCT  TCC  GGC  TGG  CTG  GTT  TAT  TGC  TGA
 G    *    S    C    R    T    T    S    A    L    G    P    S    G    W    L    V    Y    C    *      300

TAA  ATC  TGG  AGC  CGG  TGA  GCG  TGG  GTC  TCG  CGG  TAT  CAT  TGC  AGC  ACT  GGG  GCC  AGA  TGG
 *    I    W    S    R    *    A    W    V    S    R    Y    H    C    S    T    G    A    R    W      320

TAA  GCC  CTC  CCG  TAT  CGT  AGT  TAT  CTA  CAC  GAC  GGG  GAG  TCA  GGC  AAC  TAT  GGA  TGA  ACG
 *    A    L    P    Y    R    S    Y    L    H    D    G    E    S    G    N    Y    G    *    T      340

AAA  TAG  ACA  GAT  CGC  TGA  GAT  AGG  TGC  CTC  ACT  GAT  TAA  GCA  TTG  GTA  ACT  GTC  AGA  CCA
 K    *    T    D    R    *    D    R    C    L    T    D    *    A    L    V    T    V    R    P      360

AGT  TTA  CTC  ATA  TAT  ACT  TTA  GAT  TGA  TTT  AAA  ACT  TCA  TTT  TTA  ATT  TAA  AAG  GAT  CTA
 S    L    L    I    Y    T    L    D    *    F    K    T    S    F    L    I    *    K    D    L      380

GGT  GAA  GAT  CCT  TTT  TGA  TAA  TCT  CAT  GAC  CAA  AAT  CCC  TTA  ACG  TGA  GTT  TTC  GTT  CCA
 G    E    D    P    F    *    *    S    H    D    Q    N    P    L    T    *    V    F    V    P      400

CTG  AGC  GTC  AGA  CCC  CGT  AGA  AAA  GAT  CAA  AGG  ATC  TTC  TTG  AGA  TCC  TTT  TTT  TCT  GCG
 L    S    V    R    P    R    R    K    D    Q    R    I    F    L    R    S    F    F    S    A      420

CGT  AAT  CTG  CTG  CTT  GCA  AAC  AAA  AAA  ACC  ACC  GCT  ACC  AGC  GGT  GGT  TTG  TTT  GCC  GGA
 R    N    L    L    L    A    N    K    K    T    T    A    T    S    G    G    L    F    A    G      440

TCA  AGA  GCT  ACC  AAC  TCT  TTT  TCC  GAA  GGT  AAC  TGG  CTT  CAG  CAG  AGC  GCA  GAT  ACC  AAA
 S    R    A    T    N    S    F    S    E    G    N    W    L    Q    Q    S    A    D    T    K      460

TAC  TGT  CCT  TCT  AGT  GTA  GCC  GTA  GTT  AGG  CCA  CCA  CTT  CAA  GAA  CTC  TGT  AGC  ACC  GCC
 Y    C    P    S    S    V    A    V    V    R    P    P    L    Q    E    L    C    S    T    A      480

TAC  ATA  CCT  CGC  TCT  GCT  AAT  CCT  GTT  ACC  AGT  GGC  TGC  TGC  CAG  TGG  CGA  TAA  GTC  GTG
 Y    I    P    R    S    A    N    P    V    T    S    G    C    C    Q    W    R    *    V    V      500

TCT  TAC  CGG  GTT  GGA  CTC  AAG  ACG  ATA  GTT  ACC  GGA  TAA  GGC  GCA  GCG  GTC  GGG  CTG  AAC
 S    Y    R    V    G    L    K    T    I    V    T    G    *    G    A    A    V    G    L    N      520
```

57

```
GGG GGG TTC GTG CAC ACA GCC CAG CTT GGA GCG AAC GAC CTA CAC CGA ACT GAG ATA CCT
 G   G   F   V   H   T   A   Q   L   G   A   N   D   L   H   R   T   E   I   P     540

ACA GCG TGA GCA TTG AGA AAG CGC CAC GCT TCC CGA AGG GAG AAA GGC GGA CAG GTA TCC
 T   A   *   A   L   R   K   R   H   A   S   R   R   E   K   G   G   Q   V   S     560

GGT AAG CGG CAG GGT CGG AAC AGG AGA GCG CAC GAG GGA GCT TCC AGG GGG AAA CGC CTG
 G   K   R   Q   G   R   N   R   R   A   H   E   G   A   S   R   G   K   R   L     580

GTA TCT TTA TAG TCC TGT CGG GTT TCG CCA CCT CTG ACT TGA GCG TCG ATT TTT GTG ATG
 V   S   L   *   S   C   R   V   S   P   P   L   T   *   A   S   I   F   V   M     600

CTC GTC AGG GGG GCG GAG CCT ATG GAA AAA CGC CAG CAA CGC GGC CTT TTT ACG GTT CCT
 L   V   R   G   A   E   P   M   E   K   R   Q   Q   R   G   L   F   T   V   P     620

GGC CTT TTG CTG GCC TTT TGC TCA CAT GTT CTT TCC TGC GTT ATC CCC TGA TTC TGT GGA
 G   L   L   L   A   F   C   S   H   V   L   S   C   V   I   P   *   F   C   G     640

TAA CCG TAT TAC CGC CTT TGA GTG AGC TGA TAC CGC TCG CCG CAG CCG AAC GAC CGA GCG
 *   P   Y   Y   R   L   *   V   S   *   Y   R   S   P   Q   P   N   D   R   A     660

CAG CGA GTC AGT GAG CGA GGA AGC GGA AGA GCG CCT GAT GCG GTA TTT TCT CCT TAC GCA
 Q   R   V   S   E   R   G   S   G   R   A   P   D   A   V   F   S   P   Y   A     680

TCT GTG CGG TAT TTC ACA CCG CAG ATG GTG CAC TCT CAG TAC AAT CTG CTC TGA TGC CGC
 S   V   R   Y   F   T   P   Q   M   V   H   S   Q   Y   N   L   L   *   C   R     700

ATA GTT AAG CCA GTA TAC ACT CCG CTA TCG CTA CGT GAC TGG GTC ATG GCT GCG CCC CGA
 I   V   K   P   V   Y   T   P   L   S   L   R   D   W   V   M   A   A   P   R     720

CAC CCG CCA ACA CCC GCT GAC GCG CCC TGA CGG GCT TGT CTG CTC CCG GCA TCC GCT TAC
 H   P   P   T   P   A   D   A   P   *   R   A   C   L   L   P   A   S   A   Y     740

AGA CAA GCT GTG ACC GTC TCC GGG AGC TGC ATG TGT CAG AGG TTT TCA CCG TCA TCA CCG
 R   Q   A   V   T   V   S   G   S   C   M   C   Q   R   F   S   P   S   S   P     760

AAA CGC GCG AGG CAG GAT CTC GAT CCC GCG AAA TTA ATA CGA TAC ACT ATA GGG AGA CCA
 K   R   A   R   Q   D   L   D   P   A   K   L   I   R   Y   T   I   G   R   P     780

CAA CGG TTT CCC TCT AGA AAT AAT TTT GTT TAA CTT TAA GAA GGA GAT ATA ATG CCA GAC
 Q   R   F   P   S   R   N   N   F   V   *   L   *   E   G   D   I   M   P   D     800

CTG AAG AAT GTC AAG TCC AAG ATC GGC TCC ACT GAG AAC CTG AAG CAC CAG CCG GGA GGC
 L   N   V   K   S   K   I   G   S   T   E   N   L   K   H   Q   P   G   G   G     820

GGG AAG GTG CAG ATA ATT AAT AAG AAG CTG GAT CTT AGC AAC GTC CAG TCC AAG TGT GGC
 G   K   V   Q   I   I   N   K   K   L   D   L   S   N   V   Q   S   K   C   G     840

TCA AAG GAT AAT ATC AAA CAC GTC CCG GGA GGC GGC AGT GTG CAA ATA GTC TAC AAA CCA
 S   K   D   N   I   K   H   V   P   G   G   G   S   V   Q   I   V   Y   K   P     860

GTT GAC CTG AGC AAG GTG ACC TCC AAG TGT GGC TCA TTA GGC AAC ATC CAT CAT AAA CCA
 V   D   L   S   K   V   T   S   K   C   G   S   L   G   N   I   H   H   K   P     880

GGA GGT GGC CAG GTG GAA GTA AAA TCT GAG AAG CTT GAC TTC AAG GAC AGA GTC CAG TCG
 G   G   G   Q   V   E   V   K   S   E   K   L   D   F   K   D   R   V   Q   S     900

AAG ATT GGG TCC CTG GAC AAT ATC ACC CAC GTC CCT GGC GGA GGA AAT AAA AAG ATT GAA
 K   I   G   S   L   D   N   I   T   H   V   P   G   G   G   N   K   K   I   E     920

ACC CAC AAG CTG ACC TTC CGC GAG AAC GCC AAA GCC AAG ACA GAC CAC GGG GCG GAG ATC
 T   H   K   L   T   F   R   E   N   A   K   A   K   T   D   H   G   A   E   I     940

GTG TAC AAG TCG CCA GTG GTG TCT GGG GAC ACG TCT CCA CGG CAT CTC AGC AAT GTC TCC
 V   Y   K   S   P   V   V   S   G   D   T   S   P   R   H   L   S   N   V   S     960

TCC ACC GGC AGC ATC GAC ATG GTA GAC TCG CCC CAG CTC GCC ACG CTA GCT GAC GAG GTG
 S   T   G   S   I   D   M   V   D   S   P   Q   L   A   T   L   A   D   E   V     980

TCT GCC TCC CTG GCC AAG CAG GGT TTG GAA TTC CGA TCC GGC TGC TAA CAA AGC CCG AAA
 S   A   S   L   A   K   Q   G   L   E   F   R   S   G   C   *   Q   S   P   K    1000

GGA AGC TGA GTT GGC TGC TGC CAC CGC TGA GCA ATA ACT AGC ATA ACC CCT TGG GGC CTC
 G   S   *   V   G   C   C   H   R   *   A   I   T   S   I   T   P   W   G   L    1020

TAA ACG GGT CTT GAG GGG TTT TTT GCT GAA AGG AGG AAC TAT ATC CGA TAA
 *   T   G   L   E   G   F   F   A   E   R   R   N   Y   I   R   *              1039
```

Figure 3.2: DNA and amino acid sequences of the pRK172 expression vector containing the TauΔ1-250 DNA of interest (highlighted region). This figure was made to check that the DNA sequence associated with the plasmid sent by Tokyo Metropolitan Institute of Medicine matched the known amino acid sequence for Tau 251-441.

3.2.3 TRANSFORMATION INTO *E. COLI*

Transformation entails altering the genome of competent cells through the introduction of an exogenous engineered plasmid vector, which usually contains antibiotic resistance genes and genes to synthesize proteins of interest. In this research two *E. coli* cell lines were transformed; XL1Blue and BL21 (DE3) for plasmid storage and recombinant expression, respectively.

3.2.3.1   TRANSFORMATION INTO XL1BLUE CELLS

50μL of *E. coli* XL1 Blue cells were thawed on ice before the addition of 1.7μL of β-mercaptoethanol (Agilent Technologies, UK) to improve cell wall permeability and then left on ice for 10 minutes (Brzobohaty and Kovac, 1986). Under sterile conditions 5μL of plasmid pRK-172 DNA was added and gently mixed before leaving on ice for 30 minutes. Cells were then heat shocked at 45°C for 45 seconds and returned to ice for 2 minutes to allow *E. coli* to take up the plasmid. Cells were slowly supplemented with 900μL of sterile SOB media and then incubated at 37°C for 1 hour with agitation. Using aseptic technique 200μL of culture was distributed over the surface of LB agar plates containing 0.1% ampicillin and incubated at 37°C overnight. As the plasmid contained ampicillin resistance, any growth on the agar plates suggested that it had been successfully taken up by the *E. coli*. Individual colonies were selected and transferred into 30ml sterile LB media containing 0.1% ampicillin and incubated at 37°C overnight. From this overnight culture 50% glycerol stocks were produced and frozen at -80°C for future use.

3.2.3.2   TRANSFORMATION INTO *E. COLI* BL21 (DE3) CELLS

Following the same transformation methodology (**Section 4.1.3.1**), plasmid vectors were also transformed into *E. coli* BL21(DE3) expressing cell-line (Agilent Technologies, UK) to enhance protein expression. Producing glycerol stocks of this cell-line ensured that overnight cultures could be prepared immediately; without having to first isolate the DNA from the XL1 Blue cell-line and transforming into BL21 (DE3).

3.2.4 PRODUCTION OF TAU
3.2.4.1   RECOMBINANT PROTEIN EXPRESSION

Using a pipette tip scratching from the glycerol stocks previously mentioned, overnight cultures of *E. coli* containing the pRK-172 plasmid vector were prepared in 30ml LB media containing 0.1% ampicillin. This culture was utilised to inoculate 1L of sterile LB media which was incubated at 37°C with agitation until an OD_{600} of 0.6 was reached. This ensured adequate growth without the formation of any toxic species. When OD_{600} was suitable, 1ml of culture was collected for SDS-PAGE analysis and culture was induced with 1mM isopropyl β-D-thiogalactoside (IPTG) which bound to the LacI repressor causing a conformational change. This resulted in the liberation of the LacUV5 promoter which is otherwise inhibited by the LacI repressor. Consequentially T7 polymerase was able to express which subsequently bound to the T7 promoter which drives the expression of the TauΔ1-250 peptide. Following guidelines from Hasegawa et al. (1998), protein expression was optimised for induction incubation at 37°C for 3 hours and with agitation following experimental inductions at various temperatures which were sampled (20μL) on an hourly basis over 5 hours and overnight for SDS-PAGE.

3.2.4.2   CELL HARVEST AND LYSIS

To harvest the cells after induction, cells were centrifuged at 5,000 RPM for 15 minutes at 4°C. Cells were re-suspended in lysis buffer (50mM PIPES, 1mM EGTA, 1mM DTT, 0.5mM PMSF, 0.5μg/ml leupeptin, pH 6.8) and frozen at -20°C to assist lysis. After thawing, cells were sonicated at 20 microns for 6 cycles of 30 seconds with 60 second breaks on ice. Lysed cells were centrifuged at 15,000 rpm for 15 minutes at 4°C to remove cell debris. Supernatant was collected and supplemented with 1% β-mercaptoethanol to prevent disulphide cross bridging and dimer formation which could affect subsequent column binding. Tau as an intrinsically disordered protein is heat-stable (Uversky, 2019; KrishnaKumar and Gupta, 2017). The crude protein mix was boiled at 100°C for 5 minutes (to degrade bacterial cell wall for protein release and to denature contaminating proteins) and then centrifuged again at 15,000 rpm for 15 minutes at 4°C before recovering the supernatant.

3.2.4.3   IMMOBILISED CATION-EXCHANGE CHROMATOGRAPHY

The heat-stable supernatant of the *E. coli* was collected and loaded onto a sulphopropyl (SP) sepharose

column (bed volume 3ml), pre-equilibrated in purification buffer (50mM PIPES, 1mM EGTA, 1mM DTT,

pH 6.8). TauΔ1-250 has an isoelectric point (pI) of 9.5. To remove any non-specifically binding proteins

the column was washed in purification, followed by purification buffer + 0.1M NaCl. Proteins were

eluted with purification buffer +0.35M NaCl and collected as 1ml fractions. Finally, the column was

washed with purification buffer +1M NaCl to flush the column out. 1mL elution fractions were

collected and protein concentrations were analysed using a Nanodrop 2000 (Thermo Scientific, UK).

Fractions with high protein concentration were pooled for ammonium sulphate precipitation. 20μL of

the pooled sample was analysed by SDS-PAGE.

3.2.4.4   AMMONIUM SULPHATE PRECIPITATION

The pooled elution fractions were brought to 35% ammonium sulphate. This solution was left mixing

at 4°C for 3 hours to allow precipitation to occur before centrifugation at 21,000 x g using an 'FA-45-

24-11 rotor' in an 'Eppendorf Centrifuge 5424'. The supernatant was removed, and pellet was

reconstituted in ddH20. Supernatant was then dialysed against Tris buffer (30mM), pH 7.5 overnight

and subsequently frozen at -20°C (Takahashi et al., 2015).

3.2.4.5   DIALYSIS AND ULTRACENTRIFUGATION

A suitable length of 14kDa BioDesignDialysis Tubing™ (Thermofisher Scientific, USA) was washed with

ddH$_2$O for 10 seconds, three times. The inside of the tubing was filled with ddH$_2$O three times and

emptied to remove glycerol. A knot was tied at one end of the tubing and capped off before sample

was loaded. Once sample was loaded a knot was tied in the other end and capped. Sample was

suspended using a float and was dialysed against 4L of 30mM Tris (30mM), pH 7.5, with three washes:

2 hours, 2 hours and overnight. Dialysed sample was transferred to a falcon tube and DTT (1mM) was

added, before boiling sample for 3 minutes. Sample was ultracentrifuged at 113,000x g for 20 minutes

at 4°C (using Ti 70.1 rotor and 10.4ml ultra-centrifuge tubes) and supernatant (Tau monomers) was collected.

3.2.4.6   PROTEIN CONCENTRATION QUANTIFICATION

Protein concentration was determined through ultraviolet absorbance at A280 and corrected using **Equation 10** which takes into consideration the number of tryptophan, tyrosine and cystine residues:

$$Equation\ 10: \quad \varepsilon(280)\ (M^{-1}\ cm^{-1}) = (\#W\ x\ 5500) + (\#Y\ x\ 1490) + (\#C\ x\ 125)$$

The extinction coefficients for 1M solutions of tryptophan, tyrosine and cystine are 5500 M^{-1} cm^{-1}, 1490 M^{-1} cm^{-1} and 125 M^{-1} cm^{-1} respectively. Cystines are dimers of two cysteine molecules joined via disulphide bonding. The calculated extinction coefficient was then divided by protein molecular weight to give concentration in the absorbance of a 1mg/ml solution of target protein (Gill and von Hippel, 1989 and Pace et. al, 1995).

3.2.4.7   SDS POLY-ACRYLAMIDE GEL ELECTROPHORESIS (PAGE)

To determine the level of expression and purity of the end-product, SDS-PAGE was conducted at each stage of the process, using 15% polyacrylamide gels in a Bio-Rad gel electrophoresis system. 16µL of each sample was mixed with 2 µL of 10x sample buffer (20% v/v 1M Tris, 40% glycerol, 2% β-mercaptoethanol, 5% v/v 0.5M EDTA, 4% SDS and 29% ddH20). To assist the denaturing process samples were heated at 95°C for 5 minutes before being loaded onto 15% polyacrylamide stacking gel. 5µL of PageRuler™ Unstained Broad Range Protein Ladder (Thermo Scientific) was loaded into the first well to serve as a reference baseline. Gels were run at 200V for approximately 1 hour which following completion were stained with 10% v/v acetic acid and 6% v/v Coomassie blue G-250 overnight with agitation. Gels were then treated with 10% acetic acid de-stain and imaged on UV light using the Chemidoc™ XRS+ System and Image Lab 4™ software.

3.3 TAUΔ1-250 AGGREGATION

Each Tau aggregation mix replicate consisted 60µL of monomeric TauΔ1-250 (20µM), ThT (15µM), heparin (5µM), dithiothreitol (1mM) and Tris (30mM), pH 7.4. Samples were aggregated at 37˚C with 10 seconds of shaking every 10 minutes for 24 hours. Heparin concentration was calculated using the average of the estimated molecular weight range reported by the manufacturer. General salts and chemicals such as were sourced from Fisher Scientific (Newcastle, UK) and Sigma-Aldrich Ltd. (Gillingham, UK). Heparin sodium salt was sourced from porcine intestinal mucosa with an average MW of 4650 Da and obtained from Iduron (Manchester, UK).

3.3.1 THIOFLAVIN-T (ThT) FLUORESCENCE

Each Tau aggregation mix replicate consisted 60µL of monomeric TauΔ1-250 (20µM), ThT (15µM), heparin (5µM), dithiothreitol (1mM) and Tris (30mM), pH 7.4 in a black clear flat bottom 384 well microplate (Corning®) at 37˚C for 24 hours. When investigating the effect of inhibitors, various concentrations were co-incubated. Condition were conducted in at least in triplicate. Plates were monitored for fluorescence every 10 minutes following a 10s shake of the plate (λex=442nm, λem=483nm) in a FlexStation 3 microplate reader or a BioTek Synergy 2 microplate reader (Wolfe et al., 2010). Fluorescence was taken as an average of each triplicate experiment. Statistical analysis data was expessed as mean ± standard error of mean. ThT was sourced from Sigma-Aldrich Ltd. Standard Tau vs Inhibitor experiment concentrations were equimolar to keep experiments even. One factor repeated measures ANOVA + Tukey post hoc statistical analysis investigated lead peptides.

3.3.2 CONGO RED BIREFRINGENCE

Sixty microlitre mixtures of monomeric Tau (20µM), heparin (5µM) dithiothreitol (1mM) and various concentrations of inhibitor were incubated in Tris (30mM), pH 7.5, in a micro Eppendorf tube at 37˚C for 24 hours. Each condition was conducted at least in triplicate. After 24 hours, samples were mixed with Congo red (90µM) and 10 µL was placed on a microscope slide and left to dry in a dessicator. Samples were analysed on a a Zeissp axioscope A1 microscope in transmission mode. An unpolarsised

light source was passed through a linear polariser, then through the sample and then projected onto a second polariser. Samples were observed at 10x objective lens with 0° polarised lens and 90° polarised lenses for uncrossed and crossed measurements, respectively.

3.3.3 CIRCULAR DICHROISM

Using the same aggregation conditions as above, TauΔ1-250 was aggregated under the same conditions as above and then pipetted into a Quartz cuvette and far-UV CD measurements were obtained using a Chirascan plus qCD spectrometer (Applied Photophysics) between 180 and 260nm with a bandwidth of 1 nm and a path length of 2mm. CD is further discussed in **Section 5.2.3**.

3.3.4 TRANSMISSION ELECTRON MICROSCOPY

TauΔ1-250 (20μM) was aggregated under the same conditions as above. Samples were loaded onto Formvar/Carbon 300 mesh carbon-coated copper grids (Agar Scientific) at a volume of 10μL per grid and left for 3 minutes. Excess sample was wicked away before each grid was counter stained with 10μL of filtered 2% phosphotungstic acid, pH 2. After 2 minutes of staining excess phosphotungstic acid was wicked away by allowing the solution to soak into Whatman filter paper. Grid samples were loaded onto a Jeol JEM-1010 electron microscope and were visualised and photographed at various magnifications under the training and supervision of Dr. Nigel Fullwood at Lancaster University. Several random fields were photographed per sample. Fibrils presented as transparent as they are less dense than the phosphotungstic acid which presented as black areas. This model of electron microscope utilised gelatin and silver bromide film which after exposure to light subsequently required processing in a dark room under red light. Wearing protective Marigold gloves, the developer (Ilford Phenisol) was mixed with water at a 1:4 ratio at 20°C. Film was agitated in developer for 10 seconds per minute for 4 minutes. This reduced the silver bromide which was exposed to electron, into metallic silver. Film was gently agitated in water for 1 minute to wash away excess developer and then agitated in Fixer for 10 seconds per minute for 4 minutes. This stabilised the film and washed away unreduced silver bromide. Film was then left to wash in water for 1 hour to remove anything unbound to the film.

Detergent was pipetted into the water bath before removing the film to ensure even drying. Film was dried overnight before being scanned into digital format. Repeats were performed in triplicate across independent experimental repeats.

3.3.5 PRODUCTION OF RI-AG03 LIPOSOMES

Liposomes were prepared using sphingomyelin, cholesterol and 1,2-distearoyl-sn-glycero-3-phosphoethanolamine-N-[maleimide(polyethylene glycol)-2000] (DSPE-PEG-MAL) in a molar ratio of 47.5:47.5:5. Lipids were resuspended in chloroform/methanol at 2:1 and then dried under nitrogen gas stream. Complete evaporation was ensured by one hour under vacuum. The dried lipid film was resuspended in PBS with vortexing and sonication for ~5-15 minutes. They were then frozen in liquid nitrogen and defrosted at 45°C several times to disrupt multimellar liposomes. Using a Mini-Extruder with two Hamilton 1000µl syringes at each end, the liposomes were extruded 11 times through a 100 nm pore polycarbonate filter under 20 bar nitrogen pressure at room temperature to produce ~130 nm liposomes. To covalently link peptide inhibitors, these liposomes were incubated with solid RI-AG03-Cys at 1.2 x 2.5% total lipid concentration for 2 hours at 37°C and incubated overnight at 4°C. Peptides reacted with the lipids via click chemistry. CysOH denotes cysteine capped with OH to the C-terminal to prevent further elongation. Maleimide is a sulfhydryl-reactive chemical group and at pH 6.5-7.5, it selectively crosslinks with the free/reduced sulfhydryl group on the side-chain of cysteine to form a stable and non reversible covalent thioether linkage, as seen in **Figure 3.3**. To remove unbound peptides, the sample was centrifuged at 171,000g for 1 hour and then resuspended in PBS. Amount of RI-AG03 in the liposome fraction was quantified using BSA assay and the amount of phosopholipid was quantified using the Phospholipid C test from Fujifilm WAKO diagnostics USA (Gregori et al., 2017).
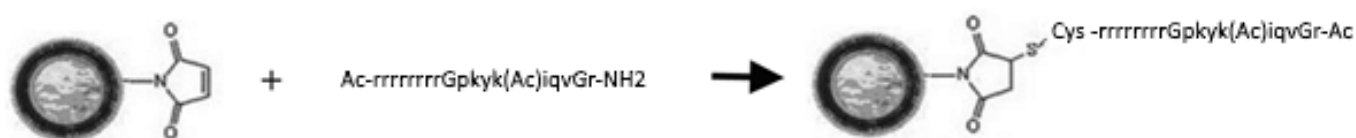
Figure 3.3: Illustration of RI-AG03 linking to a liposome using a maleimide linker, via an additional cysteine amino acid.

3.4 RI-AG03 TOXICITY IN HEK-293 CELLS

Tau is largely found intracellularly so it is important for RI-AG03 to be able to act within cells. An enzyme stability assay was conducted to determine if RI-AG03 was resistant to enzymatic degredation. Following this a lactose dehydrogenase (LDH) cytotoxicity assay was conducted to investigate potential toxicity of RI-AG03 in SH-5Y5 cells. Due to availability, a cell uptake assay was conducted in HEK-293 cells to confirm proof of principle that RI-AG03 could penetrate cells, before conducting experiments in *Drosophila*.

3.4.1 CULTURING PROTOCOL

The hood and equipment were cleaned with ethanol prior to use. Equipment (not including fluids) were placed inside the hood and steralised with UV for at least 20 minutes. Growth medium used in cell culture was Dulbecco's Modified Eagle Medium/Ham's F12 (DMEM/F12) in a 1:1 ratio, supplemented wih 10% FBS and 1% antibiotics (Streptomycin and Penicillin 1:1 ratio) to prevent contamination. Cells were incubated at 37°C and 5% CO_2. Growth medium was replaced every 3-7 days with pre-warmed growth medium and cells were split once they reached 80% confluency. To split cells in T-75 flasks; old medium was aspirated, and cells were washed with 5 mL 1x PBS to wash away any excess old medium. This was important as medium inhibits trypsin which is used to detatch cells from the flask. PBS was removed and 5 mL 1x trypsin was added to the cells which were subsequently incubated for 5-10 minutes at 37°C, 5% CO_2. The flask was gently agitated, and cells were examined under a microscope to ensure they had detached. 5 mL pre-warmed growth medium was added to neutralise the trypsin. Cells suspended in growth medium were transferred to a sterile Falcon tube and spun at 1,000 RPM for 5-10 minutes at 20°C. Supernatant was decantered into the waste and the pellet was resuspended in 1 mL growth medium and transferred into a fresh T-75 flask which was supplemented with an additional 9 mL growth medium. Cells were incubated at 37°C, 5% CO_2.

3.4.2 ENZYME STABILITY

RI-AG03 amino acid sequence was processed using ExPASy peptide cutter tool (Gasteiger et al., 2005). RI-AG03 (20µM) was incubated at 37 °C for 24 hours with and without an equimolar concentration of Trypsin. To determine stability, samples and controls were run on SDS-PAGE gels, following methodology previously described.

3.4.3 CELLULAR UPTAKE

VWR pcs Cover Glass 13 mm were sterilised in 100% ethanol and placed flat into wells of a 12 well plate. HEK-293 (human embryonic kidney) cells were seeded into individual wells at 20,000 cells and supplemented with 5(6)-carboxyfluorescein (absorption maximum at 494 nm and emission maximum of 512 nm) tagged RI-AG03 (15µM) and DMEM/10% FBS pre-warmed to 37°C. Cells were incubated at 37°C and 5% CO_2 for 24 hours before being fixed using 4% formaldehyde and washed with TBS. Samples were mounted to microscope slides using ProLong™ Gold Antifade Mountant and visualised on a Nikon Eclipse Ti fluorescent microscope using the FITC filter.

3.4.4 CELL TOXICITY

HEK-293 cells were incubated in DMEM/10% FBS at 37°C and 5% CO_2 and transferred during the exponential growth phase to a 96 well plate at 10,000 cells/100 µl per well. RI-AG03 was dissolved in 30mM Tris (pH 7.5) and was supplemented at 0, 2, 4, 10, 15, 20, 30, 40 and 100 µM to the growth medium in triplicate and incubated as previously over 24 hours. Potential peptide toxicity towards the cells was determined using the Pierce™ LDH Cytotoxicity Assay Kit.

3.5 TESTING RI-AG03 IN A ROUGH-EYE *DROSOPHILA MODEL*.

2N4R wild type human Tau fly line 51361 was sourced from the '*Bloomington Drosophila Stock Centre'*. These flies were homozygous stable Tau flies recombined to GMR stable lines. Control flies had the driver by itself (GMR-GAL4). No crosses were conducted. Preliminary experiments were conducted before *in vivo* testing. *Drosophila* media preparation involves high temperatures and RI-AG03 was added to the fly food. Thermal stability CD was conducted to ensure temperature did not change RI-AG03 secondary structure e.g. adopting β-sheet structure. Fly media was changed every week, so RI-AG03 had to be stable for this period and was confirmed using reversed phase ultra high-performance liquid chromatography mass spectrometry (RP-UHPLC).

3.5.1 THERMAL STABILITY

Using the same aggregation conditions in **Section 3.3**, TauΔ1-250 was incubated in a Quartz cuvette with the temperature steadily increasing from 20-90˚C over 5 hours. Far-UV CD measurements were obtained every two minutes using a Chirascan plus qCD spectrometer (Applied Photophysics) between 180 and 260nm with a bandwidth of 1 nm and a path length of 2mm.

3.5.2 MASS SPECTROMETRY

RP-UHPLC positive ion electrospray ionisation mass spectrometry of RI-AG03 was conducted using a maXis (Bruker Daltonics, Bremen, Germany) time of flight (TOF) mass spectrometer, with the assistance of Dr. Julie Herniman at the Department of Chemistry at Southampton University. Samples (50μM) were diluted 50:50 in water. Injection sample volumes of 2 μL were introduced to the mass spectrometer via a Dionex Ultimate 3000 autosampler and UHPLC pump at a flow rate of 600 μL/min. UHPLC was performed using a Restek Force C18 (50 mm x 2.1 mm 1.7μm) column and a column temperature of 40˚C. Solvent used were: A (water + 0.2% formic acid) and solvent B (acetonitrile + 0.2% formic acid, with a gradient of 0% A for 2 minutes, 100% B until 7.8 minutes, held at 100% B for 2.2 minutes. UHPLC, instrument control and processing softwares used were Chromeleon Xpress, Bruker otofControl V 3.2 (Build 41) and Bruker DataAnalysis V 4.0, respectively.

3.5.3 ROUGH-EYE MODEL

Human Tau$_{441}$ and *Drosophila* Tau$_{370}$ amino acid sequences were compared to ensure that *Drosophila* Tau$_{370}$ did not contain VQIINK or VQIVYK sequences which would interact with the binding sequence of RI-AG03. In FASTA format the following sequences for human Tau$_{441}$ and *Drosophila* Tau$_{370}$ were inputted into BLAST blastp suite to determine similarities in amino acid alignment. **Appendix C** confirmed that Drosophila Tau$_{370}$ does not contain VQIINK or VQIVYK sequences.

Human Tau$_{441}$ sequence: $_1$ **MAEPRQEFEV MEDHAGTYGL GDRKDQGGYT MHQDQEGDTD AGLKESPLQT PTEDGSEEPG SETSDAKSTP TAEDVTAPLV DEGAPGKQAA AQPHTEIPEG TTAEEAGIGD TPSLEDEAAG HVTQARMVSK SKDGTGSDDK KAKGADGKTK IATPRGAAPP GQKGQANATR IPAKTPPAPK TPPSSGEPPK SGDRSGYSSP GSPGTPGSRS RTPSLPTPPT REPKKVAVVR TPPKSPSSAK SRLQTAPVPM PDLKNVKSKI GSTENLKHQP GGGKVQIINK KLDLSNVQSK CGSKDNIKHV PGGGSVQIVY KPVDLSKVTS KCGSLGNIHH KPGGGQVEVK SEKLDFKDRV QSKIGSLDNI THVPGGGNKK IETHKLTFRE NAKAKTDHGA EIVYKSPVVS GDTSPRHLSN VSSTGSIDMV DSPQLATLAD EVSASLAKQG L** $_{441}$

Drosopihila Tau$_{370}$ sequence: $_1$ **MADVLEKSSL LDAVPPLGDP HPPLPHQQLQ QEAAAAAAAN AAPPAPPQQQ QPPPHQLQQQ QPQQQQLQQK PANARANQDQ KEGDNDSGVD ESTQEKDRNG PNSPSSPVKT PTSTSSKPDK SGTSRPPSAT PSNKSAPKSR SASKNRLLLK TPEPEPVKKV PMNKVQVGHA PSPNLKAVRS KIGSLDNATY KPGGGHVKIE SKKIDIKAAP RIEAKNDKYM PKGGEKKIVT TKLQWNAKSK IGSLENAAHK PGGGDKKIET LKMDFKDKAK PKVGSTANVK HQPGGGDIKI QTQKLEIKAQ SKVGSLDNVK HKPGGGEKKI FDDKDYLKNV EHSVALTTPP TQFALQGRLI ATIHLEFGLC NSDCVCNNIF ESLFK** $_{370}$

Training in the fly lab was provided and experiments were supervised by Dr. Shreyasi Chatterjee. An appropriate volume of fly food was prepared based on the standard Bloomington fly media recipe as seen in **Table 3.2**, following standard methodology (Bloomington Drosophila Stock Centre, 2019). Based on experimental data at Southampton University, an approximate concentration of Tau found in the heads of mutant *Drosophila* was calculated. RI-AG03 was mixed into the fly food at different concentrations; 0.08μM, 0.8μM, 20μM and 40μM. Homozygous stable Tau flies recombined to GMR stable lines (GMR-hTau) were used in this research. The 'healthy' control was the driver by itself (GMR-GAL4). Four fresh homozygous males and four homozygous flies' females were incubated per vial containing 10 mL fly food supplemented with RI-AG03 at 25°C. An equal number of healthy flies were also introduced to drug food in another separate vial. Parents were discarded after hatching larvae in the drug food. Once the larvae had matured to adult flies, they were transferred to fresh vials weekly and incubated at 25°C. Flies were monitored daily using a Nikon microscope and 1-day old live flies

were imaged (n=5/condition) and processed on ImageJ. One factor repeated measures ANOVA was conducted with Tukey post hoc testing using IBM SPSS Statistics 23.

Ingredients	Amount required
Distilled water (L)	1
Malt extract (g)	46.2
Sugar (g)	48
Agar (g)	6
Soya flour (g)	10
Yeast (g)	17.5
Yellow Maize Meal (g)	73.1
Extra water (ml)	80
Propionic acid (ml)	5

Table 3.2: Bloomington fly media recipe per litre (Bloomington Drosophila Stock Centre, 2019)

3.5.4 SCANNING ELECTRON MICROSCOPY

Flies were euthanised and fixed in 2.5% glutaraldehyde in PBS at Southampton University in collaboration with Dr. Shreyasi Chatterjee. Samples were prepped for SEM and analysed in collaboration with Dr. Nigel Fullwood. Three 5-minute washes in PBS were performed, before dehydrating the sample for 30 minutes at each ethanol concentration of 50%, 70%, 80%, 90%, 100%. hexamethyldisilazane (Sigma Aldrich, UK) has reduced surface tension and was used to dry SEM samples and reduce sample fracturing by providing strength through cross-linking proteins. Two one-hour changes of hexamethyldisilazane was conducted and then left in hexamethyldilizane overnight with the top off vial under a fume hood; allowing hexamethyldisilizane to sublimate off. Samples were sputter coated with gold for 4 minutes on an Edwards 150A sputter coater. They were then mounted on JEOL SEM stubs under a stereo microscope and examined using a JEOL 5600 scanning electron microscope.

4.   DESIGNING PEPTIDIC TAU

AGGREGATION PEPTIDE INHIBITORS

4.1   INTRODUCTION

The purpose of this *in silico* chapter provides informed guidance on where to begin when designing peptide-based aggregation inhibitors for Tau. The information provided includes the predicted binding potential for peptides towards their target and if the peptides interact with themselves. If the peptides have high interaction together, they could potentially seed aggregation which is undesirable. Predictions based on the results in this chapter provided indications for which amino acid sequence to target in Tau and which peptide inhibitor amino acid sequences may bind and inhibit aggregation. This approach provided some evidence-based direction on which peptides may work. This process saved money in the wet lab by filtering out peptides that were predicted to be unsuitable aggregation inhibitors. Evidence of potentially successful inhibitors were taken forward into the following chapter to be tested in the wet lab.

4.1.2   PROTEIN THERAPEUTICS

Protein drugs are becoming increasingly prevalent due to their functional versatility, specificity and low on-target toxicity as potential diagnostic and therapeutic molecules (Carter, 2011).   More specificity they are less likely to interact with other things but can still be toxic. With small molecules the unwanted effects are off-target, however with anti-bodies they can be too specific and in worst cases this can be fatal. Protein drugs can be utilised for a broad array of diseases such as administering endogenous insulin, interleukin or growth hormone supplements for diabetes, cancer, and auto-immune diseases, respectively (Elvin et al., 2013; Sormanni et al., 2015). Of the 239 US Food and Drug Administration approved peptide and protein therapeutics and their 380 drug variants, only 7 are used in neurological disorders, whereas there are 89, 80, 74 and 61 drug varients for metabolic disorders,

immunological diseases, haematological diseases and cancer therapy, respectively (Usmani et al., 2017). Protein drugs are generally delivered subcutaneously as the preferential route of delivery as they are not normally orally active, however they can also be administered intra-nasally which is more suitable for neurologically acting drugs. Therapeutic doses are often found as concentrated formulations of ≥50 mg/ml which could possibly aggregate. This poses a potential issue especially with regards to developing a peptide aggregation inhibitor that specifically targets pathogenically aggregating proteins such as Tau. Therefore, it is important when desgning a peptide aggregation inhibitor that they are sufficiently polar and hydrophilic to avoid self-association which may result in loss of activity, toxicity and seeding Tau aggregation. However, If the peptide is too polar and hydrophilic, it may lose binding affinity and specificity to its molecular target, and so a fine balance must be made to ensure solubility whilst retaining some aggregation-prone sequences on their surface (Sormanni et al., 2015).

4.1.3 TARGET SEQUENCE

Tau aggregation is largely facilitated by two hexapeptide motifs at the beginning of the second and third repeat domains of Tau which adopt β-sheet structure, namely [275]VQIINK[280] and [306]VQIVYK[311], respectively (Ganguly et al., 2015). Substituting either of these sequences renders Tau unable to assemble (Von Bergen et al., 2001). As these two sequences play a formidable role in Tau aggregation, they make excellent therapeutic targets to disrupt pathogenic activity. The importance of these hexapeptides originate from their capacity to conformationally change from unordered to β-sheet structure (Von Bergen et al., 2005; Murkrasch et al., 2005). Perez et al, (2007) demonstrated that deletion of [306]VQIVYK[311] in Tau prevents heparin induced aggregation and that incubating Tau with VQIVYK hexapeptide stimulates aggregation. The interaction of [306]VQIVYK[311] with [275]VQIINK[280] is believed to produce twisted PHF-like filaments (Von Bergen et al., 2000). 4R Tau includes both [306]VQIVYK[311] and [275]VQIINK[280] sequences, whereas 3R Tau only includes the [306]VQIVYK[311] sequence, therefore the latter may be a more suitable primary target. [306]VQIVYK[311] is situated on the carboxyl-terminal half of Tau and is mainly responsible for microtubule binding and pathological aggregation,

forming the core of PHF's (Jeganathan et al., 2008; Von Bergen et al.,2006; Lee et al., 1989). Meng et al., (2012) mentioned that recombinant 4R Tau fragment (specifically Tau$_{244-372}$) was unable to form fibrils when [306]VQIVYK[311] and [275]VQIINK[280] (included in 3R Tau) were deleted, suggesting their essential role in aggregation. This is supported by Ganguly et al., (2015) who concluded that [306]VQIVYK[311] has a greater propsensity of aggregation than [275]VQIINK[280] or mutant [275]VQIINK[280]ΔK280 and that heterodimers of [306]VQIVYK[311] and [275]VQIINK[280] were more stable than homodimers of [275]VQIINK[280]. This suggests the interaction between these two hexapeptides are important in Tau$_{441}$ aggregation. They also concluded that mutant [275]VQIINK[280]ΔK280 bound more strongly to [306]VQIVYK[311] than [275]VQIINK[280] and so suggested this as a possible mechanism for the pathological loss of normal Tau function. Mizushima et al., (2007), reported that the R3 peptide demonstrated the highest self-association ability whereas R2 peptide featured long lag times of 6 hours. Sawaya et al., (2007) conducted crystallographic studies of [306]VQIVYK[311] hexapeptides and concluded that they stack in parallel β-sheets whereby two mating sheets form a steric zipper by coming together with their hydrophobic side chains orientating inwards. Solid-state NMR and electron paramagnetic resonance studies also support this finding as well as that [275]VQIINK[280] can occupy parallel β-sheet or disordered arrangements (Daebel et al., 2012; Margittai and Langen, 2004). Zheng et al., (2011) used x-ray crystallography on the VQIVYK peptide (**Figure 4.1**) and identified that this peptide formed anti-parallel-layered parallel β-sheet structures. This structure interacted with other VQIVYK parallel β-
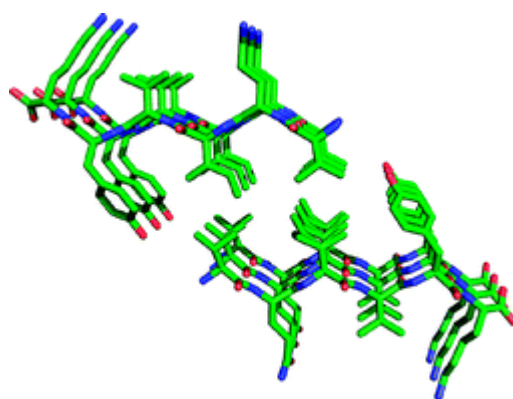
Figure 4.1: X-ray crystallographic structure of Tau derived VQIVYK peptide forming antiparallel-layered parallel β-sheets (Zheng et al., 2011).

sheets via edge-to-edge hydrogen bonding, face-to-face β-sheet layer interactions and in-register orientation and packing of side chains, particularly isoleucine and valine which form a hydrophobic core (Zheng et al., 2011). As Tau binds to microtubules via the four repeat domains it is important that the inhibitors do not interfere with the normal functioning of microtubules. It is suggested that taxol may outcompete Tau for binding sites on β-tubulin. Kar et al. (2003), nanogold labled a 4R-Tau repeat motif and observed that Tau bound on the inner surface of β-tubulin close to the taxol binding site, as seen in **Figure 4.2**.
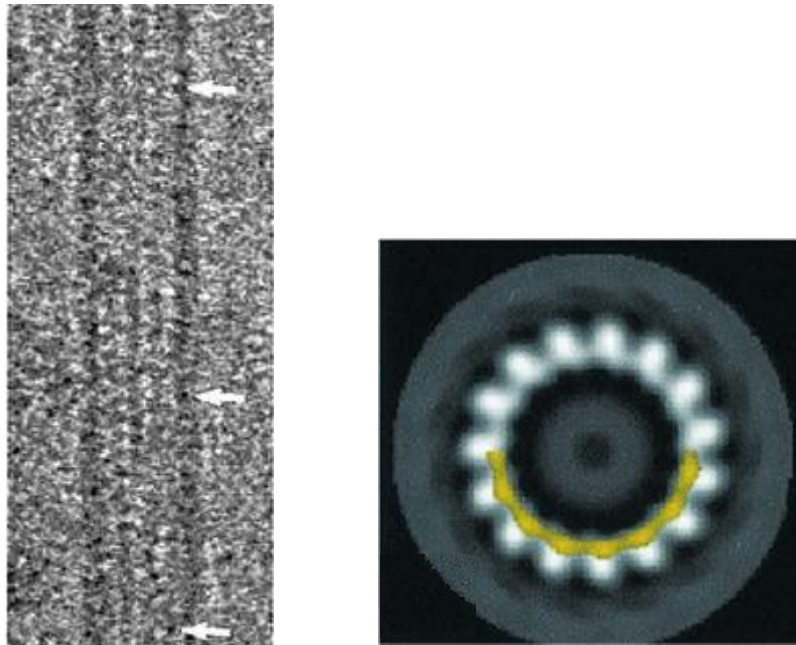
Figure 4.2: Tau binding to the inside of microtubules. **A:** EM image of a frozen hydrated microtubule with bound nanogold labelled 4R-Tau (indicated with arrows) **B:** Reconstructed end-on view of microtubule where tubulin is co-assembled with nanogold lebelled Tau (yellow). Notice that Tau is bound on the inside of the microtubule (Kar et al., 2003).

The binding energy within the repeats when bound to microtubules is delocalised through a series of weak interactions (affinity ~10^{-7}M) by three or four 18 amino acids, separated by 13-14 linker sequences which do not bind. This suggests that Tau exists flexibly on microtubules with the potential to migrate along the surface, however this flexible nature could suggest that Tau may be easily displaced (Butner and Kirschner, 1991). The low binding affinity of Tau to microtubules is also mentioned by Kar et al., (2003) who proposed that loops within the repeat motifs of bound Tau

stabilise microtubules with a low affinity so that assembly is reversible. These loops have the PGGG sequence similarity to the α-tubulin extended loop and binds to the same region inside microtubules where taxol (a known microtubule stabiliser) does on β-tubulin. Research done by Tsvetkov et al., (2012) agrees that there is a low affinity binding site for Tau to tubulin with a Tau:tubulin stoichiometry of 0.8, however, that there is also another binding site of high affinity with a Tau:tubulin stoichiometry of 0.2. It was suggested by Jho et al., (2010) that Tau repeat domains bind to microtubules via their net positive charge interacting with the negatively charged residues in tubulin monomers. As Kar et al., (2003) suggested that repeat motifs bind to the insides of microtubules and the N terminal projection runs along a protofilament on the outside of microtubules. This could suggest that peptide inhibitors specific to Tau repeat domain motifs may be less likely to interact with normal Tau within microtubules. Hyperphosphorylated Tau recruits Tau and aggregates, however normal Tau does not behave like this. Since Tau requires an inducer of some kind to initiate aggregation, normal Tau should not recruit and bind peptide inhibitors.

Kadavath et al., (2015) reported that the binding residues responsible for binding Tau to microtubules are also responsible for pathogenic aggregation of Tau; suggesting that physiological interaction competes with pathogenic misfolding. As a result, it is imperative that healthy functioning of Tau on microtubules is not hindered. As all repeats are reported to bind to microtubules this means that 3R and 4R Tau both bind to microtubules which indicates that the second repeat absent in 3R is not entirely necessary for this binding. This is supported by Kadavath et al., (2015) who suggested that 3R and 4R isoforms use similar mechanisms to bind to microtubules based on similar signal broadening profiles. Although, R4 Tau is reported to bind much more strongly to microtubules, with great importance at the lysine residue in VQIINK which is suggested to be one three most critical lysine residues responsible for interactions with microtubules. Acetylation at this position impaired microtubule interaction and increased cytosolic Tau (Mietelska-Porowska et al., 2014). Deletion of this residue causes Tau to aggregate, even without the presence of a polyanionic inducer. Developing a peptide inhibitor which interferes with lysine$_{280}$ may be detrimental. Mietelska-Porowska et al., (2014)

and Mukrasch et al. (2007), stated that the important Tau residues for microtubule interaction include [240]KSRLQTAPV[248], [275]VQINKKLDLS[285], [297]IKHV[300], [225]KVAVVRT[231] and [370]KIETHK[375]. Kadavath et al., (2015) stated that protofilaments are stabilised by Tau binding to hydrophobic pockets between α-β-tubulin heterodimers potentially due to an allosteric mechanism. Flexible regions in between the repeat domains of Tau may suggest a dynamic mode of binding to the same α-tubulin molecule and that VQIINK may be responsible for this. As a result, VQIVYK which is present in all Tau isoforms may be a more suitable target. Using multiscale molecular dynamics simulations, Xu et al., (2016) noted that in a phosphorylated environment the domain movements in the filament core become more exposed to the solvent environment, especially the third and second repeats, as seen in **Figure 4.3**. VQIVYK and VQIINK are found in these repeat domains, respectively. This means that in an AD brain which is largely phosphorylated, these sequences would be suitable therapeutic targets. **Figure 4.3** demonstrates these regions in un-phosphorylated Tau are not exposed to the solvent environment which may lead to the possibility of un-phosphorylated Tau being unaffected by the peptide inhibitors. This research will design peptide aggregation inhibitors to target the [306]VQIVYK[311] and [275]VQIINK[280] sequences of Tau.
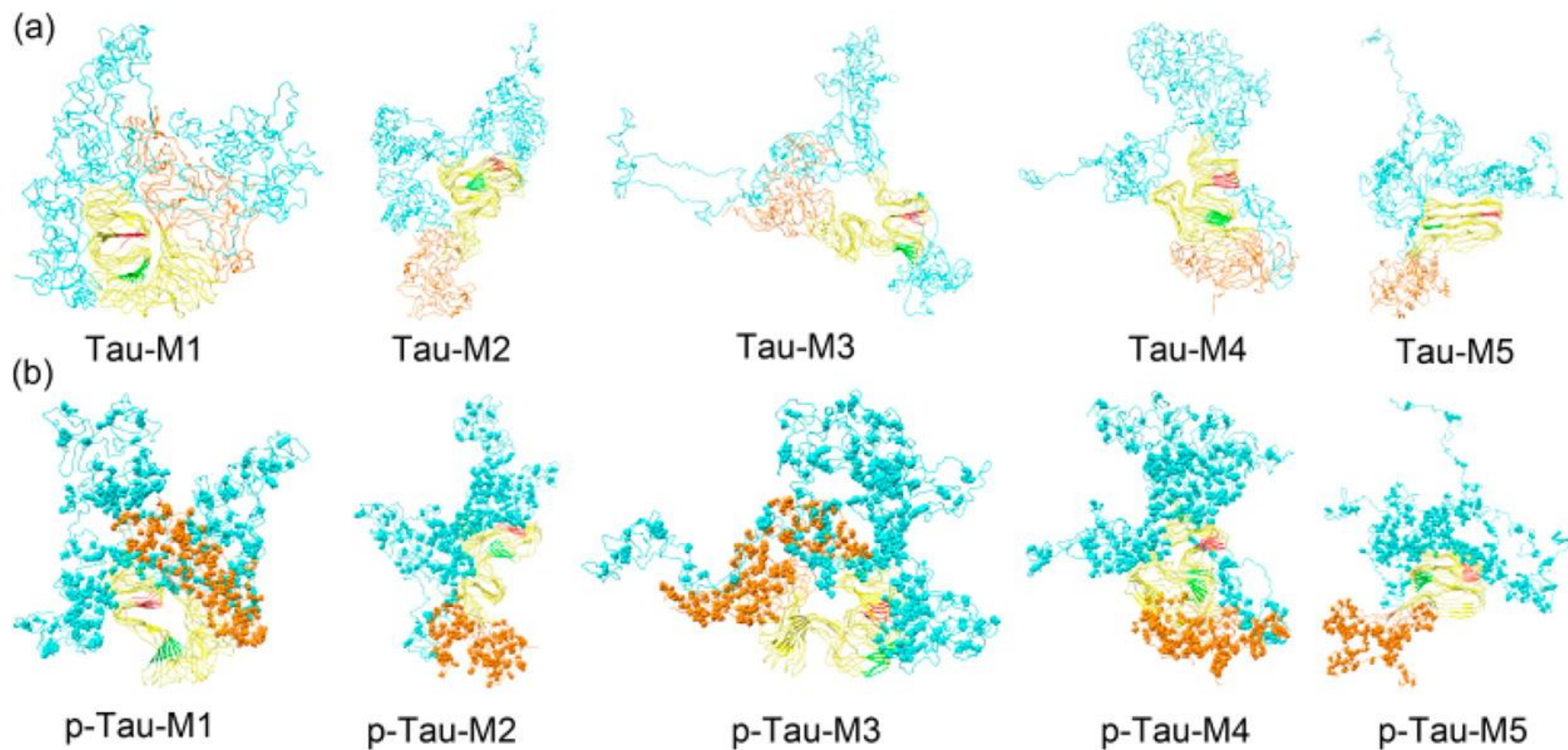
Figure 4.3: Represents conformations for different normal (a) and hyper-phosphorylated (b) Tau filaments. Tau filament N-terminus, repeat domain, and C-terminus are shown in cyan, yellow, and orange, respectively. 275VQIINK280 and 306VQIVYK311 represented as red and green, respectively (Xu et al., 2015).

4.1.4 DESIGN

Tau will generally interact with itself at [306]VQIVYK[311] and [275]VQIINK[280] as discussed in **Section 4.1.3**. These targets are useful to manipulate self-association propensity. By generating a clone clone of these sequences, they can potentially cap this self-association by preventing Tau from binding on top or by altering the aggregation pathway in an off-pathway manner. As the peptide inhibitor binding sequence represents an internal portion of the Tau amino acid sequence it is important to acetylate and amidate the inhibitors N and C-terminus, respectively. This removes the positive charge on the N-terminal and neutralises the C-terminal. This blocks both ends of the inhibitor, preventing potential unnatural introduction of charged groups which do not exist in the native complementary sequence, thereby increasing the likelihood of the inhibitor being recognised by its complementary sequence. Capping the N and C-terminus also provides the inhibitor with additional resistances to exopeptidases which is important for a potential therapeutic (Kim and Seong, 2001). Acetylation and amidation of the N and C-terminal reduces the peptide solubility, therefore additional measures must be employed to ensure solubility remains viable. C-terminal amidation is also reported by Matharu et al. (2010), to increase the activity in preventing oligomer formation. Flanking the peptide binding sequence with spacers such as glycine may improve the peptide binding ability by distancing other potentially interfering amino acids, such as cell penetrating sequences, which are necessary as Tau aggregates form intracellularly. Other important amino acids include proline which are natural β-sheet breakers and provides rigidity to the structure. Eisenberg and Sawaya (2017), highlighted that amyloid steric zippers (previously discussed in **Section1.4.4**) share common features (**Figure 4.4**) including 1) hydrogen bonding of dipolar amide N-H and C=O groups which stack β-strands together with 4.8 A° spacing, 2) hydrogen bond ladders can be formed between layers of the β-strands via amides located in glutamine and asparginine side chains, 3) tyrosine, serine and threnonine can also form hydrogen bond ladders, 4) paired sheets are almost completely devoid of water, save for a few hydrogen bonds between them. This kind of information can be utilised to develop a peptide inhibitor which can interfere in these important processes in order to prevent aggregation. This research will investigate

altering the properties of the inhibitor through addition of hydrophilic and polar molecules, acetylation and using glycine spacers, to make sure the inhibitor does not self aggregate and to improve its inhibitory properties.
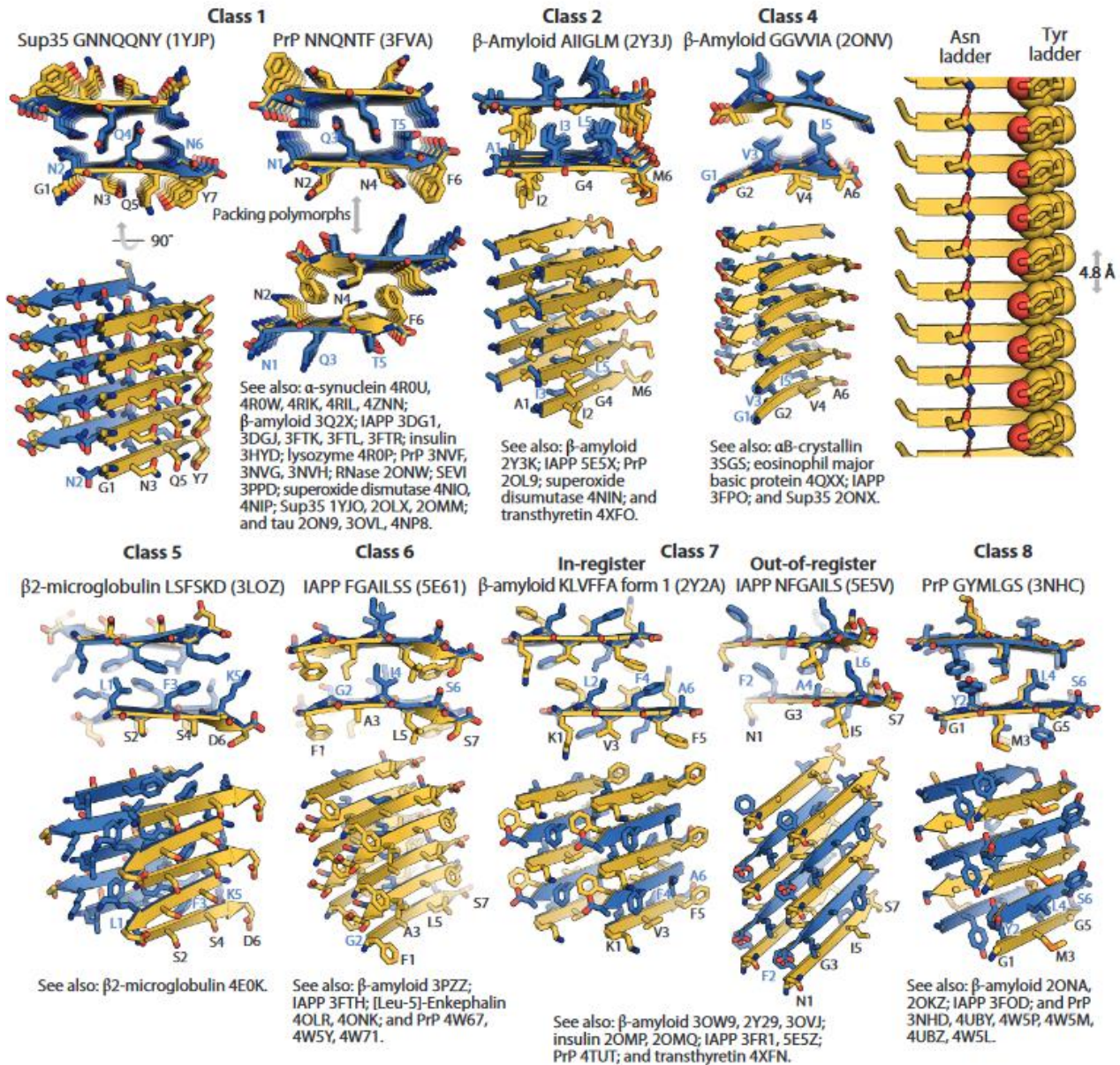
Figure 4.4: Represents a selection of published amyloid steric zipper crystal structures both parallel and perpendicular to their fibril axes. The face and back of each strand are coloured blue and gold, respectively. Also demonstrates the organisation of steric zippers into separate symetry classes depending on orientation the two sheets of each zipper. Asparagine and tyrosine hydrogen bond ladders from GNNQQNY with 4.8 A˚ spacing are visualised in the top right illustration (Eisenberg and Sawaya, 2017).

4.1.5 ICM-PRO DOCKING

Molecular docking is a powerful tool for structure-based drug design and accurately predicting potential interactions between novel ligands (either small molecules or peptides) and receptors (Neves et al., 2019). The third part of this chapter aimed at using ICM-Pro to assist in designing peptide aggregation inhibitors by assessing their binding behaviour to their target protein.

ICM-Pro uses five interaction potentials to represent a receptor pocket, including van der Waals potential for heavy atom probe (generic carbon of 1.7 Å radius), wan der Waals potential for hydrogen atom probe, optimised electrostatic term, hydrophobic term and loan pair based potential reflecting hydrogen bonding directional preferences. The energy terms calculated are based on the all-atom vaccum force field ECEPP/3 which is specific for peptides and proteins and conducts energy minimisations including hydrogen bond potentials, torsion potentials additional terms to quantify solvation free energy and entropic contributions (Molsoft, 2019; Shaumann et al., 1990). These force fields are parameters utilised to calculate the potential energy of atoms in molecular dynamics simulations and are derived from experimental data. "All-atom" refers to the provision of parameters for all types of atoms within a system. The biased probability Monte Carlo procedure randomly and continuously sample different binding comformations and globally optimises ligand coordinates within the grid potential maps space (Abagyan and Totrov, 1994).

First random moves are introduced to one of the ligands rotational, translational or conformational variables, then energy function terms are minimised and desolvation energy is calculated (Neves et al., 2012). These random moves to the ligand are regulated by the Metropolis selection criterion algorithm which determines if final minimised conformations are accepted or rejected based on if they meet favourable energy conditions (Metropolis et al., 1953). These processes are repeated until the maximum number of conformations are sampled. Conformations are ranked based on their ICM-score which is calculated and weighted according to the ligands internal force-field energy, ligand loss of entropy between bound/unbound states, hydrogen bond interactions between the ligand and

receptor, polarity solvation energy differences between bound/unbound states, electrostatic energy, hydrophobic energy and hydrogen bond desolvation (Arthur et al., 2019). This is discussed in further detail by Neves et al. (2012).

Molecular docking simulations will provide informed guidance on where to begin when designing peptide-based aggregation inhibitors for Tau. The information provided includes the predicted binding potential for peptides towards their target and if the peptides interact with themselves. If the peptides have high interaction together, they could potentially seed aggregation which is undesirable. Predictions based on the results in this chapter provided indications for which amino acid sequence to target in Tau and which peptide inhibitor amino sequences may bind and inhibit aggregation. This approach provided some evidence-based direction on which peptides may work. This process saved money in the wet lab by filtering out peptides that were predicted to be unsuitable aggregation inhibitors. Evidence of potentially successful inhibitors were taken forward into the following chapter to be tested in the wet lab. ICM-Pro does not use confidence scores, the peptides are ranked by their ICM-score corresponding to their energy.

4.2 RESULTS

4.2.1 IDENTIFYING "HOT SPOT" SEQUENCE IN TAU

When developing peptide-based therapeutics against pathogenic proteins such as Tau for AD, it is important to identify sequences which contribute to pathogenic behaviour. Once these are known they can then be targeted in order to inhibit pathogenic behaviour. **Figures 4.5** and **4.6** aimed to identify chief motifs responsible for Tau aggregation.

In simple words the Camsol algorithm investigates the instrinsic solubility of peptides by assessing hydrophobicity, charge at neutral pH, α-helic propensity and β-strand propensity over a window of seven amino acids. The Aggrescan algorithm however, investigates the aggregation propensity of peptides based on previous experimental data, over several windows (5 for < 75 residues, 7 for < 175 residues, 9 for < 300 residues, and 11 for > 300 residues). By adapting these algorithms they can be used to predict a peptides behaviour with regards to target binding and aggregation. Hydrophobic interactions play a key role in aggregation. Camsol was used to investigate potential hydrophobic targets in Tau_{441}. VQIVYK was the only hexapeptide highlighted as exceptionally hydrophobic, as seen in **Figure 4.5.** Aggrescan was used to investigate potential aggregation hot spot targets in Tau_{441} and highlighted VQIVYK as the only hexapeptide above the aggregation hot spot threshold as seen in **Figure 4.6.** VQIINK and VQIVYK were chosen as suitable targets to take forward as potential targets. Although VQIINK did not come up as particularly hydrophobic in **Figure 4.5**, it did slightly peak over the aggregation hot spot threshold in **Figure 4.6.** In addition, the hexapeptide itself is touted in literature to have crucial involvement in Tau aggregation, therefore it was deemed a worthy target to investigate further.
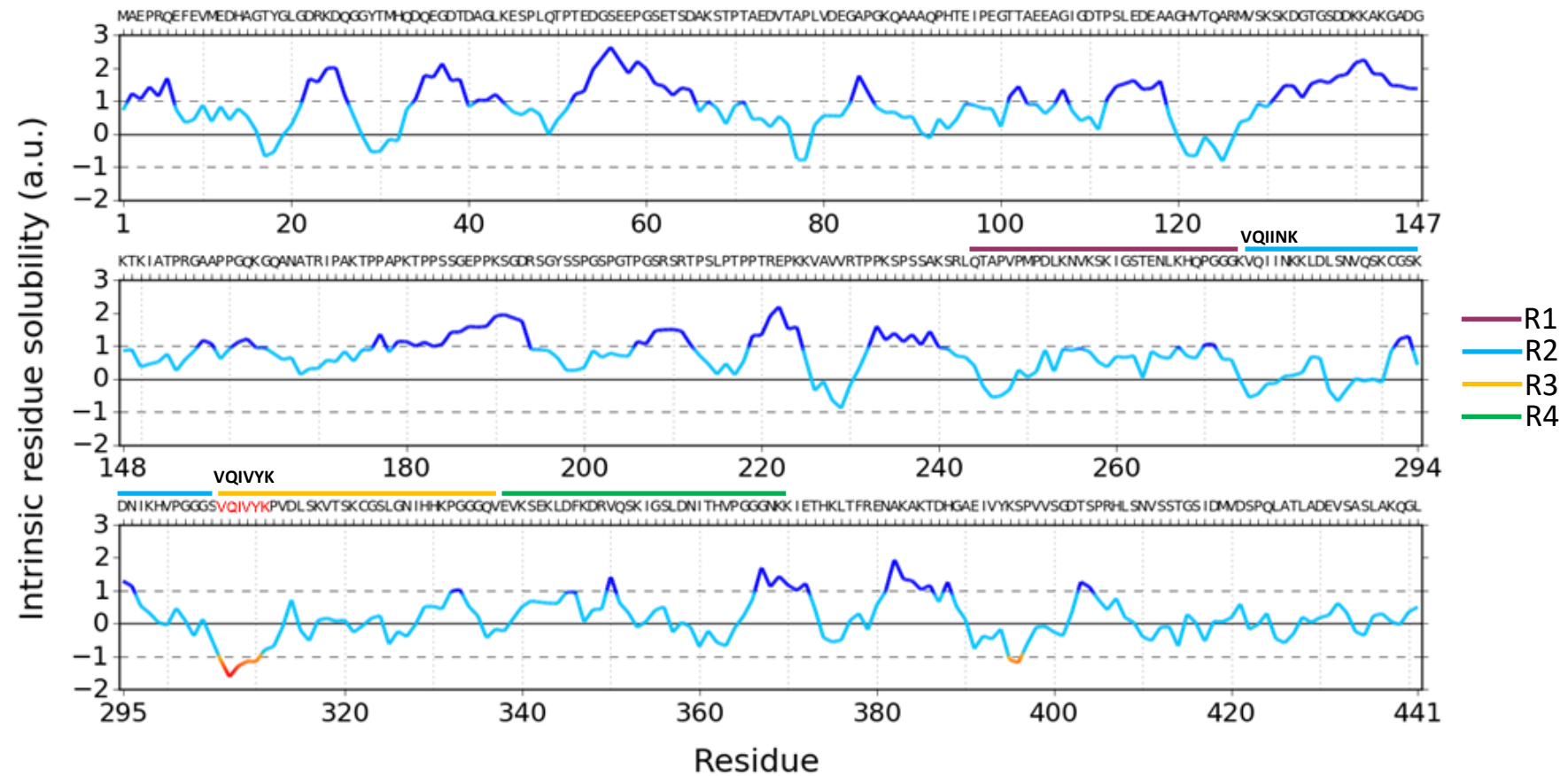
Figure 4.5: Intrinsic residue solubility values for Tau$_{441}$ residues using CamSol. Note that VQIVYK contains hydrophobic residues (V and I) and the hexapeptide flags as an aggregation hot spot. Repeats 1-4 are highlighted in purple, blue, yellow and green, respectively. Repeats 1-4 are highlighted in purple, blue, yellow and green, respectively. The blue line regions indicate soluble regions, whereas the red line regions indicate low solubility regions.
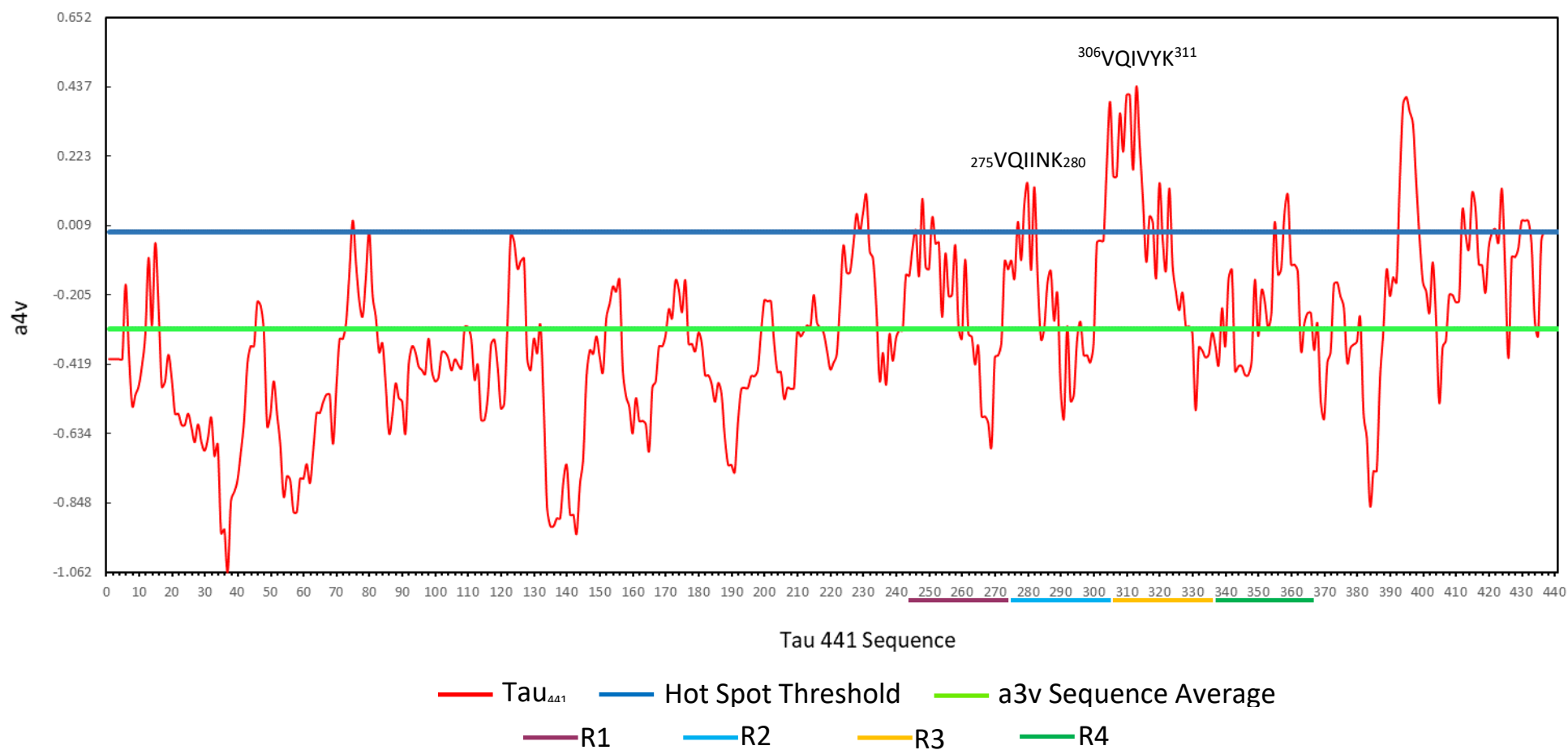
Figure 4.6: Average aggregation propensity values for Tau$_{441}$ residues using AGGRESCAN. Note that the hexapeptide VQIVYK massively surpasses the hot spot threshold. Repeats 1-4 are highlighted in purple, blue, yellow and green, respectively. Hexapeptides above the blue hot spot threshold are considered aggregation hot spot sequences (high propensity to aggregate).

4.2.2 DESIGNING PEPTIDE INHIBITORS

Using the chosen targets from **Section 4.2.1**, the second part of this results chapter aimed to design and evolve a suitable peptide which can successfully bind to its target (which in humans is intracellular) and in addition to also inhibit Tau aggregation.

As hexapeptides VQIINK and VQIVYK both form fibrils it was important to make changes to their sequence to prevent them from being able to seed aggregation. **Tables 4.1** and **4.2** demonstrate the exhaustive mutagenesis of the second isoleucine in VQIINK and the second valine in VQIVYK and predicts their aggregation propensity using Aggrescan. The native hexapeptide sequences are used as reference points and are located on the far-right hand column.

The rationale behind choosing these sites are thus: The intention was to reduce the aggregation propensity of the peptide inhibitor so to avoid potential self-association whilst also maintaining target specificity. Since VQIINK and VQIVYK both have VQIxxK motifs, these were left unchanged as they are useful reference sequences for the inhibitor to bind to Tau with. For VQIVYK the tyrosine residue was not chosen for mutagenesis because as an aromatic amino acid it is a useful as an anchoring residue through aromatic stacking interactions. For these reasons the original hexapeptide could not be altered too much to avoid risking loss of target specificity. As hydrophobic amino acids have great influence in increasing aggregation propensity, the hydrophobic amino acids in the centre of each hexapeptide were investigated.

The optimal amino acid replacement for the second isoleucine in VQIINK (**Table 4.1**) and the second valine in VQIVYK (**Table 4.2**) was lysine, in both instances. This hydrophilic amino acid lowered the average aggregation propensity. Not too little that the average aggregation propensity was still too high, nor not so much that the peptide would lose affinity to its target site in Tau. It lowered it to just below the hot spot threshold. Histidine was rejected as a replacement for valine as its hydrophobicity matched the native VQIVYK.

Residue substitution	A	C	G	V	L	M	F	S	T	W	Y		VQIVYK
a3v Sequence Average (a3vSA):	0.358	0.465	0.275	0.630	0.594	0.516	0.656	0.315	0.338	0.537	0.557		**0.668**
Number of Hot Spots (#HS):	1	1	0	1	1	1	1	1	1	1	1		**1**
Normalized #HS for 100 residues:	16.667	16.667	0.000	16.667	16.667	16.667	16.667	16.667	16.667	16.667	16.667		**16.667**
Area of the profile Above Threshold (AAT):	1.286	2.118	0.688	3.405	3.127	2.516	3.613	0.951	1.126	2.681	2.839		**3.701**
Total Hot Spot Area:	1.286	2.118	0	3.405	3.127	2.516	3.613	0.951	1.126	2.681	2.839		**3.701**
Total Area:	1.126	1.766	0.627	2.756	2.542	2.072	2.916	0.868	1.003	2.199	2.321		**2.984**
AAT per residue:	0.214	0.353	0.115	0.568	0.521	0.419	0.602	0.159	0.188	0.447	0.473		**0.617**
THSA per residue:	0.214	0.353	0	0.568	0.521	0.419	0.602	0.159	0.188	0.447	0.473		**0.617**
Normalized a4v Sequence Sum for 100 residues (Na4vSS):	18.8	31.6	8.8	51.4	47.1	37.7	54.6	13.6	16.3	40.2	42.7		**55.9**

Residue substitution	R	N	D	Q	E	H	K	P		VQIVYK
a3v Sequence Average (a3vSA):	0.158	0.147	0.058	0.159	0.129	0.192	**0.209**	0.309		**0.668**
Number of Hot Spots (#HS):	0	0	0	0	0	0	**0**	0		**1**
Normalized #HS for 100 residues:	0	0	0	0	0	0	**0**	0		**16.667**
Area of the profile Above Threshold (AAT):	0.395	0.383	0.276	0.397	0.361	0.437	**0.457**	0.322		**3.701**
Total Hot Spot Area:	0	0	0	0	0	0	**0**	0		**3.701**
Total Area:	-0.078	-0.140	-0.674	-0.069	-0.250	0.129	**0.231**	0.828		**2.984**
AAT per residue:	0.066	0.064	0.046	0.066	0.060	0.073	**0.076**	0.054		**0.617**
THSA per residue:	0	0	0	0	0	0	**0**	0		**0.617**
Normalized a4v Sequence Sum for 100 residues (Na4vSS):	-5.3	-6.5	-17.2	-5.1	-8.7	-1.2	**0.9**	12.8		**55.9**

Table 4.1: Average aggregation propensity value VQxVYK where x is consecutively replaced with every amino acid. **A:** aggregatory residues, **B:** non-aggregatory residue Note the replacement of isoleucine massively reduces the aggregation propensity. Residues coloured red, blue and black are hydrophobic, hydrophilic or neutral, respectively.

Residue substitution	A	C	G	I	L	M	F	S	T	W	Y		VQIVYK
a3v Sequence Average (a3vSA):	0.396	0.503	0.313	0.706	0.632	0.554	0.694	0.353	0.376	0.575	0.595		**0.668**
Number of Hot Spots (#HS):	1	1	1	1	1	1	1	1	1	1	1		**1**
Normalized #HS for 100 residues:	16.667	16.667	16.667	16.667	16.667	16.667	16.667	16.667	16.667	16.667	16.667		**16.667**
Area of the profile Above Threshold (AAT):	1.582	2.414	0.934	3.998	3.423	2.812	3.909	1.247	1.422	2.977	3.136		**3.701**
Total Hot Spot Area:	1.582	2.414	0.934	3.998	3.423	2.812	3.909	1.247	1.422	2.977	3.136		**3.701**
Total Area:	1.354	1.994	0.855	3.212	2.770	2.300	3.144	1.096	1.231	2.427	2.549		**2.984**
AAT per residue:	0.264	0.402	0.156	0.666	0.571	0.469	0.651	0.208	0.237	0.496	0.523		**0.617**
THSA per residue:	0.264	0.402	0.156	0.666	0.571	0.469	0.651	0.208	0.237	0.496	0.523		**0.617**
Normalized a4v Sequence Sum for 100 residues (Na4vSS):	23.3	36.1	13.4	60.5	51.7	42.3	59.1	18.2	20.9	44.8	47.2		**55.9**

Residue substitution	R	N	D	Q	E	G	H	K	P		VQIVYK
a3v Sequence Average (a3vSA):	0.196	0.185	0.096	0.197	0.167	0.313	0.230	**0.247**	0.347		**0.668**
Number #HS:	0	0	0	0	0	1	0	**0**	0		**1**
Normalized #HS for 100 residues:	0	0	0	0	0	16.667	0	**0**	0		**16.667**
Area of the profile Above Threshold (AAT):	0.441	0.428	0.322	0.443	0.406	0.934	0.495	**0.556**	1.078		**3.701**
Total Hot Spot Area:	0	0	0	0	0	0.934	0	**0**	0		**3.701**
Total Area:	0.150	0.088	-0.446	0.159	-0.022	0.855	0.357	**0.459**	1.056		**2.984**
AAT per residue:	0.073	0.071	0.054	0.074	0.068	0.156	0.083	**0.093**	0.180		**0.617**
THSA per residue:	0	0	0	0	0	0.156	0	**0**	0		**0.617**
Normalized a4v Sequence Sum for 100 residues (Na4vSS):	-0.7	-2.0	-12.7	-0.6	-4.2	13.4	3.4	**5.4**	17.4		**55.9**

Table 4.2: Average aggregation propensity value VQIxYK where x is consecutively replaced with every amino acid. **A:** aggregatory residues, **B:** non-aggregatory residues. Note the replacement of valine massively reduces the aggregation propensity. Residues coloured red, blue and black are hydrophobic, hydrophilic or neutral, respectively.

Figures 4.7 and 4.8 represent the aggregation propensity and intrinsic residue solubility, respectively, for each of the following peptides: VQIVYK, VQI**H**YK, VQI**K**YK and VQ**K**VYK. In **Figure 4.7** VQI**H**YK, VQI**K**YK and VQ**K**VYK were well under the hot spot threshold which VQIVYK exceeded. Although in **Table 4.2** histidine generated a similar aggregation propensity value to lysine; VQI**H**YK was rejected for further investigation based on **Figure 4.8** as it had the same intrinsic solubility score as native VQIVYK. VQI**K**YK retained a degree of insolubility unlike VQ**K**VYK which reported to be very soluble.
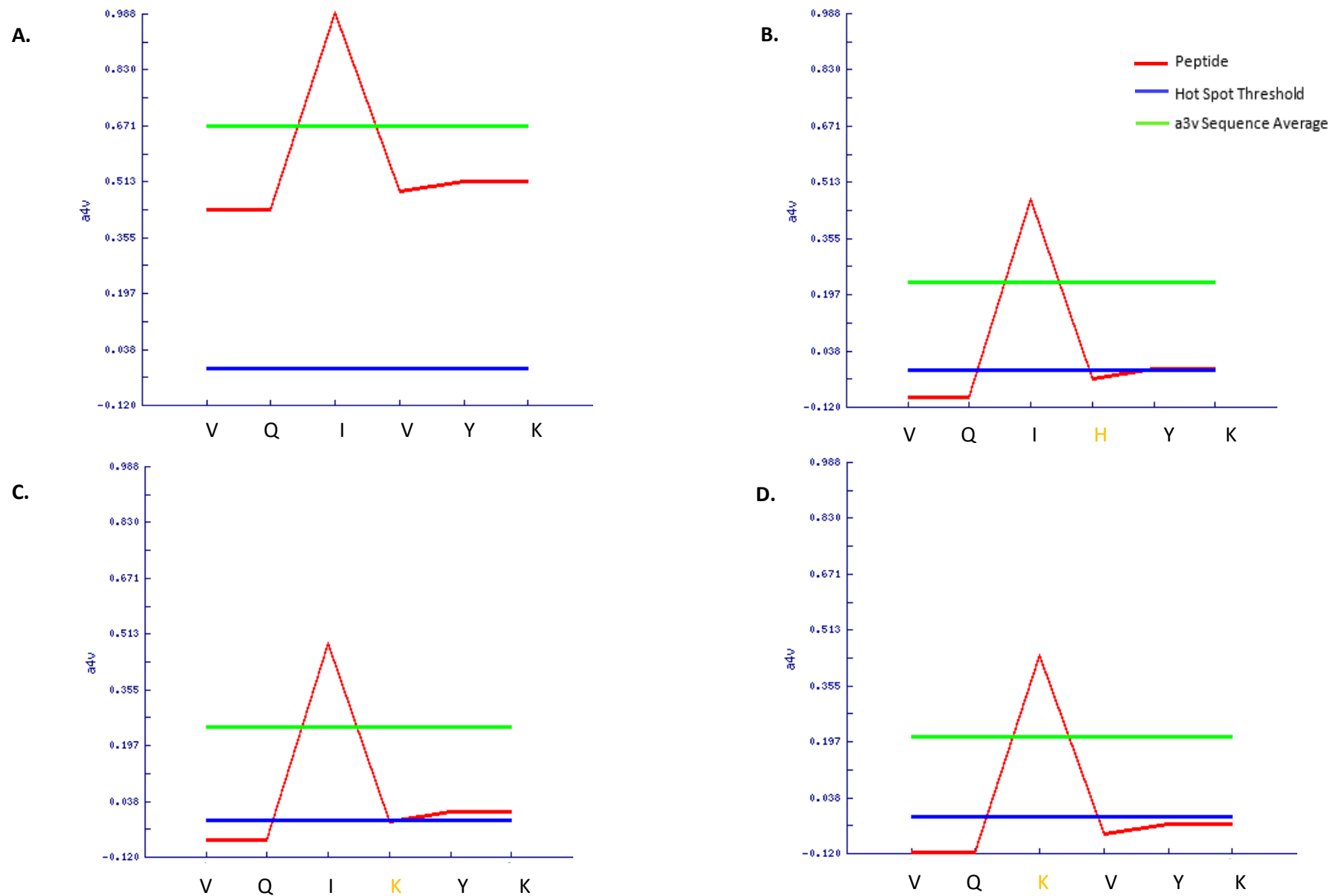
Figure 4.7: Aggrescan calculations for the average aggregation propensity value for Tau residues 301-315. Residues highlighted in orange are mutated; **A:** Native VQIVYK; **B:** VQIHYK; **C:** VQIKYK; **D:** VQKVYK. Note the replacement of either isoleucine or valine reduces the aggregation propensity.
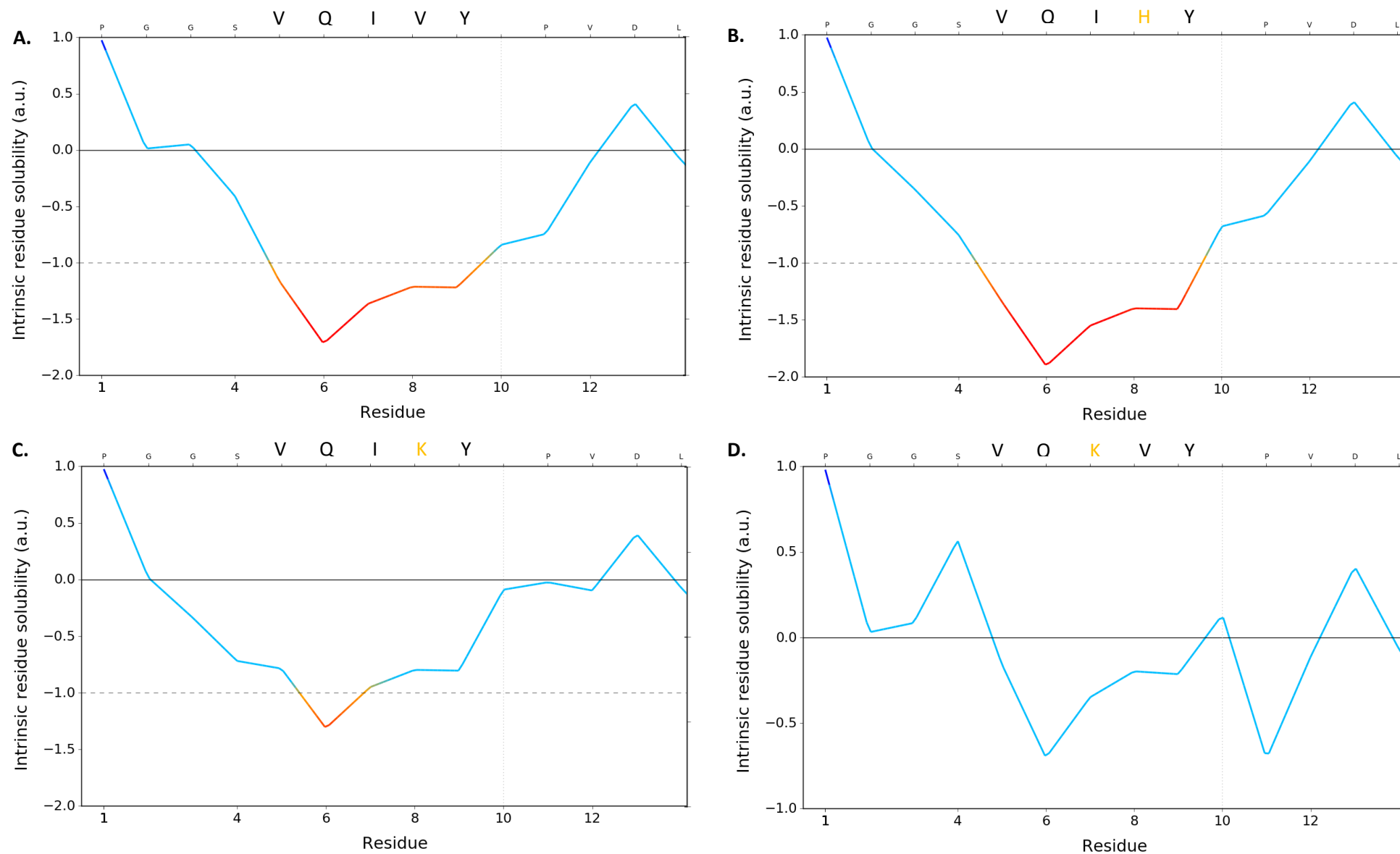
Figure 4.8: CamSol calculations of the Intrinsic residue solubility for Tau residues 301-315. Residues highlighted in orange are mutated. **A:** Native VQIVYK; **B:** VQI**H**YK; **C:** VQI**K**YK; **D:** VQ**K**VYK. Note the importance of isoleucine rather than valine for intrinsic solubility within the VQIVYK

4.2.3 ACETYLLYSINE

Figure 4.9. demonstrated that the circled regions indicating the [306]VQIVYK[311] sequence are rich in hydrogen bond acceptors. By acetylating the substituted lysine in the peptide inhibitor [Ac-VQI**K**YK-NH2], this lysine residue becomes a hydrogen bond donor and it may promote interaction with [306]VQIVYK[311] (circled), which has many hydrogen bond acceptors. Heparin predominantly has hydrogen acceptor sites, and it was also predicted that heparin would likely bind to the hydrogen bond donor sites in the centre and the outside of the protofilaments.

Paired Helical Filament   **Straight Filament**
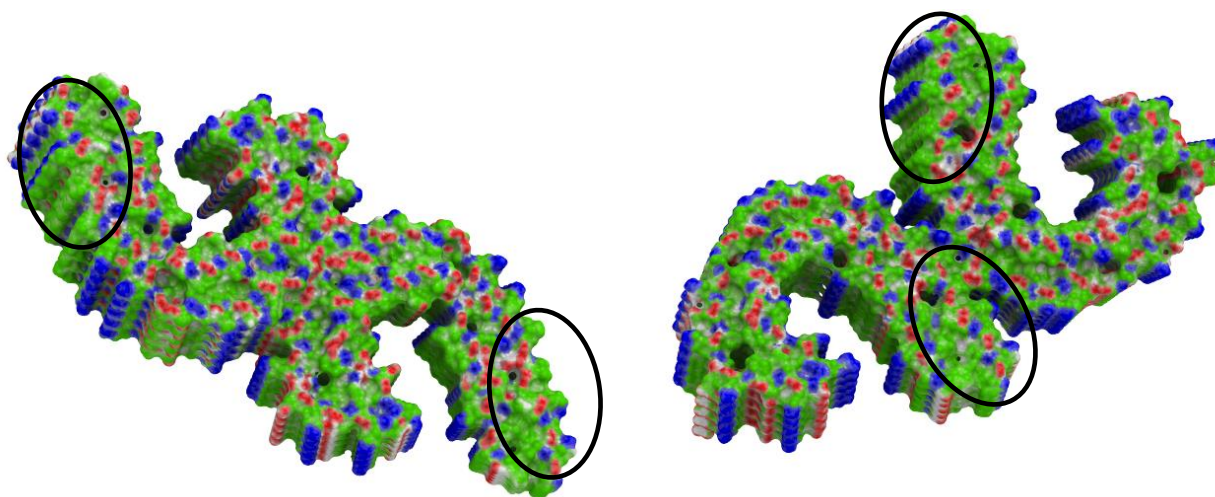
Figure 4.9: Binding properties of PDB 5o3l PHF and PDB 5o3t SF, including hydrophobic areas (green), hydrogen bond acceptor potential (red) and hydrogen bond donor potential (blue). VQIVYK sequences are circled in black. This figure demonstrates that the outside of Tau consists mainly of hydrogen bonding donors whereas perpendicular to the fibril axis of Tau are mainly hydrogen bonding acceptors.

4.2.4 OPTIMAL DOCKING AREA (ODA) FOR INHIBITORS

Peptide inhibitors were named to help quickly identify their features in the lab. The following three nomenclature refer to their peptide binding residues: AG02 corresponds with [RG-VQIVYK-GR], AG02ΔI corresponds with [RG-VQ**K(Ac)**VYK-GR] and AG02ΔV corresponds with [RG-VQI**K(Ac)**YK-GR].

Figure 4.10 was used to predict sites on the following peptides which were likely for protein-protein interactions. This was useful to identify important recognition and binding residues for the peptide inhibitors AG02 [RG-VQIVYK-GR], AG02ΔI [RG-VQ**K(Ac)**VYK-GR] and AG02ΔV [RG-VQI**K(Ac)**YK-GR]. Position 5 and 7 (from left to right) on these sequences play an important role in binding. In the native peptide, position 5 and 7 entails isoleucine and tyrosine, respectively. This confirmed the choice of keeping isoleucine which is important in native binding and to keep tyrosine which can act as an anchoring molecule via aromatic stacking. The preferred mutation around these bases of interactions to modulate hydrophobic interactions was AG02ΔV [RG-VQI**K(Ac)**YK-GR].

AG02:

[RG-VQIVYK-GR]
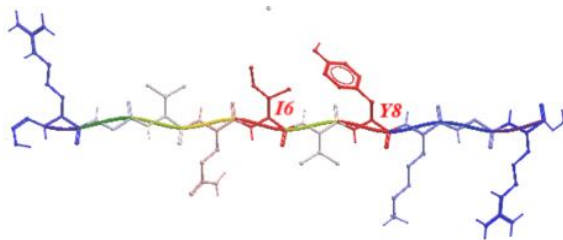
AG02ΔI:
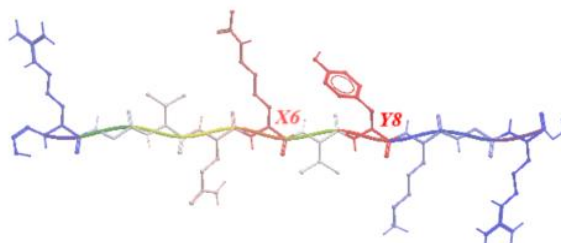
[RG-VQK(Ac)VYK-GR]

AG02ΔV:

[RG-VQIK(Ac)YK-GR]
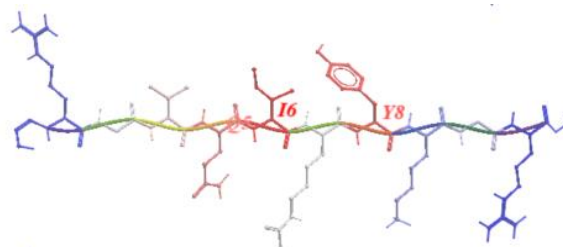
Figure 4.10: Optimal docking areas for 1) AG02 [RG-VQIVYK-GR] which includes I6 and Y8, 2) AG02ΔI [RG-VQK(Ac)VYK-GR] which includes X6 and Y8 (X6 denotes acetyllysine), 3) AG02ΔV [RG-VQIK(Ac)YK-GR] which includes Q7, I6 and Y8. Notice I6 and Y8 are important binding molecules for these peptides. X6 denotes acetyllysine.

AG02ΔI [RG-VQ**K(Ac)**VYK-GR] and AG02ΔV [RG-VQI**K(Ac)**YK-GR] were docked onto copies of themselves to see how strongly they interact with themselves. **Table 4.3** demonstrated that AG02ΔI associated with itself much more strongly than AG02ΔV did. From this it was predicted that AG02ΔV would be a more suitable inhibitor as there was less likelihood of it self-associating.

Ligand	Self Association of peptides					
	ICM Score	H Bond Score	Hydrophobicity	Van der Waals	Eintl	Dsolv
AG02ΔI	-34.24	-8.26	-7.02	-48.46	20.76	4.01
AG02ΔV	-24.07	-7.62	-5.96	-47.87	25.36	4.78

Table 4.3: Triplicate average of computationally calculated values describing self-association properties of AG02ΔI and AG02ΔV. **ICM score** of < -32 suggests a strong bind; **Natom** denotes the number of atoms in the docked ligand; **Nflex** denotes the number of rotatable torsions; **Hbond** denotes hydrogen bond energy; **Hphob** denotes hydrophobic energy to expose a surface to water; **VwInt** denotes strong van der Waals interaction energy (< 0); **Eintl** denotes strong ligand internal conformation energy (< 0); **Dsolv** denotes desolvation of exposed hydrogen bond donors and acceptors; **SolEl** denotes solvation electrostatics energy change upon binding; **mfScore** denotes potential of average force score; **dTSc** denotes loss of entropy via rotatable side-chains.

4.2.5 ASSESSING PDB STRUCTURE QUALITY

Before docking simulations were conducted it was advised to test the quality of the PDB structure in case there are errors e.g. incomplete data. This supported an informed decision approach when subsequently conducting docking experiments by providing evidence based confidence into the decisions being made. The QMEAN of PDB structures were scored to describe the local geometry over 3 consecutive amino acids, long range residues interactions, residues burial status, solvent accessibility and predicted/calculated secondary structure. These scorings are then compared to an ensemble of alternative models in order to select the best model (Benkert et al., 2008). **Figure 4.11** did not pass the minimum score of -5.00, however **Figures 4.12**, **4.13** did and were taken forward for docking experiments.

5o3t SF.pdb - QMEAN4 Value: -5.12

A.

B.

C.
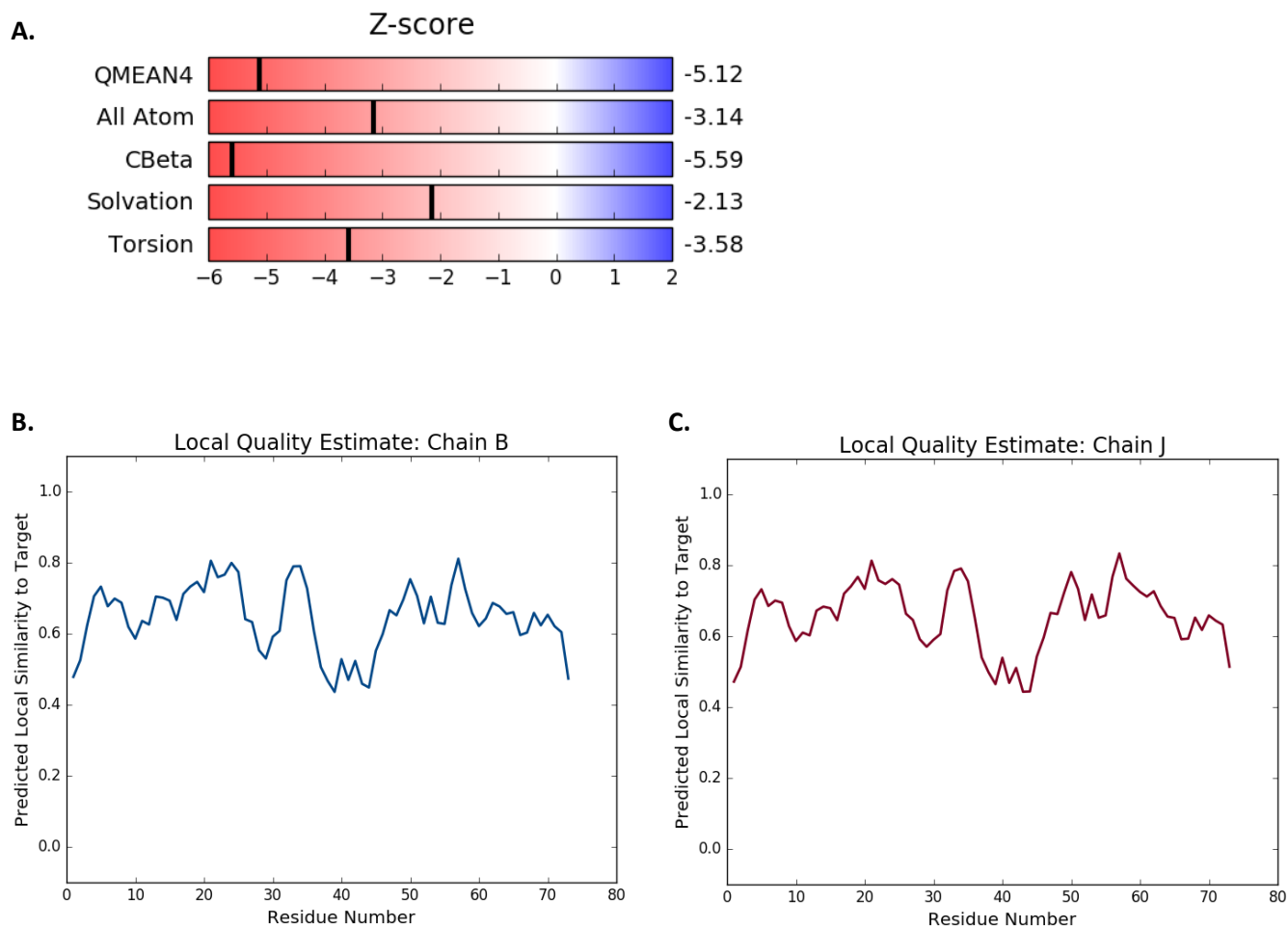
Figure 4.11: Predicted structure quality of PDB 5o3t SF. **A:** QMEAN4 score was less than -5 (-5.12) and deemed unsuitable for further computational analysis. **B-C**: Predicted local similarity to target was below 0.6 suggesting low local quality scores.
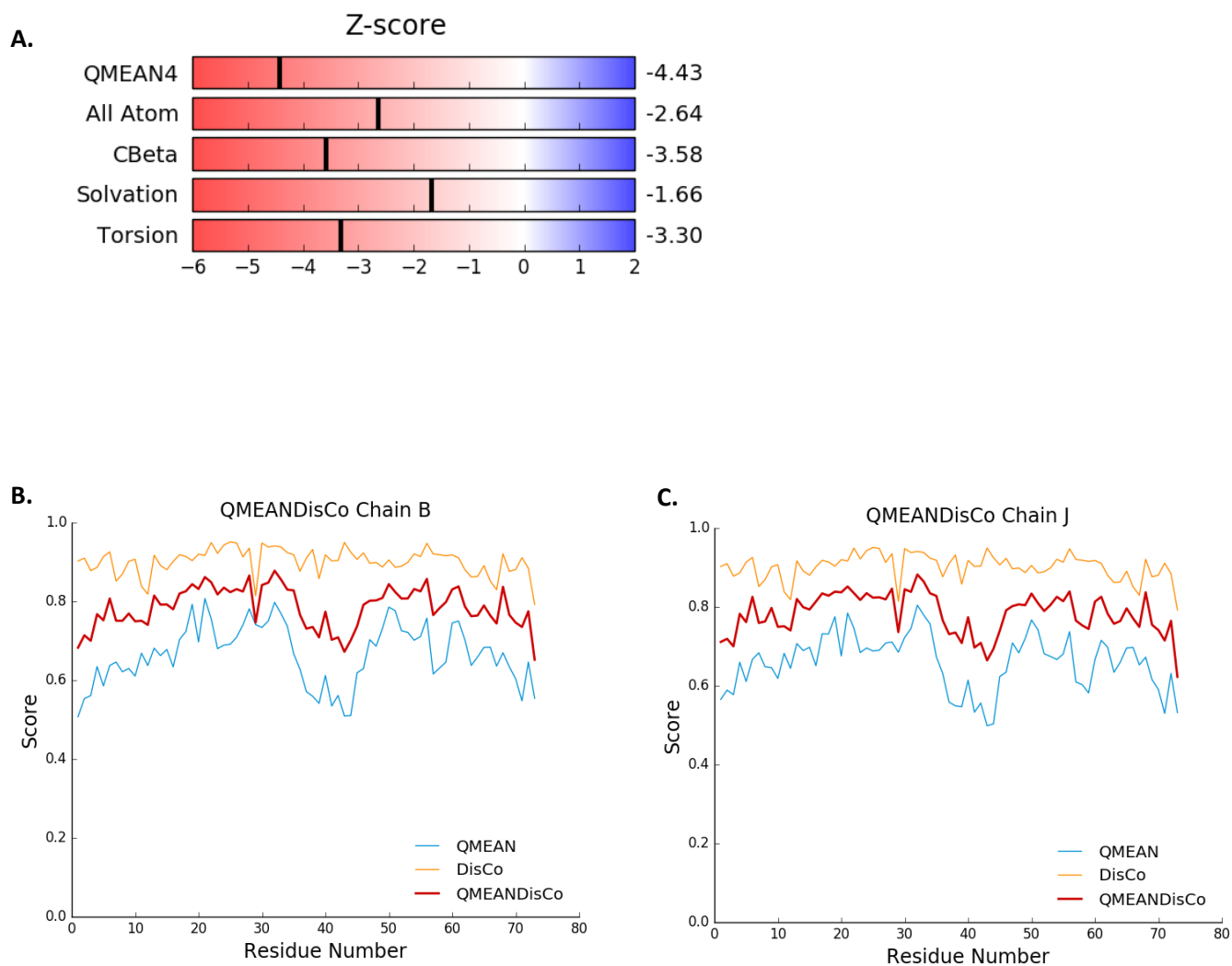
Figure 4.12: Predicted structure quality of PDB 5o3l PHF. **A:** QMEAN4 score was greater than -5 (-4.43) and deemed suitable for further computational analysis. Scores less than -0.4 suggest global models of low quality. **B-C**: Predicted local similarity to target was above 0.6 suggesting high local quality scores.
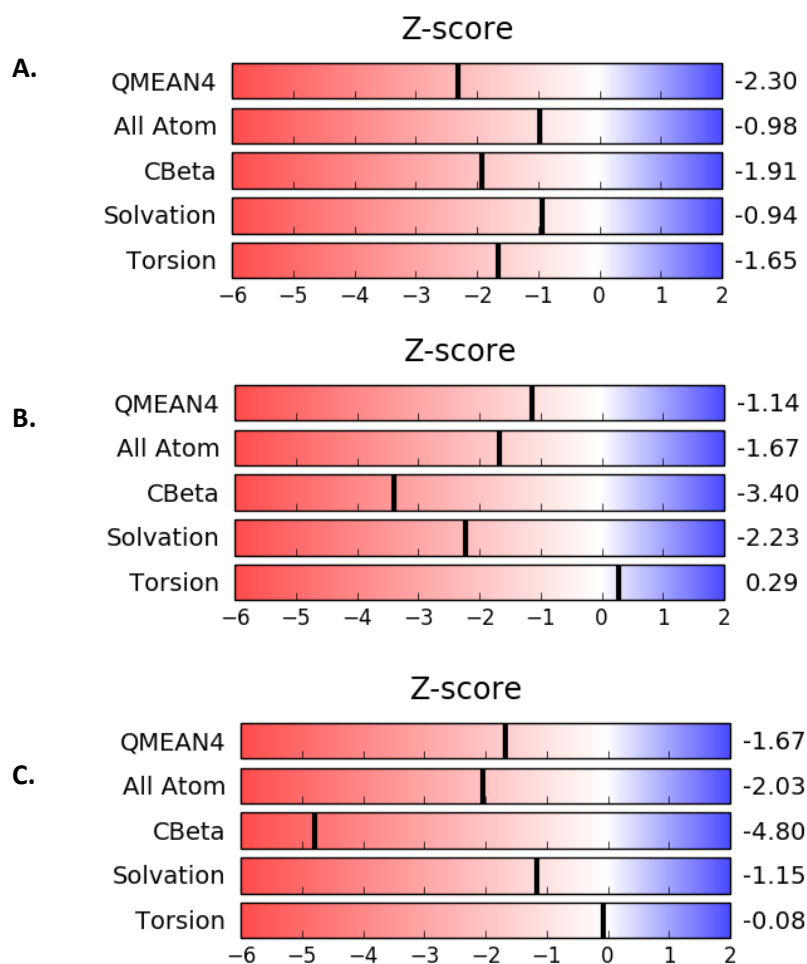
Figure 4.13: QMEAN4 values. **A:** 6QJH.pdb heparin-induced 2N4R Tau snake filament = -2.30, **B:** 6QJM.pdb heparin-induced 2N4R Tau twisted filament = -1.14, **C:** 6QJP.pdb heparin-induced 2N4R Tau jagged filament = -1.67. All structures scored satisfactory global quality. Structures from Zhang et al. (2019).

4.2.6 TAU SMALL MOLECULE BINDING POCKETS AND BINDING PARTNERS

Figure 4.14 illustrates the main binding pockets on Tau$_{306-378}$ and describes the raw data used to calculate

the pockets. This was investigated to predict where other important binding locations may be in relation

to the theoretical peptide inhibtor binding location.

A.

B.
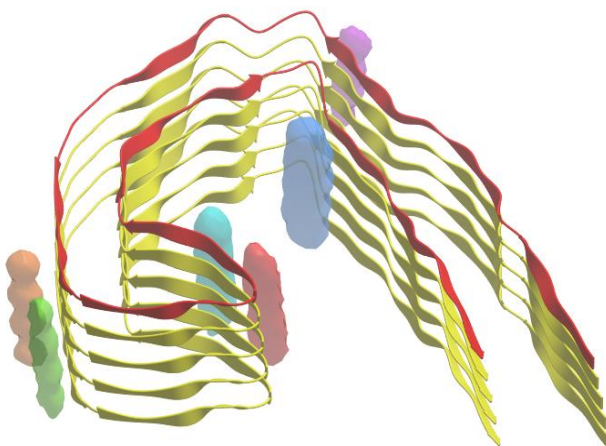
Pocket	Volume (Å)	Area (Å)	Hydrophobicity	Buriedness	DLID	Nonsphericity
Blue	385.87	348.64	65%	0.88	0.63	1.36
Red	246.90	277.80	60%	0.67	-0.65	1.46
Cyan	243.74	266.78	68%	0.77	-0.06	1.41
Green	124.59	185.91	40%	0.53	-2.15	1.54
Orange	118.43	180.00	66%	0.80	-0.53	1.54
Purple	104.99	173.52	47%	0.58	-1.93	1.61

Figure 4.14: ICM-Pro display of PDB 5o3l using the icmPocketFinder function, **A:** Six binding pockets were predicted and displayed in blue, red, cyan, green, orange and purple, **B:** Raw data describing the compactness of the binding pockets which are calculated based on the **Volume** of the pocket; **Area** of the pocket; **Hyrdophobicity** signifying pocket surfaces in contact with hydrophobic protein residues; **Buriedness** suggesting how open (> 0.5) or closed (1.0) pockets were; **DLID** is the druggability of the pocket (> 0.5); **Nonsphericity** representing pocket sphericity (1.0 is spherical).
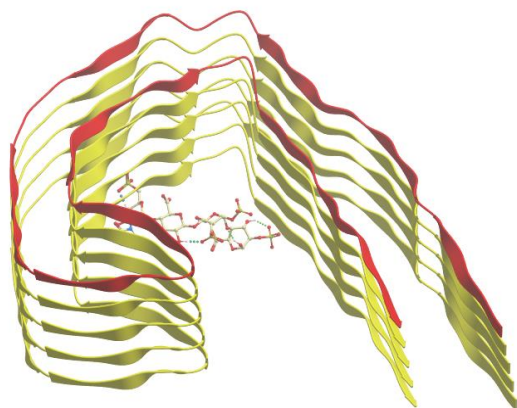
A. *Sodium Heparin*   **B.** *Thioflavin-T*   **C.** *Diothiothreitol*
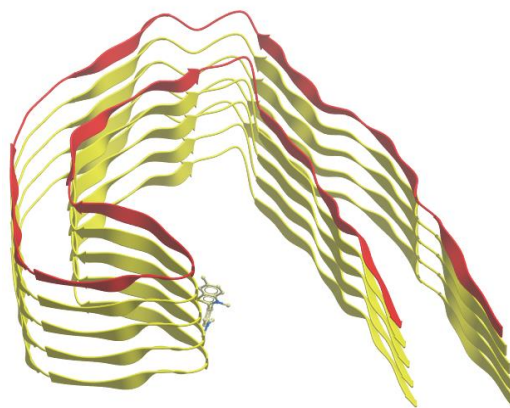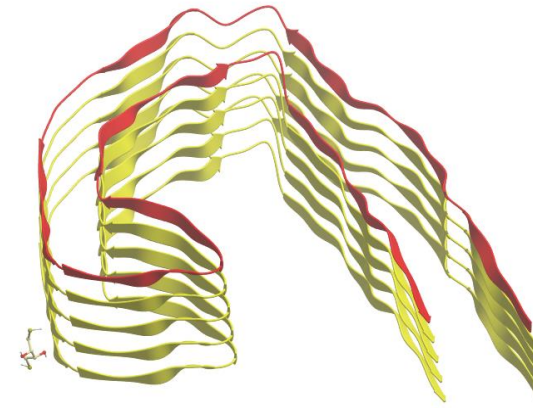
D.

Compound	PubChem ID	ICM Score	H Bond Score	Hydrophobicity	Van der Waals	Eintl	Dsolv	SolEl	mfScore
Sodium Heparin	22833565	-34.73	-10.77	-4.11	-32.35	1.24	23.24	-8.43	-86.57
Thioflavin-T	16953	-28.45	0.00	-5.17	-25.99	1.74	-4.50	5.06	7.60
Dithiothreitol	446094	-12.86	-2.82	-2.10	-12.11	1.31	2.81	1.04	-6.47

E.

Sodium Heparin

Thioflavin-T

Dithiothreitol

VQIVYK

100

Figure 4.15: ICM-Pro display of PDB 5o3l with computationally docked compounds at their highest energy binding sites Tau$_{306-378}$; **A:** Sodium Heparin; **B:** ThT; **C:** DTT; **D:** Raw data describing the docked compounds. ICM score of < -32 suggests a strong bind; H bond Score denotes hydrogen bond energy; Hydrophobicity denotes hydrophobic energy to expose a surface to water; Van der Waals denotes strong van der Waals interaction energy (< 0); Eintl denotes strong ligand internal conformation energy (< 0); Dsolv denotes desolvation of exposed hydrogen bond donors and acceptors; SolEl denotes solvation electrostatics energy change upon binding; mfScore denotes potential of average force score. **E:** Superimposed image of **A-C** with highlighted binding pockets. Compounds in the Tau aggregation mix maximally bind to different binding pockets in PDB 5o3l. DTT binds to the green pocket, ThT binds to the red pocket and Heparin binds to the blue pocket. Circled in black is the theoretical binding site for the peptide inhibitor.

As peviously mentioned in **Section 3.3.1**, The Tau aggregation mix included sodium heparin (to induce aggregation of Tau), ThT (reporter dye) and DTT (to prevent disulphide cross-bridging). **Figure 4.15** illustrates the predicted binding locations for sodium heparin, ThT and DTT on $Tau_{306\text{-}378}$ and describes the raw data used to calculate the binding sites. This provided some indication of where these molecules predicted binding sites were in relation to each other. This was an important prediction so that there was a degree of confidence that these molecules may not competitively bind with one another or with the theoritcal $^{306}VQIVYK^{311}$ binding location of the peptide inhibitor.

4.2.7 PEPTIDE INHIBITOR DOCKING AREAS ON TAU

A.

B.

C.

Residue	avgeODA	
	A	B
V306	-12.08	-20.13
Q307	-6.56	-16.66
I308	-11	-17.86
V309	-7.36	-12.48
Y310	-6.15	-9.01
K311	-4.34	-8.92
P312	-4.4	-6.29
V313	-6.74	-8.20
D314	-6.21	-6.59
L315	-4.87	-4.96
S316	-1.61	-0.90
K317	1.82	2.15
V318	0.61	0.42
T319	-0.81	3.11
S320	-0.93	2.74
K321	0.32	4.70
C322	-2.02	3.90
G323	-1.07	-0.37
S324	0.45	-0.80

Residue	A	B
L325	-1.72	-6.10
G326	-1.55	-8.99
N327	0.55	-2.44
I328	-4.33	-9.02
H329	-0.9	-5.60
H330	-1.88	-8.60
K331	-1.53	-2.13
P332	-1.16	-1.07
G333	-0.48	-1.02
G334	0.21	0.67
G335	0.18	0.40
Q336	0.84	1.59
V337	-0.47	-0.01
E338	1.73	1.96
V339	-0.74	0.54
K340	2.25	3.14
S341	-1.02	-0.27
E342	2.02	1.32
K343	4.31	3.69

Residue	A	B
L344	-2.68	-2.45
D345	5.87	-0.71
F346	-4.29	-2.18
K347	6.49	3.67
D348	1.85	0.65
R349	1.87	1.12
V350	-1.69	-2.55
Q351	1.12	-0.14
S352	-1.83	-0.84
K353	1.7	1.38
I354	-4.21	-0.89
G355	0	0.10
S356	0.87	0.27
L357	0	-0.34
D358	6.19	-0.49
N359	0.7	-0.73
I360	-2.55	-2.31
T361	-7.94	-8.63
H362	-6.08	-8.82

Residue	A	B
V363	-7.94	-9.07
P364	-2.39	-7.45
G365	0	-5.41
G366	0	-4.38
G367	-0.52	-6.91
N368	1.2	-5.43
K369	1.39	-3.23
K370	-2.15	-2.68
I371	-0.52	-1.27
E372	0.18	-2.32
T373	0.61	0.12
H374	-4.16	-1.75
K375	3.91	2.68
L376	-6.1	-10.95
T377	-4.87	-7.07
F378	-20.58	-18.50

Figure 4.16: Optimal docking areas for PDB 5o3l PHF on **A:** top of PHF, including V306, Q307, I308, V309 and F378; **B:** bottom of PHF including V306, I308 and F378. **C**: Average optimal docking area values for PDB 5o3l PHF for **A** and **B.**

Figure 4.16 demonstrates that residues V_{306}, Q_{307}, I_{308}, V_{309} and F_{378} for the PHF structure PDB 5o3I are the optimal docking areas for peptides. Interestingly VQIV residues are target residues for the peptide inhibitor. Note that Isoleucine is highlighted as an important docking area for Tau as well as for the inhibitor in **Figure 4.10**. This is probably due to the highly hydrophobic nature of isoleucine which promotes hydrophobic interactions.

Peptide binding sequences were docked onto Tau to predict which residues they would interact with. **Figure 4.17** illustrates that the predicted binding site for VQIVYK peptide to its complementary [306]VQIVYK[311] sequence in Tau$_{306-378}$ is variable as the peptide is bound in parallel to the top of the protofilament but is bound in anti-parallel to the bottom of the protofilament. This docking experiment served as a control to test if VQIVYK bound to its complementary [306]VQIVYK[311] sequence in Tau.

A.

B.
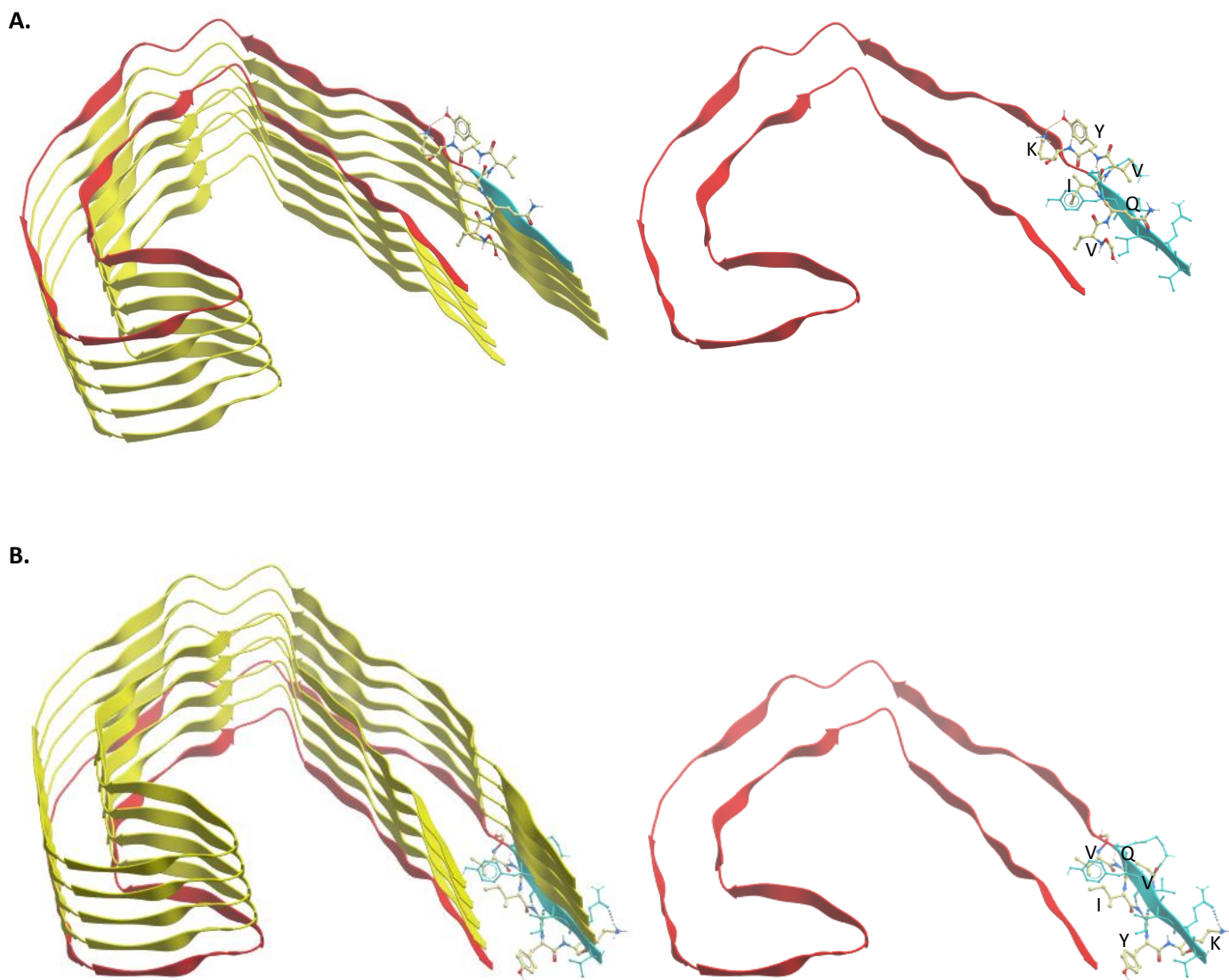
Figure 4.17: VQIVYK bound to complementary [306]VQIVYK[311] sequence (cyan) on the PDB 5o3l PFF structure. **A:** bound in parallel and shifted to the top of the protofilament, **B:** bound in anti-parallel to the bottom of the protofilament. Experiment was run with maximum sampling effort.

Figure 4.18 illustrates the predicted binding sites for VQIK(Ac)YK to its complementary ^{306}VQIVYK^{311} sequence in Tau$_{306-378}$. VQIK(Ac)YK bound in parallel in both instances however also interacted with amino acids in the parallel β-sheet. Increasing the length of the peptide (to include cell penetrating peptide) would not be possible to dock accurately. This docking experiment served as an indication if the inhibitor binding sequence bound close to its complementary ^{306}VQIVYK^{311} sequence in Tau.

A.

B.
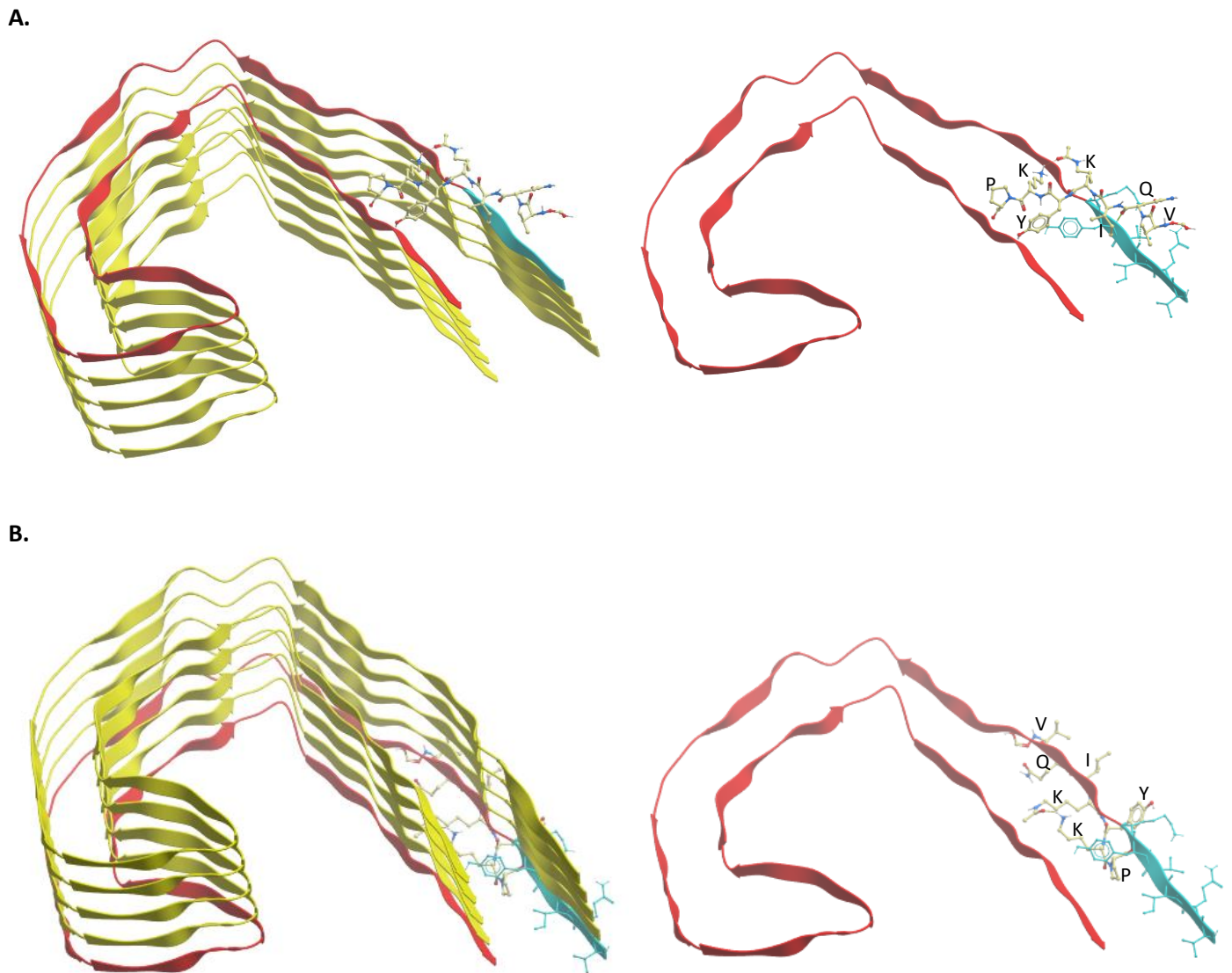
Figure 4.19: VQIK(Ac)YKP bound close to the ^{306}VQIVYK^{311} sequence (cyan) in PDB 5o3l PFF structure. **A:** bound in parallel to the top of the protofilament, **B:** bound in anti-parallel to the bottom of the protofilament. Notice it the peptide is shifted to interact with the amino acids following ^{306}VQIVYK^{311} in Tau. Experiment was run with maximum sampling effort.

Figure 4.19 illustrates the predicted binding sites for VQIK(Ac)YKP to its complementary [306]VQIVYK[311] sequence in Tau[306-378]. Addition of proline appeared to bind in a distinctly different manner compared to the native VQIVYK peptide and the modified sequence without proline. Increasing the length of the peptide (to include cell penetrating peptide) would not be possible to dock accurately. This docking experiment served as an indication to see how the bind would change with an additional proline.

A.

B.
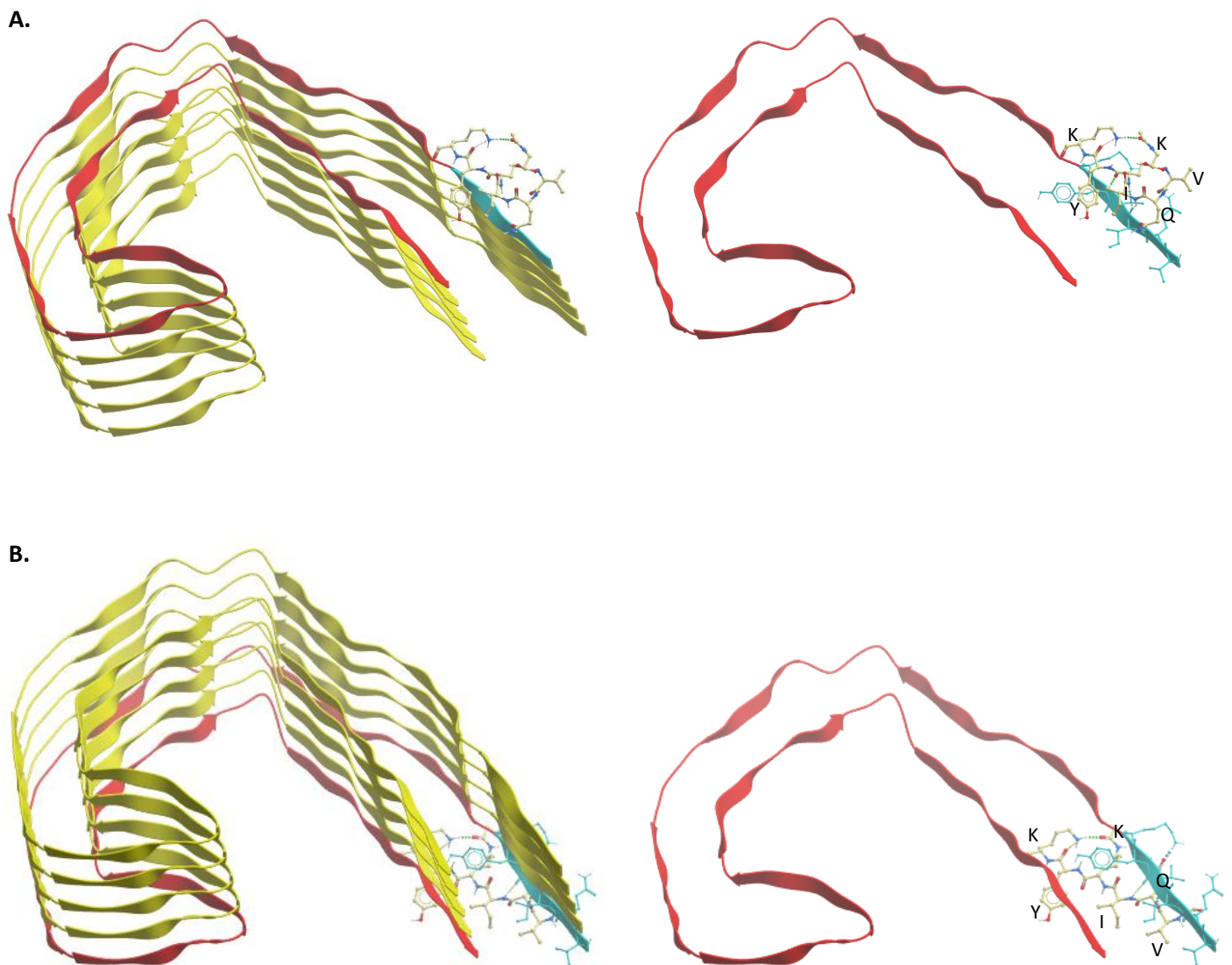
Figure 4.18: VQIK(Ac)YK bound to [306]VQIVYK[311] sequence (cyan) in PDB 5o3l PFF structure. **A:** bound in parallel to the top of the protofilament, **B:** bound in parallel to the bottom of the protofilament and extending to interact with the parallel β-sheet to [306]VQIVYK[311]. Experiment was run with maximum sampling effort.

Table 4.4 Summarises the raw data for the average (n=3) of peptides docking to Tau$_{306-378}$. Based on the ICM score, the control peptide VQIVYK bound more strongly to the top of the protofilament than modified VQIK(Ac)YK did, however with the additional proline, VQIK(Ac)YKP bound the most strongly. When binding to the bottom of the protofilament however, VQIK(Ac)YK bound the most strongly.

A.

Ligand	Bound to top of PHF							
	ICM Score	H Bond Score	Hydrophobicity	Van der Waals	Eintl	Dsolv	SolEl	mfScore
VQIVYK	-15.49	-8.28	-5.68	-40.66	19.83	13.61	17.60	-61.58
VQIK(Ac)YK	-11.40	-4.41	-6.02	-31.54	6.09	9.46	9.07	-41.93
VQIK(Ac)YKP	-18.90	-10.88	-7.28	-39.04	17.44	19.29	11.86	-105.84

B.

Ligand	Bound to bottom of PHF							
	ICM Score	H Bond Score	Hydrophobicity	Van der Waals	Eintl	Dsolv	SolEl	mfScore
VQIVYK	-21.15	-7.59	-6.24	-34.26	13.88	14.15	2.05	-62.82
VQIK(Ac)YK	-25.51	-7.80	-5.77	-40.01	17.89	11.96	-0.28	-85.69
VQIK(Ac)YKP	-19.67	-10.91	-6.80	-40.02	13.77	18.58	15.91	-67.79

Table 4.4: Summary table of the average computationally calculated values describing the docked compounds to Tau$_{306-378}$, as seen in **Figure 4.17-4.19**. **A**: peptides bound to the top of the PHF, **B**: peptides bound to the bottom of the PHF. **ICM score** of < -32 suggests a strong bind; **H bond Score** denotes hydrogen bond energy; **Hydrophobicity** denotes hydrophobic energy to expose a surface to water; **Van der Waals** denotes strong van der Waals interaction energy (< 0); **Eintl** denotes strong ligand internal conformation energy (< 0); **Dsolv** denotes desolvation of exposed hydrogen bond donors and acceptors; **SolEl** denotes solvation electrostatics energy change upon binding; **mfScore** denotes potential of average force score.

Table 4.5 Summarises the raw data for the highest energy bindings of peptides docking to Tau$_{306-378}$. Based on the ICM score, the control peptide VQIVYK bound more strongly to the top of the protofilament than modified VQIK(Ac)YK did, however with the additional proline, VQIK(Ac)YKP bound the most strongly. When binding to the bottom of the protofilament VQIVYK and VQIK(Ac)YKP bound with similar energy, however VQIK(Ac)YK bound the most strongly, despite forming less hydrogen bonds.

A.

Ligand	ICM Score	No. H Bonds	Highest Energy Bindings to Top of PHF
			H Bonds
VQIVYK	-16.36	4	V1-I308; V4-Y310; V6-P312; Y5-K6
VQIK(Ac)YK	-13.45	6	Q2-I308; I3-I308; K(Ac)4-I308; Y5-Y310; K(Ac)4-K6; Y5-K6
VQIK(Ac)YKP	-28.23	7	Q2-I308; Q2-Y310; K(Ac)4-Y310; Y5-H374; K6-P312; P7-H374, K(Ac)4-K6

B.

Ligand	ICM Score	No. H Bonds	Highest Energy Bindings to Bottom of PHF
			H Bonds
VQIVYK	-24.22	7	V1-K311; Q2-K311; Q2-K311; V4-V309; V4-V309; K6-Q307; K6-Q307
VQIK(Ac)YK	-26.20	6	V1-Q307; V1-V309; Q2-K311; I3-V309; K4(Ac)-K6; K6-K6
VQIK(Ac)YKP	-22.50	8	V1-K317; Q2- S316; I3-L315; I3-L315; I3-V313; Y5-V313; P7-K311; K(Ac)4-K6

Table 4.5: ICM scores, number of hydrogen bonds and hydrogen bond partners for **A:** highest energy bindings to the top of the PHF, **B:** highest energy bindings to the bottom of the PHF Potential.

Figure 4.20 illustrates the potential binding sites for the predicted lead sequence Ac-VQIK(Ac)YKP-NH2 on to three differently folded heparin-induced 2N4R Tau filaments: **A:** 6QJH snake filament, **B:** 6QJM twister filament, **C:** 6QJP jagged filament. The potential binding locations include the target VQIVYK (red), VQIINK (black) and DLLSNV (blue). It was previously mentioned in **Section 4.1.3**, that during Tau aggregation, VQIVYK and VQIINK interact. Since the peptide inhibitor is designed to bind to [306]VQIVYK[311], it was hypothesised that it may also bind with [275]VQIINK[280] based on this logic. [282]LDLSNV[287] packs directly opposite [306]VQIVYK[311], therefore is was also hypothesised that the inhibitor could potentially bind here also.
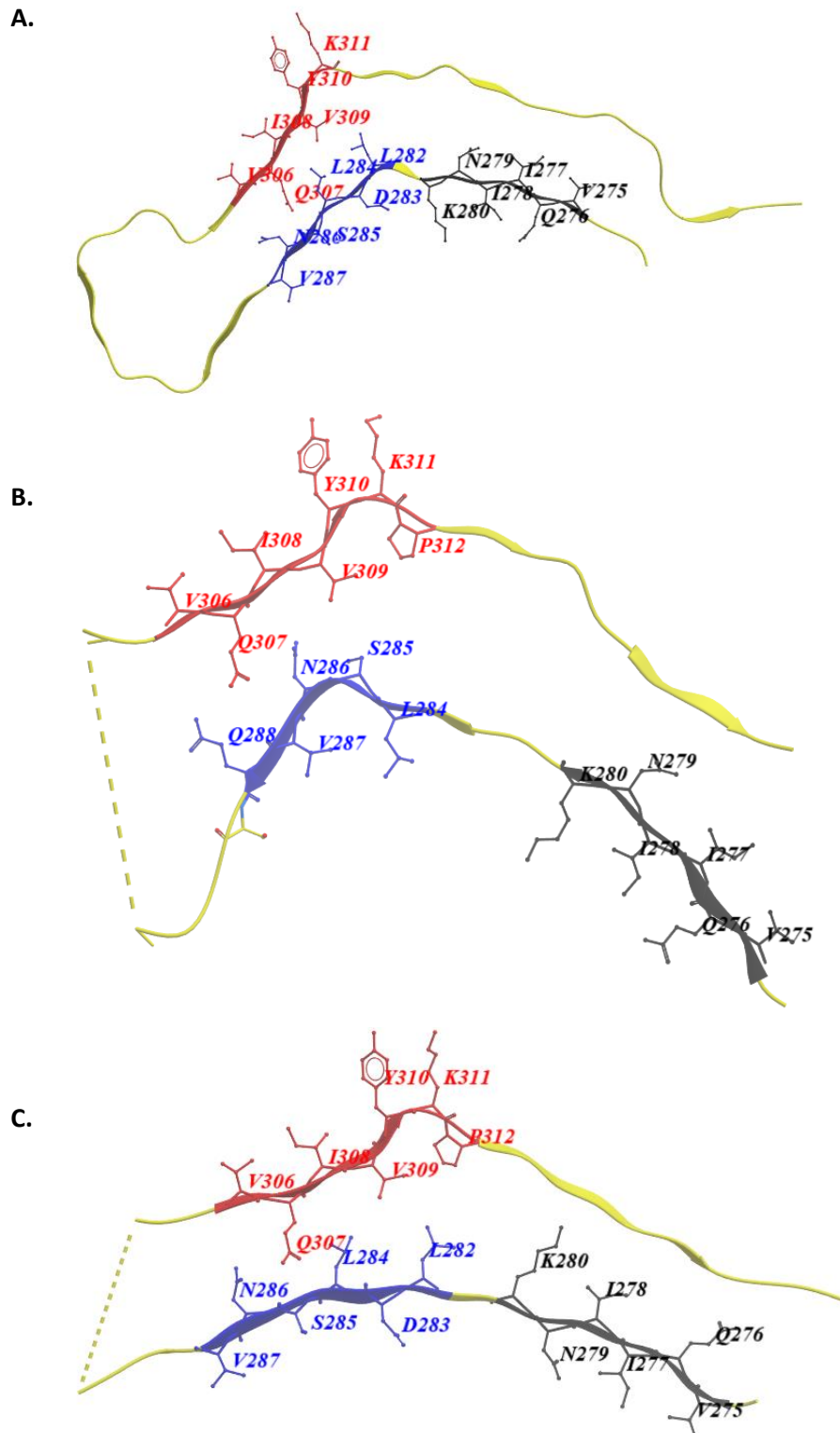
Figure 4.20: Potential binding sites for, **A:** 6QJH heparin-induced 2N4R Tau snake filament, **B:** 6QJM heparin-induced 2N4R Tau twister filament, **C:** 6QJP heparin-induced 2N4R Tau jagged filament. Cryo-EM structures from Zhang et al. (2019).

Figure 4.21 illustrates the predicted peptide binding sites on the heparin-induced 2N4R Tau snake

filament: **A:** VQIVYK (control peptide) binds in parallel to both [306]VQIVYK[311] and [275]VQIINK[280] sequences, **B:**

VQIK(Ac)YKP binds in anti-parallel to [306]VQIVYK[311] and in parallel to [275]VQIINK[280].

A.

B.
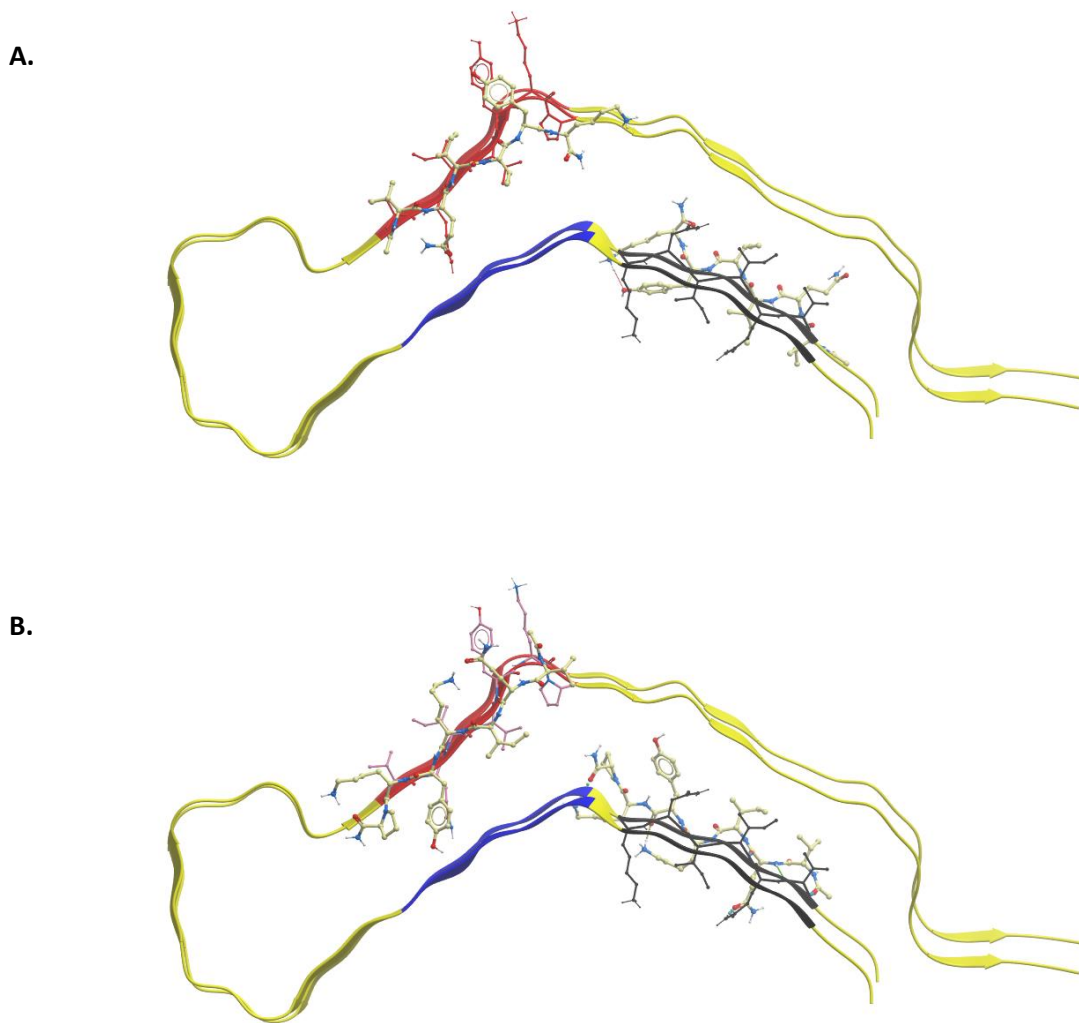
Figure 4.21: Docked peptides to PDB 6QJH heparin-induced 2N4R Tau snake filament; each binding to the [306]VQIVYK[311] and [275]VQIINK[280] sequences. **A:** Ac-VQIVYK-NH$_2$ binding in parallel to the filament, **B:** Ac-VQIK(Ac)YKP-NH$_2$ binding in anti-paralell to the filament at [306]VQIVYK[311] position and in parallel at the [275]VQIINK[280] position.

Table 4.6 summarises raw data for the predicted peptide binding sites of Ac-VQIVYK-NH2 and Ac-VQIK(Ac)YKP-NH2 on the heparin-induced 2N4R Tau snake filament. Based on the ICM-score, VQIVYK bound with higher energy to [275]VQIINK[280] than it did with its complementary [306]VQIVYK[311] sequence, whereas VQIK(Ac)YKP bound with higher energy to its complementary sequence [306]VQIVYK[311] than it did with [275]VQIINK[280]. These differences are marginal.

A.

Ligand	Receptor	ICM Score	No. H Bonds	Binding Positions
				H Bonds
VQIVYK	VQIVYK	-17.55	7	Ace-V306; Q2-V306; Q2-Q307; Q2-I308; V4-I308; V4-Y310; K6-V313
	VQIINK	-22.11	8	V1-V275; Q2-C322; -I3-V275; I3-I277; Y5-I277; Y5-N279; K6-N279; Y5-K6
VQIK(Ac)YKP	VQIVYK	-20.19	11	Q2-Y310; Q2-Y310; K(Ac)4-Y310; K(Ac)4-Y310; Y5-N286; Y5-S285; K6-V306; K6-V306; K6-G302; Q2-K4, K6-P7
	VQIINK	-17.45	10	Ace-Y310; Q2-V275; Q2-V276; Q2-I277; K(Ac)4-I277; K(Ac)4-N297; Y5-S316; P7-L282; K4-P7; K6-P7

B.

Ligand	Receptor	ICM Score	H Bond Score	Hydrophobicity	Van der Waals	Eintl	Dsolv	SolEl
VQIVYK	VQIINK	-22.11	-9.19	-6.37	-31.07	11.37	21.41	-2.13
VQIVYK	VQIINK	-20.58	-9.81	-6.21	-31.40	9.63	26.02	-0.76
VQIVYK	VQIVYK	-17.55	-9.59	-5.42	-34.72	16.92	22.61	4.47
VQIK(Ac)YKP	VQIVYK	-20.19	-11.19	-6.13	-37.51	10.69	28.59	5.88
VQIK(Ac)YKP	VQIINK	-17.45	-12.86	-6.72	-38.09	11.99	33.37	11.28
VQIK(Ac)YKP	VQIVYK	-16.16	-9.25	-5.75	-36.30	7.72	24.60	9.55

Table 4.6: Summarises the raw data for the highest energy bindings and hydrogen bond data of peptides (VQIVYK and VQIK(Ac)YKP) dockedto the snake filament, **A:** peptides binding to the [306]VQIVYK[311] and [275]VQIINK[280] sequences, **B:** Summarise the top 3 binding poses of VQIVYK and VQIK(Ac)YKP to the snake filament.

Figure 4.22 illustrates the predicted peptide binding sites on the heparin-induced 2N4R Tau snake

filament: **A:** VQIVYK (control peptide) binds in parallel to its complementary [306]VQIVYK[311] sequence, **B-C:**

VQIK(Ac)YKP binds in parallel and in anti-parallel to [306]VQIVYK[311], respectively.

A.

B.   C.
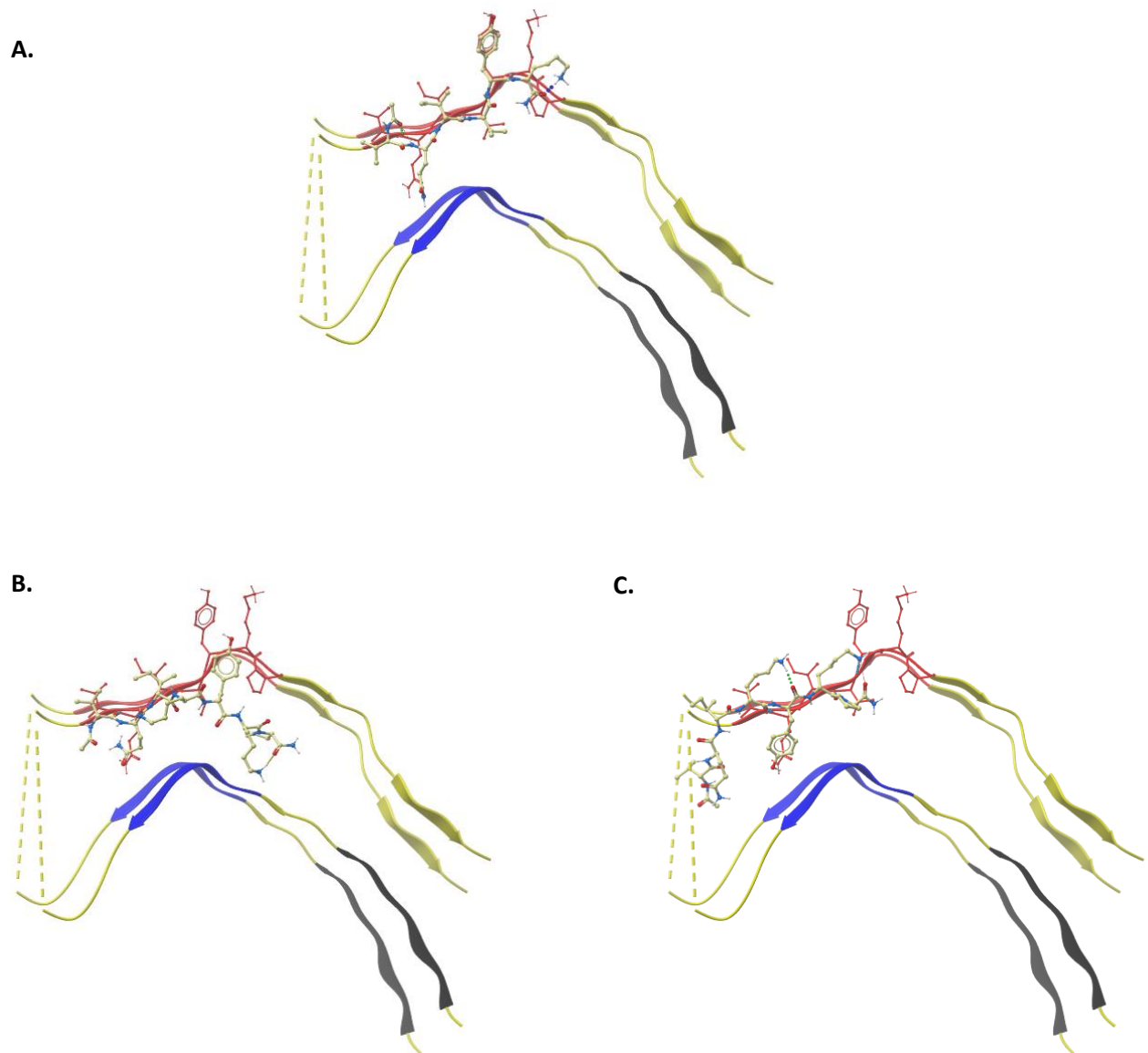
Figure 4.22: Docked peptides to PDB 6QJM heparin-induced 2N4R Tau twister filament; each binding to the [306]VQIVYK[311] sequence. **A:** VQIVYK binding in parallel to fibril, **B:** VQIK(Ac)YKP binding in paralell to the fibril but slightly shifted, **C:** VQIK(Ac)YKP binding anti-parallel to fibril.

Table 4.7 summarises raw data for the predicted peptide binding sites of VQIVYK and VQIK(Ac)YKP on the heparin-induced 2N4R Tau twister

filament. Based on the ICM-score, VQIVYK bound with higher energy to ^{306}VQIVYK^{311} than VQIK(Ac)YKP did.

A.

Ligand	Receptor	ICM Score	No. H Bonds	Binding Positions
				H Bonds
VQIVYK	VQIVYK	-32.14	8	Ace-Q307; Q2-Q307; I3-Q307; I3-V309; Y5-V309; Y5-K311; Ace-Q2; Ace-Q2; K6-CONH$_2$
VQIK(Ac)YKP	VQIVYK	-22.95	9	V1-S305; V1-Q307; Q2-Q288; I3-Q307; I3-N286; Y5-S285; CONH$_2$-D283; Q2-K4; K6-P7

B.

Ligand	Receptor	ICM Score	H Bond Score	Hydrophobicity	Van der Waals	Eintl	Dsolv	SolEl
VQIVYK	VQIVYK	-32.14	-11.08	-5.24	-41.46	13.69	21.67	2.11
VQIK(Ac)YKP	VQIVYK	-22.95	-8.00	-6.79	-38.94	3.04	29.24	-1.48
VQIK(Ac)YKP	VQIVYK	-20.64	-10.47	-6.83	-38.40	4.22	36.12	1.85
VQIK(Ac)YKP	VQIVYK	-19.97	-8.99	-6.48	-39.18	2.01	34.61	1.71

Table 4.7: Summarises the raw data for the highest energy bindings and hydrogen bond data of peptides (VQIVYK and VQIK(Ac)YKP) docked to the twister filament; **A:** peptides binding to the ^{306}VQIVYK^{311} sequences; **B:** Summarise the top 3 applicable bindings poses and locations of VQIVYK and VQIK(Ac)YKP to the snake filament.

Figure 4.23 illustrates the predicted peptide binding sites on the heparin-induced 2N4R Tau jagged

filament. VQIVYK (control peptide) bound in parallel to both [306]VQIVYK[311] and [275]VQIINK[280] sequences,

whereas VQIK(Ac)YKP bound in parallel only to [306]VQIVYK[311].

A.
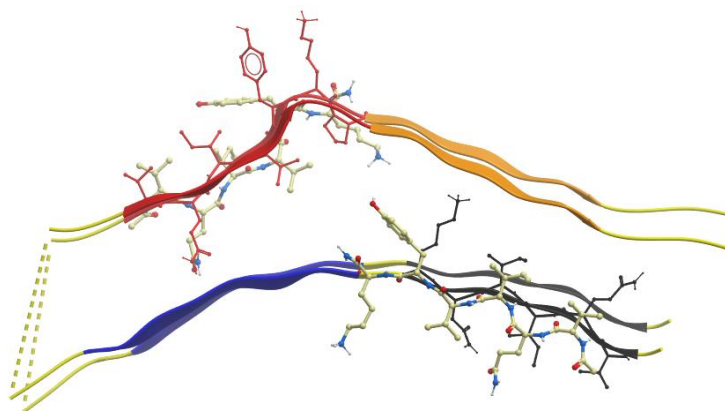
B.
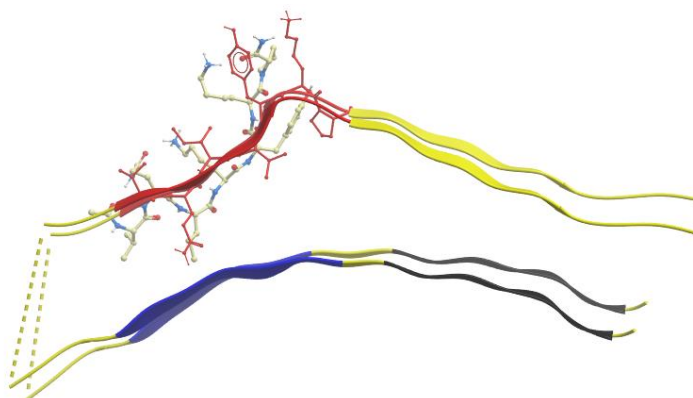
Figure 4.23: Docked peptides to PDB 6QJP heparin-induced 2N4R Tau jagged filament. **A:** VQIVYK binding in parallel to fibril at the [306]VQIVYK[311] and [275]VQIINK[280] positions, **B:** VQIK(Ac)YKP binding in parallel at the VQIVYK position.

Table 4.8 summarises raw data for the predicted peptide binding sites of VQIVYK and VQIK(Ac)YKP on the heparin-induced 2N4R Tau snake filament. Based on the ICM-score, VQIVYK bound with higher energy to [306]VQIVYK[311] sequence than it did with [275]VQIINK[280], whereas VQIK(Ac)YKP bound only to its complementary sequence [306]VQIVYK[311]. VQIK(Ac)YKP bound to [306]VQIVYK[311] more strongly than VQIVYK did.

A.

Ligand	Receptor	ICM Score	No. H Bonds	Binding Positions
				H Bonds
VQIVYK	VQIVYK	-21.87	7	V1-S305; V1-Q307; I3-Q307; I3-V309; Y5-V309; Y5-K311; CONH$_2$-P312
VQIVYK	VQIINK	-17.29	7	V1-V275; V1-I277; I3-I277; I3-N279; Y5-N279; Y5-K281; CONH$_2$-K281
VQIK(Ac)YKP	VQIVYK	-25.48	10	V1-S305; Q2-S305; Q2-P307; K(Ac)4-Q307; K(Ac)4-V309; K6-V309; P7-K311; V1-Q2; Q2-K(Ac)4; K6-P7

B.

Ligand	Receptor	ICM Score	H Bond Score	Hydrophobicity	Van der Waals	Eintl	Dsolv	SolEl
VQIVYK	VQIVYK	-21.87	-11.17	-6.25	-36.93	14.67	25.35	7.09
VQIVYK	VQIINK	-17.29	-9.71	-6.53	-28.72	14.27	20.31	2.39
VQIVYK	VQIVYK	-14.29	-8.73	-6.19	-32.52	15.91	20.55	6.82
VQIK(Ac)YKP	VQIVYK	-25.48	-8.03	-5.64	-35.80	1.59	20.06	0.64

Table 4.8: Summarises the raw data for the highest energy bindings and hydrogen bond data of peptides (VQIVYK and VQIK(Ac)YKP) docked to the jagged filament; **A:** peptides binding to the [306]VQIVYK[311] and [275]VQIINK[280] sequences as applicable; **B:** Summarises the top 3 bindings poses and locations of VQIVYK and VQIK(Ac)YKP to the jagged filament.

4.3   DISCUSSION

Figures 4.5 and **4.6** illustrated the intrinsic residue solubility profile and the A4V for Tau_{441}, respectively. In both figures, VQIVYK is highlighted as the sequence with the lowest intrinsic solubility profile and the highest aggregation propensity. Based on this it was determined that the most suitable sequence to target using a peptide aggregation inhibitor was the [306]VQIVYK[311] sequence. This coincides with the literature which highlights the importance of [306]VQIVYK[311] for the aggregation of Tau. Perez et al, (2007) demonstrated that deletion of [306]VQIVYK[311] in Tau prevents heparin induced aggregation and that incubating Tau with VQIVYK hexapeptide stimulates aggregation. This data is also supported by the fact that when the Aβ sequence is run through these algorithms, they highlight the [16]KLVFF[20] sequence as the aggregatory seqeunce.

When developing peptide aggregation inhibitors with high selectivity for their pathogenic target sequence(s), it is important that the inhibitor itself does not have propensity to self-associate; thus, self-defeating the original purpose of an aggregation inhibitor. Based on the findings in **Figures 4.5** and **4.6**, a peptide inhibitor to target [306]VQIVYK[311] must share some similarities to bind to its complementary sequence. Professor David Allsop's research group developed a successful Aβ aggregation inhibitor utilising the [16]KLVFF[20] binding sequence; widely appreciated as the aggregation hot-spot for Aβ (Taylor et al., 2010). Following similar logic whilst at the same time safeguarding the possibility of peptide self-association, potential modifications to [306]VQIVYK[311] were investigated. **Tables 4.1 and 4.2** demonstrates aggregation propensity for VQxVYK and VQIxYK, respectively. 'x' denotes amino acid substitutions of the native Tau [306]VQIVYK[311] sequence with alternative amino acids. All conformations of VQxKYK and VQIxYK which contained hydrophobic residues except proline were identified as aggregation hot-spots. This is likely because proline is widely acknowleged as a β-sheet breaker due to the bulkiness of its pyrrolidine ring placing steric comformational constraints on its preceding residue and that its dihedral angle fixed at

-65˚ is incompatible with β-sheets (Zhang et al., 2019; Li et al., 1996). As a result of these constraints, proline interferes with hydrogen bonding between Tau molecules and generates disordered structures. This is supported by mutations P301L and P301S in Tau which accelerates aggregation (Barghorn et al., 2000). Conformations containing hydrophilic residues cysteine, serine, threonine and tyrosine also identified as aggregation hot spots. This suggests that substituting the native hydrophobic amino acids with any hydrophilic residue does not necessarily lower the hexapeptide aggregation propensity below the aggregation threshold. Na4vSS values are the final calculated aggregation propensity values. For both VQxKYK and VQIxYK, lysine was chosen as the optimum replacement as VQ**K**VYK and VQI**K**YK had higher Na4vSS values than the other conformations, except proline. A high Na4vSS value but below the aggregation threshold was desired as it is a logical assumption that there is a fine line between pathogenic aggregation and functionality of proteins. If the Na4vSS value was too low, then it may result in a weak interaction with its target sequence [306]VQIVYK[311]. Proline was not deemed suitable to be included in the centre of a binding sequence due to its rigidity placing steric conformational constraints within the peptide binding sequence.

Aggregation hot spots are defined as regions (excluding regions containing proline) with ≥ 5 continuous residues with an aggregation propensity greater than the "hot spot" threshold. Sequences which exceed the hot-spot threshold are predicted to be aggregation prone. Camsol calculates the intrinsic solubility profile of 7 amino acid sequence windows and illustrates hydrophilic and hydrophobic regions with blue and red, respectively (Sormani et al., 2015). CamSol calculates the intrinsic solubility profile by evaluating as intrinsic factors the amino acid residue aggregation propensity, hydrophobicity, charge and secondary structure propensity (Arslan et al., 2019). **Figures 4.7** and **4.8** suggests the aggregation propensity and intrinsic residue solubility, respectively, for each of the following peptides: VQIVYK, VQ**K**VYK and VQI**K**YK. The entire control VQIVYK sequence was well above the hot-spot threshold and was highlighted as a highly

insoluble sequence. VQ**K**VYK was globally under the hot-spot threshold, with lysine (position 3) locally exceeding the threshold and according to CamSol was not particularly hydrophobic.

VQI**K**YK was also globally under the hot-spot threshold, with isoleucine (position 3) locally exceeding the threshold and according to CamSol isoleucine (position 3) was considered particularly hydrophobic. Based on these data, isoleucine appears to be highly important for hydrophobic binding interactions in VQIVYK. This is supported by the C-beta carbon in isoleucine having two non-hydrogen substituents attached to it, resulting in restricted conformations and being involved in binding/substrate recognition (Betts and Russel, 2003). Peptide solubility is important; however, they also need to be able to bind to their molecular targets which requires aggregation-prone sequences of amino acids e.g. VQI (Sormanni et al., 2015). As [306]VQIVYK[311] sequences interact with one another perpendicularly to the fibril axis (as seen below in **Figure 4.24**) through hydrophobic interaction, VQI**K**YK was favoured to be the more suitable binding sequence.
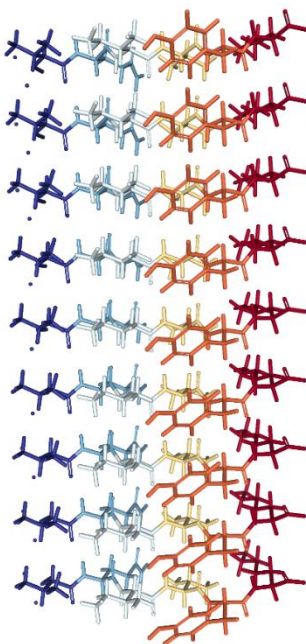
Figure 4.24: Atomic resolution structure of Tau [306]VQIVYK[311] peptide determined by MicroED, demonstrating perpendicular stacking to the fibril axis (de la Cruz et al., 2017).

Using ICM-Pro, PDB 5o3l PHF and PDB 5o3t SF were analysed using the binding properties mesh as seen in **Figure 4.9**. This mesh scans all residues for their ability to form hydrogenbonds and identifies, hydrogen bond donors, hydrogen bond acceptors and hydrophobic areas. Hydrogen bond donation is an electrostatic interaction. Hydrogen bonding occurs when the partial positive charge from a hydrogen atom bound to an electronegative atom, usually Nitrogen, Oxygen and Fluorine (hydrogen bond donor) attracts a lone pair of electrons attached to another electronegative atom (hydrogen bond acceptor). These non-covalent bond interactions are important for binding. Electron donors are reducing agents which donate electrons to another compound. When aggregating Tau, the presence of polyanions such as heparin are necessary to initiate nucleation. In Tau-heparin interactions, hydrogen bond donor sites on Tau will donate their positively charged hydrogens to hydrogen bond acceptor sites on heparin, which is negatively charged. The area for this interaction to occur is predicted to be within the horse-shoe shape of Tau as seen in **Figure 4.9**. Here heparin can act as a scaffold via its sulfate groups and interact with oligomers through electrostatic interactions. Lysine acetylation is a common modification and by acetylating lysine it loses its ability to accept hydrogen bonds and is rendered solely a Brønsted acid where it can only donate hydrogen bonds to Brønsted bases, which are hydrogen bond acceptors (European Bioinformatics Institute, 2019). The outer regions perpendicular to the fibril axis are largely positively charged, whereas the inner regions following the fibril axis are largely negatively charged. As a result, by acetylating the substituted lysine at position 4 in the VQI**K**YK sequence it may promote binding to or near its complementary sequence within the negatively charged region, perpendicular to the fibril axis. It also removes the charge on lysine which could interfere with binding as positive charges must be neutralised for Tau to bind stably (Guo et al., 2017). As acetyllysine is polar and valine is non-polar, introduction of VQIK(Ac)YK may decrease the hydrophobicity of the hot-spot sequence in native Tau. Zhang et al. (2019), stated that lysine positive charges must be neutralised for Tau to form stable filaments; therefore, this modification may allow the inhibitor to bind with more stability.

ODA (optimal docking area) analyses surfaces for favourable energy change once buried as a protein-protein complex to identify. The ODA was calculated for AG02, AG02ΔI and AG02ΔV in **Figure 4.10** which revealed that positions 5 (isoleucine) and 7 (tyrosine) are important for docking, even when isoleucine was replaced with acetyllyisine in AG02ΔI. This agrees with the Aggrescan and CamSol data which formed the initial basis of the prediction that VQI**K**YK would bind better than VQ**K**VYK. Berhanu and Masunov, (2012), stated that [306]VQIVYK[311] forms an apolar dry interface via the side chains of V1 and I3 with tyrosine which further highlights the importance of isoleucine and tyrosine in the VQIVYK peptide. Both isoleucine and tyrosine are also on the side which packs tightly with the 4th repeat in the hydrophobic PHF core (Fitzpatrick et al., 2017). Naruto et al. (2010), reported that CH/π interactions between isoleucine and tyrosine in VQIVYK is essential for dry interface formation of steric zippers. This interaction can be seen in **Table 4.9** when tyrosine from VQIVYK is CH/π hydrogen bonding with isoleucine in [275]VQIINK[280]. These interactions occur between soft acids and bases, in polar or non polar environments and are weaker than classical hydrogen bonds, however have proven to be very important interactions regarding molecular recognition, assembly and behaviour. However, the strength of CH/π bonds involving acetylenic groups are more similar to classical hydrogen bonds (Nishio, 2011). The acetyllysine in VQIK(Ac)YKP demonstrated to interact with the VQIVYK tyrosine in the PHF (**Table 4.8**) and the snake filament (**Table 4.9**). Retaining isoleucine and tyrosine in the binding sequene of the peptide inhibitor are clearly important binding molecules for VQIVYK interactions. The introduction of acetyllysine also seems to play a role in enhancing interactions. AG02ΔV [RG- VQI**K**(Ac)YK-GR] contains the acetyllysine on position 6 (valine) which packs tightly with the 2nd repeat (Zhang et al., 2019). [275]VQIINK[280] is in the 2nd repeat and is touted as the other highly aggregatory hexapeptide in Tau. Interfering with residues in the 2nd repeat was deemed favourable as this could potentially disturb the usual pathogenic folding of [275]VQIINK[280] as well as [306]VQIVYK[311], which are both neccessary hexapeptides for Tau aggregation. Having the acetyllysine at position 6 (valine) instead of position 5 (isoleucine) retained the docking propensity for glutamine at position 4, which is also

seen with AG02 [RG-VQIVYK-GR]. This similarity to the native sequence suggests AG02ΔV [RG-VQI**K**(Ac)YK-GR] to be a more favourable binding protein than AG02ΔI [RG-VQ**K**(Ac)VYK-GR]. To investigate potential self-association of AG02ΔI [RG-VQ**K**(Ac)VYK-GR] and AG02ΔV [RG-VQI**K**(Ac)YK-GR] they were docked onto themselves in ICM-Pro. **Table 4.3** demonstrated that AG02ΔI binding sequence [VQ**K**(Ac)VYK] interacted with itself more strongly than the binding sequence of AG02ΔV [VQ**K**(Ac)VYK] by having lower ICM, hydrogen bond, hydrophobicity, van der Waals and solvation electrostatics energy change scores. This confirmed the choice for ceasing progression of AG02ΔI [RG-VQ**K**(Ac)VYK-GR] (which was the weaker optimal docking protein and was predicted to self associate) and progressing with the development of AG02ΔV [RG-VQI**K**(Ac)YK-GR]. This binding sequence was then modified to include proline [RG-VQI**K**(Ac)YKP-GR] which as previously described has useful β-sheet breaker properties. Von Bergen et al (2000), demonstrated that mutation of any resiude from VQIVYK into proline results in severe inhibition of Tau aggregation due to interrupting necessary chain conformations. Since Tau aggregation largely occurs intracellularly, the inhibitor was modified to include octa-arginine for use as a cell penetrating peptide (CPP) motif. From this AG03 [RG-VQI**K**(Ac)YKP-GRRRRRRRR] was proposed and the core binding sequence retained similar ODA values as AG02ΔV [RG-VQI**K**(Ac)YK-GR], as seen in **Figure 4.10**. PDB 5o3l PHF and PDB 5o3t SF were the only viable Tau structures available at the time for the docking simulations required for this thesis. Before working with these structures, they were first assessed for their structure quality with SWISS-MODEL by relating their structural features to similar sized experimental stuctures (Benkert et al., 2011). This supported an informed decision approach when subsequently conducting docking experiments by providing evidence based confidence into the decisions being made. PDB 5o3t SF failed to provide a satisfactory QMEAN4 threshold value and was rejected for further use (**Figure 4.11**). When assessing PDB 5o3l PHF with SWISS-MODEL a low global quality QMEAN4 value was generated (**Figure 4.12**); however, still deemed acceptable. QMEAN mainly uses statistical potentials of mean force that compare interactions observed in the model such as pairwise interactions, dihedral angles etc. and

with what would be expected from high resolution X-ray structures in a probabilistic manner. As seen in **Figure 4.25**, PDB 5o3I PHF is a structure from aggregated Tau and does not follow the dogma of a nicely packed globular protein, and as a result it may be why the generated global quality score was poor. These structures have been ground breaking and perhaps due to their unique structure not previously seen in the PDB is why global quality score was poor.
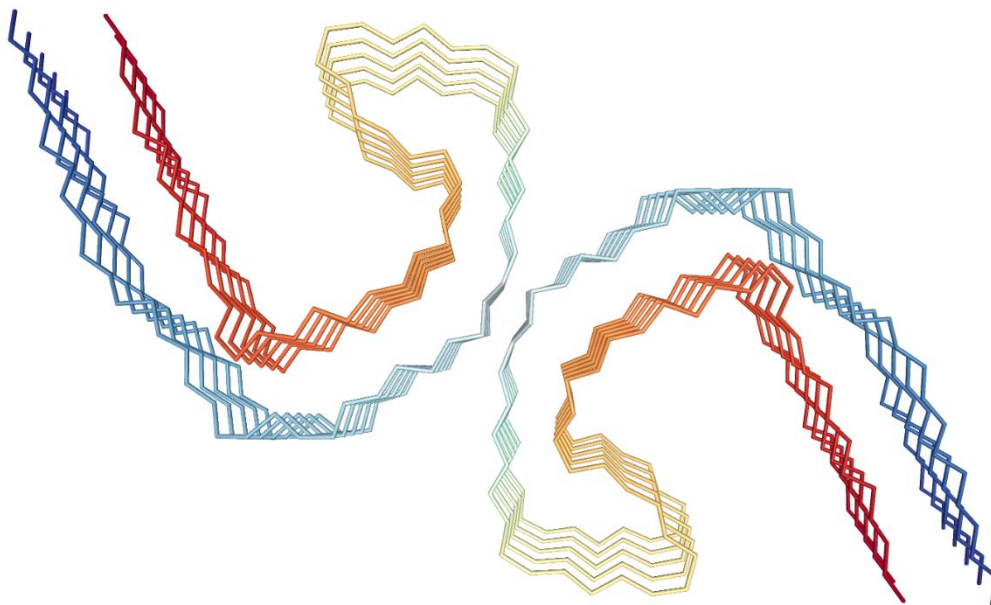
Figure 4.25: PDB 5o3I cryo-EM structure of PHF in AD brain (Fitzpatrick et al., 2017).

QMEANDisCo is agnostic of actual physical interactions and assesses the consistency of interatomic distances with ensembles of constraints extracted from homologous structures in the PDB. Since the actual structure 5ol3 PHF is in the PDB, QMEANDisCo generates good quality local residue scores, with average QMEANDisCo scores for chains B and J as 0.78 (out of 1). Based on this the structure passed the criteria for the set methodology of pre-requisite docking experiments. QMEAN values for 6QJH.pdb snake filament, 6QJM.pdb twisted filament and the 6QJP.pdb jagged filament were scored with good quality, as seen in **Figure 4.13**, and so were also subsequenty used for docking experiments. To verify that the peptide inhibitor would not interfere with other compounds in the aggregation mix (Thioflavin-T, Sodium heparin and DTT) used to aggregate Tau *in vitro*, small molecule binding pockets were investigated using

ICMPocketFinder on ICM-Pro. This was an important prediction before testing the inhibitors *in vitro,* otherwise fluorescence reports would not be truly measuring the effect of the inhibitors on Tau aggregation. They would instead be measuring how the inhibitors prevent heparin and ThT from interacting with Tau to generate fluorescence signal. **Figure 4.14** highlights six potential pockets where small molecules can bind to the PHF core and provides information on each pocket. Only one pocket located between residues ^{362}HVPGGNK^{369} scored high enough to be considered druggable according to its DLID score, which are measurements of the likelihood a pocket will bind a drug-like molecule (Sheridan et al., 2010). Once pockets were identified, compounds from the Tau aggregation mix (Heparin, ThT and DTT) were docked onto the 5o3l PHF structure. Heparin, ThT and DTT all appeared to dock at their highest energy to the blue, red and green pockets, respectively, as seen in **Figure 4.15**. This demonstrated that these compounds did not compete with one another for binding sites on Tau, which meant that heparin is freely able to interact with Tau to promote fibrilisation and that ThT is able to freely interact with Tau. Both heparin and ThT bind to Tau very strongly with ICM-scores of -34.73 and -28.45. It is important these strongly binding compounds have differet binding areas to one another and that of the ^{306}VQIVYK^{311} sequence, otherwise the peptide inhibitor would be in competition to the binding sites and produce false results. ODA was also performed on the sequence to determine the optimum docking areas for peptides. **Figure 4.16** highlighted residues V_{306}, Q_{307}, I_{308}, V_{309} and F_{378} which is perfect as the peptide inhibitor is designed to target the ^{306}VQIVYK^{311} sequence. By summarising the aggregation mix predicted binding sites and the predicted peptide binding site, there was now confidence that these molecules would be less likely to interfere with one another. From this it was predicted that any phenomena seen *in vitro* regarding inhibition of Tau aggregation would be because of the inhibitor binding to Tau.

LEADS-PEP is a benchmark data set consisting of 53 protein-peptide complexes which serves for evaluation of docking softwares in terms of their efficiency assessment of docking and scoring performance (Hauser and Windshügel, 2016). Hauser and Windshügel (2016), demonstrated that very few

complexes were docked reproducibly using peptide lengths over 8 residues, and none of 12 residue peptides were re-docked correctly by any of the methods tested as computational difficulty of docking grows exponentially with length. In 2018 MolSoft ICM-Pro ranked first place by outperforming other methods for docking pose and affinity prediction accuracy for all targets in the Drug Design Data Resource (D3R) Grand Challenge 3 (Lam et al., 2019). The D3R Grand Challenge 3 is a blind community-wide test enabling developers to validate their methods and compare them to others. AG03 is 18 residues long which is outside of the general applicability domain of flexible ligand docking protocols (Hauser and Windshügel, 2016). It was feasible instead to use VQIVYK sequence (as the native control) and two versions of the inhibitor binding sequence, VQIK(Ac)YK and VQIK(Ac)YKP in docking simulations onto the top and bottom of PDB 5o3l PFH fibril axis. Both VQIVYK and VQIK(Ac)YKP docked in parallel to their complementary [306]VQIVYK[311] sequence in the native protein, both at the top and bottom of the fibril axis, as seen in **Figure 4.17** and **4.19**. VQIK(Ac)YKP docked in an anti-parallel manner next to the [306]VQIVYK[311] complementary sequence. Within the context of a Tau fibril, [306]VQIVYK[311] organises into parallel face-to-face β-strands within the same β-sheet layer and protofilaments are formed by mating identical β-sheet layers in an anti-parallel fashion, as seen above in **Figure 4.25** (Eisenberg et al., 2017; Ganguly et al., 2015; Berhanu and Masunov, 2012). Cheon et al. (2012), observed that free VQIVYK peptides formed β-sheets consisting of both parallel and anti-parallel strands which stacked to then form disordered or irregular protofilaments. This may suggest why VQIK(Ac)YKP docked in an anti-parallel manner. Ganguly et al. (2015), stated that peptides which promote anti-parallel alignments usually have slower aggregation kinetics than parallel alignments due to increased difficulty mating β-sheets together. This finding agrees with x-ray structures solved by Sawaya et al., (2007).

According to **Table 4.4**, VQIK(Ac)YKP docked most strongly to the top of the fibril axis, however bound with similar energy to the bottom of the fibril axis when compared with the control VQIVYK. peptide This is made apparent when observing the number of hydrogen bonds formed in **Table 4.5**; the control made

7 hydrogen bonds whereas VQIK(Ac)YKP made 8. VQIK(Ac)YKP demonstrated its ability to not only bind the native residues of [306]VQIVYK[311], but also with amino acids in the R4 opposing chain, perhaps due to the added rigidity of proline affecting the fold of VQIK(Ac)YKP.

Structure quality was assessed for 2019 structures: PDB 6QJH Q6JM and 6QJP which are heparin-induced induced 2N4R Tau snake, twisted and jagged filaments, respectively (**Figure 4.13**). All three structures scored good global quality scores of -2.30, -1.14 and -1.67, respectively. The interaction of [306]VQIVYK[311] with [275]VQIINK[280] is believed to produce twisted PHF-like filaments, therefore if VQIK(Ac)YKP can bind to [06]VQIVYK[311] perhaps it can also bind to [275]VQIINK[280] due all three sharing the same VQIxxK sequence (Von Bergen et al., 2001). **Figure 4.20** highlights potential additional inhibitor binding sites, including the [275]VQIINK[280] sequence and the [282]LDLSNV[287] sequence (which in the snake, twister and jagged PDB filament structures) packs directly opposite the [306]VQIVYK[311] sequence and resembles an amphiphilic amyloidogenic motif (Seidler et al., 2018). The VQIVYK control peptide docked in parallel to its complementary VQIVYK sequence on the snake filament, however VQIK(Ac)YKP docked in an anti-parallel comformation, as seen in **Figure 4.21**. Both control peptide and VQIK(Ac)YKP also docked in parallel to the VQIINK sequence, suggesting that the inhibitor can target the two main aggregation sequences in Tau. **Table 4.6** demonstrated that VQIK(Ac)YKP *in-silico* docks with more affinity to the [306]VQIVYK[311] sequence than the control peptide does, whereas the control peptide had a stronger affinity to bind to [275]VQIINK[280]. The observation of VQIVYK binding strongly to [275]VQIINK[280] is supported by Ganguly et al., (2015) who demonstrated that [306]VQIVYK[311] forms stable heterodimers with [275]VQIINK[280] and that homodimers of [306]VQIVYK[311] and heterodimers of [306]VQIVYK[311] and [275]VQIINK[280] have stronger interactions than homodimers of [275]VQIINK[280]. When docking to the twister filament both control peptide and VQIK(Ac)YKP docked in parallel to the native [306]VQIVYK[311] sequence as seen in **Figure 4.22**. Both docks were strong, however the control peptide had an exceptionally higher binding score as seen in **Table 4.7**. In this structure neither peptide bound to the [306]VQIVYK[311] sequence, however VQIK(Ac)YKP, in addition to

binding to its target sequence, also simultaneously bound to S305, Q288, N286 and S285 in the parallel R2 region which packs next to [306]VQIVYK[311]. Interestingly with the jagged filament structure, the control peptide docked in parallel to both its complementary sequence and the [275]VQIINK[280] sequence, however VQIK(Ac)YKP only docked in parallel to the [306]VQIVYK[311] sequence but with greater binding energy than the control peptide (**Figure 4.23** and **Table 4.8**). Both [275]VQIINK[280] and [306]VQIVYK[311] sequences contain a VQIxxK recognition motif which was favourable to maintain in the inhibitor. The fifth amino acid (from left to right) in [275]VQIINK[280] and [306]VQIVYK[311] are amino acids asparagine and tyrosine, respectively. Asparagine can accept two hydrogen bonds and donate two hydrogen bonds, whereas tyrosine can get involved in aromatic stacking interactions. These two amino acids play important roles in binding and may interact via polar-π interactions involving a polar molecule (asparagine) interacting with a quadrupole moment (benzene ring in tyrosine). Quadruple moments in molecules arise from the uneven distribution of charge (Chakravarty et al, 2018). In addition to this, the data suggests that both VQIVYK and VQIK(Ac)YKP may be able to bind the [306]VQIVYK[311] and the [275]VQIINK[280] sequence, perhaps making it a VQIxxK specific peptide, as well as the ability to additionaly bind neighbouring residues, which may inhibit aggregation. The summary on the next page in **Table 4.9** demonstrated that VQIK(Ac)YKP binds with similar intensity to its target when compared with the native control. Both peptides were also predicted to interact with [275]VQIINK[280]. VQIK(Ac)YKP binds to the general region of [305]SVQIVYKP[312] which includes hydrogen bonding to residues G302, H374, N286, S285, Q288. It also binds to the general region of [274]HVQIINKK[281] which includes hydrogen bonding to residues L282, N297, Y310, S316. Notice that H374 (from HVQIINKK sequence) is involved in the [306]VQIVYK[311] bind and that Y310 (from the SVQIVYKP sequence) is involved in the [75]VQIINK[280] bind, suggesting that the inhibitor may be able to interact with the [306]VQIVYK[311] and [275]VQIINK[280] residues simultaneously. As the peptide inhibitor was observed to bind to its target sequence [306]VQIVYK[311] in an anti-parallel manner, it may also alter the aggregation pathway. According to Feinstein et al. (2016), anti-parallel Tau dimers mediated via two N-terminal tails forming an electrostatic zipper,

promote microtubule bundling which may provide an additional benefit to this peptide inhibitor as a microtubule stabiliser (Rosenberg et al., 2008). In summary the best inhibitor binding region chosen to take forward was VQIK(Ac)YKP because it contains the advantageous deletion of valine, the replacement with acetyllysine and the addition of beta sheet breaker proline on the N terminus. This peptide demonstrated a lower predicted tendancy to self associate (perhaps due to the replacement of valine and the addition of proline) but bound to Tau with similar intensity as the native control (perhaps due to the acetyllysine promoting hydrogen bond interactions with the [306]VQIVYK[311] target) and with a greater number of hydrogen bonds, as seen in **Table 4.9**.

Structure	Receptor	VQIVYK ligand			VQIK(Ac)YKP ligand		
		Orientation	Best ICM score	H. bonds	Orientation	Best ICM score	H. bonds
PHF	VQIVYK (top)	Parallel	-16.36	4	Parallel	-28.23	7
	VQIVYK (bottom)	Anti-parallel	-24.22	7	Anti-parallel	-22.50	8
Snake	VQIVYK	Parallel	-17.55	7	Anti-parallel	-20.19	11
	VQIINK	Parallel	-22.11	8	Parallel	-17.45	10
Twister	VQIVYK	Parallel	-32.14	8	Parallel	-22.95	9
Jagged	VQIVYK	Parallel	-21.87	7	Parallel	-25.48	10
	VQIINK	Parallel	-17.29	7	-	-	-

Table 4.9: Summary of the strongest energy bindings, orientations and number of hydrogen bonds for VQIVYK and VQIK(Ac)YKP docked onto PDB: 5o3l PHF, 6QJH snake filament, 6QJM twister filament and 6QJP jagged filament. Significantly stronger energy bindings are highlighted in grey.

5. DEVELOPMENT OF TAU AGGREGATION

INHIBITORS

This chapter explores the recombinant expression and purification of Tau251-441 (TauΔ1-250) and testing the peptide inhibitors against TauΔ1-250 aggregation using ThT fluorescence assays, CD, Congo red birefringence and TEM. The lead peptide inhibitor is adapted to include retroinversion of its sequence – meaning the sequence uses D-amino acids instead of L-amino acids and the sequence is reversed. This adapted lead peptide is also investigated for its effectiveness when attached to a liposome.

5.1   EXPRESSION OF RECOMBINANT TAUΔ1-250

5.1.1 PROTEIN EXPRESSION

~50mg of Tau protein was required for this research to test and develop successful peptide aggregation inhibitor candidates. It was unfeasible to purchase Tau protein (Sigma Aldrich) at the required quantities due to cost, therefore in-house production was necessary. In this research TauΔ1-250 fragment was used instead of full-length Tau as the plasmid was already in the lab and this protein fragment aggregates in ~8 hours whereas full length Tau aggregation can take up to ~72hours (Crespo et al., 2018; Taniguchi et al., 2005). This slow aggregation of full-length Tau may be due to its high proportion of polar and hydrophilic molecules. Recombinant expression of TauΔ1-250 in *Escherichia coli* (*E.coli*) was conducted in order to facilitate the aim of this research. *E. coli* expression systems can produce high yields of protein in a short amount of time for a low cost. Disadvantages include no eukaryotic post-translational modifications and improper folding for some proteins.

5.1.2 CATION EXCHANGE COLUMN CHROMATOGRAPHY

Cation exchange chromatography is the separation of negatively charged or polar molecules. There are two phases; the stationary phase, where positively charged proteins bind to the negatively charged column, and the mobile phase which is the elution of the column. Elution of proteins can be achieved by changing the pH or ionic strength of the mobile phase, resulting in ion exchange on the column. In this research the stationary phase column consistsed of negatively charged SP-sepharose polymers which retained cations. At a protein isoelectric pH, the net charge is neutral, however if the pH is shifted above or below the protein isoelectric point the net charge becomes negative or positive, respectively. TauΔ1-250 (pI 9.5) was positively charged because it was reconstituted in purification buffer (pH 6.8), therefore Tau was attracted to the negative beads of the cation exchange column. To secure the protein of interest the column was eluted using NaCl. Na^+ ions compete with positively charged proteins bound to the negatively charged column, causing those proteins to elute. Neutral and negative ions such as Cl^- do not bind to the column and pass through the mobile phase. Differently charged molecules elute at different concentrations of NaCl.

5.1.3 AMMONIUM SULPHATE PRECIPITATION

Ammonium sulphate precipitation is a technique used to precipitate proteins out from a solution. This is achieved through the manipulation of three main interactions between proteins and water: 1) hydrogen bonding between water and polar groups such as Serine, Threonine and Tyrosine, 2) ion hydration between charged side chains such as Arginine, Glutamic acid and Lysine and 3) hydrophobic hydration between Valine, Isoleucine, Leucine and Phenylalanine (Wingfield, 2001). When low levels of salts are introduced to a solution ("salting-in"), they help to stabilise proteins due to their charge, the same way magnesium stabilises the backbone of DNA. Native globular proteins maintain their solubility at ~0.3-0.4g water per gram protein. At high salt concentrations ("salting-out"), the salt has a higher affinity to interact

with water, resulting in fewer protein-water interactions at the hydration layer due to increased solvent

surface tension. (Bhattacharyya et al., 1988, Rupley et al., 1983 and Green and Hughes, 1955). This results

in increased hydrophobic interactions between protein and water; causing proteins to decrease their

surface area to minimise contact with the salts by self associating and subsequently precipitating out of

solution (Wingfield, 2001).

5.2   TAU AGGREGATION EXPERIMENTS

In this research, TauΔ1-250 was used instead of full-length Tau for aggregation experiments as it aggregates faster and more readily (Kumar et al, 2014). Tau is difficult to aggregate *in vitro* without an inducer due to its hydrophilic nature, as demonstrated by having ~38% hydrophilic amino acids. Hydrophobic conditions are required to bring the Tau molecules together, so they can begin the aggregation process. Induced aggregation kinetics for Tau fibril formation is characterised by a lag phase, followed with a period of exponential growth and reaching a plateau at equilibrium (Chirita et al., 2005). The most studied aggregation assays use either polyanions or fatty acids in oxidative or reductive conditions, respectively (Ward et al., 2013; Barghorn and Mandelkow, 2002). The two common anionic surfactants are heparin and arachidonic acid which both induce the formation of PHFs in 3R isoform Tau (contains three microtubule-binding repeat domains) whereas fibrils are less twisted when aggregating 4R isoform Tau (contains four microtubule-binding repeat domains) and are straighter (Barghorn and Medelkow, 2002). Heparan sulfate is a glycosaminoglycan with a structure very similar to heparin and co-exists with Tau in the nerve cells of AD patients (Uversky and Lyubchenko, 2013). Calamai et al., (2006) stated that removing the sulphate groups from heparin or adding magnesium or calcium ions suppresses aggregation. This suggests that Tau aggregation is rather influenced by electrostatics instead of the nature of negatively charged polymers (Sibille et al., 2006). According to literature heparin appears to be the most widely used polyanion aggregation inducer as it is much cheaper than other inducers such as Arachadonic acid (Pickhardt et al., 2007; Li et al., 2009; Hattori et al., 2008; Yao et al., 2003). Depending on the isoform, Tau generally has a pI of 8.3-10.0, so is positively charged at neutral pH (Von Bergen et al., 2005). K18 is a recombinant construct of Tau that only comprises the 4R repeat domains and has a pI of 10.39 and a net charge of +9 at neutral pH (Jeganathan et al., 2008). Tau repeat domains are positively charged and are attracted to negatively charged microtubules, however lose their positive charge upon

phosphorylation (Gong and Iqbal, 2008). Since TauΔ1-250 (entails the 4R domain plus the N terminus) has a pI of 9.3, it will also have a high net positive charge at neutral pH. Amongst all known biological molecules, heparin has the highest negative charge density allowing it to overcome positive charges in Tau (Cox and Nelson, 2004). This reduces the activation energy required for aggregation; thereby accelerating fibril growth (Zhu et al., 2010). **Figure 5.1** demonstrates the kinetic role of heparin allowing one heparin molecule to attract two Tau monomers and undergo conformational changes to form an aggregation nuclei dimer.
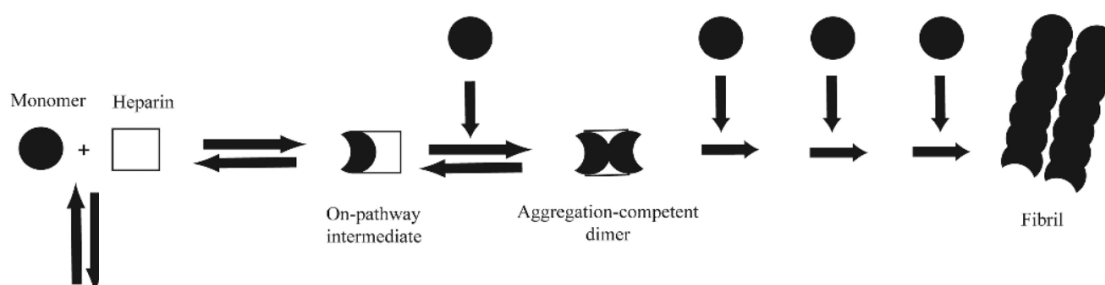
Figure 5.1: Illustrative model demonstrating a single heparin molecule binding two Tau monomers to form an aggregation competant dimer (Ramachandran and Udgaonkar, 2011).

Figure 5.2 illustrates an inverted-U curve where the rate of fibril formation is observed for dependence on the concentration of heparin. (Ramachandran and Udgaonkar, 2011). Insufficient heparin results in a reduced rate of aggregation, ~1:2 Tau:heparin yields the fastest rate of aggregation, however exceeding this ratio causes unbound heparin to increase ionic strength which inhibits aggregation and increasing lag
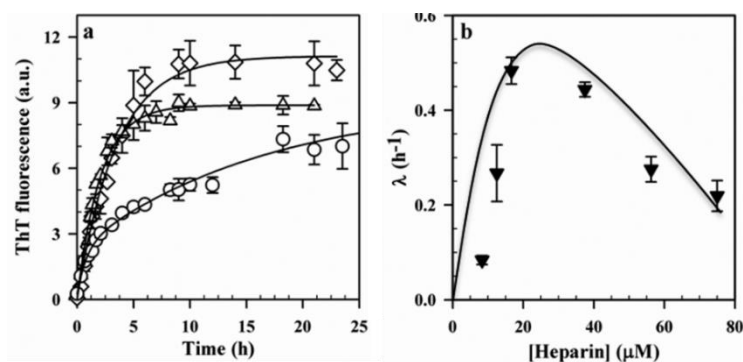
Figure 5.2: Aggregation kinetic model of K18 50μM a) in the presence of different heparin concentrations at pH 7: 8.3μM (○), 16.6μM (Δ), and 56.2μM (◊) b) Apparent ThT monitered kinetics rate constant plotted against heparin concentration (Ramachandran and Udgaonkar, 2011).

times (Ramachandran and Udgaonkar, 2011; Zhu et al., 2010; Jeganathan et al., 2008). Similar patterns for rate of fibril formation is also dependent upon concentration of protein present. To compare exponential growth phases more clearly a conservative molar ratio of Tau:heparin commonly used is 4:1.

Other potential inducers of aggregation include: poly-glutamate, RNA, alkyl sulphate detergents, docosahexaenoic acid, quinones, taurine and hexafluoro-2-propanol (Kampers et al., 1996; Lim et al., 2014; Barghorn and Mandelkow, 2002; Elbaum-Garfinkle et al., 2010; Santa-Maria et al., 2004; Santa-Maria et al., 2007; Konno et al., 2004). Fatty acids and detergents behave in a different manner in comparison to negatively charged polymers such as heparin and RNA which freely bind with Tau and act as scaffolds. Instead, fatty acids and detergents form negatively charged micelles by sequestering their hydrophobic tails inwards and displaying their hydrophilic heads outwards. Once they exceed the critical micellar concentration they then behave as inducers of aggregation through their negatively charged outer surface (Ramachandran and Udgaonkar, 2011; Barghorn and Mandelkow, 2002). This negative charge attracts Tau proteins causing increases in concentration which enables the Tau to aggregate by overcoming the required energy barrier (Chirita and Congdon, 2005). As Tau forms hydrophobic interactions, it reduces its interactions with water promoting fibrilisation. This hypothesis correlates to *in vivo* observations whereby PHFs are often bound to organelle membranes, suggesting that perhaps disturbances in lipid metabolism may affect their byproducts or membranes in general and thus induce the aggregation cascade of Tau (Kuret et al., 2005).

Proteins usually either have a net positive or negative charge depending on the pH of the solution they are in as this alters the electrostatic properties of the protein surface. Typically, at low pH they have a net positive charge whereas at high pH they have a net negative charge. At a pH that equals a specific protein isoelectric point the net charge becomes neutral and the protein becomes more insoluble as there is less repulsion between molecules resulting in an increase in hydrophobicity and aggregation. According to Ruffin et al. (2014), hippocampal neurons in in CO_2/HCO_3^- containing media have a pH of ~7.03–7.46 and

extracellular pH of ~7.35 (Raley-Susman et al., 1991; Schwiening and Boron, 1994; Bevensee et al., 1996; Church et al., 1998; Vincent et al., 1999). Physiological pH (7.4) was used for the research in this thesis as it is similar to the human brain and because within the pH ranges of ~5-10 heparin is efficient in various buffers. Outside of these pH values would cause the reaction to break down due to the disappearance in the pattern of charged interactions (Jeganathan et al., 2008). Addition of an appropriate buffer to the aggregation mix is necessary to resist changes in pH. Sigmoidal ThT growth curves representing amyloid aggregation are characteristcally divided into three main phases: 1. lag (represents thermodynamically unfavourable nucelus formation), 2. Growth (thermodynamically favourable growth) and 3. Plateau (when the concentration of monomers has reached equilibrium). Barghorn and Mandelkow (2002) observed sigmoidal ThT curves when aggregating Tau in phosphate buffered saline (PBS). However, Ramachandran and Udgaonkar (2011), confirmed PBS follows sigmoidal kinetics but was not very reproducible; whereas Tris buffer was more reproducible but appearedd to follow single-exponential kinetics without any lag phase at pH 7.5, in both the absence and presence of NaCl (**Figure 5.3**).
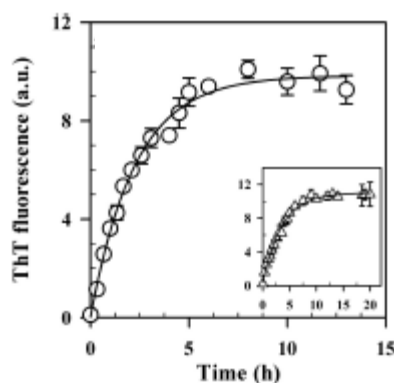
Figure 5.3: K18 fibril formation in presence of heparin. ThT fluorescence of 50µM K18 with 37.5µM heparin in 25mM Tris, 50mM NaCl, 1mM DTT, pH7 at 37°C. (Ramachandran and Udgaonkar, 2011).

Many aggregation protocols use 37°C corresponding to physiological temperature (Yao et al., 2003, Pickhardt et al., 2005, Hattori et al., 2008 and Li et al., 2009). This coincides with Uversky et al., (2001) who suggested that elevating temperatures promoted partial folding through a hydrophobicity-driven collapse. Aggregation is a result of electrostatics and should be conducted at 37°C and at a pH which also

mimics *in vivo* conditions.All Tau isoforms comprising the four microtubule-binding repeat domains contain two cysteine residues at C291 and C322 which can form intermolecular and intramolecular disulphide bonds upon oxidation to produce covalent dimers or compact monomers, respectively (Walker et al, 2012). Aggregation studies using mutant Tau containing only one cysteine residue lead to the conclusion that these intermolecular disulphide bonds facilitate PHF assembly in 3R Tau (Meraz- Ríos et al., 2010; Sugino et al., 2009; Kuret et al., 2005; von Bergen, 2000; Barghorn and Mandelkow, 2002; Di Noto et al., 1999). This is supported by *in vitro* studies which suggested that intramolecular disulphide bonds between the two cysteines retard Tau aggregation as they prevent intermolecular disulphide bonding (Walker et al., 2012). **Figure 5.4** demonstrates that aggregating K19 (3 repeat domains of Tau without the second repeat) in reducing conditions reduced rate and extent of aggregation whereas the opposite was found for K18 (4 repeat domains of Tau).
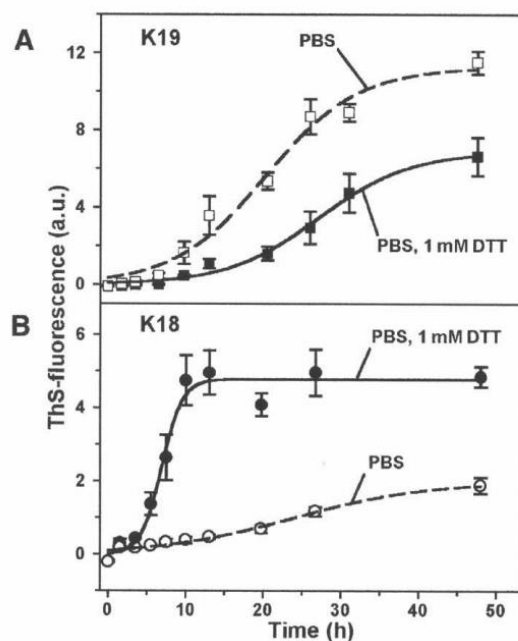
Figure 5.4: Aggregation kinetics. **A:** K19 in oxidising conditions, **B:** K18 in oxidising conditions. PHFs in A) reducing and oxidative conditions using ThS fluorescence (Barghorn et al., 2005). Thioflavin-S (ThS) is an alternative dye to ThT to monitor fibril formation, however reports higher background signal.

Sahara et al., (2007) stated that Tau mutants without any cysteine residues still aggregated to form fibrils over a 24-hour period; suggesting a more complicated role for intramolecular disulphide bonds. It is important to note that the pathological AD brain includes both 3R and 4RTau which undergoes oxidative rather than reducing conditions to encourage aggregation (Zhu et al., 2010). Ibáñez-Salazar et al. (2017), demonstrated that by inducing oxidative stress in human fibroblast primary cultures transfected with Tau-gene or untransfected, resulted in higher immunopositivity to phospho-Tau within cell nuclei in both models. Fatty acid oxidatation was postulated by Gamblin et al. (2000), to stimulate Tau aggregation *in vitro*, rather than cysteine dependent oxidation of Tau. In short, 4R Tau readily forms fibrils in a reduced environment but fibril formation is impaired with oxidation, whereas 3R Tau fibril formation is impaired in a reduced environment but readily forms fibrils with oxidation. For the purpose of the *in vitro* experiments in this thesis, DTT was used in the 4R Tau aggregation mix as a reducing agent. This prevented Tau from locking itself into compact monomers through cysteine disulphide cross bridging and provided necessary charge compensation to enhance the rate and extent of aggregation.

Aggregating conditions (incubation times and temperatures, voltage, ionic concentration, the buffer pH and the length of Tau used) are important to take into consideration such as (Jeganathan et al., 2008). The main driving forces for Tau repeat domain filament formation involves intermolecular disulphide bond production, electrostatic interactions, hydrophobic interactions and non-covalent interactions like hydrogen bonding (Zhu et al., 2010). Peptide inhibtiors can be made proteolytically stable through N-methylation or retroinversion which alters the structural configuration of peptide backbones; rendering them inaccessible to proteolytic enzymes (Cody et al., 1997). These modofications will be explored for the lead peptide inhibitor.

5.2.1 THIOFLAVIN-T FLUORESCENCE

Although ThT fluorescence does not quantitatively measure fibrilisation it was used in this research to indicate the presence of amyloid. Thioflavin-T (ThT) and Thioflavin-S (ThS) are thiazine salt dyes which have positive and negative charges, respectively, as ThS is a sulfonated derivative of ThT. They are commonly used to detect real time amyloid assembly by selectively binding (between pH 5-9) in parallel to the long axis of β-sheets along surface side-chain grooves and have also been proposed to bind to cavities as either planar monomers or dimers, respectively (Wu et al., 2008, Krebs et al., 2005, Stsiapura et al., 2007, Voropai et al., 2003, Stsiapura et al., 2008, Friedhoff et al. 1998, Groenning et al., 2007). Cavities with an 8–9 Å diameter may be present in the centre or between protofilaments during association into protofibrils/fibrils (Blake and Serpell, 1996, Serpell and Smith, 2000, Jiménez et al., 1999, Malinchik et al., 1998, Elam et al., 2003). ThT has a central C-C bond as seen in **Figure 5.5** flanked by freely
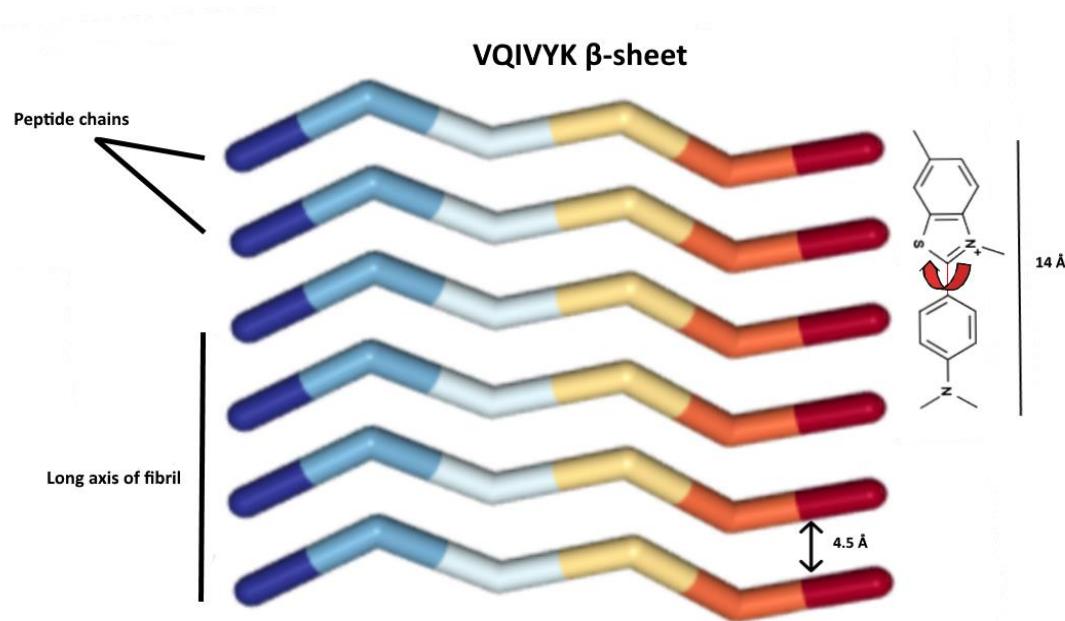
Figure 5.5: Schematic of the chemical structure of Thioflavin-T ordered in parallel with its long axis to the long axis of the Tau VQIVYK fibril (The Protein Data Bank De la Cruz, et al., 2017). In an extended conformation ThT requires ~3-4 continuous β-strands in a β-sheet. Note Thioflavin-T C-C bond which rotates upon binding to β-sheet (red) resulting in the compounds fluorescent properties to red shift with enhanced emission maxima at 482 nm when excited at 450 nm (adapted from Groenning, 2010).

oscillating benzothiazole and aminobenzoyl rings. Upon binding to consecutive β-sheet strands this oscillation becomes restricted by rotating the C-C bond and locking it into a stabilised high energy state ThT-amyloid complex (Girych et al., 2014; Chan et al., 2015). This prevents movement of electrons; keeping ThT in its locally excited state which causes a red shift in its fluorescent properties resulting in fluorescence at emission maxima 482 nm when excited at 450 nm in the presence of amyloid (Wolfe et al., 2010; LeVine, 1999; Girych et al., 2014, Amdursky et al. 2012). ThT does not modulate fibrilisation of Tau due to its positive charge and small supramolecular structure (Kuret et al., 2005).

According to LeVine (1997), ThS is less suitable than ThT for kinetic analysis as ThS fluorescence may interfere with the determination of fibril bound species. LeVine (1999), described that in solution ThS generates high background fluorescence (~x10) rendering it unsuitable for quantitative analysis (Wegmann et al., 2018). This is supported by Kuret et al. (2005), who suggested that ThS is a semi-quantitative method for estimating aggregation of Tau. In summary kinetic based experiments in this thesis will be conducted using ThT at excitation and emission maxima of 450 and 482 nm, respectively. Xue et al. (2017), concluded that ThT has very little effect at influencing aggregation kinetics at concentrations of 20µM and below and that 50µM or more may influence the aggregation curve.

5.2.2 CONGO RED BIREFRINGENCE

This technique was used to investigate if the inhibitors could prevent Tau from forming β-sheet secondary structures. Birefringence denotes the different refractive indices observed by horizontal and vertically polarised light. Congo red dye is the current gold standard for detecting amyloid in tissue as it binds to amyloid and displays a characteristic apple green birefringence when viewed under polarized light. Amyloid is significantly different in its secondary structural compositions in comparison to other insoluble proteins, in that its core has an exceptionally high β-sheet content, whereby hydrogen bonds run in parallel to the fibre axis and β-strands are perpendicular; having a distance of ~4.7Å between each β-

strand, according to X-ray diffraction (Rambran and Serpell, 2008). The exact mechanism as to how Congo red binds to amyloid is unknown, however it is reported that Congo red binds with high affinity to β-sheets, in a similar fashion as ThS does, which is also sulfonated (LeVine, 1993).

5.2.3 CIRCULAR DICHROISM

This technique was also used in conjunction with congo red birefringence to investigate if the inhibitors could prevent Tau from forming β-sheet secondary structures. CD is a spectroscopic technique which determines the secondary structure and folding properties of proteins and conformations of other macromolecules by analysing samples over a range of wevelengths. Regarding proteins, CD can also be used to investigate pH, heat or solvent induced changes and protein un/folding. CD measures molecules with chiral centres, whose spectral measreuments can be either positive or negative as a result of greater absorption of either left handed or right handed circularly polarised light, respectively (Li et al, 2009). These positive and negative measurements are manifested as peaks and troughs, respectively, when viewing a CD spectrum. Left and right handed circularly polarised light can be summarised through **Figure 5.6**.
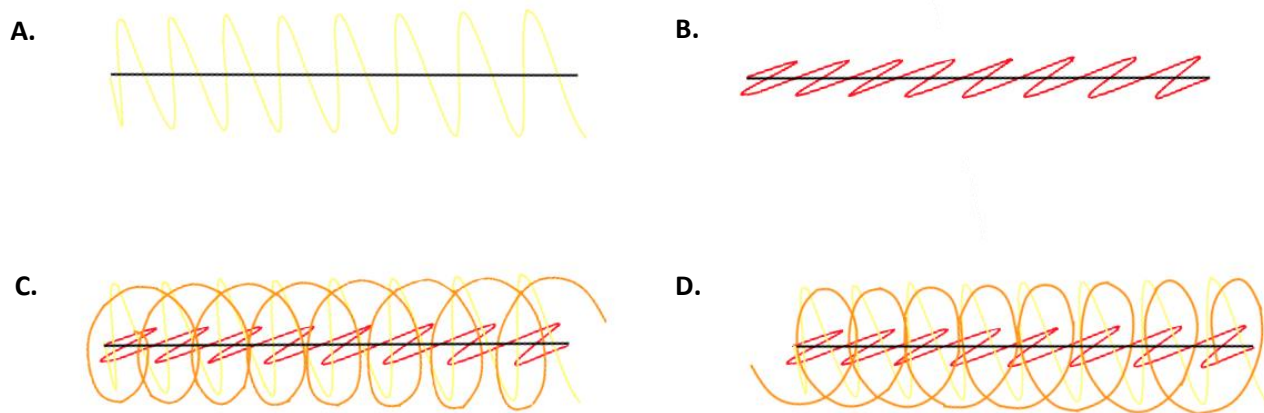
Figure 5.6: Demosntrates (along z-axis) A: vertically polarised light, B: horizontally polarised light, C: left circularly polarised light, D: right circularly polarised light.

In CD monochromatic light passes through a polariser which polarises the light and then into a photoelastic modulator (modulates polarisation of light sources) to form left and right handed circularly polarised light. Left handed circularly polarised light ossilates about the propagation direction in a clockwise fashion, whereas right handed circularly polarised light ossilates in an anti-clockwise fashion. As circularly polarised light reaches an optically active sample e.g. a protein; some light will be differentially absorbed. The electronic structure of the protein results in characteristic bands in respective regions of the CD spectrum. Secondary structures such as α-helices, β-sheets, β-turns and unordered can be determined from distinct spectra in the far UV as seen in **Figure 5.7.**
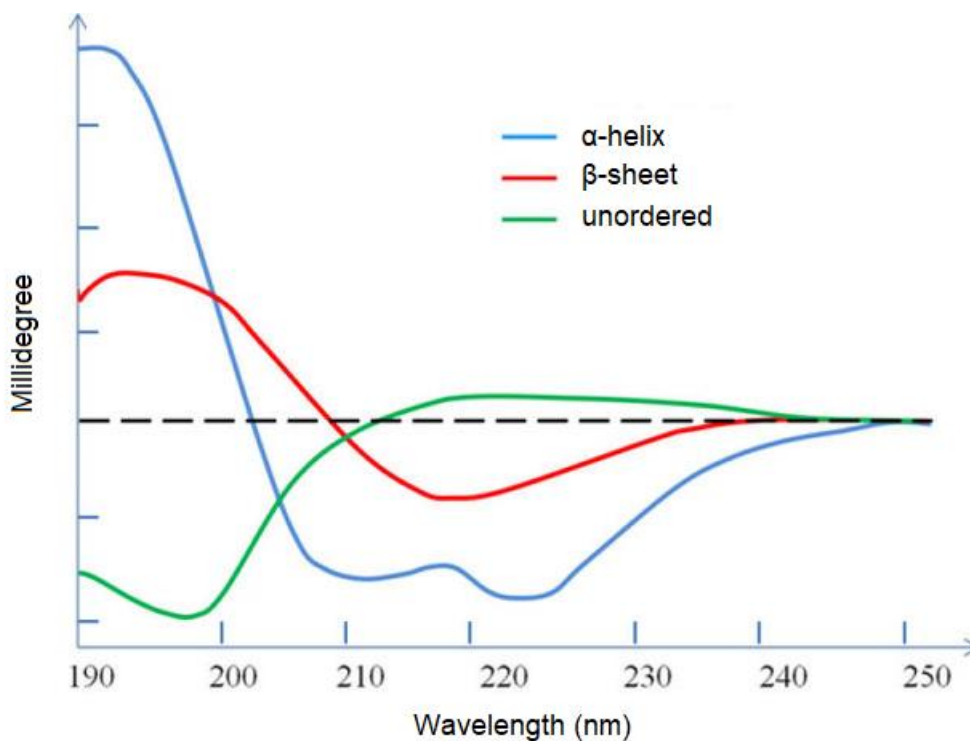
Figure 5.7: Examples of far-UV CD spectra for α-helices, β-sheets and unordered (adapted from Wei et al., 2014)

5.2.4 TRANSMISSION ELECTRON MICROSCOPY (TEM)

As ThT could potentially bind to both fibrillar and non-fibrillar β-sheets and emit fluorescence, TEM was employed in this research to validate the ThT results. In existing literature, TEM has been utilised extensively to monitor formation of oligomers and amyloid fibrils *in vitro* and to qualitatively identify specific characteristics such as fibril length, width curvature, smoothness (for example Tau_{441} fibrils displaying a fuzzy coat due to the N terminus of Tau_{441}), bends and twists (Goldsbury et al., 2000 and Thorn et al., 2008). TEM is a microscopy technique which uses the same basic principles as simple optical microscopy, however instead of using light, it uses electons; which results in much more powerful resolution. An electron gun fires a beam of electrons produced by thermic emission of a super-heated tungsten wire. This beam of electrons is focused by condenser lenses in a vacuumed space before reaching the specimen suspended grid. As the beam passes through the specimen, certain parts are transmitted which are focused by the objective lens. This produces an enlarged visible image on a fluorescent screen of the specimen. This process can be summarised by **Figure 5.8**.
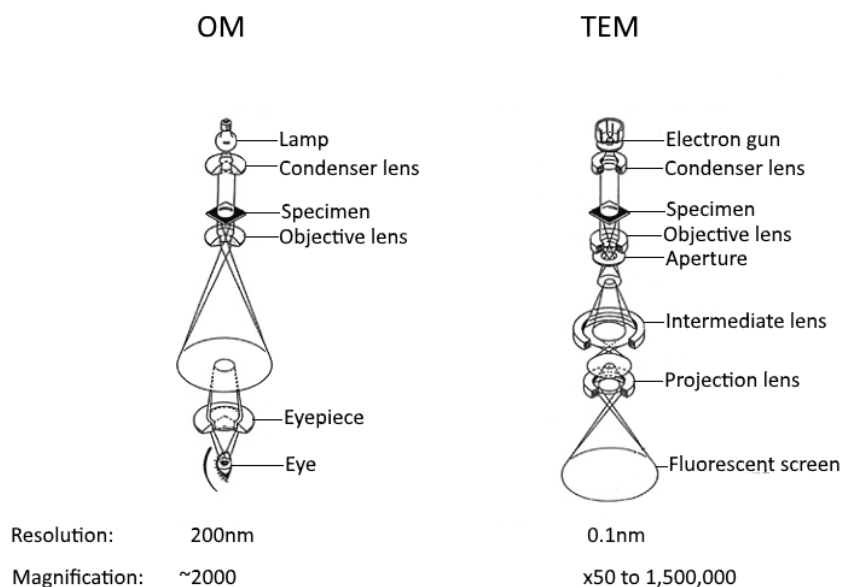
Figure 5.8: Comparison of the layout and the light/electron beam path of an optical microscope and transmission electron microscope, respectively TEM (Adapted from Jeol, 2019)

142

5.3 RESULTS

In addition to the peptides discussed in **Section 4,** a variety of other peptides were also drafted for analysis in the wet lab. Tau aggregation is largely facilitated by charge interactions. These peptides utilised arginine residues to investigate the effects of their global charge and local charge (depending on the terminus arginine residues were added to) on Tau aggregation. Peptide inhibtiors used a nomenclature to make it easier to identify their properties when working in the lab. AG01 refers to the core binding sequence VQIINK, whereas AG02 refers (to VQIVYK), AG02ΔI (refers to VQ**K**VYK with original replacement of isoleucine with lysine), AG02ΔV (refers to VQI**K**YK with the original replacement of the second valine with lysine) and AG03 (which refers to VQIK(Ac)YKP). Peptide inhibitors were flanked with at least 1 glycine followed by 1 arginine. The number of arginines were counted for each peptide inhibitor, therefore, AG02R5 would be RG-VQIKYK-GRRRR. **Table 5.1** summarises the peptides used in this chapter.

Peptide ID	Sequence	Purity %
AG01	Ac - R G <u>V Q I I N K</u> G R - NH$_2$	>90
AG02	Ac - R G <u>V Q I V Y K</u> G R - NH$_2$	>90
AG02R4	Ac - R R G <u>V Q I V Y K</u> G R R - NH$_2$	>90
AG02R5	Ac - R G <u>V Q I V Y K</u> G R R R R - NH$_2$	>90
AGR502	Ac - R R R R G <u>V Q I V Y K</u> G R -N H$_2$	>90
AG02PR5	Ac - R G <u>V Q I V Y K P</u> G R R R R - NH$_2$	>90
AG02R6	Ac - R R R G <u>V Q I V Y K</u> G R R R - NH$_2$	>90
AG02R9	Ac - R G <u>V Q I V Y K</u> G R R R R R R R R R - NH$_2$	>90
AG02TAT	Ac - R G <u>V Q I V Y K</u> G R Y G R K K R R Q R R R - NH$_2$	>90
AG02ΔI	Ac - R G <u>V Q K(Ac) V Y K</u> G R - NH$_2$	>90
AG02ΔV	Ac - R G <u>V Q I K(Ac) Y K</u> G R - NH$_2$	>90
AG03	Ac - R G <u>V Q I K(Ac) Y K P</u> G R R R R R R R R R - NH$_2$	>95
AG03-Cys	Ac - R G <u>V Q I K(Ac) Y K P</u> G R R R R R R R R R C - OH	>95
Scramble AG03	Ac – R G Q P K I K(Ac) Y V G R R R R R R R R R - NH$_2$	>95
AG03M	Ac - R G <u>V(m) Q I(m) K(Ac) Y(m) K P(m)</u> G R R R R R R R R R - NH$_2$	>95
RI-AG03	Ac - r r r r r r r r r G <u>p k y k(ac) i q v</u> G r - NH$_2$	>95
FAM-RI-AG03	Ac - k(FAM) r r r r r r r r r G <u>p k y k(ac) i q v</u> G r - NH$_2$	>95
Poly-R	R R R R R R R R R - NH$_2$	>95
TAT	Ac - Y G R K K R R Q R R R - NH$_2$	>95

Table 5.1 List of peptide inhibitor designs customly synthesised for research in this thesis. Underlined sequence corresponds to Tau binding region. Peptide inhibitors were custom made by Peptide Synthetics (Fareham, UK) with >90% purity and Severn Biotech (Kidderminster, UK) with >95% purity; determined by HPLC-MS. Peptide HPLC-MS data can be found in **Appendix D-V.**

5.3.1 PLASMID ANALYSIS
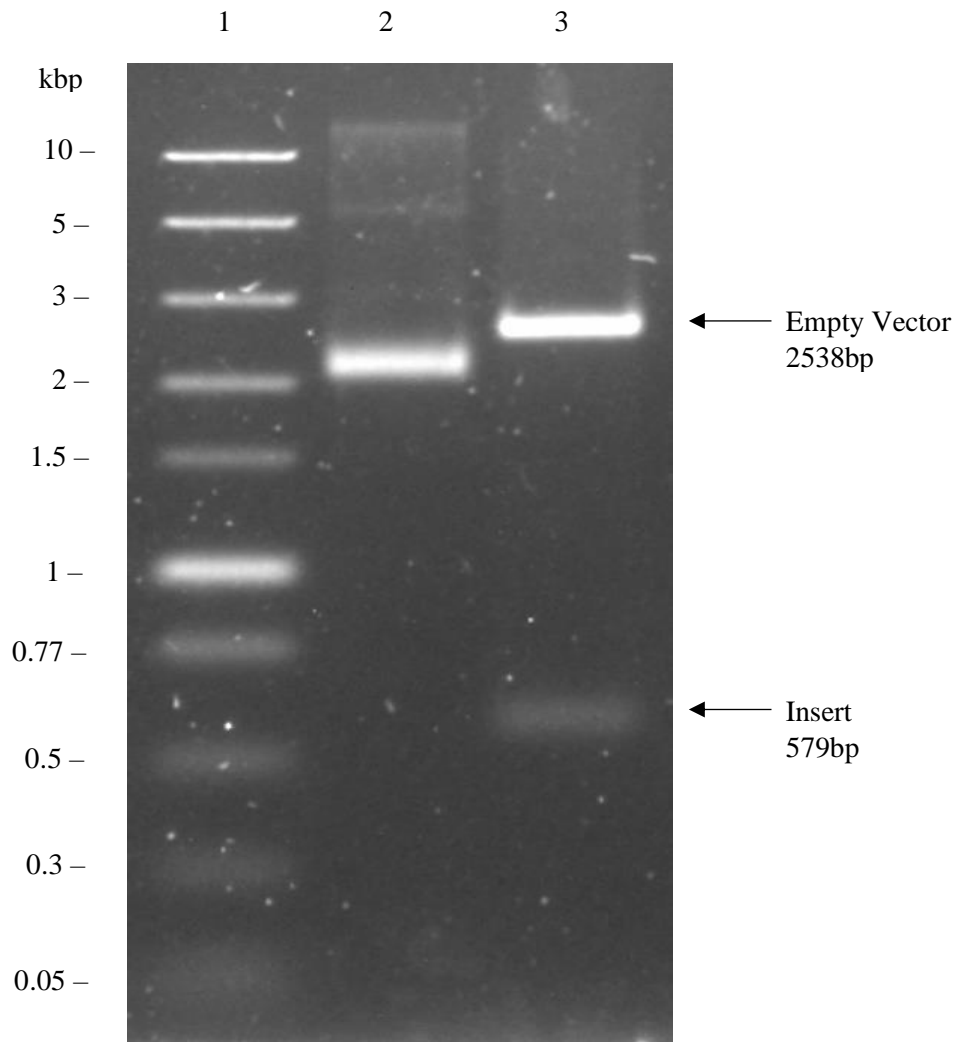
Figure 5.9: Agarose gel of the uncut circular plasmid of the pRK172 expression vector containing the of TauΔ1-250 DNA of interest and a cut version using *Nde*I and *Eco*RI enzymes. 1: Fast DNA Ladder, 2: Uncut circular plasmid, 3: Cut plasmid + *Nde*I + *Eco*RI.

Figure 5.9 confirmed the successful DNA digest and the size of the sequences for the TauΔ1-250 insert

and the pRK172 empty vector, as compared to the DNA sequence.

5.3.2 TAU EXPRESSION AND PURIFICATION

5.3.2.1   EXPRESSION OF TAU

Following successful transformation of TauΔ1-250 pRK172 expression plasmid into *E.coli* BL21 (DE3) expressing cell line, an expression protocol was devised and optimised to express large quantities of Tau in LB media and ampicillin (0.1%). Protein expression was optimised for induction incubation at 37°C for 3 hours and with agitation following experimental inductions (at 26°, 37° and 42° for over 1-24 hours), which the cell culture samples were sampled (18µL) on an hourly basis over 5 hours and overnight for SDS-PAGE, as seen in **Figure 5.10**. Successful expression of Tau is indicated by the band at 20 kDa which is absent prior to induction with IPTG (1mM). Optimum temperature and duration of induction with IPTG was determined to be 3 hours at 37°C due to the thicker bands in comparison to the 26°C and 42°C controls. After overnight incubations, Tau expression appeared to be lost due to the culture becoming saturated causing basal leakage of the expression system resulting in plasmid instability from leaky T7 expressions ystem (Sturdier, 2005). Lysed cells will also have been exposed to proteolysis.
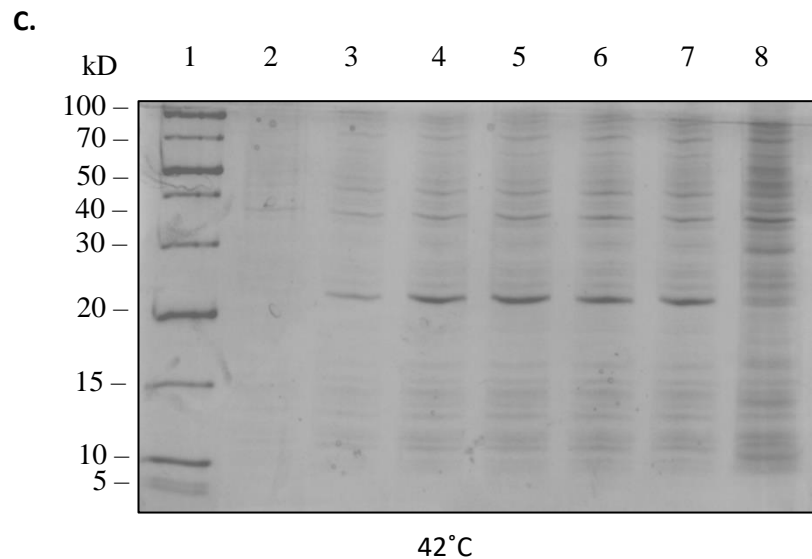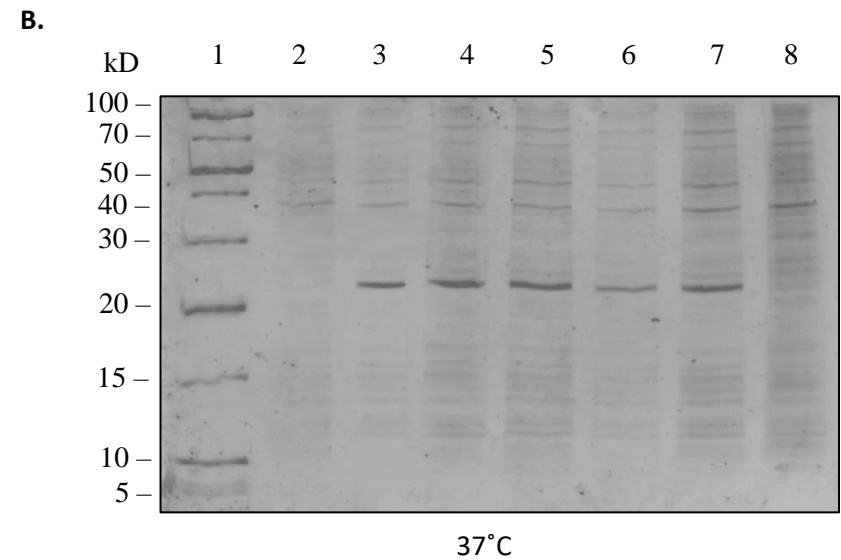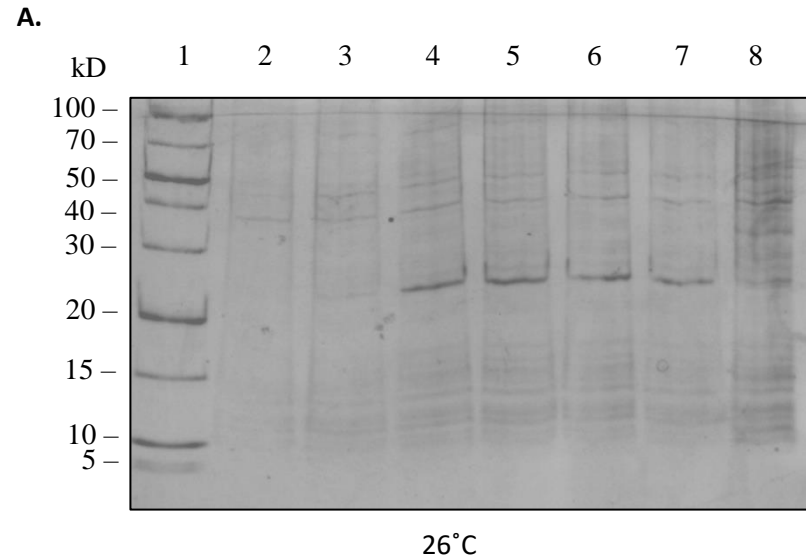
Figure 5.10: Coomassie staining of 15% SDS PAGE gels of *E.coli* BL21 (DE3) pre and post induction with IPTG (1mM) for 1, 2, 3, 4, 5 hours and overnight (**A**-**C**). Samples were incubated at various temperatures to determine the optimum. **A**: incubated at 26°C. **B**: incubated at 37°C. **C**: incubated at 42°C. Lanes 1: PageRuler Unstained Broad Range Protein Ladder (Thermo Scientific), 2: Before induction with IPTG, 3: 1hour, 4: 2 hours, 5: 3 hours, 6: 4 hours, 7: 5 hours, 8: over-night. The optimum temperature and time was 37°C for 3 hours.

5.3.2.2   PURIFICATION OF TAU

After successfully expressing Tau, purification was necessary which was achieved via cell harvesting, lysis and cell debris removal. **Figure 5.11** demonstrates that most impurities are removed after boiling and ultra-centrifuging the cell lysate, however a significant amount of Tau (or other proteins of similar molecular weight) appears to be lost in the latter stage. When conducting cation exchange chromatography, a significant amount of Tau is again lost. After washing the column with a series of NaCl concentrations, very few impurities remain. The 1M NaCl wash suggests that all the Tau had been removed from the column. After ammonium sulphate precipitation and dialysis, most of the impurities had been removed leaving behind an average >90% pure stock of Tau, as determined by **Figure 5.13**. Native Tau is a highly hydrophilic and intrinsically disordered protein which has a lack of a defined secondary structure, therefore the conformational properties of Tau in this state demonstrate a lower dependence on temperature. Tau is therefore heatstable and refolds correctly after heat treatment. Mild heat treatment of neuronal cells demonstrated Tau to bind DNA and enhance DNA repair (Sultan et al., 2011).
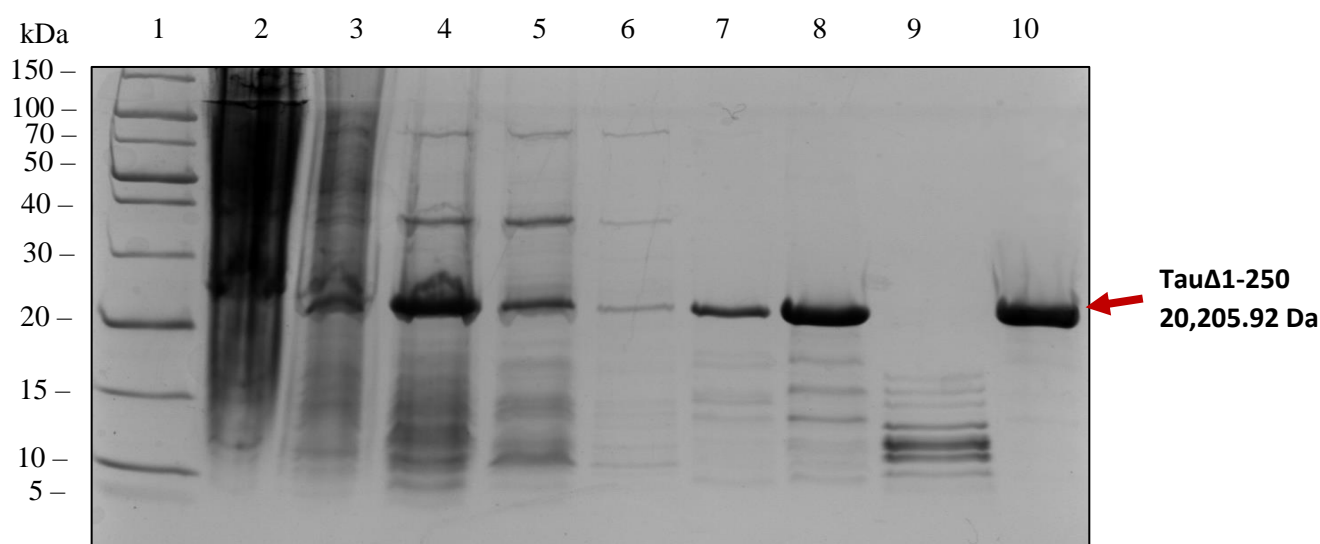
Figure 5.11: 15% SDS PAGE gel of samples from each stage of the Tau purification process; cell lysate, post centrifugation, post boiling, flow through, 0.1M NaCl wash, 0.35M NaCl wash, 1M NaCl wash, $(NH4)_2SO_4$ precipitation and dialysis. Lanes 1: Ladder, 2: Cell lysate, 3: Post centrifugation, 4: Post boiling + centrifugation, 5: Flow through, 6: 0M NaCl wash, 7: 0.1M NaCl wash, 8: 0.35M NaCl, 9: 1M NaCl wash, 10: $(NH_4)_2SO_4$ precipitation +dialysis.

The final concentration of Tau was determined using a Nanodrop 2000 (Thermo Scientific) and corrected

using the equation in **Section 3.2.4.5**. Accuracy of protein concentration was confirmed using the Pierce™

BCA Protein Assay as seen in **Figure 5.12**. Expression yields of purified Tau had n yield of ~10mg/L culture.

The graph shows a standard curve with equation $y = 120.37x^2 + 638.21x$, $R^2 = 0.9978$. The y-axis is labeled "Absorption (562nm)" ranging from 0 to 2500, and the x-axis is labeled "Concentration (µg/ml)" ranging from 0.000 to 2.500.
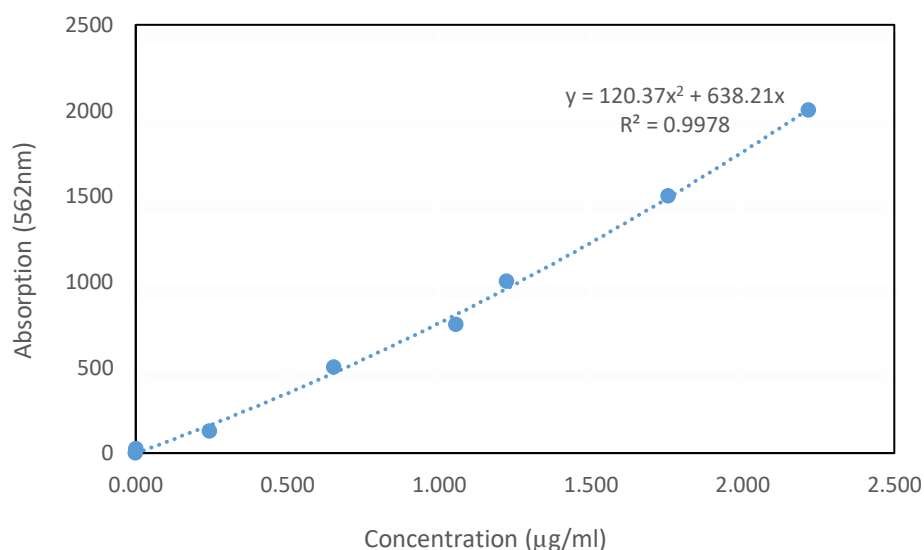
Figure 5.12: Standard curve for bovine serum albumin in the BCA protein assay.

Figure 5.13 demonstrates densitometric analysis of the purified Tau samples. This type of analysis

determines the densities of any present bands which are directly proportional to the concentration of

protein present (Smith and Veenstra, 2003). The average purity of Tau was >90%.
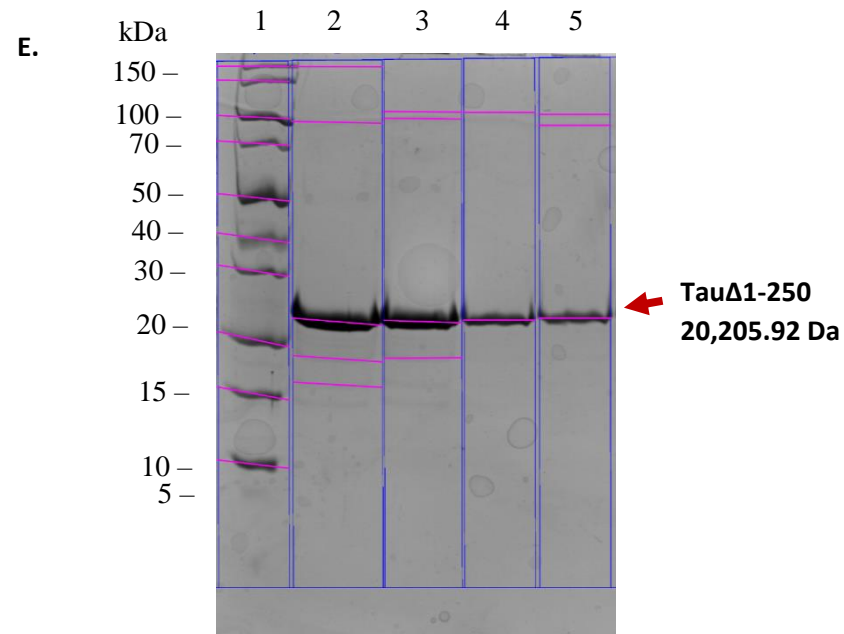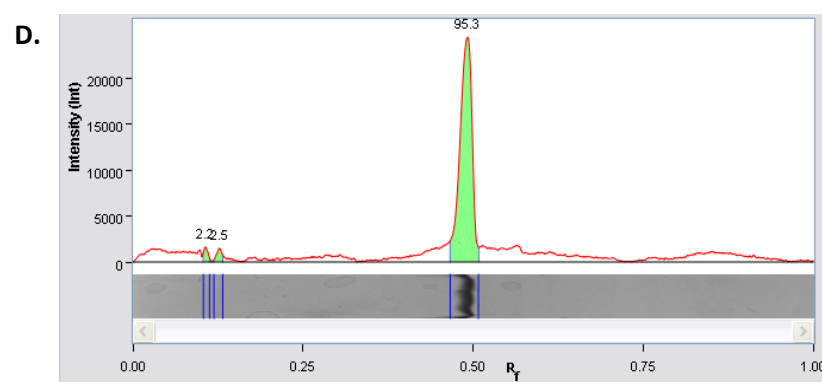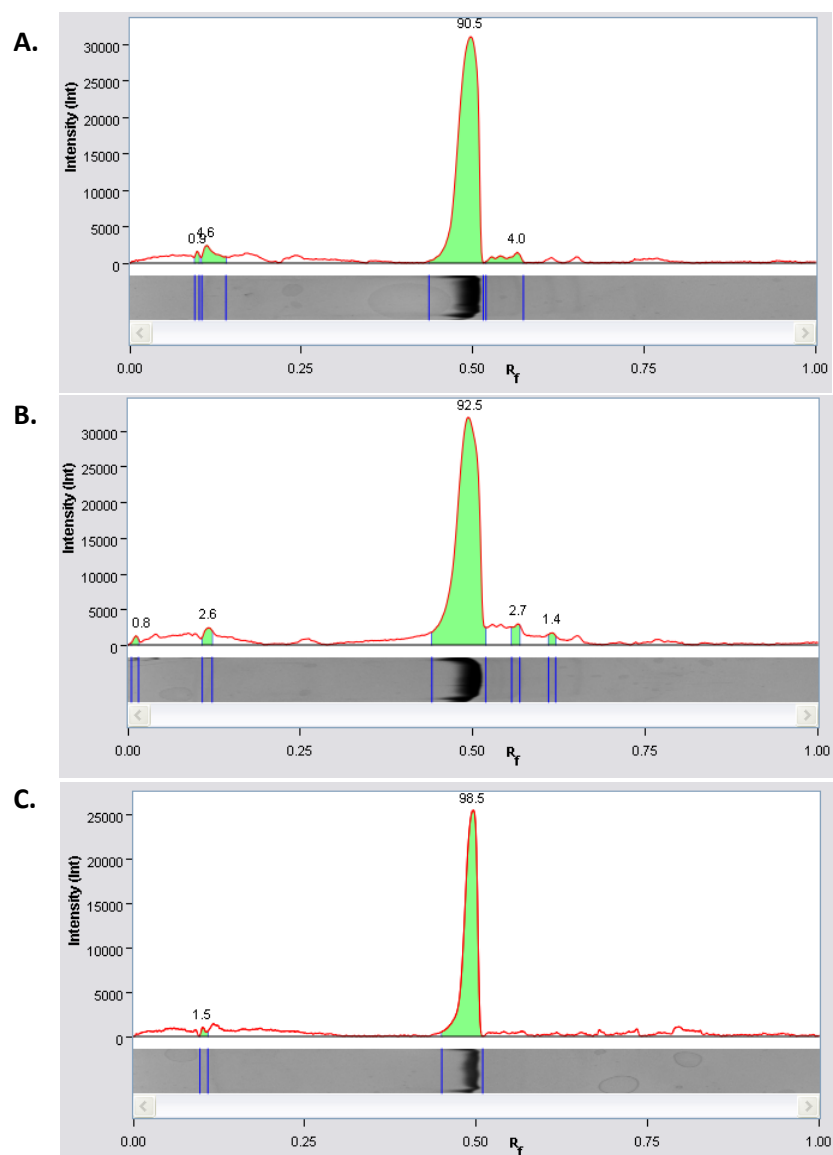
Figure 5.13: Densitometric analysis of Tau samples. **E**: 15% SDS PAGE gel of purified Tau samples from separate expression batches. **A-D**: detected band purity from lanes 2-5, respectively. Average purity of each Tau band was >90%.

5.3.3 EFFECT OF HEPARIN ON TAU AGGREGATION

The graph shows ThT Fluorescence (A.U.) on the y-axis (0 to 2000) versus Heparin Concentration (µM) on the x-axis (0 to 100). A red arrow points to the peak labelled "5µM heparin". Inset table:

Model	BiHill
Equation	$y = Pm/(1+(Ka/x)^{Ha})/(1+(x/Ki)^{Hi})$;
Plot	Mean
Pm	1849.94586 ± 42.91517
Ka	1.21973 ± 0.04643
Ki	32.02029 ± 3.77947
Ha	6.20329 ± 8.25157
Hi	1.28574 ± 0.26288
Reduced Chi-Sqr	0.3073
R-Square(COD)	0.99671
Adj. R-Square	0.98353

Figure 5.14: Thioflavin data using FlexStation 3. End-point aggregation of TauΔ1-250 (20 µM) with increasing concentrations of heparin; 0µM, 1.25µM, 2.5µM, 5µM, 10µM, 20µM, 100µM. Fitted with the '*Biphasic Hill equation*' on OriginPro.

End-point aggregation data (after 24 hours) i.e. final fluorescence data points for Tau aggregated with increasing concentrations of heparin can be seen in **Figure 5.14.** End point data was plotted to observe the relationship between heparin concentration and fluorescence signal. This demonstrated that heparin is necessary for the aggregation of Tau, and that the ratio of heparin to Tau plays an important role as well. The optimal ratio of Tau to heparin on this Figure is 4:1. At higher heparin to Tau concentrations, aggregation of Tau becomes increasingly retarded due to unbound free heparin increasing the ionic strength of the medium (Zhu et al., 2010). The bi-phasic hill equation reflects the binding of heparin to Tau as a function of heparin concentration.

150

5.3.4 CONTROLLING FOR HEPARIN
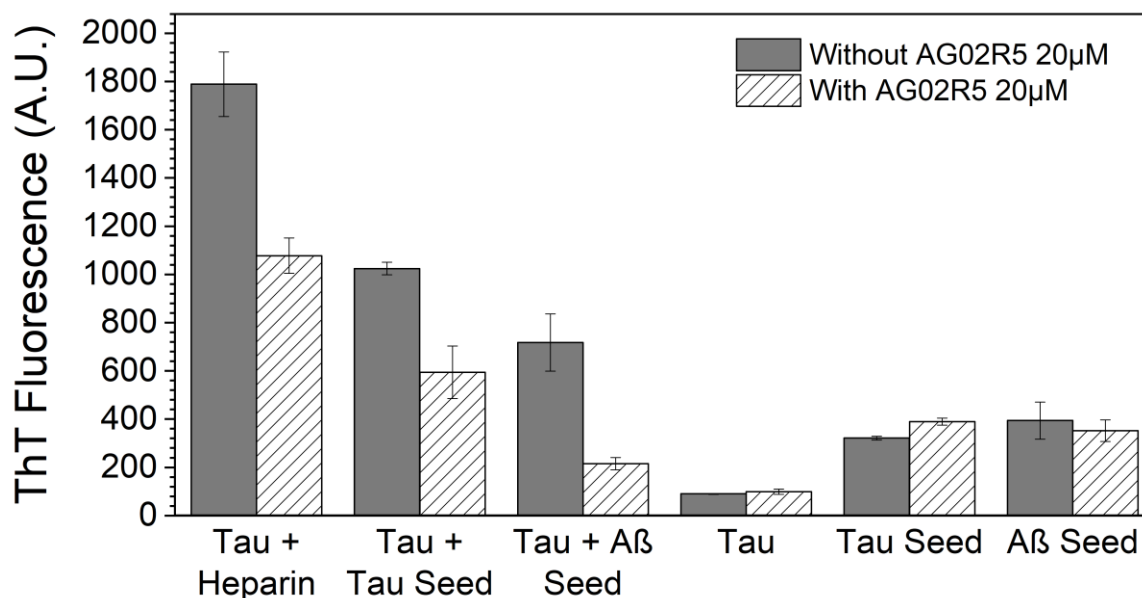
Figure 5.15: Thioflavin data using FlexStation 3. Average end-point aggregation of TauΔ1-250 (20 µM) with either heparin, Tau seed or Aβ seed to induce aggregation, with and without AG02R5 (20 µM). Experiments were conducted in triplicate and error bars are reported as standard deviation of the mean.

It was a concern that the positively charged arginine residues would sequester heparin and prevent heparin from interacting with Tau. AG02R5 was used in **Figure 5.15** as it was the lead peptide tested at the time. This figure demonstrated that AG02R5 can inhibit Tau aggregation in the presence of not only heparin, but also Tau seeds and Aβ seeds. This demonstrated that the inhibitor does not simply interfere with heparin binding to Tau through charge interactions to reduce fluorescence signal.

The binding sequence for each inhibitor was based on the VQIVYK sequence of Tau which on its own can self assemble and aggregate to form fibrils. For this reason, it was important to test that the inhibitors would not seed themselves to form fibrils. **Figure 5.16** demonstrated that AG01 [RG-VQIINK-GR] appeared to self associate considerably more than AG02 [RG-VQIVYK-GR], therefore additional experiments were conducted using AG02. AG02R4 [RRG-VQIVYKG-RR], AG02R5 [RG-VQIVYK-GRRRR], AGR502 [RRRRG-VQIVYK-GR], AG02PR5 [RG-VQIVYKP-GRRRR], AG02R9 [RG-VQIVYK-GRRRRRRRR] and AG02TAT [RG-VQIVYK-GRYGRKKRRQRRR] did not appear to self associate based on the fluorescence signal. AG02R5 and AGR502 investigated if the position of polyarginine had any significant effect on inhibition of Tau aggregation, however none was observed. Increasing the number of arginines past 5 did not seen to show any added inhibitory effects against Tau aggregation. AG02R9 and AG02TAT were designed for cell penetration and were compared to see any difference for inhibition of Tau aggregation. No differences were seen, however AG02R9 seemed to self-associate less than AG02TAT. AG02ΔI [RG-VQK(Ac)VYK-GR] self associated the most, whereas AG02ΔV [RG-VQIK(Ac)YK-GR] aggregated much less, despite having one difference in amino acid replacement compared to the native sequence. Although not much difference was seen for AG02PR5 when comparing it with AG02R5, the additional proline was still taken forward as this is also its natural position in native Tau. The angle change was hypothesised to be more effective when used in conjunction with a longer polyarginine chain to provide more binding interference. After combining several elements from these previous inhibitors, AG03 [RG-VQIK(Ac)YKP-GRRRRRRRR] was tested. It did not self associate and reduced Tau aggregation the most based on the fluorescence signal. AG03 was chosen as the lead peptide candidate for further development to make it proteolytically stable via N-methylation or retroinversion.

5.3.5 EFFECT OF INHIBITORS ON TAU AGGREGATION

A.
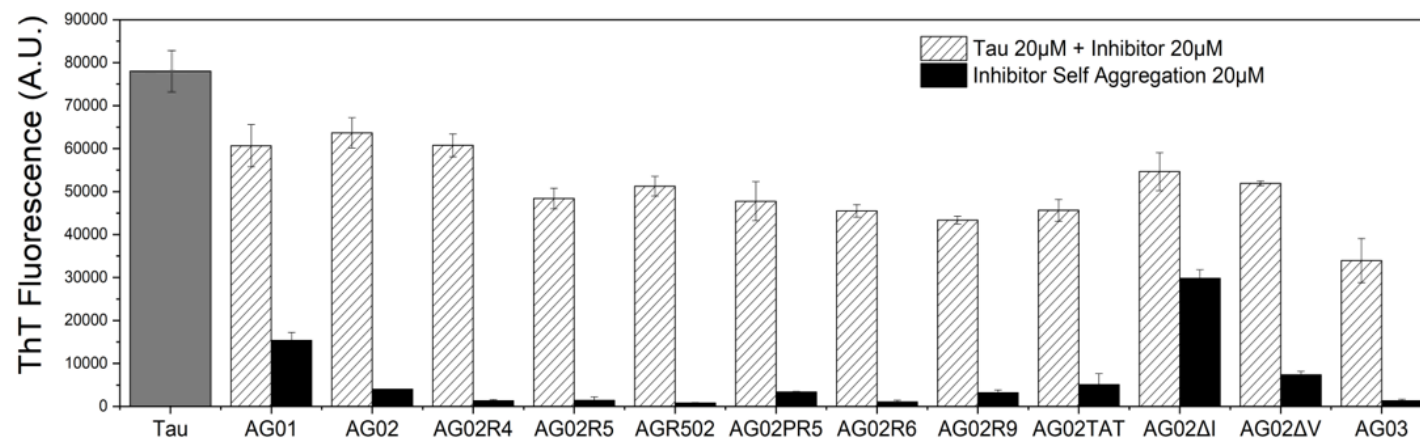
B.
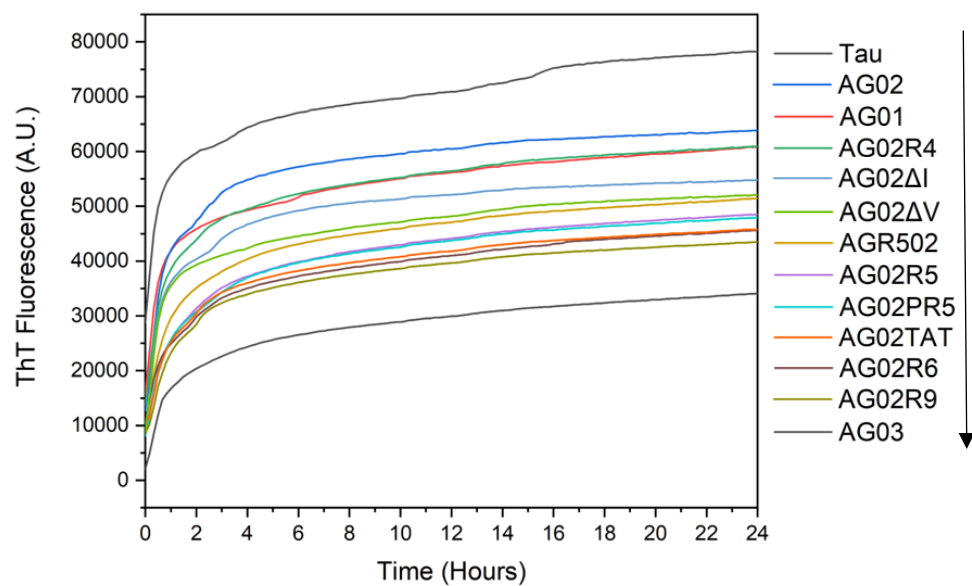
Figure 5.16: Thioflavin data using a Synergy2 plate reader. **A:** End-point (24 hr) aggregation of TauΔ1-250 (20 μM) with different peptide inhibitors (white) and attempted self assembly of inhibitors without presence of Tau (black). **B:** Aggregation kinetics of TauΔ1-250 (20 μM) incubated with different peptide inhibitors and labeled in descending order of fluorescence intensity. Experiments were conducted in triplicate and error bars are reported as standard deviation of the mean.

5.3.6 EFFECT OF RETRO-INVERSO AG03 ON TAU AGGREGATION
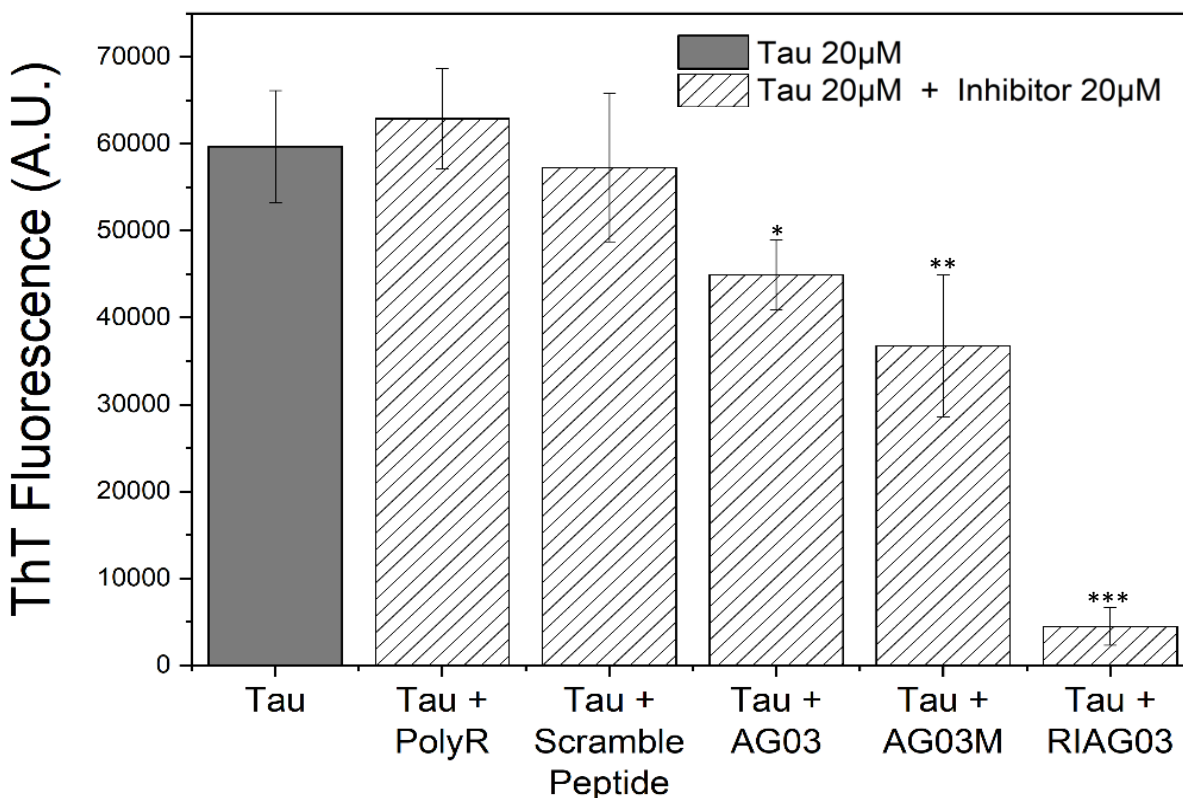
Figure 5.17: Thioflavin data using a Synergy 2 plate reader. End-point (24 hr) aggregation of TauΔ1-250 (20 μM) with equimolar concentrations of either octa-arginine, scrambled AG03 peptide, AG03, N-methylated AG03 and retro-inverso AG03. Experiments were conducted in triplicate and error bars reported as standard deviation. $P > 0.05$, * $P \leq 0.05$, ** $P \leq 0.01$, *** $P \leq 0.001$.

Figure 5.17 demonstrated that after 24 hours of incubation at 37˚C, AG03 [RG-VQIK(Ac)YKP-GRRRRRRRR] inhibited aggregation of Tau by ~30% and that a core binding sequence scrambled version of itself [RG-QPKIK(Ac)YV-GRRRRRRRR] and the octa-arginine chain on its own [RRRRRRRR] were unable to inhibit aggregation. This showed that it was not just the combination of amino acids causing inhibition i.e. through charge effects, but that the location of the amino acids was important. To make AG03 proteolytically stable it was N-methylated to form AG03M [RG-V(m)QI(m)K(Ac)Y(m)KP(m)-GRRRRRRRR] or retroinverted to form RI-AG03 [RG-QPKIK(Ac)YV-GRRRRRRRR]. When testing these theoretical proteolytically stable peptides, AG03M reduced inhibition fluorescence slightly when compared to AG03, however RI-AG03 reduced fluorescence by >90%.

5.3.7 RI-AG03 DOSE RESPONSE

A.

B.

Model	DoseResp
Equation	y = A1 + (A2-A1)/(1 + 10^((LOGx0-x)*p))
Plot	Mean
A1	2.35309 ± 1.37045
A2	2147.4327 ± 319.76373
LOGx0	7.83351 ± 2.09466
p	-0.08265 ± 0.00777
Reduced Chi-Sqr	0.85496
R-Square (COD)	0.99933
Adj. R-Square	0.99904

IC_{50} 7.83µM
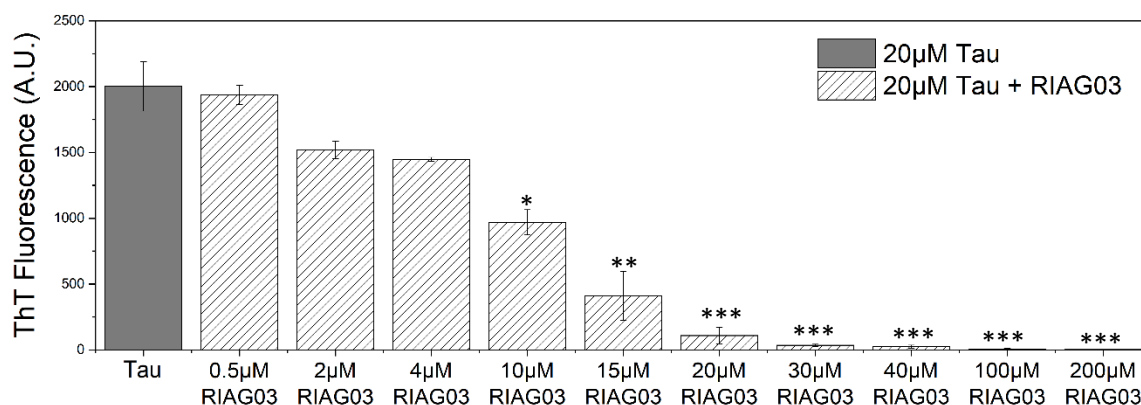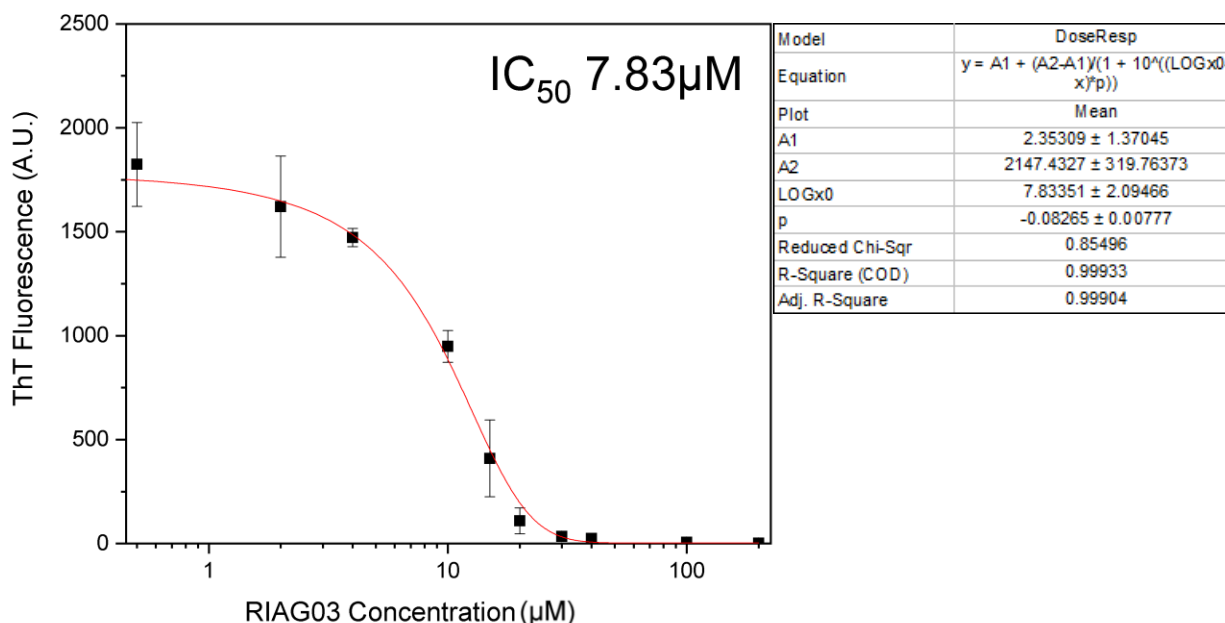
Figure 5.18: Thioflavin data using a FlexStation 3 plate reader, **A:** End-point (24hr) aggregation of TauΔ1-250 (20 µM) demonstrating the dependence of TauΔ1-250 inhibition by RI-AG03. **B:** A $\log^{10}$ scatter graph of the same data employing a curve fitting algorithm to calculate the IC50 (the concentration of RI-AG03 required for 50% inhibition of Tau aggregation) of 7.83 µM.
$P > 0.05$, * $P \leq 0.05$, ** $P \leq 0.01$, *** $P \leq 0.001$

Figure 5.18 demonstrated that there is a negative correlation between inhibitor concentration and TauΔ1-250 aggregation. The more inhibitor present, the greater the inhibition of Tau aggregation. Both the Tau stock solution and inhibitors were solubilised in 30 mM Tris solution. Looking at the data it is unlikely that inhibition was caused by the Tris because the Tau control also contained 30 mM Tris.

5.3.8 RI-AG03 VS TAU SEEDS
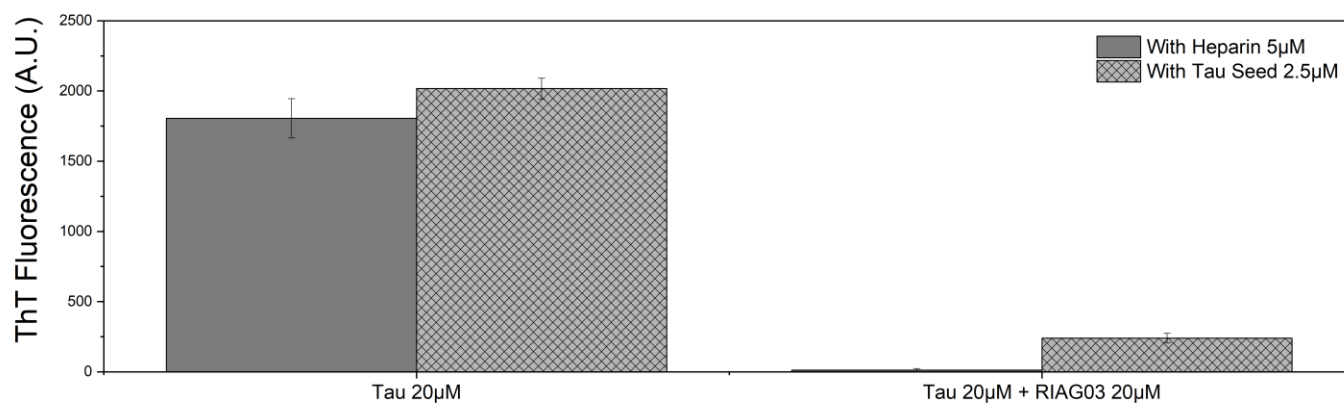
Figure 5.19: Thioflavin data using a FlexStation 3 plate reader. End-point aggregation of TauΔ1-250 (20μM) with equimolar RI-AG03, in the presence of heparin or Tau seed.

Figure 5.19 demonstrated that RI-AG03 is as potent at inhibiting aggregation of TauΔ1-250 in the presence of Tau seeds as it is heparin. The residual fluorescence with the Tau seeds is presumable due to the presence of a small amount of these pre-formed aggregates.

5.3.9 RI-AG03 VS GROWTH PHASE
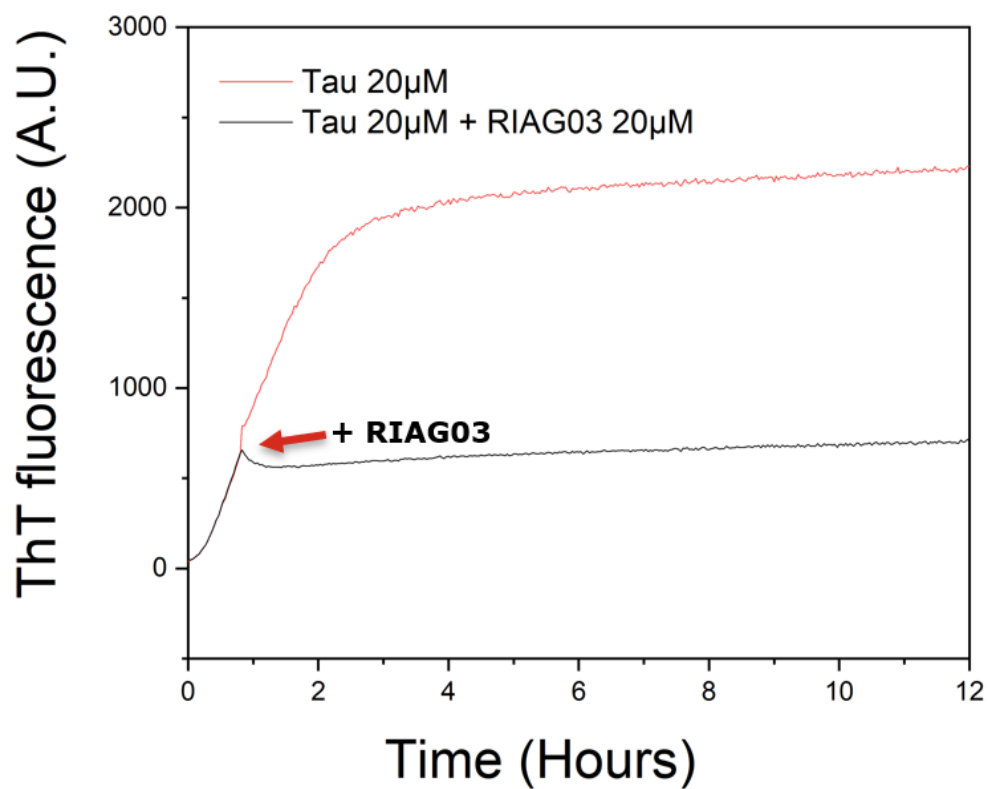
Figure 5.20: Thioflavin data using a FlexStation 3 plate reader. Aggregation kinetics of TauΔ1-250 (20µM), and after adding RI-AG03 (20µM) after one hour of aggregation.

Figure 5.20 demonstrated that after adding RI-AG03 after one hour, it can halt the aggregation of TauΔ1-250 during the elongation phase of aggregation.

5.3.10 RI-AG03 INHIBITS β-SHEET FORMATION
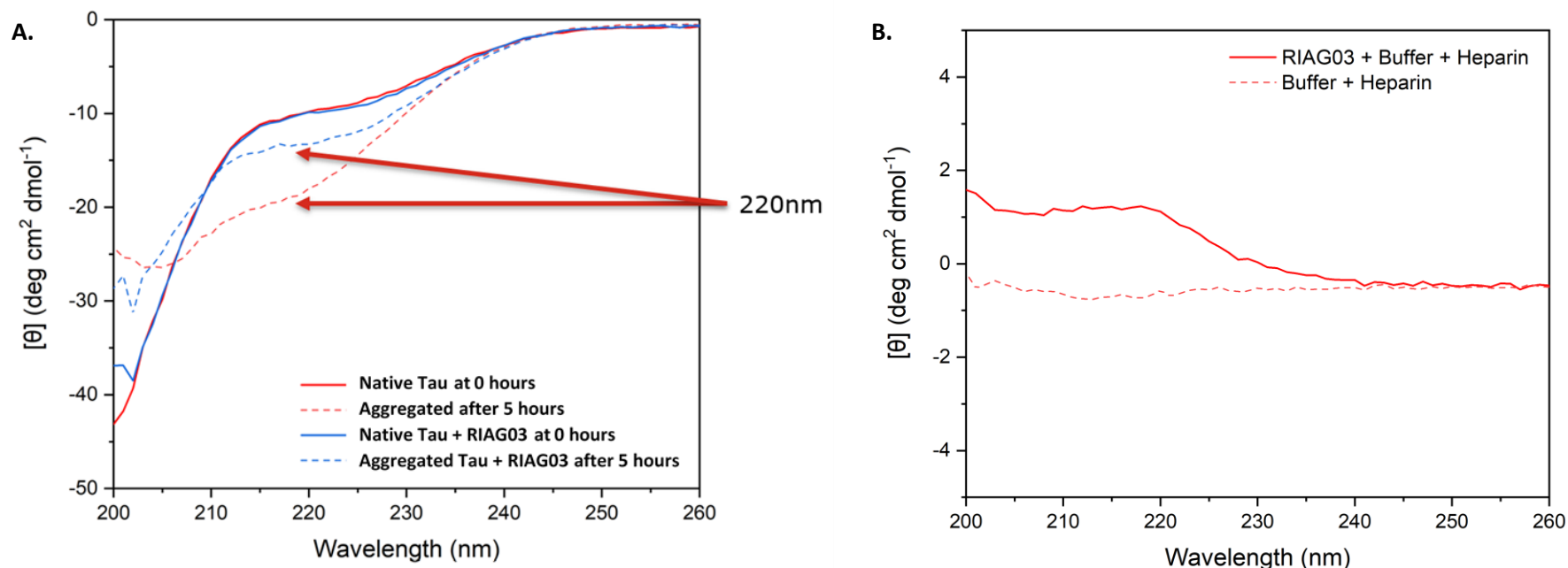
Figure 5.21: CD spectroscopy data **A:** After incubation with heparin and RI-AG03 at 37°C for 5 hours; TauΔ1-250 (20µM) has a reduction in β-sheet content (at 220 nm) compared to control. **B:** After incubation with heparin (5µM) at 37°C for 24 hours; RI-AG03 does not gain secondary structure.

Figure 5.21 A, demonstrated that RI-AG03 partially prevents TauΔ1-250 from shifting from unordered to β-sheet structure, as seen by a reduced dip at 220nm, when compared to the control. The figure also suggests that in both samples, insoluble material is being formed due to a reduction of signal in the y-axis, suggesting protein is precipitating out of solution. **Figure 5.12 B** demonstrated that RI-AG03 has no secondary structure and that heparin does not force RI-AG03 to transition into a defined secondary structure. This was useful to investigate because it helped to validate the phenomena observed in **Figure 5.21 A;** that changes in spectra were not associated with changes in the secondary structure of the inhibitor.

Uncrossed lens   **90˚ Crossed lens**

TauΔ1-250 Control

TauΔ1-250 + RI-AG03

100 μm
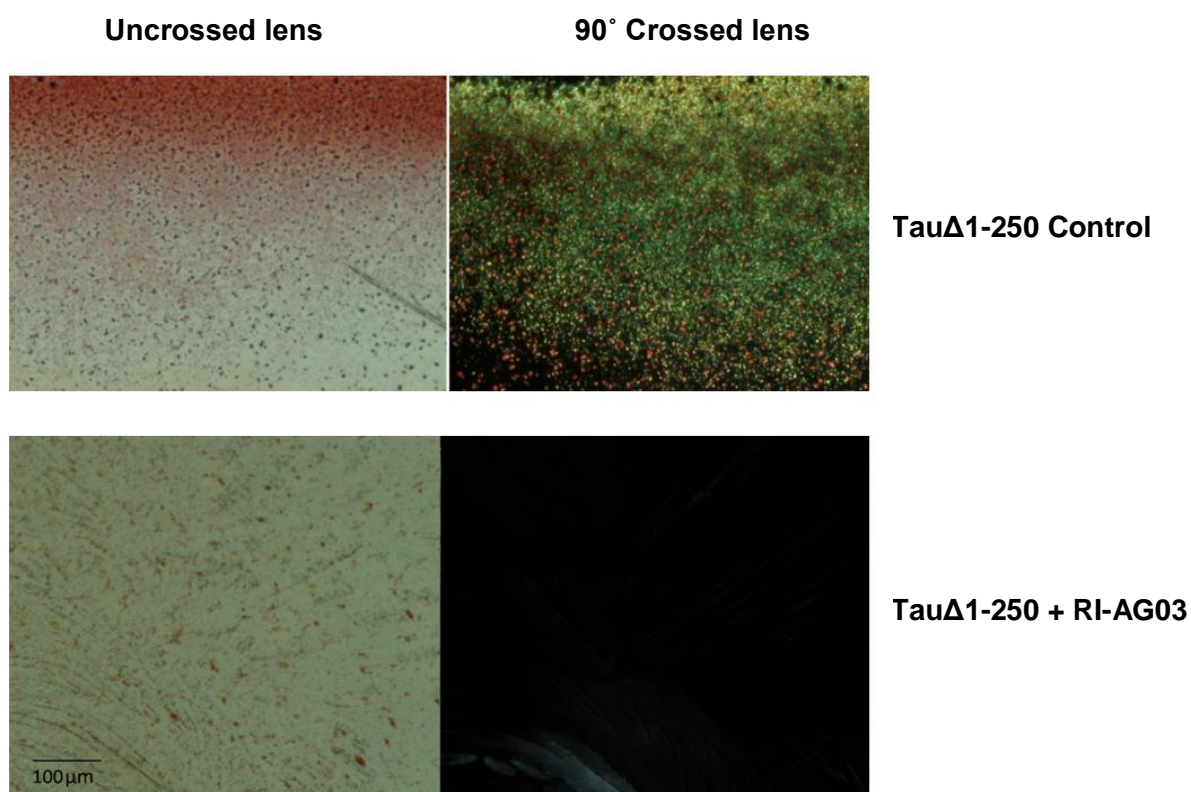
Figure 5.22: Birefringence data using Zeiss axioscope A1 microscope. TauΔ1-250 with and without the presence of RI-AG03, stained with congo red and visualised under uncrossed lens and crossed (90˚) polarising lens.

Figure 5.22 demonstrated that TauΔ1-250 when stained with congo red, appears red when viewed under uncrossed polarisers, however when viewed between crossed polarisers at 90˚C, the sample emits an apple green coloured birefringence. This suggests that the protein has β-sheet secondary structure. When TauΔ1-250 is incubated with RI-AG03 and stained with congo red, it appears red when viewed under uncrossed polarisers, however when viewed between crossed polarisers at 90˚C, no birefringence can be seen. This suggests that the protein formed has much less β-sheet content.

5.3.11 EFFECT OF RI-AG03 ON FIBRIL MORPHOLOGY
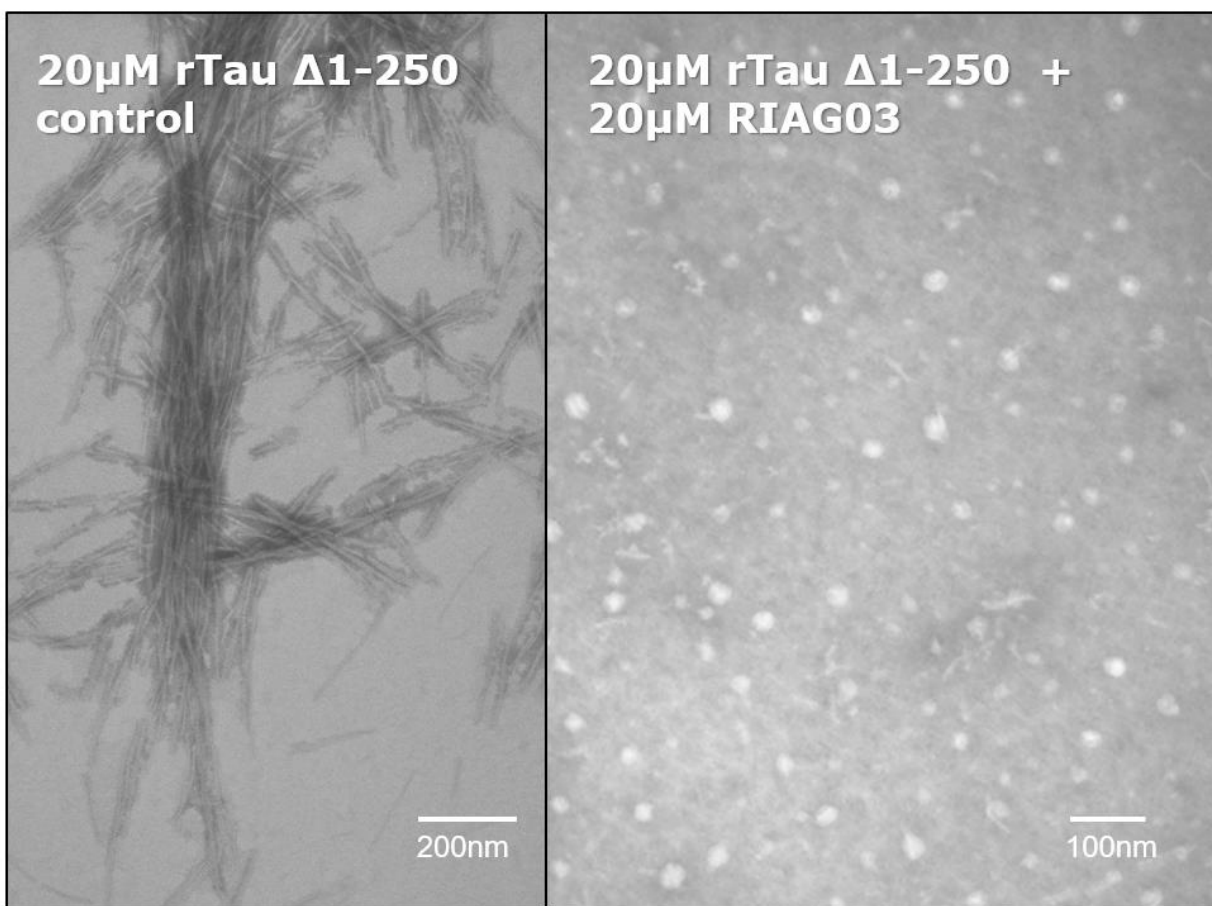
Figure 5.23: Negative stain TEM images using a Joel JEM-1010 following aggregation of TauΔ1-250 (20 µM) at pH 7.4 in the presence of Tris buffer (30 mM), DTT (1 mM), heparin, (5 µM), with and without RI-AG03 (20 µM) and incubated at 37°C for 24 hr. Note absence of fibrils in the presence of RI-AG03. Repeats were performed in triplicate across independent experimental repeats.

Figure 5.23 demonstrated that when aggregated using heparin, TauΔ1-250 formed fibrils, however when in the presence of equimolar RI-AG03, no fibrils were formed; Instead ~36nm diameter spherical structures are formed, as quantified by **Table 5.2**.

Table 5.2 provided quantitative analysis of the TEM images, suggesting that the inhibitor altered the

normal pathogenic aggregation pathway by locking Tau into ~36 nm diameter structures instead of

forming fibrils.

	Area (nm²)	Perimeter (nm)	Diameter (nm)
Mean	1024.30	112.53	35.82
Minimum	456.03	75.70	24.10
Maximum	1868.88	153.25	48.78
Standard Deviation	262.16	14.46	4.60
Skewness	0.41	0.13	0.13

Table 5.2: Table quantifying area, perimeter and diameter of 200 oligomeric-like structures seen in TEM images from Tau incubated with RI-AG03, using iTEM software.

5.3.12   LIPOSOME RI-AG03 VS FREE PEPTIDE
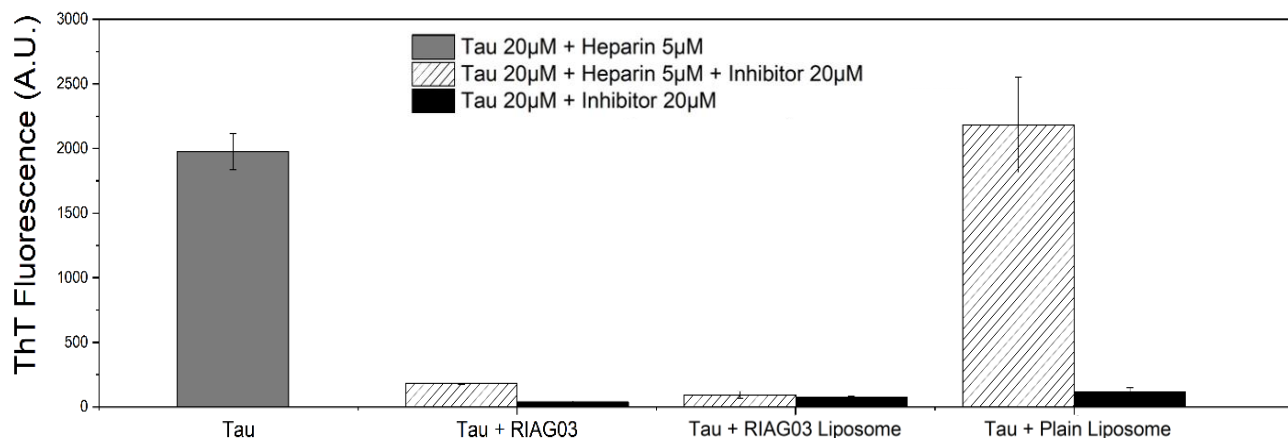
Figure 5.24: Thioflavin data using FlexStation 3. Aggregation of TauΔ1-250 (20µM) alone (grey), TauΔ1-250 with equimolar concentration of either RI-AG03, RI-AG03 Liposomes or plain liposomes (white) and RI-AG03, RI-AG03 Liposomes or plain liposomes alone (black); using conditions as before. Concentration of liposomes was calculated from the molecular mass of the components of the liposome.

Figure 5.24 demonstrates that after 24 hours of incubation at 37˚C, RI-AG03 reduced aggregation of of TauΔ1-250 by ~87% whereas RI-AG03 decorated liposomes (total lipid concentration 20 µM, peptide concentration 0.5µM) reduced aggregation ~94%. Plain liposomes did not inhibit aggregation at all. When incubated without TauΔ1-250, neither condition appeared to self associate into ThT reactive species.

5.4 DISCUSSION

This first part of this chapter successfully completed the aim of recombinantly producing Tau via a bacterial expression system at a large scale. TauΔ1-250 was used instead of full-length Tau as it aggregates much faster as it consists of all four repeat domains and the C-terminus but without the flanking N terminus containing the positively charged proline rich regions present (Gustke et al., 1994). Full length Tau can take days to aggregate whereas TauΔ1-250 plateaus at ~4-8 hours (Okuda et al., 2015). This was advantageous as it meant that there was a much quicker turnover of results, less machine time use, less risk of contamination or having to include antimicrobials such as sodium azide which could subsequently interfere. Potential problems of using a more aggressively aggregating fragment of Tau are that the inhibitors may be ineffective at keeping up with the rate of aggregation in the fragments, however could be useful in a more clinically relevant setting with full length Tau which aggregates more slowly. Another downside of using TauΔ1-250 is that it does not include the N-terminus and so may be less clinically relevant than using full-length Tau and inhibitors may behave differently if the fuzzy coat from the N terminus in Tau is present. In both cases, if either full-length TauΔ1-250 was synthesised, neither would be phosphorylated, which is another drawback to clinical relevance as in AD the Tau is hyperphosphorylated. Alternatively, inhibitors could be tested against recombinant Tau proteins which are phosphorylated *in-vitro* using kinases such as ERK2 kinase (Despres et al., 2017). Producing enough pathophysiologically relevant hyperphosphorylated Tau is a major hurdle. Sui et al. (2015), used the Zippers-Assisted Catalysis sytem which co-expresses 1N4R Tau and GSK-3β in *E. coli* as leucine zipper fusion proteins, to produce hyperhosphorylated Tau. It is important to note that proteins produced chemically, rather than recombinantly may have different characteristics, such as in the way they fold, which will alter the aggregation potential (Finder et al., 2010). It is also important to note that heparin induced Tau filaments are polymorphic and are different to those seen naturally in AD and Picks disease

(Fichou et al., 2018 and Zhang et al., 2019). Although *in-vitro* experiments using recombinant Tau protein have their limitations, they are still a decent guideline to predict what may occur *in vivo*. To understand what would truly occur in a clinically relevant setting, *in vivo* experimentation is necessary. Based on the average of four separate purified expression batches, purity of Tau was ~94%. The low yield of 10mg/L culture for this prep may be accountable for the loss of protein during the early centrifugal stages of the purification process and again during the 0.1M NaCl wash stage. The gel bed could be increased to allow more binding of Tau to the column, which may result in a reduced amount of 20kDa protein in the flow through. KrishnaKumar and Gupta (2017), stated that recombinant Tau expression is a challenge because BL21(DE3) usually provides low yields due to *E.coli* synonomously using non-preferential codons, particularly those which encode arginine and proline residues as they obstruct translation. Due to the intrinsically disordered nature of Tau it is also prone to bacterial proteolysis which results in further loss of protein yield (Suskiewicz et al., 2011). Nevertheless, the purity of the product was acceptable based on densitometric analysis shown in **Figure 5.13.** To improve Tau protein yields deficient tRNA can be supplemented which enhances translation. Direct boiling without a previous cell lysis step also improves yield as it reduces the duration for proteases to potentially interact with Tau (KrishnaKumar and Gupta 2017).

The second part of this chapter focused on developing and investigating potential peptide-based inhibitors of Tau aggregation derived from the hot spot binding region corresponding to residues [306]VQIVYK[311]. The rationale being the prevention of monomeric or misfolded Tau molecules from interacting at this accessible binding site; thereby impeding further aggregation. The techniques utilised to determine this were ThT fluorescence (**Sections 5.2.1-7**), CD (**Section 5.2.8**), Congo red birefringence (**Section 5.2.8**) and TEM (**Section 5.2.9**). The two peptides that were used as a starting point for peptide development were VQIINK and VQIVYK. Although VQIINK did not come up in the Aggrescan and Camsol results, the literature suggests plays a very important in Tau aggregation and that it interacts with VQIVYK,

therefore, it was worth investigating Mukrasch et al., 2005; Von Bergen et al., 2000). Heparin was used to induce aggregation of Tau, however the optimum ratio of heparin:Tau had to be first determined, as too low a concentration of heparin may not be enough and too high may retard aggregation due to unbound free heparin increasing the ionic strength of the medium. Tau aggregation was also retarded for the same reasons from experiments using increasing salt concentrations with a fixed heparin concentration (Zhu et al., 2010). According to Goedert et al. (1996), the formation of Tau filaments is dependent upon the concentration of Tau and on the ratio of Tau:sulphated glycosaminoglycan. Both Ferrari and Rüdiger (2019) and Ambadipudi et al. (2017), mention that the optimal ratio of Tau:heparin:Tau is 4:1. According to **Figure 5.14** the optimum ratio of Tau:heparin was 4:1 which corresponds to the ratio used by other researchers as well (Ambadipudi et al, 2017; Hattori et al., 2008, Yao et al., 2003, Jeganathan et al., 2008, Goedert et al., 1996). Since heparin is electronegative as it has high sulphur content and the inhibitors are electropositive as they contain polyarginine chains, it is plausible to assume the two may interact. This was important to elucidate to determine whether true inhibition of aggregation was occurring or reductions in ThT signal were the result of the inhibitor sequestering heparin from solution (due to attracting charges) and thereby preventing heparin from interacting with Tau and initiating nucleation. **Figure 5.15** suggests that the inhibitors do not reduce aggregation as a function of sequestering heparin from solution through charge interactions. It shows that the inhibiors also prevent Tau from aggregating when the inducer of aggregation is Tau seeds, or Aβ seeds, instead of heparin. However, a better way of establishing this would be to test the inhibitors against aggregation of TauΔK280 which aggregates without heparin. It has been demonstrated that the prion-like spread of extracellular Tau aggregates into neurones via micropinocytosis is mediated by heparan sulfate on the surface of cell surfaces but in cultured cells and primary neurones this process is inhibited by heparin. As a result, it was suggested that the glycosamino glycan and Tau interaction has a more prominant relationship in AD pathology than previously appreciated (Zhao et al., 2017; Holmes et al., 2013).

Evolutionary step	Peptide ID	Sequence	Self associate?	Better inhibitor?	Conclusion for lead peptide
1 binding sequence	AG01	Ac - R G V Q I I N K G R - NH$_2$	✓		Chose sequence which did not self associate
	AG02	Ac - R G V Q I V Y K G R - NH$_2$	X	✓	
2 charge effects	AG02R4	Ac - R R G V Q I V Y K G R R - NH$_2$	X		Kept poly-arginine chain on N terminus
	AG02R5	Ac - R G V Q I V Y K G R R R R - NH$_2$	X	✓	
	AGR502	Ac - R R R R G V Q I V Y K G R -N H$_2$	X		
	AG02R6	Ac - R R R G V Q I V Y K G R R R - NH$_2$	X		
3 β-sheet breaker	AG02R5	Ac - R G V Q I V Y K G R R R R - NH$_2$	X		Kept proline β-sheet breaker
	AG02PR5	Ac - R G V Q I V Y K P G R R R R - NH$_2$	X		
4 cell penetration	AG02R9	Ac - R G V Q I V Y K G R R R R R R R R - NH$_2$	X	✓	Chose poly-arginine over TAT
	AG02TAT	Ac - R G V Q I V Y K G R Y G R K K R R Q R R R - NH$_2$	X		
5 acetyllysine	AG02ΔI	Ac - R G V Q K(Ac) V Y K G R - NH$_2$	✓		Chose sequence which did not self associate
	AG02ΔV	Ac - R G V Q I K(Ac) Y K G R - NH$_2$	X	✓	
6 choose lead peptide	AG02R9	Ac - R G V Q I V Y K G R R R R R R R R - NH$_2$	X		Chose poly-arginine over TAT
	AG02TAT	Ac - R G V Q I V Y K G R Y G R K K R R Q R R R - NH$_2$	X		
	AG03	Ac - R G V Q I K(Ac) Y K P G R R R R R R R R - NH$_2$	X	✓	
7 proteolytic stability	AG03M	Ac - R G V(m) Q I(m) K(Ac) Y(m) K P(m) G R R R R R R R R - NH$_2$	X		Chose retro-inversion
	RI-AG03	Ac - r r r r r r r r G p k y k(ac) i q v G r - NH$_2$	X	✓	

Lead peptide = RI-AG03 [Ac - r r r r r r r r G p k y k(ac) i q v G r - NH2]

Table 5.3: Table describing the evolutionary steps for the peptide inhibitor. 1) chose the target binding sequence, 2) investigated charge effects associated with aggregation, 3) utilising a rigid amino acid to disrupt chain interactions, 4) attaching a cell penetrating sequence so the inhibitor can enter cells to target Tau, 5) utilising accetyllysine to promote binding to VQIVYK, 6) integrated previous peptide designs to form AG03 and tested its effectiveness, 7) testing the effectiveness of AG03 when it is changed to be proteolytically stable so it does not degrade in cells or *in vivo*.

The data from **Figure 5.16** and **Figure 5.17** summarised in **Table 5.3** explains the evolution of the inhibitors where the first step chose the initial binding sequence. As AG01 [RG-VQIINK-GR] self associated and AG02 [RG-VQIVYK-GR] did not, the latter was chosen for further development. Since Tau aggregation is largely facilitated by electrostatic interactions, the second step was to test charge effects. Peptides AG02R4 [RRG-VQIVYK-GRR], AG02R5 [RG-VQIVYK-GRRRR], AGR502 [RRRRG-VQIVYK-GR] and AG02R6 [RG-VQIVYK-GRRRRR] investigated the effects of different chain lengths of positively charged arginines on the N and C terminals, in different conformations. There appeared to be some added inhibitory effect with additional chained arginine residues, until reaching ~5 arginine residues, at which little difference is seen with additional residues. There also appeared to be no prominent difference to which terminus the arginne residues were located. The third step examined AG02PR5 [RG-VQIVYKP-GRRRR] which had the addition of proline added to the end of the VQIVYK peptide core to mimick its natural position in the native Tau sequence. Proline is reported as a β-sheet breaker and provides rigidity to peptides and prevents backbone interactions which are essential for amyloid aggregation. Since the polyarginine chain followed the peptide binding region, the proline residue will change the angle direction the chain projects at. Based on experiments there appeared to be little difference with the addition of proline, however it was retained as an evolutionary step as it may be more useful with a longer poly-arginine chain attached to it to obstruct Tau interactions. The fourth step investigated potential cell penetrating sequences and the peptides tested were AG02R9 [RG-VQIVYK-GRRRRRRRR] and AG02TAT [RG-VQIVYK-GRYGRKKRRQRRR]. Again, there appeared to be little difference with regards to additional inhibition when comparing them to AG02R5, however AG02TAT appeared to self aggregate slightly more, so polyarginine was retained. The fifth step investigated the predictions from chapter 1 with regards to replacing isoleucine or valine with acetyllysine. AG02ΔI [RG-VQK(Ac)VYK-GR] and AG02ΔV [RG-VQIK(Ac)YK-GR] demonstrated inhibition to aggregation however AG02ΔI self associated, therefore it was discarded and AG02ΔV was retained. The combination of acetyllysine residues seen in AG02ΔI and AG02ΔV was not used because the peptide would

lose specificity by changing the hexapeptide recognition sequence and hydrophobic interactions too much, thus preventing it from binding to its target.

Elements from AG02PR5 (proline), AG02R9 (octa-arginine chain) and AG02ΔV (replacement of valine with acetyllysine) were combined to form AG03 [RG-VQIK(Ac)YKP-GRRRRRRRR]. Octa-arginine was desireable as Tau aggregation occurs intracellularly, so the inhibitor would need to be able to cross cell membranes. AG03 demonstrated enhanced inhibitory effects at ~53% inhibition when compared to AG02R9 and AG02TAT which inhibited aggregation at ~40. **Figure 5.17** confirmed that the inhibitory properties of AG03 were not simply due to the polyarginine positive charge or due to the global charge of the peptide residues. Polyarginne and a scrambled version of AG03 were tested, both of which displayed no inhibitory properties. Before testing in cells, AG03 had to be made proteolytically stable, therefore two versions of it were created: An N-methylated version AG03M [RG-V(m)QI(m)K(Ac)Y(m)KP(m)-GRRRRRRRR] and a retro-inverted version RI-AG03 [rrrrrrrrG-pkyk(ac)iqv-Gr].

Based on ThT fluorescence, AG03M did not appear to have any additional inhibitory effects when compared to AG03, however RI-AG03 inhibited aggregation by ~94%. Therefore RI-AG03 was chosen as the lead peptide to be taken forward for additional experiments. A dose-dependent experiment of RI-AG03 was conducted to establish potency whereby an IC50 of 7.83 µM was calculated, as seen in **Figure 5.18**. RI-AG03 demonstrated its ability to inhibit aggregation of Tau in the presence of Tau seeds and to also prevent further aggregation of Tau when added during the growth phase of aggregation as seen in **Figures 5.19 and 5.20, respectively** (**Section 5.2.6**). Individual L- and D- amino acids are optical isomers of each other, however the retro-inverted RI-AG03 sequence is not an enantiomer of its original AG03 sequence. Although the sidechains for AG03 and RI-AG03 havie similar orientations, the difference between them is that the amino acid backbones are reversed, and the resulting hydrogen bonds are therefore different. In addition, the N and C terminal domains are on opposite ends due to inversion of the peptide sequence. The stability of amyloid fibres is generated by backbone interactions, so it is

impressive that RI-AG03 still has activity with a reversed backbone. These findings suggest that the subtle changes in peptide inhibitor backbone and N and C terminal domains can influence aggregation. The increased solubility of the amide functional group in RI-AG03 may offer greater inhibitory properties when it is localised close to the Valine in the inhibitor binding sequence. Ree et al. (2018), stated that affixing an acetyl group on the N-terminal amino group results in altered charge, hydrophobicity and size of the terminus; resulting in altered binding properties. Moving the more hydrophobic acetyl group further away from the binding sequence may also be beneficial as it will increase the local area hydrophilicity. The acetyl methyl group may also interfere with binding. These terminal modifications may create new protein interaction surfaces, enhance peptide metabolic and enzymatic stability as well as enhance peptide activity (Ree et al., 2018). Arispe et al., (2008) mentioned that capping the N-terminus and C-terminus through acetylation and amidation, respectively, promotes aromatic interactions. This may be due to the peptide and its Tyrosine group behaving more like it does in its native form than as a peptide with open ends. This has relevance to RI-AG03 as it contains Tyrosine in the binding residue. It may also be that the bond angles in the retro peptides are not perfect mimicks and as such the D-amino acid inhibitors have slightly altered binding properties.

Professor David Allsop's research group previously developed an Aβ peptide aggregation inhibitors OR-2 [H2N-RGKLVFFGR-NH2] and its retro-inverted counterpart RI-OR2 [Ac-rGffvlkGr-NH2] which was more effective than OR-2 as an inhibitor (Matharu et al, 2010; Taylor et al., 2010). This resembles the difference between AG03 and RI-AG03 in their effectiveness as aggregation inhibitors. Taylor et al, (2010) suggested that RI-OR2 prevented aggregation of Aβ1-42 by outcompeting monomers for the KVLFF region on Aβ1-42 peptide. When tested *in vivo* with the attachment of TAT sequence to penetrate the blood brain barrier, Aβ oligomer levels were reduced in cerebral cortex of 10-month-old APPswe/PS1DE9 mice following daily i.p. injections of RI-OR2-TAT over 21 days (Parthsarathy et al., 2013). Obasse et al. (2017), developed Amylin peptide aggregation inhibitors IO8 (H2N-RGANFLVHGR-NH2) and its retro-inverted

counterpart RI-IO8 (Ac-rGhvlfnaGr-NH2). The L-amino acid inhibitor partially inhibited amylin aggregation whereas, surprisingly, the retro-inverted version stimulated aggregation. The differences between IO8 and RI-IO8 are again the reversed backbone and the N-terminal domains which are free amine and acetyl, respectively. Again, this is a conversion from positive to neutral charge in IO8 and RI-IO8, respectively. It is also important to note that in both examples the positive amine charge flanks residues on the opposite end of the sequence due to peptide inversion. To make IO8 proteolytically stable, Obasse et al (2017), N-methylated alternate amino acid residues form NI-IO8 which did not appear to have enhanced aggregation properties when compared to IO8 in ThT assays. This resembled the data in this PhD research as AG03 and AG03M seemed to be both inhibit Tau aggregation relatively equally. Alternate N-methylation of peptides blocks one face of the peptide from hydrogen bonding due to the replacement of backbone NH groups with N-methyl groups (Kokkoni et al., 2006). Therefore, simple N-methylation or retro-inversion of peptide aggregation inhibitors do not necessarily mean they will become more effective inhibitors. With regards to retroinverted peptides, changes in amino acid backbones and local charge can potentially improve inhibition of aggregation or even seed it.

RI-AG03 has a high positive charge whereas heparin is heavily negatively charged. It is important that RI-AG03 can inhibit aggregation of Tau in the presence of seeds as it acts as a control for heparin. It demonstrates that previous inhibition of heparin induced Tau aggregation was not as a result of RI-AG03 sequestering heparin rendering it unable to interact with Tau. The fact that RI-AG03 can also inhibit pathological aggregation of Tau when added during the elongation phase means that it is able to block Tau assembly even after this process has been initiated, which is promising for development of an inhibitor to slow disease progression.

Thioflavin-T fluorescence can detect the presence of β-sheet protein species, but it fails to detect the presence of oligomers. CD on the other hand can identify secondary structure of oligomeric species (Persichilli et al., 2011; Maezawa et al. 2008; Lasagna-Reeves et al., 2010); Li et al., 2009). **Figure 5.21**

demonstrates that incubation of Tau with heparin at 37°C for 5 hours results in a shift from unordered structure to β-sheet structure. When co-incubated with RI-AG03 under the same conditions there is a reduction in transition to β-sheet structure, which agrees with the Thioflavin-T data and further supported by Congo red birefringence (**Figure 5.22**). Since heparin induces aggregation of Tau, it is plausible that RI-AG03 results in the formation of Tau aggregates which are not Thioflavin-T reactive. CD data in **Figure 5.21** confirmed that RI-AG03 does not form β-sheets itself in the presence of heparin; supporting previous CD and Thioflavin-T data. The techniques discussed so far only determine secondary structure; to truly confirm the results morphological analysis is necessary.

TauΔ1-250 constructs aggregated to display highly ordered structures; both straight fibrils and PHFs with the characteristic twist. This twist is hypothesised to be due to interactions between VQIINK and VQIVYK found in the second and third repeats, respectively (Xu et al., 2016). Most of the fibrils appear to be straight (**Figure 5.23**) which agrees with the findings of Barghorn and Mandelkow, (2002) who aggregated K18 using heparin. As mentioned previously, K18 is a recombinant construct of Tau that only comprises the 4R repeat domains, whereas TauΔ1-250 also contains the C terminus. TEM data in **Figure 5.23** demonstrates that when Tau was incubated in the presence of RI-AG03 no fibrils were formed. Instead ~36nm diameter spherical structures can be seen, as quantified in **Table 5.2**, suggestive of large granular Tau oligomers (GTO) (Maeda et al., 2018). Maeda et al. (2007) suggested that once GTOs reach an average diameter of 20 nm they can form fibrils, however the structures seen in this research appear to be locked in their granular form (Cowen et al., 2015). The structures formed in the TEM images are not necessarily the same as structures formed in the sigmoidal curve of amyloid production in the absence of inhibitor. It is not known whether the Tau-inhibitor complex structures in this research were toxic however, according to literature its possible that they may not be toxic and in fact may follow an insoluble and neuroprotective pathway (Cowan et al., 2015; Ali et al., 2112). These unknowns need investigating further to be sure.

RI-AG03-Cys decorated liposomes via click chemistry in a 1:1 ratio (**Figure 5.25**). Maleimide is a sulfhydryl-reactive chemical group and at pH 6.5-7.5, it selectively crosslinks with the free/reduced sulfhydryl group on the side-chain of cysteine to form a stable and non reversible covalent thioether linkage. Total lipid
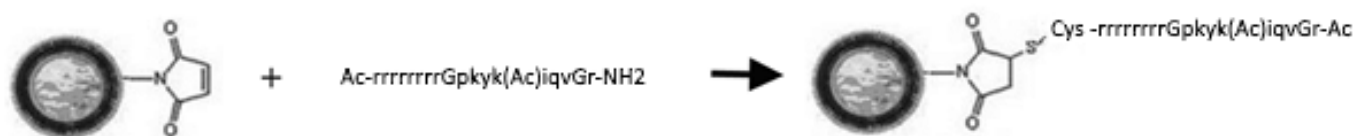
Figure 5.25: Illustrating RI-AG03 linking to a liposome using a maleimide linker, via an additional cysteine amino acid.

concentration was 20 µM but only 5% of the lipid was DSPE-PEG-MAL. Therefore only 5% of the lipid concentration (1 µM) could bind RI-AG03. Assuming 50% of the decorated peptides were outward facing and that 100% of the peptides bound; then the lipids contained ~2.5% peptide (0.5 µM). **Figure 5.24** demonstrated that liposome-peptide (0.5 µM) vs Tau (20 µM) elicited a similar inhibition response than free peptide (20 µM) vs Tau (20 µM). As a result, RI-AG03 liposome was approximately x40 better than the free peptide version. This agrees with previous research using free and peptide-bound Aβ aggregation inhibitors (Taylor et al., 2010).

One of the barriers to this research is that TauΔ1-250 is a truncated construct so it can not be certain that the structure of the *in vitro* Tau aggregates is comparable to those manifested naturally in AD (Barghorn and Mandelkow, 2002). Ultimately this leaves a blank space in our knowledge as to whether Tau is behaving in a similar fashion in the lab in comparison to the disease and if advances in inhibiting aggregation *in vitro* will be equally effective in clinical trials. In addition, it is important to note that heparin-induced filaments are different from those found in AD and Pick's disease (Fichou et al., 2018). The two types of filaments observed in AD include PHFs and SFs which are ultrastructural polymorphs consisting of two matching protofilaments with a C-shaped core comprising amino acids 304–380. The two types of filaments observed in Picks disease include narrow filaments with a J-shaped core comprising

amino acids 254-378 and wide filaments which are made from two narrow filaments (Zhang et al., 2019). Using cryo-EM, Zhang et al (2019), identified heparin-induced 2N4R filaments adopt four different conformations: snake, twister, jagged and hose filaments. These conformations have differences in loop regions based on a subtle 20° adjustment to the backbone conformation of the ^{310}YKP^{312} turn which causes alternative β-sheet packing conformations. The outward facing residues for AD and Picks filaments have alternating positive and negative charges, however in heparin-induced Tau filaments these residues are mainly positively charged. This results in R4 being disordered in heparin-induced Tau filaments (Zhang et al. 2019). The differences between disease (Alzheimer fold, Pick fold) and heparin-induced 2N4R Tau (4R-snake, 4R-twister, 4R-jagged) are summarised in **Figure 5.26**. It may be possible that since the inhibitors are targeted against VQIVYKP, they may be interfering with the backbone conformation ^{310}YKP^{312} resulting in off-pathway aggregates as previously demonstrated by the TEM image in **Figure 5.23**. This leads to further requirement to test if the structures formed in the presence of the inhibitor are toxic or not and to also test the effect of the inhibitor on Tau in an *in vivo* setting. Overall it suggests Tau has very versatile side-chain interactions resulting in variable cross-β packings, which with the right intermediate e.g. RI-AG03, could completely alter the pathogenic aggregation pathway. Seidler et al. (2018), stated that VQIVYK inhibitors can only block filament formation of 3R Tau, whereas VQIINK inhibitors can block filament formation of 4R Tau. RI-AG03 is based on the VQIVYK sequence but can block filament formation of 4R Tau, suggesting that RI-AG03 can also interact with VQIINK.
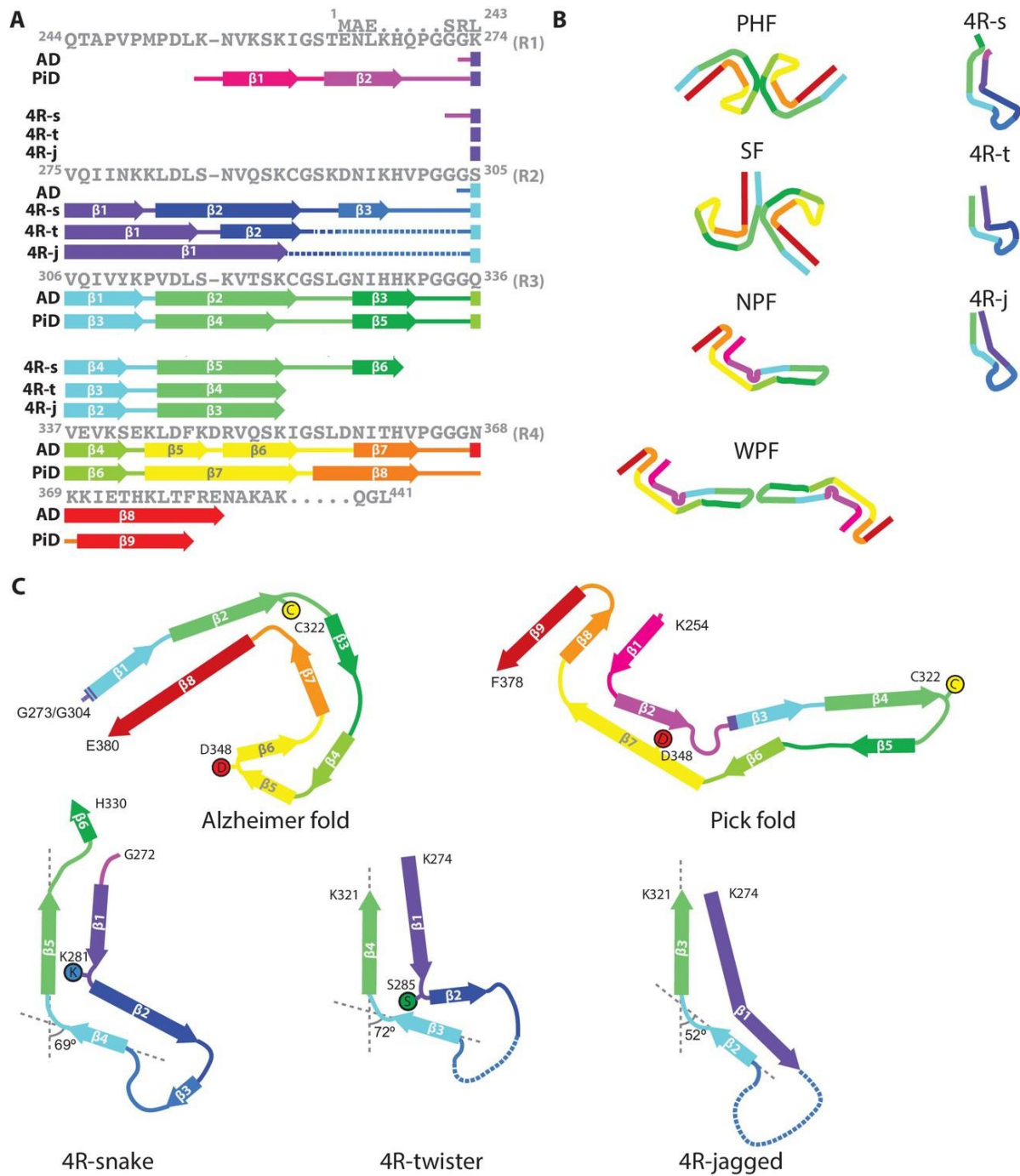
Figure 5.26: Illustration of disease and heparin-induced Tau structures. **A:** Colour coded filament β-strand and loop regions between R1–R4 for **B:** Schematic Tau folds for AD (PHF and SF), PiD (NPF and WPF), 4R-s (Snake), 4R-t (Twister) and 4R-j (Jagged). **C:** Structural differences between disease and heparin-induced 2N4R Tau filaments (Zhang et al., 2019).

6. TESTING RI-AG03 *IN VIVO*

6.1 INTRODUCTION

6.1.1 CELL UPTAKE

As Tau aggregates are formed intraneuronally it is important that the inhibitory peptide RI-AG03 can enter cells where it can inhibit Tau aggregtion. In addition, for the peptide to get into the brain it must pass through the blood-brain barrier (BBB, so it needs to be taken up and released by the cells that form the BBB. In this research the lead peptide utilises octa-arginine as a CPP enters cells via direct penetration and endocytosis. Polyarginine peptides are hydrophilic cationic CPPs due to their polar properties however mechanisms of CPP cellular uptake and delivery are still not understood completely (Langel, 2019). The structural component of arginine providing it with its cell uptake properties as a polymer is the guanidinium head group. This is supported by Yamashita et al. (2016), who demonstrated that polycitrulline was unable to penetrate cells when the nitrogen of guianidine was replaced with oxygen. The optimum arginine chain length for efficient cellular uptake are 7-15 arginine residues and the most commonly used are between 8-10 residues. Less than 7 residues may be insufficient for cell uptake and above 15 results in less efficient uptake (Mitchell et al., 2000). Futaki (2005), stated that octa-arginine has high translocation efficiency and for this reason has gained significant attention. If intracellular insoluble Tau oligomers are too difficult targets for the peptide inhinitors, then soluble extracellular Tau released from dead neurones or possibly even secreted from cells could be targeted instead. In doing so this could possibly indirectly reduce intra-neuronal Tau levels by means of shifting the equilibria of pathogenic Tau molecules. This is supported by De Calignon et al., (2012) who suggested based on animal models that Tau and aggregates can be secreted and propagated between neurones with a transynaptic mechanism like prions. As a result, potential therapeutic interventions may include preventing the initial formation of

seeds and the dispersion of extracellular soluble Tau aggregates (Giacobini and Gold, 2013). Furthermore, extracellular Tau may also be toxic on top of having a role in spreading of Tau pathology in the brain. This is supported by Frost et al., (2009) who suggested that extracellular Tau aggregates, not monomers, can be taken up by cultured cells and as a result displace tubulin, co-localise with dextran and subsequently induce fibrillation of intracellular Tau 441. Giacobini and Gold, (2013) stated that anti-Tau antibodies may reduce Tau pathology and neurodegeneration by inhibiting transynaptic transmission of Tau pathology and so acts extracellularly but may indirectly reduce intracellular Tau. RI-AG03 should be able to enter cells as it contains a the octa-arginine transit sequence which is known to be used for brain delivery of drugs as it allows cargos to cross cell membranes and enter cells, as previously discussed (Zhu et al., 2014).

6.1.2 *DROSOPHILA* ROUGH EYE MODEL OF TAUOPATHY

Drosophila melanogaster were initially introduced as a research model by Thomas Hunt Morgan and have been used to answer biological questions for over a century and are versatile enough to cover various topics in neurobiology such as degeneration, development, behaviour and cirdadian rhythems (Gistelinck et al., 2012; Bellen et al., 2010; Morgan, 1910). They are particularly useful as they do not require ethical approval, are much cheaper to conduct *in vivo* experiments on than mice are and provide a faster turn-around of results due to short their life-cycle, as seen in **Figure 6.1**. On top of short life cycles, they also have high fecundity, providing researchers with plenty of potential research samples. They are ~3 mm long and are routinely kept in small vials ~30 mL containing 5-10 mL food which can sustain the flies for around one month. Furthermore Reiter et al. (2001), suggested that ~77% of distinct disease genes in humans are orthologous to *Drosophila* sequences, providing an insight into human disease.
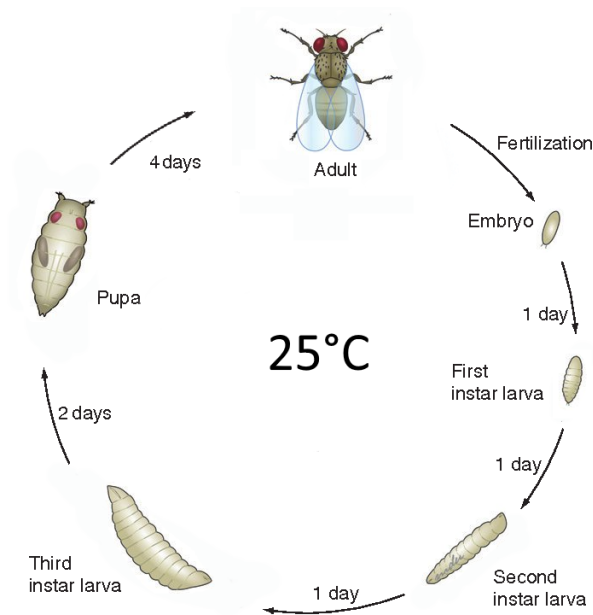
Figure 6.1: The relatively rapid life cycle of *Drosophila* at 25 ˚C takes ~10 days. Development is split into several stages including embro, larva, pupa and adult (adapted from Ong et al. 2014).

Various transgenc *Drosophila* models have been used to investigate neurodegeneration based on human expression of Tau and Aβ, particularly the rough-eye model due to association of Tau and Aβ correlating with retinal toxicity (Chouhan et al., 2016; Cao et al., 2008; Shulman and Feany, 2003). In these models' proteins are expressed solely in the eye and aggregation of these proteins results in retinal toxicity causing a loss of retinal cells, disordered ommatidia and bristle abnormalities (Chatterjee et al., 2008). The *Drosophila* Tauopathy models of aggregation replicate human disorder features such as accumulation of Tau, adult onset, progressive neurodegeneration and early death, however filamentous aggregates are not observed in these models (Wittmann, 2001). The rough-eye model is usually induced via the GMR-GAL4 (glass multiple reporter GAL4) driver and expresses proteins throughout development (Chouhan et al., 2016). The binary GAL4/UAS system has been extensively used for transgene expression in *Drosophila*. To specifically express transgenes in the developing eye one of the most commonly utilised drivers of expression is the GMR-GAL4 driver which under the control of GMR (glass multiple reporter) expresses yeast transcription factor GAL4 (Li et al., 2012). Expression of the desired transgene is then driven under control of the GAL4 sequence (Li et al., 2012; Brand and Perrimon, 1993). In this fly line full length human Tau is overexpressed and phosphorylated in the eye, which results in the formation of toxic non-filamentous aggregates. Chatterjee et al. (2009), demonstrated that this misexpression of Tau induced neurodegeneration in *Drosophila*, manifested by early onset cell death in larval eye discs and then reduced eye size and rough-eye phenotype in adults with disordered ommatidia, abnormal bristles and loss of photoreceptor neurons in the retinal architechture. In addition, abnormal wing phenotype, or missing wings may also be observed due to up and down regulation of Notch or *Drosophila wingless* (Wg) pathways under the GMR-GAL4 driver (Li et al., 2012). Cagan and Ready (1989), stated that Notch is involved in tissue remodelling and is required for the hexagonal rearrangement of pigment cells in the *Drosophila* eye. Bao (2014), suggested that Notch is involved with cell adhesion in the *Drosphila* eye through control of epithelial remodelling. Bao demonstrated that cone cells communicated with primary

pigment cells using Notch signalling. These primary pigment cells would activate transcription of genes

hbs and *sns* which code for the Nephrin group adhesion molecules that bind to Rst and Kirre. In addition,

primary pigment cells inactivated transcription of genes *rst* and *kirre* which code for the Neph 1 group.

Notch has a clear involvement in the developing eye and is also either up or down regulated by the GMR-

GAL4 driver which could skew data in some flies. These flies are also reported to display loss of nerve cells,

deficits in behaviour and a reduced lifespan (Passarella and Goedert, 2018). This agrees with phenomena

seen in humans, whereby oligomers were detected in AD brains and so were believed to be the cause of

toxicity (Ali et al, 2012; Wittman et al., 2001). Passarella and Goedert (2018), demonstrated that in a

Drosophila models of Tauopathy which over expressed Δ306–311 human Tau-383 there was reduced Tau

phosphorylation, no detectable degeneration and they had higher percentage survival. However, those

flies which did express amino acid residues 306-311 displayed rough-eye phenotype signs of degeneration

and had lower percentage of survival. They also demonstrated degeneration was evident in an age-

dependent manner, therefore investigating GMR-hTau eyes feeding on RI-AG03 over time will be

important to observe. As the rough eye model is a genetic model, to observe changes in the fly eye

phenotype or biochemistry through use of a peptide inhibitor may be challenging. This is because the flies

are genetically engineered to overexpress Tau which is a process that can not be interfered with using

peptide aggregation inhibitors. So, although the inhbitors may prevent aggregation of Tau, the flies will

continue to overexpress Tau. Furthermore, the Tau is only expressed in the eye and the inhibitors will

penetrate other cells after ingestion. This means that a small portion of the ingested inhibitor will reach

the eye. Chouhan et al. (2016), also stated that degeneration progressed with aging, therefore the most

profound effects of RI-AG03 would be seen in newly eclosed flies, as expression of Tau begins throughout

development and most of the inhibitor would be consumed during the larval stage.

6.2 RESULTS

Stability, cell-uptake and toxicity assays were conducted in preparation for experiments in *Drosophila*.

6.2.1 ENZYME STABILITY
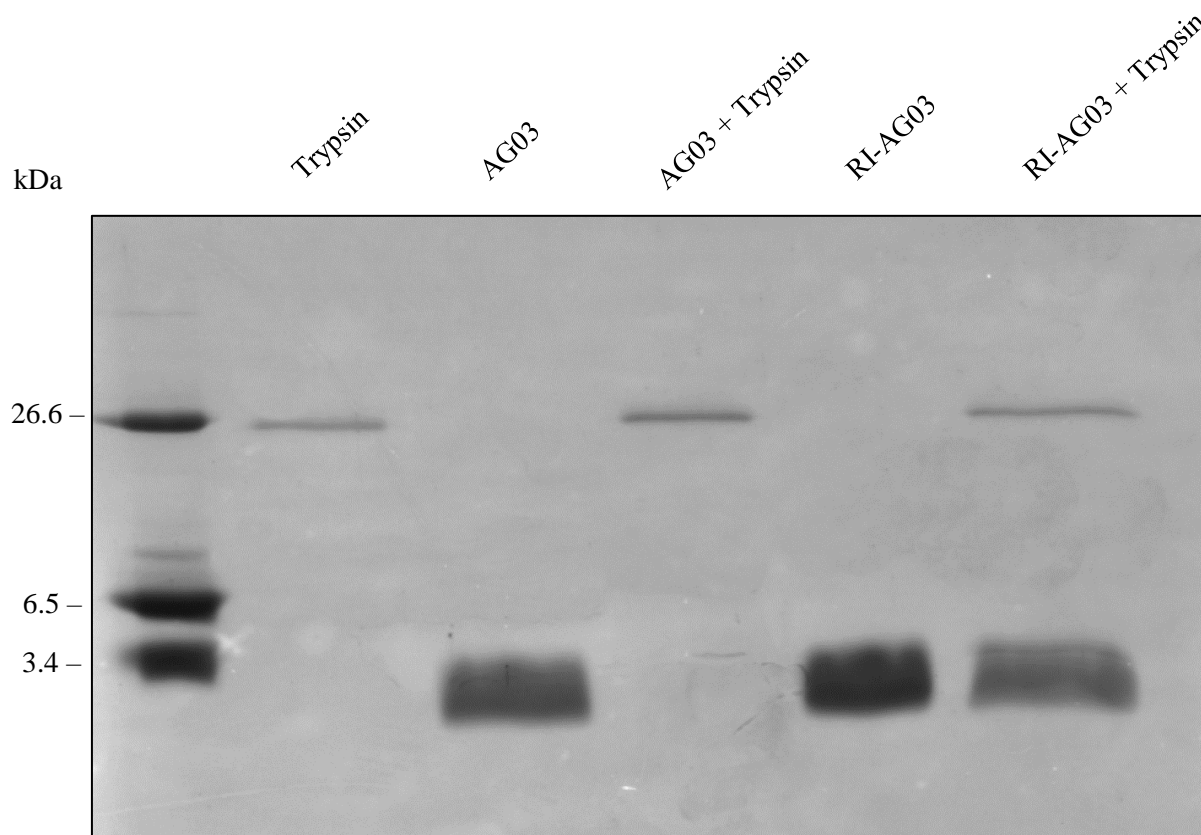
Figure 6.2: 15% SDS PAGE gels of AG03 (100µM) and RI-AG03 (100µM) treated with and without equimolar Trypsin concentration for 24-hours at 37˚C. AG03 has no signal in the presence of Trypsin whereas RI-AG03 has a strong signal in the presence of Tyrpsin. Digests were conducted in triplicate and densitometric analysis suggested a 19% reduction in signal after equimolar incubation of RI-AG03 with Trypsin for 24-hours at 37˚C.

Before conducting experiments in cells or *in-vivo,* the lead peptide had to be resistant to enzymatic degredation. Densitometric analysis of **Figure 6.2** suggested that AG03 was completely processed by trypsin, whereas RI-AG03 was only partially processed, with a 19% reduction in signal.

CELL UPTAKE AND TOXICITY

Before conducting experiments in cells or *in-vivo,* the lead peptide also had to be able to enter cells. **Figure 6.3A** demonstrated that RI-AG03 was successfully taken up into cells. The inhibitor could be in vesicles but as it contains an octa-arginine chain they may have escaped into the cytoplasm. Notice that some cells are green everywhere so the inhibitor could potentially also be in the nucleus. Before conducting experiments *in-vivo* RI-AG03 had to be tested for toxicity. **Figure 6.3B** demonstrated that after concentrations of 30μM. the peptide started becoming toxic to cells. This was deemed acceptable before testing the inhibitor in a *Drosophila* model of Taupoathy
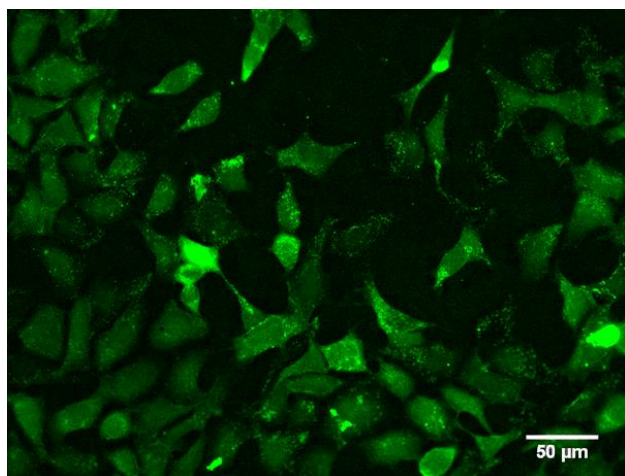
A   **B**
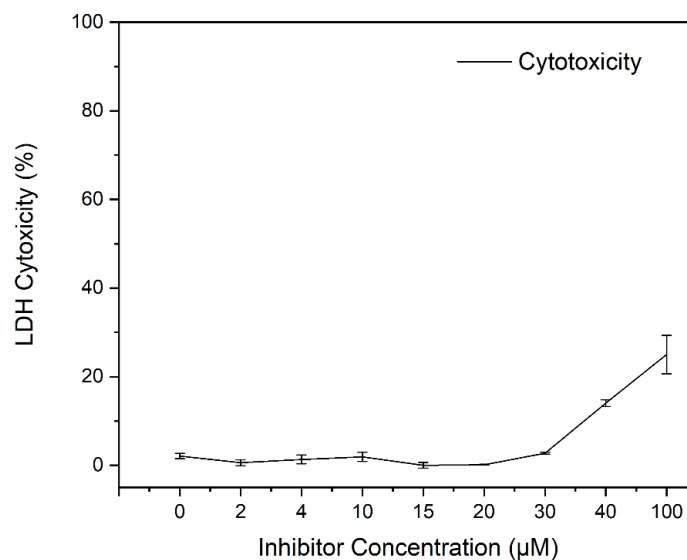
Figure 6.3: HEK-293 cells. **A:** Cellular uptake of FAM-RI-AG03 (15μM) by HEK-293 cells over 24-hours. Almost no peptide is visible in the medium, suggesting that majority of the peptide was taken up into the cells. **B:** Varying concentrations of RI-AG03 were co-incubated with HEK-293 cells and cytotoxicity was analysed using an LDH cytotoxicity kit. Toxicity begins to increase at 40μM.

6.2.3 EXTENDED STABILITY

Figure 6.4 demonstrated that RI-AG03 is stable after 8 days incubation at 25°C with a 1-hour incubation at 55°C. **Figure 6.4A** illustrates no changes in UV absorbance. **Figure 6.4B** highlights the raw charge state data. **Figure 6.4C** demonstrated the maximum entropy deconvolution of the raw data. This is an algorithm-based approach to transform the average m/z raw spectra into a zero-charge spectrum. The basic principle involves identifying realistic solutions as those with minimal information whilst simultaneously retaining compatability with the data (Raab and Jung-Richardt, 2015). This approach reduces the complexity of the data and improves resolution in comparison to raw data (Reinhold and Reinhold, 1992; Ferrige et al., 1991).

A.
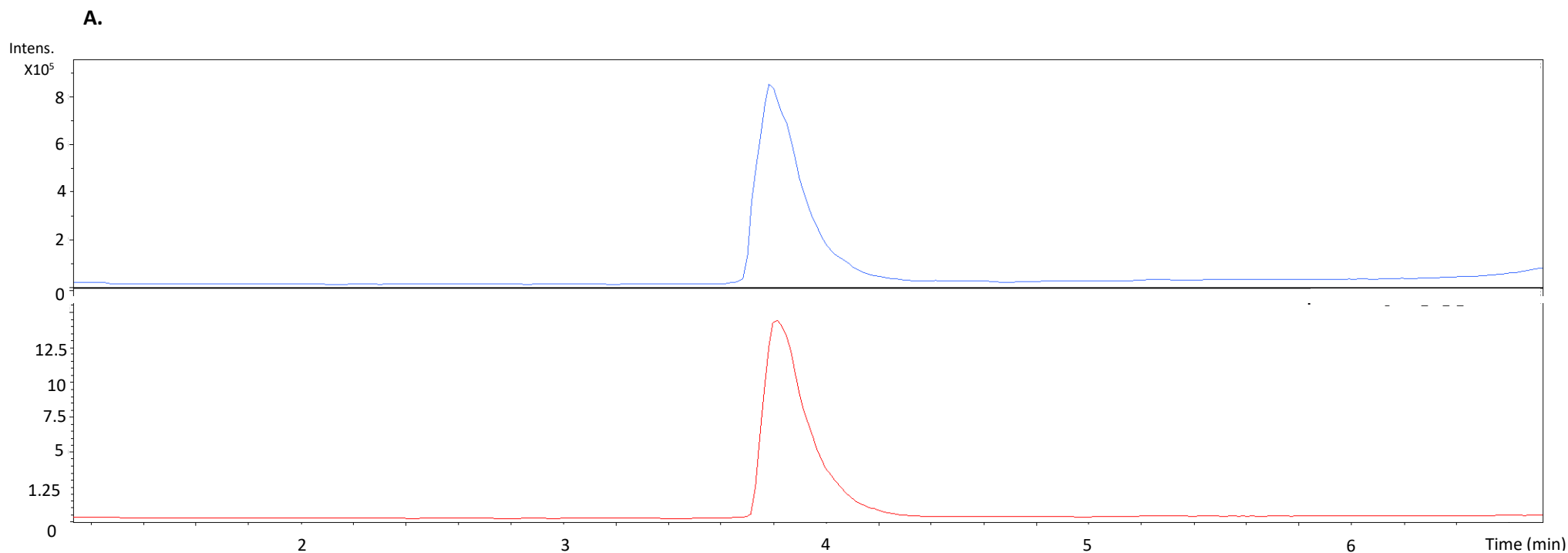
B.
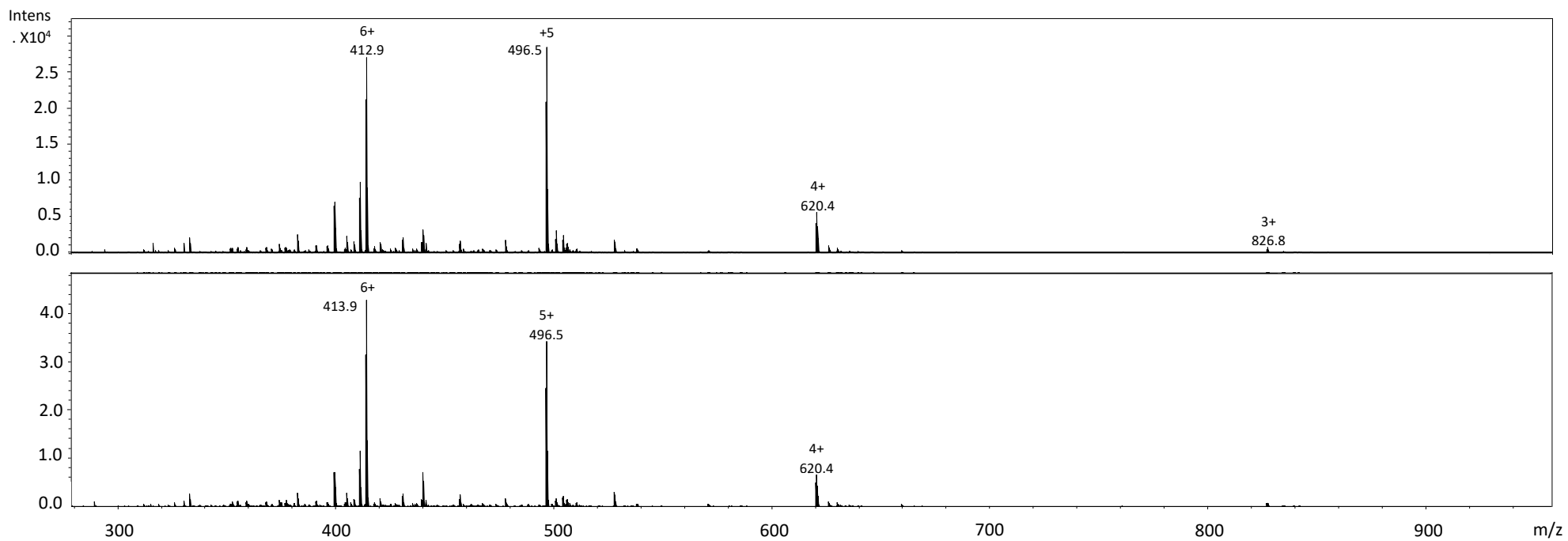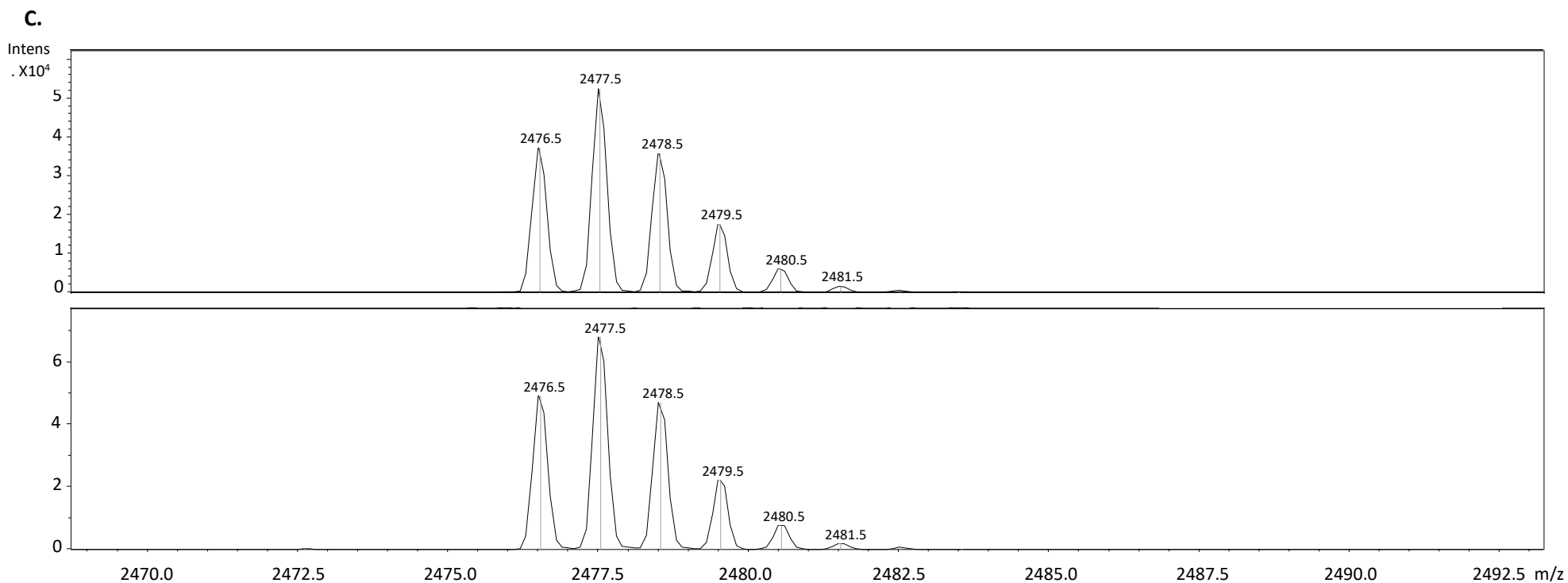
Figure 6.4: RP-UPHPLC MS data for RI-AG03 at time zero (top) and after 8 days incubation at 25˚ and heated to 55˚C for one hour (bottom). **A:** UV Chromatogram, 254 nm at **B:** MS 3.7min retention **C:** MS with maximum entropy deconvolution isotopic cluster peaks using Dalton units. This demonstrates that RI-AG03 remains unchanged over 8 days and heating.

A.
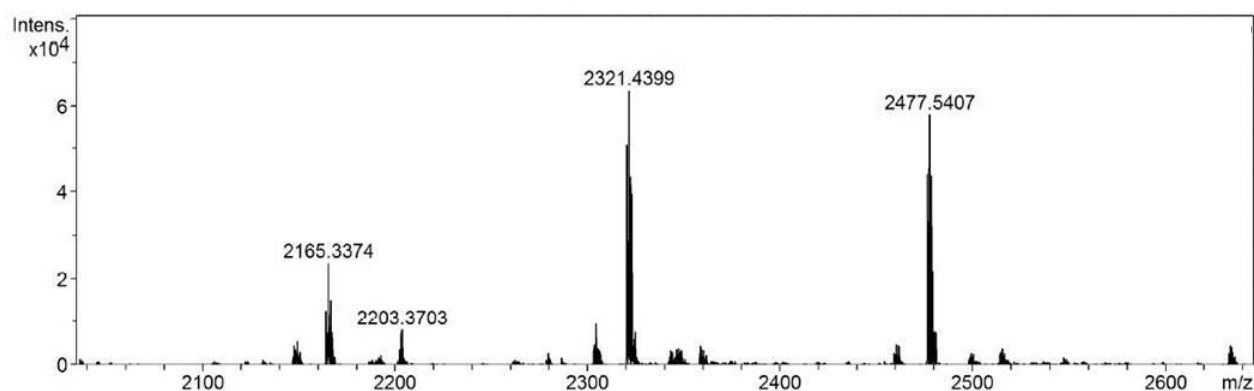
B.

Charge States	m/z		
[M+H]$^+$	2477.50	2321.00	2165.30
[M+H]$^{2+}$	1239.26	1161.20	1083.10
[M+H]$^{3+}$	826.51	774.50	722.40
[M+H]$^{4+}$	620.14	581.10	542.10
[M+H]$^{5+}$	496.31	465.10	433.80
[M+H]$^{6+}$	413.00	387.70	361.90
[M+H]$^{7+}$	354.79		
	Species 1	Species 2	Species 3

Figure 6.5: RP-UPHPLC MS data for RI-AG03 **A:** Demonstrated RI-AG03 exists as three separate species, **B:** Outlines the charge states for the three species. Species 1 ($C_{104}H_{189}N_{49}O_{22}$) has monoisotopic mass of 2476.5, RI-AG03 species 2 ($C_{98}H_{177}H_{45}O_{21}$) has a monoisotopic mass of 2320.4 (-156.1), RI-AG03 species 3 ($C_{92}H_{165}N_{41}O_{22}$) has a monoisotopic mass of 2164.3 (-156.1).

Figure 6.5 demonstrated that RI-AG03 exists as three species, each with either octa, hepta or hexa arginine chains. Variation in monoisotopic mass is due to the loss of one arginine (Mr = 174) and the addition of one H_2O molecule (Mr = 18) which equals out at 156. In electrospray the [M+H]$_+$ m/z is unknown, so it was calculated from energy state values 3+ to 6+. Therefore species 1 is the epexcted amino acid sequence [rG-pkyk(Ac)iqv-Grrrrrrrr], whereas species 2 has -1 arginine and +1 H_2O and species 3 has -2 arginine +2 H_2O compared to species 1. The hexa-arginine chain for species is below the previously discussed recommended polyarginine chain length for cell uptake.
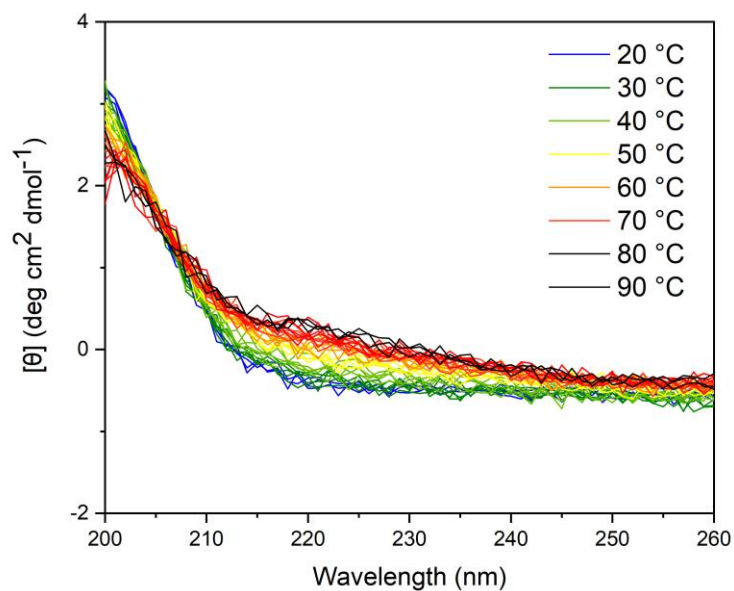
Figure 6.6: Thermal CD spectroscopy data demonstrating that temperature does not induce RI-AG03 (20μM) to adopt a specific secondary structure.

As RI-AG03 was added to the drosophila food which includes heating during preparation, it was important to determine if heat could force the inhibitor to change its secondary structure. **Figure 6.6** confirmed that RI-AG03 did not gain any secondary structure, despite being heated up to extremely high temperatures.

6.2.4 PRELIMINARY ROUGH-EYE MODEL DATA

Using BLASTP 2.8.1+ a standard align sequences protein BLAST between Human Tau 441 and Drosophila Tau 370 was conducted (**Appendix C**). The E-value suggests the number of expected hits with similar quality. lower the E-value the stronger the alignment match. The E-value for this BLASTP search was 1e-33 and suggested an identical alignment of 38% between amino acids 193-384 and 97-303 for Human Tau and Drosophila Tau, respectively (Altschul et a., 1997; Altschul et al., 2005). Neither the [306]VQIVYK[311] or the [275]VQIINK[280] sequences from TauΔ1-250 was matched to the *Drosophila* Tau.

Figure 6.7 Visually demonstrated that 1-day old GMR-hTau adults which have been fed RI-AG03 as larvae

have slighty larger eyes than untreated flies, more like those seen in the healthy control.
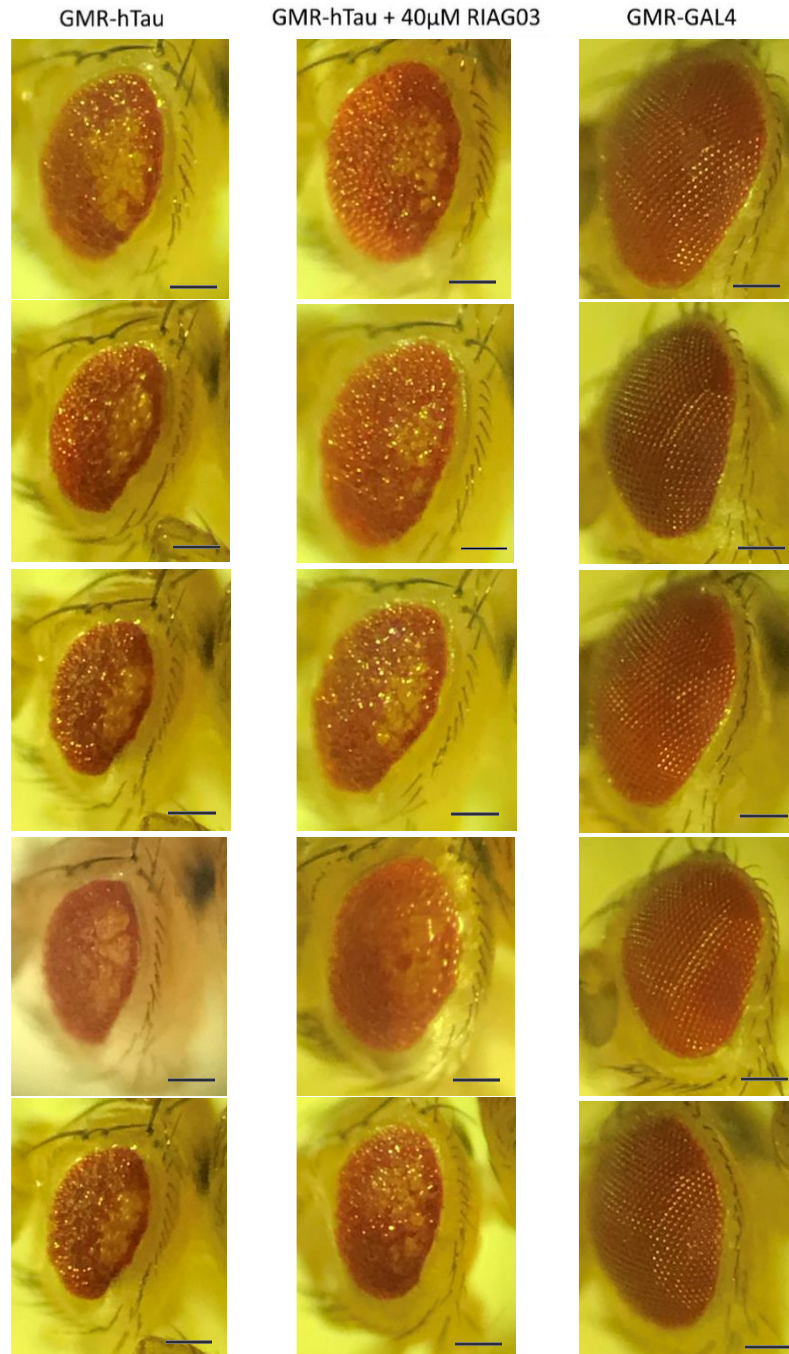
Figure 6.7: Shows experimental pilot data of *Drosophila* over-expressing Tau in the eye (GMR-hTau) and healthy Drosophila (GMR-GAL4) treated with RI-AG03 (40μM). Tau expression causes toxicity resulting in morphological changes in the eye shape and width at the middle of the eye. Notice the increased size of the eye when the Tau fly is treated with RI-AG03. Error bar = 100μm.

Figure 6.8 demonstrated that the width of the middle portion of the eye and the vertical length of the eye increased with RI-AG03 40 μM, when compared to the untreated Tau fly.
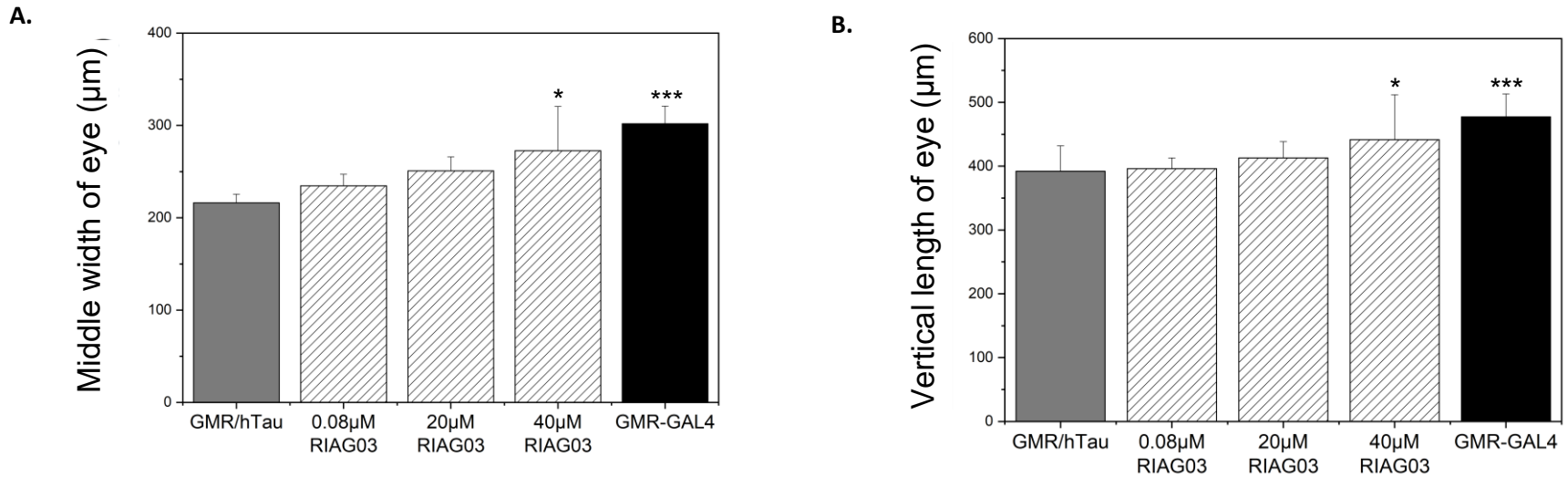
Figure 6.8: Shows experimental data of *Drosophila* over-expressing Tau in the eye (GMR-hTau) treated with various concentrations of RI-AG03 and healthy *Drosophila* control (GMR-GAL4). **A:** Width of the eye at the middle increased with 40 μM treatment. **B:** Vertical length of the eye increased with 40 μM treatment. Data presented as means (n=5/condition) and standard deviation. One factor repeated measures ANOVA + Tukey post hoc statistical analysis was conducted.

6.2.4.1 SCANNING ELECTRON MICROSCOPY

Figures 6.9 demonstrated the striking change in the ommatidia which seems most severe on the leading edge of the eyes. RI-AG03 appeared to

reduce the roughness of the eye and increase the number of bristles, resulting in a much more ordered looking eye when compared to the

healthy control.

A.
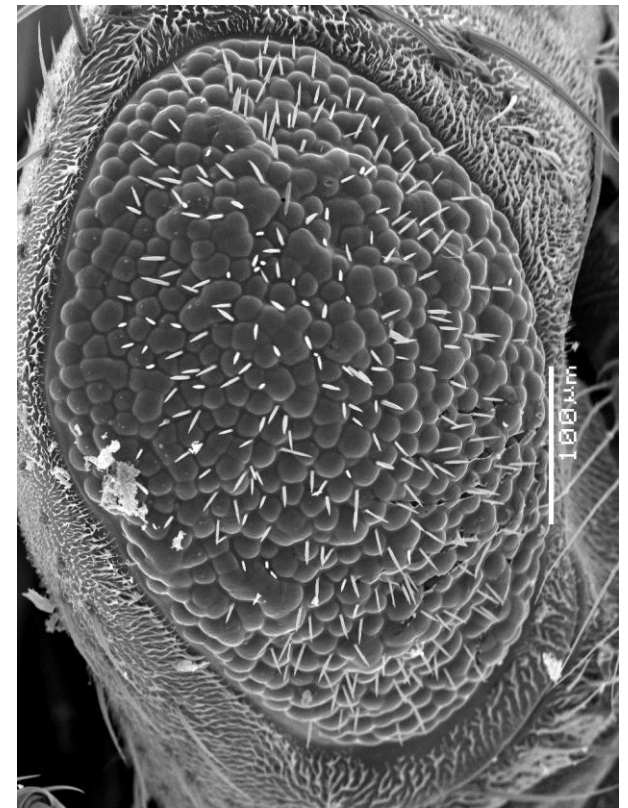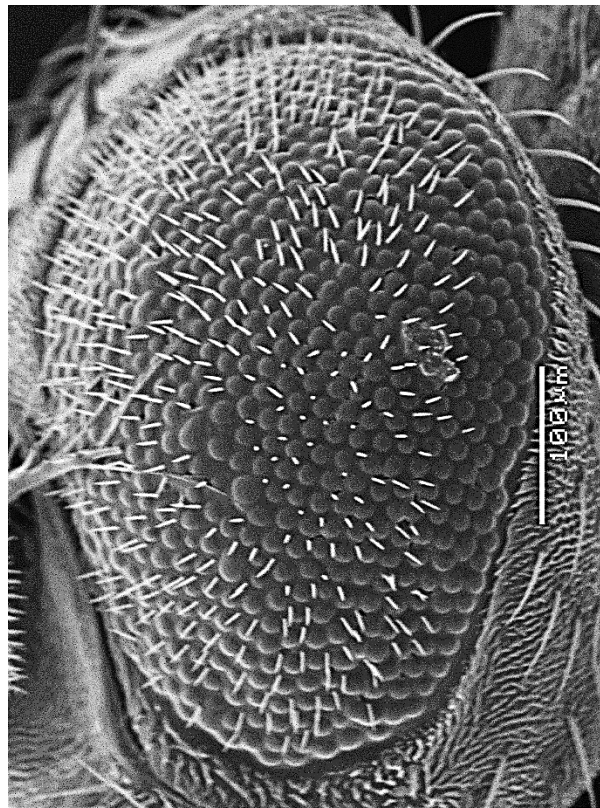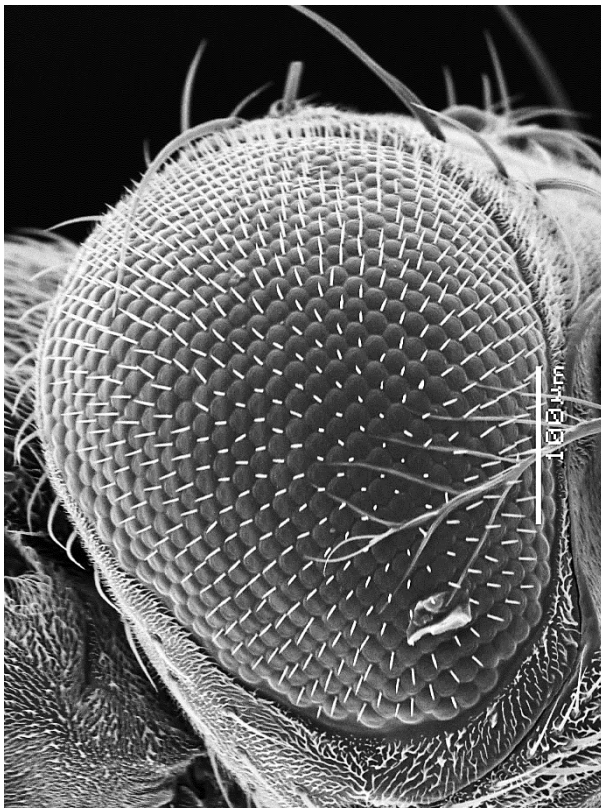
B.
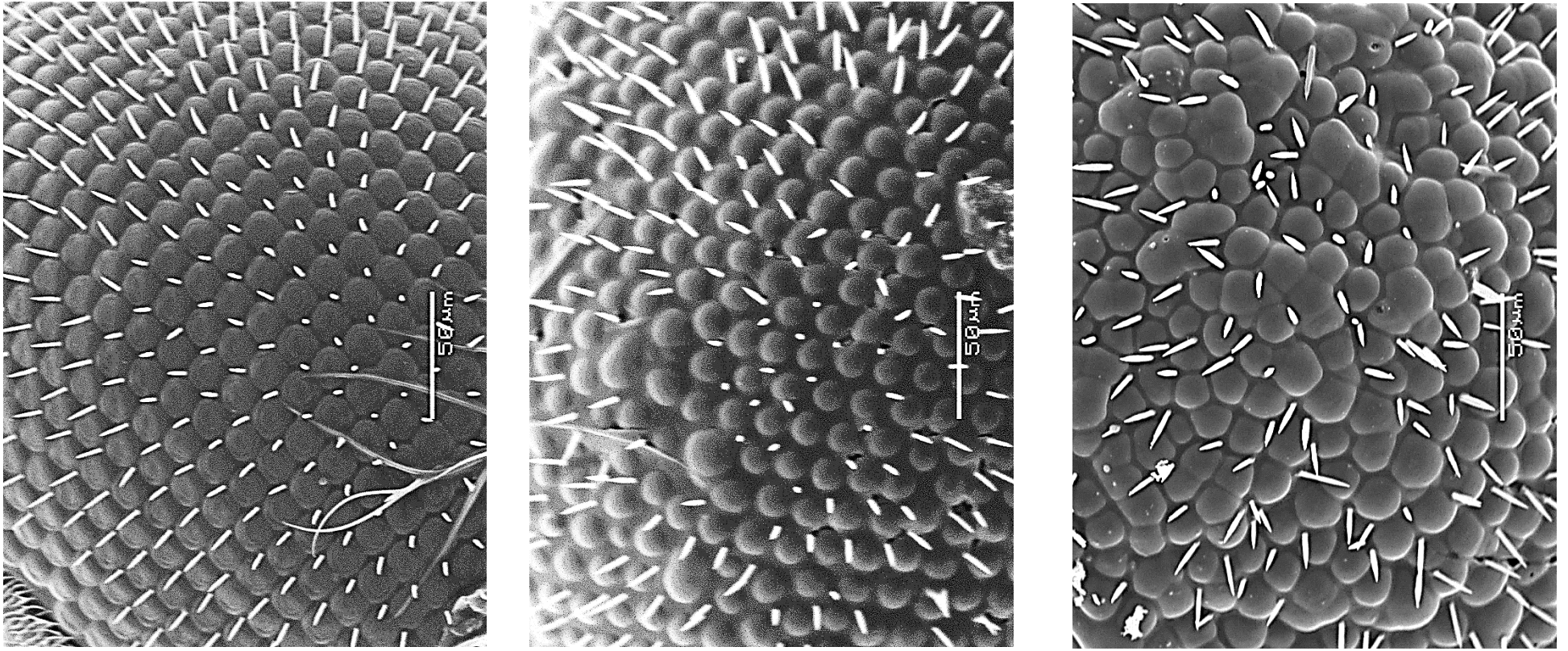
Figure 6.9: *Drosophila* eye SEM data of (from left to right) healthy GMR-GAL4, GMR-hTau treated with 20µM RI-AG03 and GMR-hTau without treatment. **A:** Notice the overall shape and size difference of the eyes **B:** Notice the ommatidia in the treated fly eye are more ordered compared to the untreated fly eye.

6.3 DISCUSSION

Before RI-AG03 could be experimented in cells and *in vivo*, proteolytic resistance first had to be confirmed. According to ExPASy peptide cutter, Trypsin cuts AG03 [RGVQIK(Ac)YKPGRRRRRRRR] at lysine and arginine residues. **Figure 6.2** demonstrated that AG03 is degraded by Trypsin but RI-AG03 is resistant to Trypsin degradation for at least 24 hours at 37°C. Proteolytic resistance is expected as RI-AG03 constitutes D-amino acids which are known to be proteolytically resistant (Taylor et al., 2010). On a molecular level the peptide can't be degraded by trypsin because the backbone is reversed and so is the conformation in the active site, therefore the catalytic triad of the trypsin molecules are not pointed in the right direction and no longer fit the residues, therefore it can not conduct cleavage. Although limited due to budget and availability of enzymes in the lab, this provided some reassurance that RI-AG03 would not be proteolytically degraded in future experiments. RI-AG03 also had to demonstrate that it could enter cells for it to be effective as an inhibitor of intracellular Tau aggregation and that itself is not toxic to cells. **Figure 6.3A** illustrated the ability of FAM-RI-AG03 to penetrate cells, perhaps through cell mediated endocytosis or an electrostatic interaction mediated process as CPPs such as polyarginne have a high capacity to cross cell membranes unaided by receptors (Oller-Salvia et al., 2016, Lu, 2012). He et al. (2016), mentioned that polyarginine utilises both direct penetration and endocytosis systems however the exact mechanisms are still poorly understood. They demonstrated that octa-arginine forms hydrophilic holes in the membranes of giant unilamellar vesicles and penetrate through. It was suggested that this interaction was based largely upon electrostatics and hydrophilic interactions. Direct penetration involves interactions between the CPP and the phosphate groups of the lipid bilayer where the the positive charges on arginines and their guanidinium side-chains nucleate theformation of transient pores (Futaki, 2005). Endocytosis pathways can be inhibited by treating cells at 4°C. Khalil et al. (2004), identified that incubation of cells treated at 4°C did not inhibit internalisation of octa-arginine. This suggests that octa-

arginine translocation is not limited to endocytosis. Macropinocytosis is a cellular uptake pathway involving polymerised actin filaments to extend from the plasma membrane like a sweeping hand to engulf cargo. Alternatively, Nakase et al. (2004), reported that uptake of octa-arginine was significantly supressed in the presence of macropinocytosis inhibitors ethylisopropylamiloride and cytochalasin D, suggesting an important role for micropinocytosis in the uptake of octa-arginine. However, Nakase et al (2004), also reported that micropinocytosis inhibitors demonstrated a greater inhibition effect for internalisation of R16 than octa-arginine, suggesting that micropinocytosis has a greater involvement in ceullar up take of R16 than octa-arginine. Upon cell uptake of CPP's, they must also be able to escape endosomes so they may exert biological activity in the cytosol. It is presumed polyarginine may cause the endosomal membranes to become leaky however this remains unclear. Calnan et al. (1991), reported that the arginine guanidinium head group forms hydrogen bonds with phosphate backbones in RNA and other phospholipids/divalent anions found in lipid bilayers Sakai et al (2004), suggested that octa-arginine can escape endosomal membranes through counteranion-mediated phase transfer, where counter anions form complexes with arginines and increase their hydrophobicity. The negative voltage within mammalian cells is a driving force for the uptake of cationic CPPs, perhaps through counteranions the positive charges can be neutralised and drive them outwards (Futaki, 2006). **Figure 6.3B** demonstrated the low toxicity levels of RI-AG03, as generally expected of a protein drug (Carter, 2011; Goodman, 2009; Leader et al., 2008). Potential side effects of using cationic cell penetrating peptides (CPPs) at high concentrations include membrane leakage and pertubation, reduction in cell viability, haemolysis and influence pore formation (Langel, 2019; Madani et al., 2011). This agrees with the increase in toxicity seen in **Figure 6.3A** at high concentrations of peptide. Kuo et al. (2009), treated human U-937 cell lines with octra-arginine and reported that octa-arginine did not release pro-inflammatory cytokines. To treat *Drosophila* with RI-AG03 the flies had to orally ingest the inhibitor. Therefore, the fly food which involves high temperatures during preparation, was supplemented with RI-AG03. The flies would feed on this drug food for 1 week

before being transferred to fresh drug food. This helped to ensure that the flies were constantly feeding

on fresh inhibitor. **Figure 6.4** illustrated that RI-AG03 is stable after 8 days incubation at 25°C with a 1-

hour incubation at 55°C; to simulate the cooling process of the *Drosophila* food. This suggested that there

is no detrimental effect to the inhibitor when it is supplemented to the hot *Drosophila* food. **Figure 6.4A**

showed no change in the UV absorbance of the sample at time zero and after 8 days incubation, suggesting

no degredation. **Figure 6.4B** highlighted the raw charge state data that was then deconvoluted in **Figure**

6.4C which considered different isotopes (e.g. 1.1% of all Carbon[12] is Carbon[13]) and demonstrated that the

neutral monoisotopic mass is 2476.50. Severn Biotech reported the molecular weight of RI-AG03 as the

average mass of 2477.99, perhaps because they used a MALDI-TOF machine without the ability to show

separate isotopes. Any change in ion numbers could be due to calibration. Changes in intensity could be

due to dilution error resulting in a change in concentration which can also affect retention time. **Figure**

6.5 showed that RI-AG03 exists as three species, each with either octa, hepta or hexa arginine chains,

respectively. This variation in monoisotopic mass resulting in these three species is due to the loss of one

arginine (Mr = 174) and the addition of one H_2O molecule (Mr = 18) which equals out at 156. The

monoisotopic mass of RI-AG03 (octa-arginine) is 2477.50, however 2477.50 − 156 = 2321.00 which is

species 2 with hepta-arginine. Therefore species 3 is 2321.00 − 156 = 2165.30. In electrospray the $[M+H]^+$

m/z is unknown, so it was calculated from energy state values 3+ to 6+. Therefore species 1 is the epexcted

amino acid sequence [rG-pkyk(Ac)iqv-Grrrrrrrr], whereas species 2 has -1 arginine and +1 H_2O and species

3 has -2 arginine +2 H_2O compared to species 1. The three species may be present due to error in peptide

synthesis and as Severn Biotech used MALDI-TOF it is possible the main peak swamped their spectra and

so they collected the peak fraction which included the three species. To ensure that RI-AG03 did not

change its fold at high temperatures when supplementing it to the fly food, thermal CD was performed.

If the inhibitor folded into β-sheets due to high temperature, then it could potentially seed aggregation

of Tau. Ambadiputi et al. (2017), demonstrated that Tau in the absence of heparin aggregates at high

temperatures >65 °C**. Figure 6.6** confirmed that RI-AG03 did not gain any secondary structure, despite being heated up to extremely high temperatures. With general confidence regarding the stability of RI-AG03, the inhibitor was taken forward for experimentation in a *Drosophila* Tau model. A BLAST was conducted (**Appendix C**) to view similarities between human Tau and Drosophila Tau to ensure that RI-AG03 did not target any VQIVYK or VQIINK sequences present in the natural Tau in the *Drosophila*. Despite sharing similarities (~38%) there are no VQIxxK sequences in the *Drosophila* Tau amino acid sequence. Therefore, there is some confidence that RI-AG03 only interacts with the Human Tau$_{441}$ in the eye rather than the with the native *Drosophila* Tau. **Figure 6.7** visually demonstrated that Tau flies treated with the inhibitor have slighty larger eyes, more like those seen in the healthy control. **Figure 6.8** provided quantitative analysis of fly eyes demonstrating that the width of the middle of the eye and the vertical length of the eye significantly increased with RI-AG03 40 µM**.** By analyzing the diameters of GMR-hTau fly eyes which were treated and untreated with RI-AG03 and comparing them to the GMR-GAL4 flies which do not express Tau in the eye, it is evident that RI-AG03 40 µM rescused eye phenotype in flies overexpressing Tau. Heidary and Fortini (2001), expressed 0N4R Tau and Δ306–311 0N4R Tau (without VQIVYK sequence) in the photoreceptors and nerve cells of Drosophila and identified that neurodegeneration occurred in the 0N4R flies but not in the Δ306–311 0N4R Tau flies. This suggests that VQIVYK is essential for Tau to assemble into toxic β-sheets. As RI-AG03 targets VQIVYK this finding also complies with the data in **Figures 6.7- 6.8** which suggest that RI-AG03 inhibits toxic Tau aggregation and that the inhibitor/Tau complexes formed were less toxic than aggregated Tau. **Figures 6.9** shows the striking change in the ommatidia which seems most severe on the leading edge of the eyes. RI-AG03 appeared to reduce the roughness of the eye and increase the number of bristles, resulting in a much more ordered looking eye when compared to the healthy control. This illustrated the ability of RI-AG03 to work *in vivo* in the rough-eye model system. It is important to note that because RI-AG03 consists of octa-arginine, it will penetrate other cells upon ingestion, therefore only very little peptide will reach the eye.

Furthermore, the peptide was demonstrated to exist as 3 separate species, one of which has nn unsufficient poly-arginine chain length for cell penetration meaning that even less inhibitor reached the eyes. It can be argued this model does not reflect neurodegeneration adequately and that the protein misfolding and toxicity is irrelevant for model of AD. Rincon-Limas et al. (2012), stated that some disease associated proteins (including Tau and Aβ) cause a rough eye phenotype whereas others such as prion protein and α-synuclein do not. They also highlighted that different phenotypes are observed in the eyes such as different size, fused ommatidia, disorganised lattice, glassu surface and loss of pigment, as seen in **Figure 6.10**. This suggests that specific pathways are interacted with, which is supported by the fact that the Aβ and Tau genes demonstrate similar phenotypes. Casas-Tinto et al. (2011), suggested that Aβ causes a rough eye phenotype whether it is photoreceptors or all cell types, providing evidence that the phenotype is caused by toxicity to photoreceptors and not by neighbouring cells.
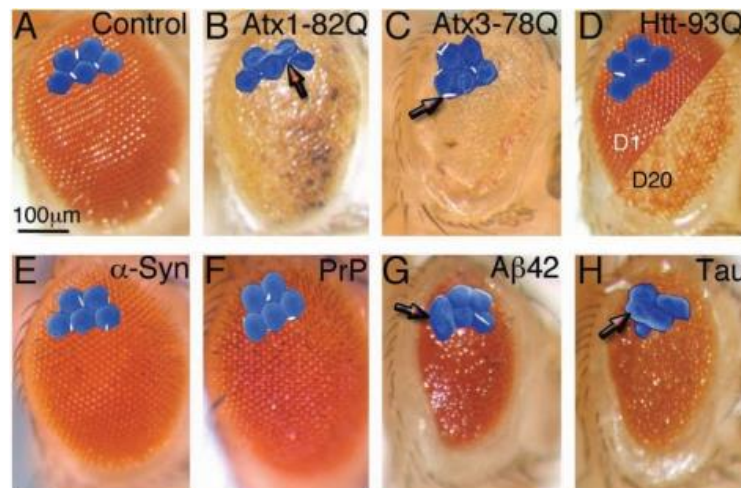
Figure 6.10: Micrographs of *Drosophila* eye disruption by different amyloidogenic protein expression. **A**: healthy control, **B**: Expressing Atx1-82Q, **C**: Expressing Atx3-78Q, **D**: Expressing Htt093Q, **E**: Expressing α-synuclein, **F**: Expressing Prion protein, **G**: Expressing Aβ, **H**: Expressing Tau (Rincon-Limas et al, 2012). Notice how both the Aβ and Tau fly eyes have a rough phenotype with reduced size and disorganised and fused ommatidia.

7. CONCLUSION

To this day there is still no clinically viable option to treat AD as the only drugs currently available are symptomatic. This leaves a huge hole in not only science but also the market. The research provided in this thesis presents a novel approach to prevent Tau aggregation using the retro-inverted peptide RI-AG03, which can also be bound to a liposome to improve efficacy.

To begin designing this peptide aggregation inhibitor the amino acid sequence of Tau was first screened for regions of low intrsinsic solubility and aggregation hot spots. The results from this highlighted region VQIVYK as the region with the lowest intrinsic solubility and the only aggregation hot spot. This provided an informed starting place to design a peptide aggregation inhibitor targeting VQIVYK. This prediction coincides with literature stating that VQIVYK is the main hexapeptide sequence for the aggregation of Tau and that in its absence Tau is unable to aggregate.

This peptide was based upon the native VQIVYK sequence in Tau so that it may retain high target selectivity. The aggregation propensity was investigated for the VQIVYK sequence with exhaustive mutagenesis the the second valine of VQI**V**YK. Mutagensis was conducted to reduce the aggregation propensity of the peptide so it would not seed aggregation as polarity and hydrophilicity are important in avoiding self-association (Sormanni et al., 2015). The second valine was chosen for mutagenesis because the VQIVYK and VQIINK sequences in Tau both share the reference motif VQIxxK. Tyrosine was not chosen for mutagenesis because as an aromatic amino acid it is useful as an anchoring residue through aromatic stacking interactions. Furthermore, following computational optimal binding experiments it was predicted that isoleucine and tyrosine are important binding molecules, which supported the rational of not altering the tyrosine residue. It is a logical assumption that there is a fine line between between pathogenic aggregation and functionality of proteins, therefore the amino acid chosen to replace valine

197

had to have a relatively high aggregation propensity, but not above the aggregation hot spot threshold. The VQIVYK binding sequence was altered using a lysine replacement for the second valine so that it no longer had the propensity to self-associate but retained a degree of intrinsic insolubility so it may bind effectively to its target. To further improve binding the newly introduced lysine was acetylated, rendering It a hydrogen bond donor. This enhanced its interactions with the hydrogen bond acceptor rich region of VQIVYK in native Tau. The natural residue in Tau after the VQIVYK sequence is proline. As proline is a known β-sheet breaker, it was included onto the end of the modified VQI**K**YK binding sequence of the inhibitor.

Molecular docking experiments predicted that VQI**K**YKP had the strongest energy bind to Tau $_{than}$ VQIVYK and VQI**K**YK did, however on average the binding conformations were very similar to each other. Both VQIVYK and VQI**K**YKP were predicted to interact with the VQIVYK and VQIINK sequences in Tau.

VQIVYK has been cited in literature to interact with VQIINK. Both peptides were predicted to mainly bind in parallel to both the VQIVYK and VQIINK sequences. This interaction of the peptides with both VQIVYK and VQIINK residues was suggested to be due to the VQIxxK recognition sequences and the asparagine and tyrosine residues in VQIINK and VQIVYK, respectively, interacting via polar-π interactions (Chakravarty et al, 2018). In some cases, however both peptides also demonstrated to also bind in anti-parallel in some cases as well. This agrees with Cheon et al. (2012), who observed that free VQIVYK peptides formed β-sheets consisting of both parallel and anti-parallel strands which stacked to then form disordered or irregular protofilaments. These predictions suggest that the inhibitors designed in this thesis are VQIxxK inhibitors as they are suggested to interact with both VQIINK (including neighbouring amino acids L282, N297, Y310, S316), and VIQVKY (including neighbouring amino acids G302, H374, N286, S285, Q288).

A variety of other peptides were also drafted for analysis in the wet lab. Tau aggregation is largely facilitated by charge interactions. These peptides utilised arginine residues to investigate the effects of

their global charge and local charge (depending on the terminus arginine residues were added to) on Tau

aggregation. The rationale behind these peptide designs was to prevent monomeric or misfolded Tau

molecules from interacting at the VQIVYK accessible binding site; thereby impeding further aggregation

Wet lab experiments were conducted using recombinantly expressed TauΔ1-250 (~94% purity). This

truncated construct only takes ~8 hours to aggregate, whereas full length Tau can take up to ~72hours to

aggregate (Crespo et al., 2018; Taniguchi et al., 2005). Tau was expressed in *E.coli* BL21(DE3) and induced

for 3 hours with IPTG at 37˚C. This Tau aggregated in the presence of heparin in an optimal Tau:heparin

ratio of 4:1.

A major concern when testing the inhibitors against heparin-induced Tau aggregation was the possibility

of the positively charged inhibitors from sequestering negatively charged heparin from solution, thereby

preventing heparin from interacting with Tau. AG02R5 [RG-VQIVYK-GRRRR] suggested that it was able to

inhibit seed-induced Tau aggregation in a ThT assay, suggesting that previous inhibition of heparin-

induced Tau was not due to the peptide sequestering heparin.

AG03 [RG-VQIK(Ac)YKP-GRRRRRRRR] comprised the valine replacement with lysine, the acetylation of this

lysine residue, the added proline residue, glycine spacers and a CPP polyarginine sequence. Although ThT

fluorescence does not quantitatively measure fibrilisation it does indicate the presence of amyloid. AG03

reduced ThT fluorescence (~30%) more than the other drafted peptide inhibitors which only comprised

at least one of these elements AG03 had. This suggested that combining these elements together

generated the most effective Tau aggregation inhibitor. The inhibitory effects of AG03 against heparin-

induced Tau were confirmed by testing a scramble peptide of AG03 and the octa-arginine sequence.

Neither the scramble peptide or octa-arginine inhibited Tau aggregation. Before testing AG03 in cells or

in vivo it had to be resistant to proteolysis, therefore an N-methylated version (AG03M) and a retro-

inverted version (RI-AG03) of AG03 were prepared. N-methylation did not appear to particularly improve

inhibitory effects against heparin-induced Tau aggregation, however retro-inversion almost completely blocked both heparin-induced and seed-induced Tau aggregation due to the reversal of the peptide backbone resulting in different hydrogen bonds. Despite the reversal of the backbone the peptide still retains activity. Ree et al. (2018), stated that affixing an acetyl group on the N-terminal amino group results in altered charge, hydrophobicity and size of the terminus; resulting in altered binding properties. RI-AG03 was also able to inhibit Tau aggregation when added during during the growth phase of Tau aggregation. The IC_{50} of RI-AG03 was calculated at 7.83μM. These data suggest that retro-inversion improved efficacy by perhaps altering the aggregation pathway of Tau. Hydrogen bond interactions calculated through molecular docking simulations illustrated that the RI-AG03 binding sequence interacted with neighbouring amino acids in addition to its target sequences, which provided additional evidence that the peptide may be able to alter the aggregation pathway of Tau. This was reinforced by TEM which showed that RI-AG03 locked Tau into spherical structures with an average diameter of ~36 nm, indicative of insoluble GTOs. These structures were not ThT or Congo red sensitive. CD demonstrated that incubation of Tau with RI-AG03 reduced β-sheet content of Tau, suggesting that the inhibitor is interfering with the way Tau normally folds in the presence of heparin.

The other peptide-inhibitors which were used to investigate different arginine chain lengths on Tau inhibition found no real difference beyond an addition of five arginnes. RI-AG03 comprised an octa-arginine sequence to provide it with cell penetrating properties which demonstrated to be enough to penetrate cells using fluorescence microscopy. After passing stability assays, RI-AG03 demonstrated to be relatively not toxic to HEK-293 cells and in a *Drosophila* model of tauopathy appeared to partially rescue the rough-eye phenotype according to light and SEM microscopy by displaying vertically longer and horizontally wider eyes in the middle portion of the eye, with more ordered ommatidia and bristles.

8.   RECOMMENDATIONS FOR FUTURE RESEARCH

It is important to confirm that the RI-AG03-Tau species formed are not toxic and so varying concentrations will be incubated with cultured neuroblastoma SH-SY5Y cells, due to the difficulties of obtaining primary neurones. MTT (3-(4,5-dimethylthiazol-2-yl)-2,5-diphenyltetrazolium bromide) and LDH assays of cell survival/proliferation will be employed to assess any undesirable toxicity on this cell type. The LDH assay is a colorimetric assay to determine cytotoxicity. When cells are damaged, they release LDH which catalyses the oxidation of lactate to form pyruvate with parallel reduction of NAD to NADH resulting in an absorbance shift which can be detected at 340 nm (Fotakis and Timbrell, 2005). The MTT assay is another colorimetric assay to determine cell viability MTT enters the mitochondria of cells where it is reduced by microchondrial succinate dehydrogenase into insoluble formazan. Cells are solubilised with organic solvent which releases the solubilised formazan and absorbance is read at 570 nm (Lie et al., 1997). DNA damage can also be assessed by detecting 8-oxo-guanine, a marker of DNA oxidation and damage. It has already been suggested in **Figure 6.3** that RI-AG03 is not overtly toxic to HEK-293 cells at concentrations of up to 30 µM, however the inhibitor-Tau complexes formed *in-vitro* have not been tested for toxicity against cells. The Ames test can also be employed to determine potential carcinogenicity by detection of point mutations in DNA. Dynamic light scattering can also be useful to determine the solubility of the inhibitor-Tau complexes formed in solution as it can identify non-fibrillar intermediates as well as fibrils. If the species formed are insoluble, they will crash out of solution.

Since Tau is a microtubule binding protein (MAP) it is important to investigate if RI-AG03 also binds, as its binding sequence is based on the VQIVYK sequence found in the microtubule binding domain of Tau. This can be achieved using a microtubule binding spin down assay kit. Microtubules can be freshly assembled in the lab using general tubulin buffer, α-tubulin, β-tubulin, MAP fraction (including Tau) and taxol solution to stabilise the microtubules. If RI-AG03 is seen to associate with microtubules it can be compared with

the NAP peptide which is a known microtubule stabiliser to see if RI-AG03 also has microtubule stabilising properties. By phosphorylating the microtubules in solution theoretically they should disassemble, however if RI-AG03 can stabilise the microtubules, there should be less occurance of disassembly.

The two main hexapeptide sequences in full length Tau responsible for aggregation are VQIINK and VQIVYK. RI-AG03 is designed to bind to VQIVYK and based on molecular docking simulations is predicted to interact with VQIVYK and VQIINK. Although RI-AG03 successfully achieved the goal of this thesis to develop a peptide-based aggregation inhibitor against Tau, the mechanism by which inhibits aggregation of Tau is still not entirely clear. It is assumed that the peptide interacts with VQIVYK and VQIINK and perhaps alters the normal aggregation pathway of heparin-induced Tau aggregation. However, it has not yet been confirmed *in-vitro* if this is occuring. By incubating VQIVYK or VQIINK hexapeptides in the presence of RI-AG03 and analysing rate and extent of aggregation via Thioflavn-T fluorescence assay, it can be determined if RI-AG03 can block fibrilisation of these hexapeptide sequences. Based on the computational predictions and the specific design of the inhibitor being a VQIxxK peptide, it should interact with both VQIVYK and VQIINK and inhibit aggregation of these hexapeptides.

RI-AG03 will be incubated in the prescence of proteolytic enzymes andanalysed using RP-HPLC with a C18 x 2.0 mm column and a gradient produced from 0.01 % trifluoroascetic acid (TFA) in dH$_2$O (Buffer A) and 0.1 % TFA in 100 % acetonitrile (Buffer B). Peptides will be eluted with a linear gradient of 0-60% acetonitrile 0.01% TFA over 40 minutes at 1 mL/min flowrate and measure absorbance at 214 nm and 275 nm. The absorbance value of 214 nm will be used because the peptide bonds in VQIVYK absorbs strongly at this wavelength. The absorbance value of 275 nm will be used because tyrosine has a distinctive absorption profile at 275 nm due to chromophores in its aromatic side chain (Prasad et al., 2017).Enzymes to be investigated will be those calculated by ExPASy to be capable of cutting L-amino acid AG03 such as Arg-C proteinase, Chymotrypsin, Clostripain, LysC, LysN, Pepsin (pH>2), Proteinase K, Thermolysin and human plasma. This will thoroughly characterise the enzymatic stability of RI-AG03.

Repeating the studies conducted in the 2N4R Tau fly eye model, and in a healthy control group with greater number of flies, to clarify whether RI-AG03 can rescue eye phenotype when observed under scanning electron microscope and confocal microscope. The normal flies and 2N4R Tau flies (n=100 per treatment) will be fed on food supplemented with two different concentrations (20 µM, 0.08 µM) of RI-AG03 and will be euthanised the day they eclosed and prepared for microscopy. Longevity and climbing assays in a pan neuronal driver 2N4R Tau ELAV Drosophila melanogaster model of Tauopathy, and in a healthy control group (Bloomington Stock Centre). The purpose is to obtain toxicity data that may be relevant to humans. The normal flies and 2N4R Tau flies (n=100 eggs per treatment) will be fed on food supplemented with two different concentrations (20 µM, 0.08 µM) of RI-AG03 and, will be monitored over a period of 2 months. The percentage of hatched eggs pupated and eclosed flies with be will be recorded. As human Tau flies are reported to have abnormalities in wing phenotype as well is potentially missing wings or limps, climbing assays will also be suitable to observe the effects of RI-AG03. Differential fractionation of 2N4R Tau in ELAV *Drosophila melanogaster* model can also be conducted to biochemically analyse the percentage difference of monomeric, oligomeric and insoluble fractions. This can indicate how RI-AG03 is interacts in *in vivo* and to what extent it can prevent aggregation.

Some experimentation has been attempted to investigate the binding affinity of RI-AG03 and liposome-RI-AG03 at the University of Rome using surface plasmon resonance however was unsuccessful due to unspecific binding of the peptide. Other potential avenues to investigate this may include NMR spectroscopy and affinity membrane chromatography. Conducting further experiments using the liposome bound RI-AG03 peptide such as CD, TEM and its effects in *Drosophila* including potential enhancement of delivery will be a logical next step for the evolution of RI-AG03.

REFERENCES

1. Abagyan, R. and Totrov, M., 1994, Biased probability Monte Carlo conformational searches and electrostatic calculations for peptides and proteins, J Mol Biol., 235(3):983-1002.

2. Abagyan, R., Kufareva, I., 2009, The flexible pocketome engine for structural chemogenomics, Methods Mol Biol., 575:249-79.

3. AC Immune, 2015, AC Immune Enters into a Worldwide License and Collaboration Agreement for Alzheimer's Disease Therapeutic anti-Tau Vaccines with Janssen Pharmaceuticals, Inc., Available at: <http://www.acimmune.com/content/news2/acimmune_janssen_20150112_final.pdf>, [Accessed 1st June 2016].

4. Adamcik, J., Mezzenga, R., 2018, Amyloid Polymorphism in the Protein Folding and Aggregation Energy Landscape, Angewandte Chem. Int. Ed. 2018, 57, 8370 – 8382.

5. Agadjanyan, M., Petrovsky, N., Ghochikyan, A., 2015, A fresh perspective from immunologists and vaccine researchers: active vaccination strategies to prevent and reverse Alzheimer's disease, Alzheimers Dement., 11(10);1246-1259.

6. Aggidis, A., Newman, J., Aggidis, G. 2015, Investigating pipeline and state of the art blood glucose biosensors to formulate next steps, Biosensors and Bioelectronics, 74;243-62.

7. Ali, Y., Ruan, K., Zhai R., 2012, NMNAT suppresses tau-induced neurodegeneration by promoting clearance of hyperphosphorylated tau oligomers in a Drosophila model of tauopathy, Hum. Mol. Genet., 21;237-250.

8. Allsop, D. and Mayes, J., 2014, Amyloid β-peptide and Alzheimer's disease Essays. Biochem, 56, 99-110.

9. Alonso, C., Mederlyova, A., Novak, M., Grundke-Iqbal, I., Iqbal, K., 2004, Promotion of hyperphosphorylation by frontotemporal dementia tau mutations, J. BiolChem., 279:34873–81. doi:10.1074/jbc.M40513120065.

10. Altschul, S., Madden, T., Schäffer, A., Zhang, J., Zhang, Z., Miller, W., Lipman, D., 1997, "Gapped BLAST and PSI-BLAST: a new generation of protein database search programs", Nucleic Acids Res. 25:3389-3402.

11. Altschul, S., Wootton, J., Gertz, M., Agarwala, R., Morgulis, A., Schäffer, A., Yu, ., 2005, "Protein database searches using compositionally adjusted substitution matrices", FEBS J. 272:5101-5109.

12. Alzforum, 2016, In First Phase 3 Trial, the Tau Drug LMTM Did Not Work. Period, Available at: <https://www.alzforum.org/news/conference-coverage/first-phase-3-trial-tau-drug-lmtm-did-not-work-period> [Accessed 5th March 2019].

13. Alzforum, 2019a, Therapeutics, Available at: <https://www.alzforum.org/therapeutics>, [Accessed 11th February 2019].

14. Alzforum, 2019b, To Block Tau's Proteopathic Spread, Antibody Must Attack its Mid-Region, Available at: <https://www.alzforum.org/news/conference-coverage/block-taus-proteopathic-spread-antibody-must-attack-its-mid-region>, [23rd April 2019].

15. Alzheimer's Association, 2015, Alzheimer's Disease Facts and Figures, Alzheimer's & Dementia, 2015;11(3)332.

16. Alzheimer's Disease International, 2015, The World Alzheimer Report 2015: 'The Global Impact of Dementia: An analysis of prevalence, incidence, cost and trends', Available at: <https://www.alz.co.uk/research/WorldAlzheimerReport2015.pdf>, [Accessed 7th October 2015].

17. Alzheimer's Society, 2014, Financial cost of dementia, Available online at: <http://www.alzheimers.org.uk/site/scripts/documents_info.php?documentID=418>, [Accessed 7th October 2015].

18. Alzheimer's Society, 2015, Types of dementia, Retrieved October 02, 2015, from Alzheimer's Society: <http://www.alzheimers.org.uk/Facts_about_dementia/What_is_dementia/> [Accessed 7th Octover 2015].

19. Ambadipudi, S., Biernat, J., Riedel, D., Mandelkow, E., Zweckstetter, M., 2017, Liquid–liquid phase separation of the microtubule-binding repeats of the Alzheimer-related protein Tau, Nature Communications, 8: 275.

20. Amdursky, N., Erez, Y., Huppert, D., 2012, Molecular Rotors: What Lies Behind the High Sensitivity of the Thioflavin-T Fluorescent Marker, Accounts of Chemical Research, 45(9);1548–1557.

21. Anand, R., Dip, K., Abbas, Mahdi, A., 2014, Therapeutics of Alzheimer's disease: Past, present and future, Neuropharmacology, 76, Part A, 27–50.

22. Andorfer, C., Acker, C., Kress, Y., Hof, P., Duff, K., Davies, P., 2005, Cell-cycle reentry and cell death in transgenic mice expressing nonmutant human tau isoforms, J Neurosci., 1;25(22):5446-54.

23. Arendt T, Stieler J, Strijkstra AM, Hut RA, Rüdiger J, Van der Zee EA, Harkany T, Holzer M, Härtig W., 2003, Reversible paired helical filament-like phosphorylation of Tau is an adaptive process associated with neuronal plasticity in hibernating animals. J Neurosci., 23:6972–81.

24. Arendt, T., Stieler, J., Holzer, M., 2016, Tau and Tauopathies, Brain Res Bull., 126(Pt 3):238-292.

25. Arispe, N., Diaz, J., Flora, M., 2008, Efficiency of Histidine-Associating Compounds for Blocking theAlzheimer's AbChannel Activity and Cytotoxicity, Biophysical Journal, 95;4879–488.

26. Arslan, M., Karadag, D., Kalyoncu, S., 2019, Protein engineering approaches for antibody fragments: directed evolution and rational design approaches, Turk J Biol, 43; 1-12.

27. Arthur, David & Uzairu, A. & Mamza, Paul & Abechi, Stephen & Shallangwa, Gideon. (2019). Molecular Docking Studies on the Interaction of NCI Anticancer Analogues with Human Phosphatidylinositol 4,5-bisphosphate 3-kinase catalytic subunit. Journal of King Saud University – Science, 31(4);1151-1166.

28. Bakota, L. and Brandt, R. 2016, Tau Biology and Tau-Directed Therapies for Alzheimer's Disease. Drugs,76(3):301-13.

29. Ballatore, C., Lee, V., Trojanowski, J., 2007, Tau-mediated neurodegeneration in Alzheimer's disease and related disorders, nature reviews neuroscience, 8;663-672.

30. Bao, S., 2014, Notch Controls Cell Adhesion in the Drosophila Eye, PLoS Genet., 10(1); e1004087.

31. Barghorn S, Davies P, Mandelkow E, 2004, Tau paired helical filaments from Alzheimer's disease brain and assembled *in vitro* contain β structure in the core domain. Biochemistry, 43:1694–1703.

32. Barghorn, S. and Mandelkow, E., 2002, Toward a Unified Scheme for the Aggregation of Tau into Alzheimer Paired Helical Filaments, Biochemistry 2002, 41, 14885-14896.

33. Barghorn, S., Biernat, J., Mandelkow, E., 2005, Purification of recombinant Tau protein and preparation of Alzheimer-paired helical filaments *in vitro*, Methods Mol Biol., 299:35-51.

34. Barghorn, S., Zheng-Fischhöfer, Q., Ackmann, M., Biernat, J., Von Bergen, M., Mandelkow, E.M., Mandelkow, E., 2000, Structure, microtubule interactions, and paired helical filament aggregation by tau mutants of frontotemporal dementias, Biochemistry, 39:11714–11721.

35. Becker, R., Greig, N., 2012, Increasing the success rate for Alzheimer's disease drug discovery and development, Expert Opinion on Drug Discovery, 7 (4), pp. 367-370.

36. Behl, C., 2012, Brain aging and late-onset Alzheimer's disease: many open questions," International Psychogeriatrics, vol. 24, supplement 1, pp. S3–S9.

37. Bellen, H., Tong, C., Tsuda, H., 2010, 100 years of Drosophila research and its impact on vertebrate neuroscience: a history lesson for the future, Nature Reviews Neuroscience, 11;514–522.

38. Benkert, P., Biasini, M., Schwede, T. 2011, Toward the estimation of the absolute quality of individual protein structure models. Bioinformatics 27;343-350.

39. Benkert, P., et al., 2008, QMEAN: a comprehensive scoring function for model quality assessment. Proteins, 71, 261–277.

40. Benkert, P., et al., 2009, QMEAN server for protein model quality estimation. Nucleic Acids Res., 37, W510–W514.

41. Benson, M., Buxbaum, J., Eisenberg, D., Merlini, G., Saraiva, M., Sekijima, Y., Amyloid nomenclature 2018: recommendations by the International Society of Amyloidosis (ISA) nomenclature committee, Amyloid, 25(4):215-219.

42. Berhanu, W., and Masunov, A., 2012, Alternative packing modes leading to amyloid polymorphism in five fragments studied with molecular dynamics, Biopolymers 98(2):131-44.

43. Betts, M., Russell, R., 2003, Amino acid properties and consequences of subsitutions In Bioinformatics for Geneticists, M.R. Barnes, I.C. Gray eds, Wiley.

44. Bevensee, M., Cummins, T., Haddad, G., Boron, W., Boyarsky, G., 1996, pH regulation in single CA1 neurons acutely isolated from the hippocampi of immature and mature rats, J Physiol., 494 (Pt 2):315-28.

45. Bhattacharyya, R., Nayak, K., Chakrabarty, A., 1988, Interaction of MgATP2- with DNA: assessment of metal-binding sites and DNA conformations by spectroscopic and thermal denaturation studies. Inorg. Chim. Acta.,153:79–86.

46. Blake, C. and Serpell, L., 1996, Synchotron X-ray studies suggest that the core of the transthyretin amyloid fibril is a continuous beta-sheet helix, Structure, 4, 989-998.

47. Blennow, K., Leon, M., Zetterberg, H., 2006, Alzheimer's disease, Lancet, 368: 387–403.

48. Bloomington Drosophila Stock Centre, 2019, BDSC Cornmeal Food<https://bdsc.indiana.edu/information/recipes/bloomfood.html>, [Accessed 3rd March 2019].

49. Boche, D., Denham, N., Holmes, C., Nicoll, J., 2010, Neuropathology after active Abeta42 immunotherapy: implications for Alzheimer's disease pathogenesis, Acta Neuropathol., 120(3):369-84.

50. Boutajangout, A., Sigurdsson, E., Krishnamurthy, P., 2011, Tau as a Therapeutic Target for Alzheimer's Disease, Curr Alzheimer Res, 8(6);666–677.

51. Bradbury, A., Sidhu, S., Dübel, S., McCafferty, J., 2011, Beyondnatural antibodies: The power of*in vitro*display technologies, Nat Biotechnol., 29:245–54.

52. Brand AH and Perrimon N (1993). Targeted gene expression as a means of altering cell fates and generating dominant phenotypes. Development 118: 401-415.

53. Brzobohaty, B. and Kovac, L., 1986, Factorsenhancing genetic transformation of intactyeast cells modify cell wall porosity. J. Gen.Microbiol. 132:3089-3093.

54. Buée L., Bussiere, T., Buee-Scherrer, V., Delacourte, A., Hof, P., 2000, Interactive report Tau protein isoforms, phosphorylation and role in neurodegenerative 1 disorders, Brain Research Reviews 33:95–130.

55. Buee, L., Delacourte, A., 1999, Comparative biochemistry of Tau in progressive supranuclear palsy, corticobasal degeneration, FTDP-17 and Pick's disease. Brain Pathol., 9;681–693.

56. Butner, K. and Kirschner, M., 1991, Tau Protein Binds to Microtubules through A Flexible Array of Distributed Weak Sites, The Journal of Cell Biology, 115(3);717-730.

57. Cagan, R., Ready, D., 1989, Notch is required for successive cell decisions in the developing Drosophila retina. Genes Dev 3: 1099–1112.

58. Calamai M, Kumita JR, Mifsud J, Parrini C, Ramazzotti M, et al., 2006, Nature and significance of the interactions between amyloid fibrils and biological polyelectrolytes. Biochemistry 45: 12806–12815.

59. Calnan, B., Tidor, B., Biancalana, S., Hudson, D., & Frankel, A. (1991). Arginine-mediated RNA recognition: the arginine fork. Science, 252(5009), 1167–1171.

60. Cao, W., Song, H., Gangi, T., Kelkar, A., Antani, I., Garza, D., Konsolaki, M., 2008, Identification of novel genes that modify phenotypes induced by Alzheimer's beta-amyloid overexpression in Drosophila. Genetics., 178:1457–71.

61. Carter, P., 2011, Introduction to current and future protein therapeutics: A protein engineering perspective. Exp Cell Res, 317:1261–9.

62. Casas-Tinto, S., Zhang, Y., Sanchez-Garcia, J., Gomez-Velazquez, M., Rincon-Limas, D., Fernandez-Funez, P., 2011, The ER stress factor XBP1s prevents Amyloid-ss neurotoxicity. Hum Mol Genet., 20(11):2144–60.

63. Castellania, R. and Perry, G., 2019, Tau Biology, Tauopathy, Traumatic Brain Injury, and Diagnostic Challenges, J Alzheimers Dis. 2019; 67(2): 447–467.

64. Chakravarty, S., Ung, A., Moore, B., Shore, J., Alshamrani, M., 2018, A Comprehensive Analysis of Anion–Quadrupole Interactions in Protein Structures, Biochemistry, 57(12);1852–1867.

65. Chan, S., Lu, L., Lam, T., Yan, S., Leung, C., Ma, D., 2015 A Novel Tetradentate Ruthenium (II) Complex Containing Tris(2- Pyridylmethyl)amine (tpa) As An Inhibitor Of Beta-amyloid Fibrillation, Curr Alzheimer Res., 12(5):434-8.

66. Chatterjee, S., Sang, T., Lawless, G., Jackson, G., 2009, Dissociation of tau toxicity and phosphorylation: role of GSK-3b, MARK and Cdk5 in a Drosophila model, Human Molecular Genetics, 18(1);164–177.

67. Cheng, J., et al., 2005, SCRATCH: a protein structure and structural feature prediction server, Nucleic Acids Res., 33, W72–W76.

68. Cheon, M., Chang, I., Hall, C., 2012, Influence of temperature on formation of perfect tau fragment fibrils using PRIME20/DMD simulations, Protein Sci. 21(10);1514-1527.

69. Chirita C. N., Congdon E. E., Yin H., Kuret J. (2005) Biochemistry 44, 5862–5872.

70. Chiti, F., Dobson, C., 2017, 2017, Protein Misfolding, Amyloid Formation, and Human Disease: A Summary of Progress Over the Last Decade., Annu Rev Biochem. 2017 Jun 20; 86:27-68.

71. Chouhan, A., Guo, C., Hsieh, Y., Ye, H., Senturk, M., Zuo, Z., Li, Y., Chatterjee, S., Botas, J., Jackson, G., Bellen, H., Shulman, J., 2016, Uncoupling neuronal death and dysfunction in Drosophila models of neurodegenerative disease, Acta Neuropathol Commun., 23;4(1).

72. Church, J., Baxter, K., McLarnon, J., 1998, pH modulation of Ca^{2+} responses and a Ca^{2+}-dependent K^+ channel in cultured rat hippocampal neurones. *J. Physiol*. 511(Pt 1), 119–132.

73. Clavaguera, F., Bolmont, T., Crowther, R., Abramowski, D., Frank, S., Probst, A., Fraser, G., Stalder A., Beibel, M., Staufenbiel, M., Jucker, M., Goedert, M., Tolnay, M., 2009, Transmission and spreading of tauopathy in transgenic mouse brain, Nat Cell Biol., ;11(7):909-13. doi: 10.1038/ncb1901.

74. Clavaguera, F., Hench, J., Lavenir, I., Schweighauser, G., Frank, S., Goedert, M., Tolnay, M., 2014, Peripheral administration of Tau aggregates triggers intracerebral Tauopathy in transgenic mice, Acta Neuropathol, 127;299–301.

75. ClinicalTrials.gov [Internet]. Bethesda (MD): National Library of Medicine (US). 2008 Feb 20 - . Identifier NCT00515333, TRx0014 in Patients With Mild or Moderate Alzheimer's Disease; Available at: <https://clinicaltrials.gov/ct2/show/NCT00515333>, [Accessed 5th March 2019].

76. ClinicalTrials.gov, 2019, Bethesda (MD): National Library of Medicine (US), Available at: <https://pubchem.ncbi.nlm.nih.gov/>, [Accessed 11th February 2019].

77. Cody, W., He, J., Reily, M., Haleen, S., Walker, D., Reyner, E, Stewart, B., Doherty, A., 1997, Design of a Potent Combined Pseudopeptide Endothelin-A/Endothelin-B Receptor Antagonist, Ac-dBhg16-Leu-Asp-Ile-[NMe]Ile-Trp21(PD 156252): Examination of Its Pharmacokinetic and Spectral Properties. Journal of Medicinal Chemistry, 40(14), 2228–2240.

78. Cohen, S., Linse, S., Luheshi, M., Hellstrand, E., White, D., Rajah, L., Otzen, D., Vendruscolo, M., Dobson, C., Knowles, T., 2013, Proliferation of amyloid-β42 aggregates occurs through a secondary nucleation mechanism Proc. Natl. Acad. Sci. U. S. A., 110, 9758– 9763.

79. Conchillo-Solé, O., de Groot, N., Avilés, F., Vendrell, J., Daura, X., Ventura, S., 2007, AGGRESCAN: a server for the prediction and evaluation of "hot spots" of aggregation in polypeptides, BMC Bioinformatics., 27;8:65.

80. Couchie D, Mavilia C, Georgieff IS, Liem RK, Shelanski ML, Nunez J., 1992, Primary structure of high molecular weight Tau present in the peripheral nervous system. Proc Natl Acad Sci U S A., 89:4378–81. doi: 10.1073/pnas.89.10.4378.

81. Cowan, C. and Mudher, A., 2013, Are tau aggregates toxic or protective in tauopathies? Front Neurol., 13;4:114.

82. Cowan, C., Quraishe, S., Hands, S., Sealey, M., Mahajan, S., Allan, D., Mudher, A., 2015, Rescue from tau-induced neuronal dysfunction produces insoluble tau oligomers, Sci Rep 5, 17191.

83. Cox, M.; Nelson D. (2004). Lehninger, Principles of Biochemistry. Freeman. p. 254.

84. Cramer, D. and Howitt, D., 2004, The Sage dictionary of statistics: a practical resource for students in the social sciences. Thousand Oaks: Sage.

85. Crespo, R., Koudstaal, W., Apetri, A. 2018, *In Vitro* Assay for Studying the Aggregation of Tau Protein and Drug Screening. *J. Vis. Exp.* (141), e58570, doi:10.3791/58570.

86. Crowe, A., James, M., Lee, V., Smith, A. 3rd, Trojanowski, J., Ballatore, C., Brunden, K., 2013, Aminothienopyridazines and methylene blue affect Tau fibrillization via cysteine oxidation. J Biol Chem., 288:11024–37.

87. Crowther, R. and Wischik, C., 1985, Image reconstruction of the Alzheimer paired helical filament, EMBO J., 4(13B);3661–3665.

88. Czerkovicz, J., Chen, W., Wang, Q., Shen, C., Wager, C., Stone, I., et al. (2018). Pan-Tau Antibody Biib076 exhibits promising safety and biomarker profile in cynomolgus monkey toxicity study. Alzheimers Dementia 13:1271.

89. Daebel, V., Chinnathambi, S., Biernat, J., Schwalbe, M., Habenstein, B., Loquet, A., Akoury, E., Tepper, K., Müller, H., Baldus, M., Griesinger, C., Zweckstetter, M., Mandelkow, E., Vijayan, V., 2012, Lange, A. B-Sheet Core of Tau Paired Helical Filaments Revealed by Solid-state NMR. J. Am. Chem. Soc., 134, 13982–13989.

90. De Calignon, A., Polydoro, M., Suárez-Calvet, M., William, C., Adamowicz, D., Kopeikina, K., Pitstick, R., Sahara, N., Ashe, K., Carlson, G., Spires-Jones, T., Hyman, B., 2012, Propagation of Tau Pathology in a Model of Early Alzheimer's Disease, Neuron, 73(4);685-697.

91. de Groot, N., Aviles, F., Vendrell, J., Ventura, S., 2006, Mutagenesis of the central hydrophobic cluster in Abeta42 Alzheimer's peptide. Side-chain properties correlate with aggregation propensities, FEBS J, 273;658-668.

92. de la Cruz, M., Hattne, J., Shi, D., Seidler, P., Rodriguez, J., Reyes, F., Sawaya, M., Cascio, D., Weiss, S., Kim, S., Hinck, C., Hinck, A., Calero, G., Eisenberg, D., Gonen, T., 2017. Atomic-resolution structures from fragmented protein crystals with the cryoEM method MicroED, Nat Methods., 14(4):399-402.

93. Desikan, R., McEvoy, L., Thompson, W., Holland, D., Brewer, J., Aisen, P., Sperling, R. and Dale, A., 2012, Amyloid-β associated clinical decline occurs only in the presence of elevated p-tau, Arch Neurol., 69(6): 709–713.

94. Despres, C., Byrne, C., Qi, H., Cantrelle, F., Huvent, I., Chambraud, B., Baulieu, E., Jacquot, E., Landrieu, I., Lippens, G., Smet-Nocca, C., 2017, Identification of the Tau phosphorylation pattern that drives its aggregation, NAS August 22, 2017 114 (34) 9080-9085.

95. Di Noto, L., DeTure, M., Purich, D., 1999, Disulfide-cross-linked Tau and MAP2 homodimers readily promote microtubule assembly. Mol. Cell Biol. Res. Commun. 2, 71–76.

96. Divinski, I., Holtser-Cochav, M., Vulih-Schultzman, I., Steingart, R., Gozes, I., 2006, Peptide neuroprotection through specific interaction with brain tubulin. J Neurochem., 98(3).

97. Dong, X., 2018, Current Strategies for Brain Drug Delivery, Theranostics. 2018; 8(6): 1481–1493.

98. Drechsel, D., Hyman, A., Cobb, M., Kirschner, M., 2017, Modulation of the dynamic instability of tubulin assembly by the microtubule-associated protein Tau, Molecular Biology of the Cell, 3(10); 1057-1194.

99. Dubois, B., Feldman, H., Jacova, C., Hampel, H., Molinuevo, J., Blennow, K., DeKosky, S., Gauthier, S., Selkoe, D., Bateman, R., Cappa, S., Crutch, S., Engelborghs, S., Frisoni, G., Fox, N., Galasko, D., Habert, M., Jicha, G., Nordberg, A., Pasquier, F., Rabinovici G., Robert, P., Rowe, C., Salloway, S., Sarazin, M., Epelbaum, S., de Souza, L., Vellas, B., Visser, P., Schneider, L., Stern, Y., Scheltens, P., Cummings, J., 2014, Advancing research diagnostic criteria for Alzheimer's disease: the IWG-2 criteria Lancet Neurol, 13;614-629.

100. Dujardin, S., Bégard, S., Caillierez, R., Lachaud, C., Delattre, L., Carrier, S., Loyens, A., Galas, M., Bousset, L., Melki, R., Aurégan, G., Hantraye, P., Brouillet, E., Buée, L., Colin, M., 2014, Ectosomes: a new mechanism for non-exosomal secretion of tau protein. PLoS One 9(6): e100760.

101.   Eckermann, K., Mocanu, M., Khlistunova, I., Biernat, J., Nissen, A., Hofmann, A., Schönig, K., Bujard, H., Haemisch, A., Mandelkow, E., Zhou, L., Rune, G., Mandelkow, E.M., 2007, The beta-propensity of Tau determines aggregation and synaptic loss in inducible mouse models of tauopathy, J Biol Chem., 26;282(43):31755-65.

102.   Eisenberg, D. and Sawaya, M., 2017, Structural Studies of Amyloid Proteins at the Molecular Level, Annu. Rev. Biochem. 2017.86:69-95

103.   Elam, J., Taylor, A., Strange, R., et al., 2003, Amyloid-like filaments and water-filled nanotubes formed by SOD1 mutant proteins linked to familial ALS, Nat. Struct. Biol, 10;461 – 467.

104.   Elbaum-Garfinkle, S., Ramlall, T., and Rhoades, E., 2010, The role of the lipid bilayer in Tau aggregation. Biophys. J. 98, 2722–2730.

105.   Elvin, J., Couston, R., van der Walle C., 2013, Therapeutic antibodies: Market considerations, disease targets and bioprocessing, Int J Pharm, 440;83-98.

106.   European Bioinformatics Institute, 2019, CHEBI:17752 - N6-acetyl-L-lysine, Available at: <https://www.ebi.ac.uk/chebi/chebiOntology.do?chebiId=CHEBI:17752> [Accessed 9th March 2019].

107.   Feinstein, H., Benbow, S., LaPointe, N., Patel, N., Ramachandran, S., Do, T., Gaylord, M., Huskey, N., Dressler, N., Korff, M., Quon, B., Cantrell, K., Bowers, M., Lal, R., Feinstein, S., 2016, Oligomerization of the Microtubule Associated Protein Tau is Mediated by its N-Terminal Sequences: Implications for Normal and Pathological Tau Action, J Neurochem., 137(6): 939–954.

108.   Fernandez-Montesinos, R., Torres, M., Baglietto-Vargas, D., Gutierrez, A., Gozes, I., Vitorica, J., Pozo, D., 2010, Activity-dependent neuroprotective protein (ADNP) expression in the amyloid precursor protein/presenilin 1 mouse model of Alzheimer's disease. J Mol Neurosci., 41:114–120.

109.   Fernandez-Recio, J., Totrov, M., Skorodumov, C., Abagyan, R., 2005, Optimal docking area: a new method for predicting protein-protein interaction sites, Proteins, 58(1):134-43.

110.   Ferrari, L. and Rüdiger, S., 2019, Recombinant production and purification of the human protein Tau, BioRxiv Preprint, 1-

111.   Ferrige, A., Seddon, M., Jarvis, S., 1991, Maximum Entropy Deconvolution in Elec-trospray Mass Spectrometry, Rapid Communications in Mass Spectrometry, 5(8);374–377.

112.   Fichou, Y., Vigers, M., Goring, A., Eschmann, N., Han, S., 2018, Heparin-induced Tau filaments are structurally heterogeneous and differ from Alzheimer's disease filaments, Chem Commun (Camb), 54(36):4573-4576.

113.   Finder, V., Vodopivec, I., Nitsch, R., Glockshuber, R., 2010, The recombinant amyloid-beta peptide Abeta1-42 aggregates faster and is more neurotoxic than synthetic Abeta1-42, J Mol Biol., 396(1):9-18.

114.   Fitzpatrick, A., Falcon, B., He, S., Murzin, A., Murshudov, G., Garringer, H., Crowther, A., Ghetti, B., Goedert, M., Scheres, S., 2017, Cryo-EM structures of tau filaments from Alzheimer's disease, Nature, 547(7662);185-190.

115.   Fotakis, G. and Timbrell, J., 2006, In vitro cytotoxicity assays: Comparison of LDH, neutral red, MTT and protein assay in hepatoma cell lines followingexposure to cadmium chloride, Toxicology Letters 160, 171–177.

116.   Frame, M., 2001, SH3 Domain, Encyclopedia of Genetics, Academic Press, Page 1825.

117.   Friedhoff, P., Schneider, A., Mandelkow, E.M., Mandelkow, E., 1998, Rapid assembly of Alzheimer-like paired helical filaments from microtubule-associated protein Tau monitored by fluorescence in solution, Biochemistry. 1998 Jul 14;37(28):10223-30.

118.   Frost, B., Jacks, R., Diamond, M., 2009, Propagation of Tau misfolding from the outside to the inside of a cell. J Biol Chem., 284(19):12845–52.

119.   Funk, K., Thomas, S, Schafer, K., Cooper, G., Liao, Z., Clark, D., Yang, A., Kuret, J., 2014, Lysine methylation is an endogenous post-translational modification of Tau protein in human brain and a modulator of aggregation propensity. Biochem. J. 462, 77– 88.

120.   Futaki, S., 2005, Membrane-permeable arginine-rich peptides and the translocation mechanisms, Adv. Drug Delivery Rev., 57(4):547-58.

121.   Futaki, S., 2006, Oligoarginine vectors for intracellular delivery: Design and cellular-uptake mechanisms. Biopolymers, 84(3), 241–249.

122.   Fyuki, K., and Hasegawa, M., 2018, Reconsideration of Amyloid Hypothesis and Tau Hypothesis in Alzheimer's Disease, Frontiers in Neuroscience, 12(25);1-11.

123.   Gamblin, C., King, M., Kuret, J., Berry, R., Binder, L., 2000, Oxidative Regulation of Fatty Acid-Induced Tau Polymerization, Biochemistry,39(46);14203-14210.

124.   Gamblin, T., Chen, F., Zambrano, A., Abraha, A., Lagalwar, S., Guil-lozet, A., et al., 2003, Caspase cleavage of tau: linking amyloid and neurofibrillary tangle in Alzheimer'sdisease., Proc Natl Acad Sci U S A, 100:10032–7.

125.   Ganguly, P., Do, T., Larini, L., LaPointe, N., Sercel, A,, Shade, M., Feinstein, S., Bowers, M., Shea, J., 2015, Tau assembly: the dominant role of PHF6 (VQIVYK) in microtubule binding region repeat R3, J Phys Chem B.,119(13):4582-93.

126.   Gasteiger E., Hoogland C., Gattiker A., Duvaud S., Wilkins M.R., Appel R.D., Bairoch A.; Protein Identification and Analysis Tools on the ExPASy Server; (In) John M. Walker (ed): The Proteomics Protocols Handbook, Humana Press (2005).

127.   Gauthier, S., Feldman, H., Schneider, L., Wilcock, G., Frisoni, G., Hardlund, J., Moebius, H., Bentham, P., Kook, K., Wischik, D.J., Schelter, B., Davis, C., Staff, R., Bracoud, L., Shamsi, K., Storey, J., Harrington, C., Wischik, C.M., 2016, Efficacy and safety of tau-aggregation inhibitor therapy in

patients with mild or moderate Alzheimer's disease: a randomised, controlled, double-blind, parallel-arm, phase 3 trial. Lancet., 10;388(10062):2873-2884. Epub 2016 Nov 16.

128.   Georgieva, J., Hoekstra, D., Zuhorn, I., 2014, Smuggling Drugs into the Brain: An Overview of Ligands Targeting Transcytosis for Drug Delivery across the Blood–Brain Barrier, Pharamaceutics, 6(4);557-583.

129.   Giacobini, E., Gold, G., 2013, Alzheimer disease therapy—moving from amyloid-β to Tau, Nature Reviews Neurology, (12):677-86.

130.   Giannakopoulos, P., Herrmann, F., Bussière, T., Bouras, C., Kövari, E., Perl, D., Morrison, J., Gold, G., Hof, P., 2003, Tangle and neuron numbers, but not amyloid load, predict cognitive status in Alzheimer's disease, Neurology, 60(9);1495-1500.

131.   Gill, S. and von Hippel, P., 1989, Calculation of protein extinction coefficients from amino acid sequence data, Anal Biochem, 1;182(2):319-26.

132.   Girych, M., Gorbenko, G., Trusova, V., dachi, E., Mizuguchi, C., Nagao, K., Kawashima, H., Akaji, K., Lund-Katz, S., Phillips, M., Saito, H.., 2014, Interaction of thioflavin T with amyloid fibrils of apolipoprotein A-I N-terminal fragment: resonance energy transfer study, J Struct Biol., 185(1):116-24.

133.   Gistelinck, M., Lambert, J., Callaerts, P., Dermaut, B., Dourlen, P., 2012, Drosophila Models of Tauopathies: What Have We Learned? International Journal of Alzheimer's Disease, 2012, Article ID 970980; 14.

134.   Giza, C., Greco, T. and Prins, M., 2018, Chapter 6 - Concussion: pathophysiology and clinical translation, Handbook of Clinical Neurology, 158;51-61.

135.   Goedert, M. and Jakes, R., 1990, Expression of separate isoforms of human tau protein: correlation with the tau pattern in brain and effects on tubulin polymerization, The EMBO Journal, 9(13);4225-4230.

136. Goedert, M. and Spillantini, M., 2017, Propagation of Tau aggregates, Molecular Brain, 10:18.

137. Goedert, M., Jakes, R., 2005, Mutations causing neurodegenerative Tauopathies. Biochim. Biophys. Acta 1739;240–250.

138. Goedert, M., Jakes, R., Spillantini, M., Hasegawa, M., Smith, M., Crowther, R., 1996, Assembly of microtubuleassociated protein Tau into Alzheimer-like filaments induced by sulphated glycosaminoglycans, Nature, 383;550-553.

139. Goedert, M., Spillantini, M., Crowther, R., 1992, Cloning of a big tau microtubule-associated protein characteristic of the peripheral nervous system, Proc Natl Acad Sci U S A., 1;89(5):1983-7.

140. Gold, G., Kövari, E., Corte, G., Herrmann, F., Canuto, A., Bussière, T., Hof, P., Bouras, C., Giannakopoulos, P., 2001, Clinical validity of Aβ-protein deposition staging in brain aging and Alzheimer disease, Journal of Neuropathology and Experimental Neurology, 60(10);946-952.

141. Goldsbury, C., Goldie, K., Pellaud, J., Seelig, J., Frey, P., Müller, S., Kistler, J., Cooper, G., Aebi, U., 2000, Amyloid Fibril Formation from Full-Length and Fragments of Amylin. Journal of Structural Biology. 130(2-3):352-362.

142. Gong, C. and Iqbal, K., 2008, Hyperphosphorylation of Microtubule-Associated Protein Tau: A Promising Therapeutic Target for Alzheimer Disease, Curr Med Chem., 15(23): 2321–2328.

143. Goodman, M., 2009, Market watch: Sales of biologics to show robust growth through to 2013. Nat Rev Drug Discov., 8;837.

144. Goodman, M., Market watch: Sales of biologics to show robustgrowth through to 2013. Nat Rev Drug Discov., 8:837.

145.   Goyal, D., Shuaib, S., Mann, S., et al., 2017, Rationally designed peptides and peptidomimetics as inhibitors of amyloid-beta (ABETA) aggregation: potential therapeutics of alzheimer's disease. ACS Comb Sci., 19:55–80

146.   Gozes, I., Iram, T., Maryanovsky, E., Arviv, C., Rozenberg, L., Schirer, Y., Giladi, E., Furman-Assaf, S., 2014, Novel tubulin and Tau neuroprotective fragments sharing structural similarities with the drug candidate NAP (Davuentide), J Alzheimers Dis., 40 Suppl 1: S23-36.

147.   Gozes, I., Morimoto, B., Tiong, J., Fox, A., Sutherland, K., Dangoor, D., et al., 2005, NAP: research and development of a peptide derived from activity-dependent neuroprotective protein (ADNP). CNS Drug Rev., 11(4):353–68.

148.   Green, A., Hughes, W., 1995, Protein solubility on the basis of solubility in aqueous solutions of salts and organic solvents. Methods Enzymol, 1:67–90.

149.   Gregori, M., Taylor, M., Salvati, E., Re, F., Mancini, S., Balducci, C., Forloni, G., Zambelli, V., Sesana, S., Michael, M., Michail, C., Tinker-Mill, C., Kolosov, O., Sherer, M., Harris, S., Fullwood, N., Masserini, M., Allsop, D., 2017, Retro-inverso peptide inhibitor nanoparticles as potent inhibitors of aggregation of the Alzheimer's Aβ peptide, Nanomedicine: Nanotechnology, Biology and Medicine, 13(2);723-732.

150.   Greig, N., Reale, M., Tata, A., 2013, Recent Pat. CNS Drug Discovery, 8;123.

151.   Grinberg, L., Wang, X., Wang, C., Sohn, P., Theofilas, P., Sidhu, M., Arevalo, J., Heinsen, H., Huang, E., Rosen, H., Miller, B., Gan, L., Seeley, W., 2013, Argyrophilic grain disease differs from other Tauopathies by lacking Tau acetylation, Acta Neuropathol., 125(4);581–593.

152.   Groenning, M., Olsen, L., van de Weert, M., Flink, J., Frokjaer, S., Jørgensen, F., 2007, Study on the binding of Thioflavin T to beta-sheet-rich and non-beta-sheet cavities, J Struct Biol., 158(3):358-69.

153.	Gu, J., Congdon, E., Sigurdsson, E.., 2013, Two novel Tau antibodies targeting the 396/404 region are primarily taken up by neurons and reduce Tau protein pathology. J Biol Chem., 288:33081–95

154.	Guo, T., Noble, W., Hanger, D., 2017, Roles of tau protein in health and disease, Acta Neuropathologica 133(5);665–704.

155.	Gustke, N., Trinczek, B., Biernat, J., Mandelkow, E. M., Mandelkow, E., 1994, Domains of Tau-protein and interactions with microtubules. Biochemistry 33, 9511–9522.

156.	Halgren, T., 1996, J Comput Chem 17(5–6):490.

157.	Hardy, J., Allsop, D., 1991, Amyloid deposition as the central event in the aetiology of Alzheimer's disease, Trends Pharmacol Sci.,12(10):383-8.

158.	Hasegawa, M., Smith, M., Goedert, M., 1998, Tau proteins with FTDP-17 mutations have a reduced ability to promote microtubule assembly, FEBS Letters, 437;1873-3468

159.	Hattori, M., Sugino, E., Minoura, K., In, Y., Sumida, M., Taniguchi, T., Tomoo, K., Ishida, T., 2008, Different inhibitory response of cyanidin and methylene blue for filament formation of Tau microtubule-binding domain, 374(1);158-163

160.	Hauser, A. and Windshügel, B., 2016, LEADS-PEP: A Benchmark Data Set for Assessment of PeptideDocking Performance, Chem. Inf. Model, 56, 188–200.

161.	He, X., Lin, M., Guo, J., Qu, Z., Xu, F., 2016, Experimental and simulation studies of polyarginines across the membrane of giant unilamellar vesicles, RSC Advances, 6(36), 30454–30459.

162.	Heidary, G. and Fortini, M., 2001, Identification and characterization of the Drosophila tau homolog. Mech. Dev. 2001; 108:171–178.

163.	Hickman, D., López-Deber, M., Ndao, D., Silva, A., Nand, D., Pihlgren, M., Giriens, V., Madani, R., St-Pierre, A., Karastaneva, H., Nagel-Steger, L., Willbold, D., Riesner, D., Nicolau, C.,

Baldus, M., Pfeifer, A., Muhs, A., 2011, Sequence-independent control of peptide conformation in liposomal vaccines for targeting protein misfolding diseases. J Biol Chem., 22;286(16):13966-76

164.   Holmes, B., DeVos, S., Kfoury, N., Li, M., Jacks, R., Yanamandra, K., Ouidja, M., Brodsky, F., Marasa, J., Bagchi, D., Kotzbauer, P., Miller, T., Papy-Garcia, D., Diamond, M., 2013, Heparan sulfate proteoglycans mediate internalization and propagation of specific proteopathic seeds, Proc. Natl. Acad. Sci. USA, 110;E3138-E3147.

165.   Hoogenboom, H., 2005, Selecting and screening recombinantantibody libraries. Nat Biotechnol., 23:1105–16.

166.   Hu W, Zhang X, Tung YC, Xie S, Liu F, Iqbal K (2016) Hyperphosphorylation determines both the spread and the morphology of tau pathology. Alzheimers Dement 12(10):1066–1077.

167.   Ibáñez-Salazar, A., Bañuelos-Hernández, B., Rodríguez-Leyva, I., Chi-Ahumada, E., Monreal-Escalante, E., Jiménez-Capdeville, M., Rosales-Mendoza, S., 2017, Oxidative Stress Modifies the Levels and Phosphorylation State of Tau Protein in Human Fibroblasts, Front Neurosci. 2017; 11: 495.

168.   International Society for Amyloidosis, 2018, Amyloidosis the Disease [online] [Accessed 23rd April 2018]. Available from: https://www.isaamyloidosis.org/

169.   Ivashko-Pachima, Y., Sayas, C., Malishkevich, A., Gozes, I., 2017, ADNP/NAP dramatically increase microtubule end-binding protein-Tau interaction: a novel avenue for protection against Tauopathy, Mol Psychiatry., 22(9):1335-1344.

170.   Jack, C., Albert, M., Knopman, D., McKhann, G., Sperling, R., Carrillo, M., Thies, B., Phelps, C., 2011, Introduction to the recommendations from the National Institute on Aging–Alzheimer's Association workgroups on diagnostic guidelines for Alzheimer's disease. Alzheimers Dement 2011;7(3):257–62

171.   Jack, C., Wiste, H., Lesnick, T., Weigand, S., Knopman, D., Vemuri, P., Pankratz, V., Senjem, M., Gunter, J., Mielke, M., Lowe, V., Boeve, B., Petersen, R., 2013, Brain β-amyloid load approaches a plateau, Neurology, 80(10);890-896.

172.   Jackson, G., Wiedau-Pazos, M., Sang. T., Wagle, N., Brown, C., Massachi. S., et al., 2002, Human wild-type tau interacts with winglesspathway components and pro-duces neurofibrillary pathologyinDrosophila.Neuron(2002)34:509–19.doi:10.1016/S0896-6273(02)00706-7.

173.   Jeganathan, S., Hascher, A., Chinnathambi, S., Biernat, J., Mandelkow, E.M., Mandelkow, E., 2008, Proline-directed Pseudo-phosphorylation at AT8 and PHF1 Epitopes Induces a Compaction of the Paperclip Folding of Tau and Generates a Pathological (MC-1) Conformation, The Journal of Biological Chemistry, 283;32066-32076.

174.   Jeganathan, S., Von Bergen, M., Mandelkow, E.M., Mandelkow, E., 2008, The Natively Unfolded Character of Tau and Its Aggregation to Alzheimer-likePaired Helical Filaments, Biochemistry, 47;10526–10539.

175.   Jeol, 2019, Scanning Electron Microscopes (SEM), Available at: <https://www.jeol.co.jp/en/science/sem.html>, [Accessed 18th January 2019].

176.   Jho, Y., Zhulina, E., Kim, M., Pincus, P., 2010, Monte carlo simulations of Tau proteins: Effect of phosphorylation. Biophys. J., 99, 2387–2397.

177.   Jicha, G., Lane, E., Vincent, I., Otvos, L., Hoffmann, R., Davies, P., 1997, A conformation- and phosphorylation-dependent antibody recognizing the paired helical filaments of Alzheimer's disease, J Neurochem., 69(5):2087-95.

178.   Jimenez, J., Guijarro, E., Orlova, J., Zurdo, C., Dobson, M., Sunde, Saibil, H., 1999, Cryo-electron microscopy structure of an SH3amyloid fibril and model of the molecular packing., EMBO J.18:815–821.

179.   Johnson, G., Stoothoff, W., 2004, Tau phosphorylation in neuronal cell function and dysfunction, Journal of Cell Science 2004 117: 5721-5729.

180.   Jones, D., (1999, Protein secondary structure prediction based on position-specific, scoring matrices. J. Mol. Biol., 292, 195–202.

181.   Kabsch, W. and Sander, C., 1983, Dictionary of protein secondary structure: pattern recognition of hydrogen-bonded and geometrical features. Biopolymers, 22, 2577–2637.

182.   Kadavath, H., Hofele, R., Biernat, J., Kumar, S., Tepper, K., Urlaub, H., Mandelkow, E., Zweckstettera, M., 2015, Tau stabilizes microtubules by binding at the interface between tubulin heterodimers, Proc Natl Acad Sci U S A., 112(24): 7501–7506.

183.   Kaffy, J., Brinet, D., Soulier, J., Correia, I., Tonali, N., Fera, K., Iacone, Y., Hoffmann, A., Khemtémourian, L., Crousse, B., Taylor, M., Allsop, D., Taverna, M., Lequin, O., Ongeri, S., 2016, Designed Glycopeptidomimetics Disrupt Protein−Protein Interactions Mediating Amyloid β-Peptide Aggregation and Restore Neuroblastoma Cell Viability, The Journal of Medical Chemistry, DOI: 10.1021/acs.jmedchem.5b01629.

184.   Kamat, P., Kalani, A., Rai, S., Swarnkar, S., Tota, S., Nath, C., Tyagi, N., 2016, Mechanism of Oxidative Stress and Synapse Dysfunction in the Pathogenesis of Alzheimer's Disease: Understanding the Therapeutics Strategies, Mol Neurobiol., 53(1): 648–661.

185.   Kampers, T., Friedhoff, P., Biernat, J., Mandelkow, E. M., and Mandelkow, E., 1996, RNA stimulates aggregation of microtubuleassociated protein Tau into Alzheimer-like paired helical filaments. FEBS Lett. 399, 344–349.

186.   Kar, S., Fan, J., Smith, M., Goedert, M., Amos, L., 2003, Repeat motifs of Tau bind to the insides of microtubules in the absence of taxol, The EMBO Journal, 22(1);70-77.

187.   Khalil, I., Futaki, S., Niwa, M., Baba, Y., Kaji, N., Kamiya, H., Harashima, H., 2004, Mechanism of improved gene transfer by the N-terminal stearylation of octaarginine: enhanced cellular association by hydrophobic core formation, Gene Ther., 11(7):636-44.

188.   Kim, K. and Seong, B., 2001, Peptide Amidation: Production of Peptide Hormones in vivo and in vitro. Biotechnol. Bioprocess Eng., 6(4);244-251.

189.   Kings College London, 2019, Tau phosphorylation sites, Available at: <http://cnr.iop.kcl.ac.uk/hangerlab/tautable>, [Accessed 28th October 2019].

190.   Kissova, I., Plamondon, L., Brisson, L., Priault, M., Renouf, V., Schaeffer, J., Camougrand, N., Manon, S, 2006, Evaluation of the roles of apoptosis, autophagy, and mitophagy in the loss of plating efficiency induced by Bax expression in yeast. J Biol Chem, 281:36187–36197.

191.   Kokkoni, N., Stott, K., Amijee, H., Mason, J., Doig, A., 2006, N-Methylated Peptide Inhibitors of,-Amyloid Aggregation and Toxicity.Optimization of the Inhibitor Structure, Biochemistry,45;9906-9918.

192.   Kolarova, M., García-Sierra, F., Bartos, A., Ricny, J., Ripova, D., 2012, Structure and Pathology of Tau Protein in Alzheimer Disease, International Journal of Alzheimer's Disease, Volume 2012, Article ID 731526, 13 pages.

193.   Konno, T., Oiki, S., Hasegawa, K., and Naiki, H., 2004, Anionic contribution for fibrous maturation of protofibrillar assemblies of the human Tau repeat domain in a fluoroalcohol solution. Biochemistry 43, 13613–13620.

194.   Kontsekova, E., Zilka, N., Kovacech, B., Novak, P., Novak, M., 2014, First-in-man Tau vaccine targeting structural determinants essential for pathological Tau-Tau interaction reduces Tau oligomerisation and neurofibrillary degeneration in an Alzheimer's disease model. Alzheimers Res Ther., 6(4):44.

195.   Krebs, M., Bromley, E., Donald, A., 2005, The binding of thioflavin-T to amyloid fibrils: localisation and implications, J Struct Biol., 149(1):30-7.

196.   Krestova, M., Hromadkova, L., Bilkova, Z., Bartos, A., Ricny, J., 2017, Characterization of isolated tau-reactive antibodies from the IVIG product, plasma of patients with Alzheimer's disease and cognitively normal, individuals. J. Neuroimmunol., 313, 16–24.

197.   KrishnaKumar, V., and Gupta, S. (2017). Simplified method to obtain enhanced expression of tau protein from E. coli and one-step purification by direct boiling. Preparative Biochemistry and Biotechnology, 47(5);530–538.

198.   Kuca, K., Soukup, O., Maresova, P., Korabecny, J., Nepovimova, E., Klimova, B., Honegr, J., Ramalhob, T., França, T., 2016, Current Approaches Against Alzheimer's Disease in Clinical Trials, J. Braz. Chem. Soc., 27(4);641-649.

199.   Kufareva, I., Rueda, M., Katritch, V., Stevens, R., Abagyan, R., GPCR Dock Participants, 2011, Status of GPCR modeling and docking as reflected by community-wide GPCR Dock 2010 assessment. Structure, 10;19(8):1108-26.

200.   Kumar, S., Tepper, K., Kaniyappan, S., Biernat, J., Wegmann, S., Mandelkow, E.M., Müller, D., Mandelkow, E., 2014, Stages and Conformations of the Tau Repeat Domain during Aggregation and Its Effect on Neuronal Toxicity, J Biol Chem, 289(29): 20318–20332.

201.   Kuo, J., Jan, M., Lin, Y., Lin, C., 2009, Interactions between octaarginine and U-937 human macrophages: Global gene expression profiling, superoxide anion content, and cytokine productionm Journal of Controlled Release, 139,197–204.

202.   Kuret J., Chirita C. N., Congdon E. E., Kannanayakal T., Li G., Necula M., Yin H., Zhong Q., 2005, Pathways of Tau fibrillization. Biochim. Biophys. Acta 1739, 167–178.

203.   Kuret, J., Congdon, E. E., Li, G., Yin, H., Yu, X., and Zhong, Q., 2005, Evaluating triggers and enhancers of Tau fibrillization. Microsc. Res. Tech. 67, 141–155.

204.   LaFerla, F., Green, K., 2012, Animal models of Alzheimer disease, Cold Spring Harbor perspectives in medicine, 2(11).

205.   Lam, P., Abagyan, R., Totrov, M., 2019, Hybrid receptor structure/ligand-based docking and activity prediction in ICM: development and evaluation in D3R Grand Challenge 3, Journal of Computer-Aided Molecular Design, 33(1);35–46.

206.   Langel, U., 2019, CPP, Cell-Penetrating Peptides, Springer, Singapore, p57.

207.   Lasagna-Reeves, C., Castillo-Carranza, D., Guerrero-Muoz, M., Jackson, G., Kayed, R., 2010, Preparation and characterization of neurotoxic Tau oligomers, Biochemistry, 49(47):10039-41.

208.   Lasagna-Reeves, C., Castillo-Carranza, D., Sengupta, U., Guerrero-Munoz, M., Kiritoshi, T., Neugebauer, V., Jackson, G., Kayed, R., 2012, Alzheimer brain-derived tau oligomers propagate pathology from endogenous tau. Sci Rep., 2:700.

209.   Leader, B., Baca, Q., Golan, D., 2008, Protein therapeutics: A summary and pharmacological classification. Nat Rev Drug Discov., 7;21–39.

210.   Lee, C., Perchiacca, J., Tessier, P., 2013, Toward aggregation-resistant antibodies by design. Trends Biotechnol., 31:612–20.

211.   Lee, G., and Leugers, C., 2012, Tau and Tauopathies, Prog Mol Biol Transl Sci., 107: 263–293.

212.   Lee, G., Neve, R., Kosik, K., 1989, The Microtubule Binding Domain of Tau Protein, Neuron, 2;1615–1624.

213.   Leroy, K., Ando, K., Laporte, V., Dedecker, R., Suain, V., Authelet, M., Heraud, C., Pierrot, N., Yilmaz, Z., Octave, J., Brion, J., 2012, Lack of tau proteins rescues neuronal cell death and decreases amyloidogenic processing of APP in APP/PS1 mice. Am J Pathol., 181:1928–1940.

214.   LeVine, H., 1999, Quantification of beta-sheet amyloid fibril structures with thioflavin T, Methods Enzymol., 309:274-84.

215.   Li, H., Rahimi, F., Sinha, S., Maiti, P. and Bitan, G., 2009, Amyloids and Protein Aggregation – Analytical Methods. Encyclopedia of Analytical Chemistry, 1–32.

216.   Li, L., Sengupta, A., Haque, N., Grundke-Iqbal, I., Iqbal, K., 2004, Memantine inhibits and reverses the Alzheimer type abnormal hyperphosphorylation of Tau and associated neurodegeneration. FEBS Lett., 21; 566(1–3):261–9.

217.   Li, S., Goto, N., Williams, K., Deber, C., 1996, Alpha-helical, but not beta-sheet, propensity of proline is determined by peptide environment, Proc Natl Acad Sci U S A, 25;93(13):6676-81.

218.   Li, W., Li, S., Zheng, H., Zhang, S., Xue, L., 2012, A broad expression profile of the GMR-GAL4 driver in Drosophila melanogaster, Genet Mol Res., 6;11(3):1997-2002.

219.   Li, X., Song, D., Leng, S., 2015, Link between type 2 diabetes and Alzheimer's disease: from epidemiology to mechanism and treatment, Clinical Interventions in Aging, 10;549–560

220.   Lim, S., Haque, M., Kim, D., Kim, D., Kim, Y., 2014, Cell-based Models To Investigate Tau Aggregation, Computational and Structural Biotechnology Journal, 12;7–13.

221.   Lipton, S., 2007, Pathologically activated therapeutics for neuroprotection, Nature Reviews Neuroscience, 8;803-808.

222.   Liu, Y., Peterson, D., Kimura, H., Schubert, D., 1997, Mechanism of Cellular 3-(4,5-Dimethylthiazol-2-yl)-2,5-Diphenyltetrazolium Bromide (MTT) Reduction, Journal of Neurochemistry, 69(2);581-593.

223.   Lovestone, S., Boada, M., Dubois, B., Hüll, M., Rinne, J., Huppertz, H., Calero, M., Andrés, M., Gómez-Carrillo, B., León, T., del Ser, T, ARGO investigators, 2015, A phase II trial of tideglusib in Alzheimer's disease, J Alzheimers Dis. 45(1):75-88.

224. Lu, W., 2012, Adsorptive-mediated brain delivery systems, Curr Pharm Biotechnol., 13(12):2340-8.

225. Madani, F., Lindberg, S., Langel, U., Futaki, S., Gräslund, A., 2011, Mechanisms of Cellular Uptake of Cell-Penetrating Peptides, J Biophys, 414729.

226. Maeda, S., Sahara, N., Saito, Y., Murayama, M., Yoshiike, Y., Kim, H., Miyasaka, T., Murayama, S., Ikai, A., Takashima, A., 2007, Granular Tau oligomers as intermediates of Tau filaments. Biochemistry, 46;3856–3861.

227. Maeda, S., Sato, Y., Takashima, A., 2018, Frontotemporal dementia with Parkinsonism linked to chromosome-17 mutations enhance tau oligomer formation, Neurobiology of Aging, 69;26-32.

228. Maezawa, I., Hong, H., Liu, R., Wu, C., Cheng, R., Kung, M., Kung, H., Lam, K., Oddo, S., Laferla, F., Jin, L., 2008, Congo red and thioflavin-T analogs detect Aβ oligomers, J Neurochem. 2008 Jan; 104(2):457-68.

229. Magen, I., Ostritsky, R., Richter, F., Zhu, C., Fleming, S., Lemesre, V., Stewart, A., Morimoto, B., Gozes, .I, Chesselet, M.. 2014, Intranasal NAP (davunetide) decreases Tau hyperphosphorylation and moderately improves behavioral deficits in mice overexpressing α-synuclein. Pharmacol Res Perspect., 2: e00065.

230. Malinchik, S., Inouye, H., Szumowski, K., Kirschner, D., 1998. Structural analysis of Alzheimer's beta (1–40) amyloid: protofilament assembly of tubular fibrils. Biophys. J. 74:537–545.

231. Mandelkow, 2013, Alzforum, Does TauRx Drug Work by Oxidizing Tau, Available at <http://www.alzforum.org/news/research-news/does-Taurx-drug-work-oxidizing-Tau>, [Accessed 3rd June 2016]

232.   Mandelkow, E., Von Bergen, M., Biernat, J., Mandelkow, E.M., 2007, Structural Principles

of Tau and the Paired Helical Filaments of Alzheimer's Disease, Brain Pathology, 17(1);83-90.

233.   Mandelkow, E.M. and Mandelkow, E., 2012, Biochemistry and cell biology of Tau protein

in neurofibrillary degeneration, Cold Spring Harb Perspect Med, (7): a006247.

234.   Margittai, M., Langen, R., 2004, Template-assisted Filament Growth by Parallel Stacking

of Tau. Proc. Natl. Acad. Sci. U.S.A., 101, 10278–10283.

235.   Martin, L., Latypova, X., Wilson, C. M., Magnaudeix, A., Perrin, M., Yardin, C., Terro, F.,

2012, Tau protein kinases: Involvement in Alzheimer's disease, Ageing Res. Rev. 12, 289–309.

236.   Martinez-Coria, H., Green, K., Billings, L., Kitazawa, M., Albrecht, M., Rammes, G.,

Parsons, C., Gupta, S., Banerjee, P., LaFerla, F., 2010, Memantine improves cognition and

reduces Alzheimer's-like neuropathology in transgenic mice. Am J Pathol 176:870–880.

237.   Matharu, B., El-Agnaf, O., Razvia, A., Austen, B., 2010, Development of retro-inverso

peptides as anti-aggregation drugs for β-amyloid in Alzheimer's disease, Peptides, 31(10);1866-

1872.

238.   Matsuoka, S., Ballif, B., Smogorzewska, A., McDonald, E. Hurov, K., Luo, J., Bakalarski, C.,

Zhao, Z., Solimini, N., Lerenthal, Y., Shiloh, Y., Gygi, S., Elledge, S., 2007, ATM and ATR substrate

analysis reveals extensive protein networks responsive to DNA damage, Science,

25;316(5828):1160-6.

239.   Matsuoka, Y., Jouroukhin, Y., Gray, A., Ma, L., Hirata-Fukae, C., Li, H., Feng, L., Lecanu, L.,

Walker, B., Planel, E., Arancio, O., Gozes, I., Aisen, P., 2008, A neuronal microtubule-interacting

agent, NAPVSIPQ, reduces Tau pathology and enhances cognitive function in a mouse model of

Alzheimer's disease. J Pharmacol Exp Ther., 325:146–153

240.   Mayes, J., Tinker-Mill, C., Kolosov, O., Zhang, H., Tabner, B., Allsop, D., 2014, β-Amyloid fibrils in Alzheimer's disease are not inert when bound to copper ions but can degrade hydrogen peroxide and generate reactive oxygen species J. Biol. Chem., 289;12052– 12062.

241.   Medina, M, 2018, An Overview on the Clinical Development of Tau-Based Therapeutics, Int. J. Mol. Sci., 19(4);1160.

242.   Medina, M., Hernández, F., Avila, J., 2016, New features about Tau function and dysfunction. Biomolecules, 6, E21.

243.   Meng, S., Zhu, Y., Guo, T., Liu, X., Chen, J., Liang, Y., 2012, Fibril-Forming Motifs Are Essential and Sufficient for the Fibrillization of Human Tau, PLoS One, 7(6): e38903.

244.   Meraz-Ríos, M., Lira-De, L., Campos-Peña, V., De Anda-Hernández, M., Mena-López, R., 2010, Tau oligomers and aggregation in Alzheimer's disease. J. Neurochem. 112, 1353–1367.

245.   Metropolis, N., Rosenbluth, A., Rosenbluth, M., Teller, A., Teller, E., 1953, Equation of State Calculations by Fast Computing Machines, J. Chem. Phys. 21, 1087; doi: 10.1063/1.1699114.

246.   Mietelska-Porowska, A., Wasik, U., Goras, M., Filipek, A., Niewiadomska, G., 2014, Tau Protein Modifications and Interactions: Their Role in Function and Dysfunction, Int J Mol Sci., 15(3): 4671–4713.

247.   Mitchell, D. J., Steinman, L., Kim, D. T., Fathman, C. G. & Rothbard, J. B. Polyarginine enters cells more efficiently than other polycationic homopolymers. J. Pept. Res. 56, 318–325 (2000).

248.   Mizushima, F., Minoura, K., Tomoo, K., Sumida, M., Taniguchi, T., Ishida, T., 2007, Marked Difference Between Self-aggregations of First and Fourth Repeat Peptides on Tau Microtubule-binding Domain in Acidic Solution, The Journal of Biochemistry, 142(1);49–54.

249.   Möller, H., Graeber, M., 1998, The case described by Alois Alzheimer in 1911. Historical and conceptual perspectives based on the clinical record and neurohistological sections, Eur Arch Psychiatry Clin Neurosci., 248(3):111-22.

250.   Molsoft, 2019, ICM-Pro User Guide v.3.8, <http://www.molsoft.com/gui/index.html>, [Accessed 3rd March 2019].

251.   Moreira, P., Santos, M., Seica, R., Oliveira, C., 2007, Brain mitochondrial dysfunction as a link between Alzheimer's disease and diabetes. J Neurol Sci., 257(1–2):206–214.

252.   Morgan, T., 1910, Sex limited inheritance in Drosophila. Science, 32:120–2.

253.   Morimoto, B., Schmechel, D., Hirman, J., Blackwell, A., Keith, J., Gold, M., 2013, A double-blind, placebo-controlled, ascending-dose, randomized study to evaluate the safety, tolerability and effects on cognition of AL-108 after 12 weeks of intranasal administration in subjects with mild cognitive impairment. Dement Geriatr Cogn Disord., 35:325–336

254.   Morozova, O., March, Z., Robinson, A., Colby, D., 2013, Conformational features of Tau fibrils from Alzheimer's disease brain are faithfully propagated by unmodified recombinant protein, Biochemistry. 2013 October 8; 52(40): 6960–6967

255.   Morris, M., Knudsen, G., Maeda, S., Trinidad, J., Ioanoviciu, A., Burlingame, A., Mucke, L., 2015, Tau post-translational modifications in wild-type and human amyloid precursor protein transgenic mice, Nat Neurosci., 2015 Aug; 18(8):1183-9.

256.   Morris, M., Maeda, S., Vossel, K., Muckle, L., 2011, The Many Faces of Tau, Neuron, 70(3):410-26.

257.   Mudher, A., Colin, M., Dujardin, S., Medina, M., Dewachter, I., Naini, S., Mandelkow, E.M., Mandelkow, E., Buée, L., Goedert, M., Brion, J., 2017, What is the evidence that tau pathology spreads through prion-like propagation? Acta Neuropathol Commun., 5: 99.

258.   Mudher, A., Shepherd, D., Newman, T., Mildren, P., Jukes, J., Squire, A., et al., 2004, GSK-3beta inhibition reverses axonal transport defects and behavioural phenotypes in Drosophila. Mol Psychiatry, 9:522–30. doi:10.1038/sj.mp.4001483.

259.	Mukrasch, M., Biernat, J., Von Bergen, M., Griesinger, C., Mandelkow, E., Zweckstetter, M., 2005, Sites of Tau Important for Aggregation Populate β-Structure and Bind to Microtubules and Polyanions, The Journal of Biological Chemistry, 280, 24978-24986.

260.	Mukrasch, M., von Bergen, M., Biernat, J., Fischer, D., Griesinger, C., Mandelkow, E., Zweckstetter, M., 2007, The "jaws" of the Tau-microtubule interaction. J. Biol. Chem., 282, 12230–12239.

261.	Nakase, I., Niwa, M., Takeuchi, T., Sonomura, K., Kawabata, N., Koike, Y., Takehashi, M., Tanaka, S., Ueda, K., Simpson, J., Jones, A., Sugiura, Y., Futaki, S., 2004, Cellular Uptake of Arginine-Rich Peptides: Roles for Macropinocytosis and Actin Rearrangement, Molecular Therap, 10(6);1011-1022.

262.	Naruto, K., Minoura, K., Okuda, R., Taniguchi, T., In, Y., Ishida, T., Tomoo, K., 2010, Interplay between I308 and Y310 residues in the third repeat of microtubule-binding domain is essential for tau filament formation, FEBS Lett., 8;584(19):4233-6.

263.	Neves, M., Totrov, M., Abagyan, R., 2012, Docking and scoring with ICM: the benchmarking results and strategies for improvement, J Comput Aided Mol Des., 26(6): 675–686.

264.	Niccoli, T. and Partridge, L., 2012, Ageing as a Risk Factor for Disease, Current Biology 22, R741–R752.

265.	Nishio, M., 2011, The CH/phydrogen bond in chemistry. Conformation, supramolecules, optical resolution and interactions involving carbohydrates, Phys. Chem. Chem. Phys., 13;13873–13900.

266.	Novak, P., Kontsekova, E., Zilka, N., Novak, M., 2018, Ten Years of Tau-Targeted Immunotherapy: The Path Walked and the Roads Ahead, Frontiers in Neuroscience, 12(798);1-14.

267.	Novak, P., Schmidt, R., Kontsekova, E., Zilka, N., Kovacech, B., Skrabana, R., Vince-Kazmerova, Z., Katina, S., Fialova, L., Prcina, M., Parrak, V., Dal-Bianco, P., Brunner, M., Staffen,

W., Rainer, M., Ondrus, M., Ropele, S., Smisek, M., Sivak, R., Winblad, B., Novak, M., 2017, Safety and immunogenicity of the tau vaccine AADvac1 in patients with Alzheimer's disease: a randomised, double-blind, placebo-controlled, phase 1 trial. Lancet Neurol 16:123–134.

268.   Obasse, I., Taylor, M., Fullwood, N., Allsop, D., 2017, Development of proteolytically stable N-methylated peptide inhibitors of aggregation of the amylin peptide implicated in type 2 diabetes, Interface Focus 7: 20160127.

269.   Oddo, S., 2008, The ubiquitin–proteasome system in Alzheimer's disease, J Cell Mol Med 12: 363–373.

270.   Oddo, S., Billings, L., Kesslak, J., Cribbs, D., LaFerla, F., 2004, Abeta immunotherapy leads to clearance of early, but not late, hyperphosphorylated tau aggregates via the proteasome, Neuron., 5;43(3):321-32.

271.   Oddo, S., Caccamo, A., Kitazawa, M., Tseng, B., LaFerla, F., 2003, Amyloid deposition precedes tangle formation in a triple transgenic model of Alzheimer's disease, Neurobiol Aging, 24: 1063–1070.

272.   Okada, H., Ouchi, Y., Ogawa, M., Futatsubashi, M., Saito, Y., Yoshikawa, E., Terada, T., Oboshi, Y., Tsukada, H., Ueki, T., Watanabe, M., Yamashita, T., Magata, Y., 2013, Alterations in α4β2 nicotinic receptors in cognitive decline in Alzheimer's aetiopathology, Brain, 136(Pt 10):3004-17.

273.   Okuda, M., Hijikuro, I., Fujita, Y., Wu, X., Nakayama, S., Sakata, Y., Noguchi, Y., Ogo, M., Akasofu, S., Ito, Y., Soeda, Y., Tsuchiya, N., Tanaka, N., Takahashi, T., Sugimoto, H., 2015, PE859, a Novel Tau Aggregation Inhibitor, Reduces Aggregated Tau and Prevents Onset and Progression of Neural Dysfunction *In vivo*, PLoS One. Feb 6;10(2):e0117511

274.   Oller-Salvia, B., Sánchez-Navarro, M., Giraltab, E., Teixidó, M., 2016, Blood–brain barrier shuttle peptides: an emerging paradigm for brain delivery, Chem. Soc. Rev., 45;4690.

275.   Ong, C., Yung, L., Cai, Y., Bay, B., Baeg, G., 2014, Drosophila melanogaster as a model

organism to study nanotoxicity, Nanotoxicology 9(3):1-8.

276.   Oz, S., Ivashko-Pachima, Y., Gozes, I., 2012, The ADNP derived peptide, NAP modulates

thetubulin pool: implication for neurotrophic and neuroprotective activities, PLoSOne;7: e51458

277.   Oz, S., Kapitansky, O., Ivashco-Pachima, Y., Malishkevich, A., Giladi, E., Skalka, N., Rosin-

Arbesfeld, R., Mittelman, L., Segev, O., Hirsch, J., Gozes, I., 2014, The NAP motif of activity-

dependent neuroprotectiveprotein (ADNP) regulates dendritic spines throughmicrotubule end

binding proteins, Molecular Psychiatry (2014) 19, 1115–1124

278.   Pace, C., Scholtz, J., Grimsley, G.,2014, Forces stabilizing proteins, FEBS Lett,

588(14):2177-84.

279.   Pace, C., Vajdos, F., Fee, L., Grimsley, G., Gray, T., 1995, How to measure and predict the

molar absorption coefficient of a protein, Protein Science (1995), 4:2411-2423.

280.   Pákáski, M.; Kálmán, J., 2008, Neurochem. Int.., 53, 103.

281.   Parsons, C., Danysz, W., Dekundy, A., Pulte, I., 2013, Memantine and Cholinesterase

Inhibitors: Complementary Mechanisms in the Treatment of Alzheimer's Disease, Neurotoxicity

Research, 24(3);358-369.

282.   Parthsarathy, V., McClean, P., Hölscher, C., Taylor, M., Tinker, C., Jones, G., Kolosov, O.,

Salvati, E., Gregori, M., Masserini, M., Allsop, D., 2013, A novel retro-inverso peptide inhibitor

reduces amyloid deposition, oxidation and inflammation and stimulates neurogenesis in the

APPswe/PS1ΔE9 mouse model of Alzheimer's disease. PLoS One., 8(1):e54769.

283.   Partridge, W., 2012 Drug transport across the blood–brain barrier, J Cereb Blood Flow

Metab. 32(11); 1959–1972.

284.   Passarella, D., Goedert, M., 2018, Beta-sheet assembly of Tau and neurodegeneration in

Drosophila melanogaster, Neurobiology of Aging, 72;98-105.

285.   Pavlou A., Reichert, J., 2004, Recombinant protein therapeutics—Success rates, market trends and values to 2010. NatBiotechnol., 22:1513–9.

286.   Pérez, M., Santa-Maria, I., Tortosa, E., Cuadros, R., Valle, M., Hernández, F., Moreno, F., Avila, J., 2007, The role of the VQIVYK peptide in tau protein phosphorylation. Journal of neurochemistry. 103. 1447-60.

287.   Persichilli, C., Hill, S., Mast, J., Muschol, M., 2011, Does Thioflavin-T Detect Oligomers Formed During Amyloid Fibril Assembly, Biophysical Journal, 100(3); supplement 1, 538a,

288.   Pickhardt, M., Larbig, G., Khlistunova, I., Coksezen, A., Meyer, B., Mandelkow, E.M., Schmidt, B., Mandelkow, E., 2007, Phenylthiazolyl-hydrazide and its derivatives are potent inhibitors of Tau aggregation and toxicity *in vitro* and in cells. Biochemistry. 46(35):10016-23.

289.   Pievani, M., de Haan, W., Wu, T., Seeley, W., Frisoni, G., 2011, Functional network disruption in the degenerative dementias, The Lancet Neurology, 10(9);829-843

290.   Pollanen, M., Bergeron, C., 2000, Modeling of a periodic instability in paired helical filaments reveals an axial repeat, Acta Neuropathol., 99(5):534-8.

291.   Pooler, A., Usardi, A., Evans, C., Philpott, K., Noble, W., Hanger, D., 2012, Dynamic association of tau with neuronal membranes is regulated by phosphorylation, Neurobiol Aging, 33(2): 431.e27-38.

292.   Povova Jana, Sery Omar, Tomaskova Hana, Vargova Lydia, Ambroz Petr, Luzny Jan, Pohlidalova Anna and Janout Vladimir, 2015, Epidemiology and Genetics of Alzheimer's Disease, J Alzheimers Dis Parkinsonism, 5(1):1000176

293.   Prasad, S., Mandal, I., Singh, S., Paul, A., Mandal, B., Venkatramani, R., Swaminathan, R., 2017, Near UV-Visible electronic absorption originating from charged amino acids in a monomeric protein, Chem. Sci., 8, 5416-5433.

294.   Prince M, Bryce R, Albanese E, Wimo A, Ribeiro W, Ferri CP. The global prevalence of dementia: a systematic review and meta-analysis. Alzheimers Dement. 2013;9(1):63–75.

295.   Protein Data Bank in Europe, 2017, EMDB › EMD-3741 Paired helical filament in Alzheimer's disease brain, Available at <http://www.ebi.ac.uk/pdbe/entry/emdb/EMD-3741> [Accessed 7th March 2019].

296.   Protein Data Bank in Europe, 2019, EMDB › EMD-4563Cryo-EM reconstruction of heparin-induced 2N4R tau snake filaments, Available at <http://www.ebi.ac.uk/pdbe/entry/emdb/EMD-4563> [Accessed 7th March 2019].

297.   Prusiner, S., 1982, Novel proteinaceous infectious particles cause scrapie, Science., Apr 9; 216(4542):136-44.

298.   Raab, S., Jung-Richardt, I., 2015, Application of Maximum Entropy Deconvolution toy-ray Skymaps, proceedings of science, 1-8.

299.   Raley-Susman, K., Cragoe, E., Sapolsky, R., Kopito, R. 1991, Regulation of intracellular pH in cultured hippocampal neurons by an amiloride-insensitive Na+/H+ exchanger, J Biol Chem., 266(5):2739-45.

300.   Ramachandran, G., and Udgaonkar, J., 2011, Understanding the Kinetic Roles of the Inducer Heparin and of Rod-like Protofibrils during Amyloid Fibril Formation by Tau Protein, The Journal of Biological Chemistry, 286(45):38948–38959.

301.   Rambran, R., and Serpell, L., 2008, Amyloid fibrils Abnormal protein assembly, Prion, 2(3): 112–117.

302.   Ree, R., Varland, S., Arnesen, T., 2018, Spotlight on protein N-terminal acetylation, Experimental & Molecular Medicinevolume 50, Article number: 90.

303.   Reinhold, B. and Reinhold, V., 1992, Electrospray Ionization Mass Spectrometry - De-convolution by an Entropy-Based Algorithm, Journal of the American Society of Mass Spectrometry, 3(3);207–215, 992.

304.   Reiter, L., Potocki, L., Chien, S., Gribskov, M., Bier, E., 2001, A systematic analysis of human disease-associated gene sequences in Drosophila melanogaster, Genome Res., 11(6):1114-25.

305.   Relkin, N., Thomas, R., Rissman, R., Brewer, J., Rafii, M., van Dyck, C., Jack, C., Sano, M., Knopman, D., Raman, R., Szabo, P., Gelmont, D., Fritsch, S., Aisen, P. 2017, Alzheimer's Disease Cooperative Study, 2017, A phase 3 trial of IV immunoglobulin for Alzheimer disease., Neurology., 88(18):1768-1775.

306.   Reuben, D., 2013, What is Dementia - Presented by Dr. David B. Reuben, UCLA Alzheimer's and Dementia Care Program, available at: <https://www.youtube.com/watch?v=wyO1qQwRHVY> [Accessed 7th Octover 2015].

307.   Riazul, A., Driver, D., Wu, S., Lozano, E., Key, S., Hole, J., Hayashi, M., Lu, J., 2017, PRECLINICAL CHARACTERIZATION OF AN ANTIBODY [LY3303560] TARGETING AGGREGATED TAU, Alzheimer's & Dementia, 13(7);592–593.

308.   Rincon-Limas, D., Jensen, K., Fernandez-Funez, P., 2012, Drosophila Models of Proteinopathies: the Little Fly that Could, Curr Pharm Des., 18(8): 1108–1122.

309.   Rissman, R., STaup, M., Roe, A., Justice, N., Rice, K., Vale, W., Sawchenko, P., 2012, Corticotropin-releasing factor receptor-dependent effects of repeated stress on Tau phosphorylation, solubility, and aggregation, Proceedings of the National Academy of Sciences 109(16):6277-82.

310.   Roberson, E., Scearce-Levie, K., Palop, J., Yan, F., Cheng, I., Wu, T., Gerstein, H., Yu, G., Mucke, L., 2007, Reducing endogenous tau ameliorates amyloid β-induced deficits in an Alzheimer's disease mouse model. Science 316: 750–754.

311.   Roberts, R., Geda, Y., Knopman, D., Cha, R., Pankratz, V., Boeve, B., Ivnik, R., Tangalos, E., Petersen, R., Rocca, W., 2008, The Mayo Clinic Study of Aging: Design and sampling, participation, baseline measures and sample characteristics. Neuroepidemiology, 30;58–69.

312.   Rosenberg, K., Ross, J., Feinstein, H., Feinstein, S., Israelachvili, J., 2008, Complementary dimerization of microtubule-associated tau protein: Implications for microtubule bundling and tau-mediated pathogenesis. Proc Natl Acad Sci USA., 105:7445–7450.

313.   Ruffin, V., Salameh, A., Boron, W., Parker, M., 2014, Intracellular pH regulation by acid-base transporters in mammalian neurons, Front Physiol., 5: 43.

314.   Rupley, J., Gratton, E., Careri, G., 1983, Water and globular proteins. Trend Biochem. Sci., 8:18–22

315.   Sadqi, M., Hernandez, F., Pan, U., Perez, M., Schaeberle, M., Avila, J., Munoz, V., 2002, R-Helix Structure in Alzheimer's Disease Aggregates of Tau-Protein, Biochemistry, 41;7150-7155

316.   Sahara N, Maeda S, Murayama M, Suzuki T, Dohmae N, Yen SH, Takashima A, 2007, Assembly of two distinct dimers and higher-order oligomers from full-length Tau, Eur J Neurosci. 25(10):3020-9.

317.   Sakai, Y., Masuda, H., Kihara, K., Kurosaki, E., Yamauchi, Y., Azuma, H., 2004, Involvement of increased arginase activity in impaired cavernous relaxation with aging in the rabbit, J Urol., 172(1):369-73.

318.   Santa-Maria, I., Hernandez, F., Martin, C. P., Avila, J., and Moreno, F., 2004, Quinones facilitate the self-assembly of the phosphorylated tubulin binding region of Tau into fibrillar polymers. Biochemistry 43, 2888–2897

319.   Santa-Maria, I., Hernandez, F., Moreno, F. J., and Avila, J., 2007, Taurine, an inducer for Tau polymerization and a weak inhibitor for amyloid-β-peptide aggregation. Neurosci. Lett. 429, 91–94.

320.   Sawaya, M., Sambashivan, S., Nelson, R., Ivanova, M., Sievers, S., Apostol, M., Thompson, M., Balbirnie, M., Wiltzius, J., McFarlane, H., Madsen, A., Riekel, C., Eisenberg, D., 2007, Atomic structures of amyloid cross- β spines reveal varied steric zippers, Nature, 447;453-457

321.   Sayas, C., Tortosa, E., Bollati, F., Ramírez-Ríos, S., Arnal, I., Avila, J., 2015, Tau regulates the localization and function of End-binding proteins 1 and 3 in developing neuronal cells, Journal of Neurochemistry, 133(5);653-667.

322.   Sayre, L., Smith, M., Perry, G., 2001, Chemistry and biochemistry of oxidative stress in neurodegenerative disease, Current Medicinal Chemistry, 8(7);721–738.

323.   Scarpini, E., Schelterns, P., Feldman, H., 2003, Treatment of Alzheimer's disease; current status and new perspectives, Lancet, 2(9)539–547.

324.   Schaumann, T., Braun, W., Wüthrich, K., 1990, The program FANTOM for energy refinement of polypeptides and proteins using a Newton – Raphson minimizer in torsion angle space, Biopolymers, 29(4-5);679-694.

325.   Schwiening, C., Boron, W., 1994, Regulation of intracellular pH in pyramidal neurones from the rat hippocampus by Na (+)-dependent Cl(-)-HCO3- exchange, J Physiol., 475(1):59-67.

326.   Seidler, P., Boyer, D., Rodriguez, J., Sawaya, M., Cascio, D., Murray, K., Gonen, T., Eisenberg, D., 2018, Structure-based inhibitors of tau aggregation, Nat Chem.,10(2);170–176.

327.   Sergeant, N., Bretteville, A., Hamdane, M., Caillet-Boudin, M.-L., Grognet, P., Bombois, S., Blum, D., Delacourte, A., Pasquier, F., Vanmechelen, E., Schraen-Maschke, S., Buée, L., 2008, Biochemistry of Tau in Alzheimer's disease and related neurological disorders. Expert Review of Proteomics, 5(2), 207–224.

328.   Serpell, L., Fraser, P., Sunde, M., 1999, X-Ray fiber diffraction of amyloid fibrils, Methods in Enzymology, 309;526-536.

329.   Serpell, L., Smith, J., 2000, Direct visualisation of the beta-sheet structure of synthetic Alzheimer's amyloid, J Mol Biol., 299(1):225-31.

330.   Serrano-Pozo, A., William, C., Ferrer, I., Uro-Coste, E., Delisle, M., Maurage, C., Hock, C., Nitsch, R., Masliah, E., Growdon, J., Frosch, M., Hyman, B., 2010, Beneficial effect of human anti-amyloid-beta active immunization on neuritemorphology and tau pathology, Brain2010; 133: 1312–27.

331.   Sheridan, R., Maiorov, V., Holloway, K., Cornell, W., Gao, Y., 2010, Drug-like Density: A Method of Quantifying the "Bindability" of a Protein Target Based on a Very Large Set of Pockets and Drug-like Ligands from the Protein Data Bank, J. Chem. Inf. Model., 50 (11), pp 2029–2040.

332.   Shubbar, M. and Smith, J., 2019, Demand Forecasting: An Open-Source Approach, SMU Data Science Review, 2(1);1-19.

333.   Shulman, J., Feany, M., 2003, Genetic modifiers of tauopathy in Drosophila. Genetics., 165:1233–42.

334.   Sibille N., Sillen A., Leroy A., Wieruszeski J. M., Mulloy B., Landrieu I., Lippens G. (2006) Biochemistry 45, 12560–12572.

335.   Sidhu, S., 2000, Phage display in pharmaceutical biotechnology. Curr Opin Biotechnol., 11:610–6.

336.   Simon, D., García-García. E., Royo, F., Falcón-Pérez, J., Avila, J., 2012, Proteostasis of tau. Tau overexpression results in its secretion via membrane vesicles., FEBS Lett 586(1):47–54.

337.   Sipe, J., Benson, M., Buxbaum, J., Ikeda, S., Merlini, G., Saraiva, M., Westermark, P., 2016, Amyloid fibril proteins and amyloidosis: chemical identification and clinical classification International Society of Amyloidosis 2016 Nomenclature Guidelines, Amyloid the Journal of Protein Folding Disorders, 23(4);209-213.

338.   Smith, A., Yaffe, K., 2014, Dementia (including Alzheimer's disease) can be prevented: statement supported by international experts. J Alzheimers Disease., 38(4):699–703

339.   Smith, G., Brett, C., Church, J., 1998, Effects of noradrenaline on intracellular pH in acutely dissociated adult rat hippocampal CA1 neurones., J Physiol., 512 (Pt 2);487-505.

340.   Smith, R. and Veenstra, T., 2003, Proteome Characterization and Proteomics, Vol 65, Amsterdam, Academ. Press, p137.

341.   Sormanni, P., Amery, L., Ekizoglou, S., Vendruscolo, M., Popovic, B., 2017, Rapid and accurate in silico solubility screening of a monoclonal antibody library., Sci. Rep., doi:10.1038/s41598-017-07800-w.

342.   Sormanni, P., Aprile, F., Vendruscolo, M., 2015, The CamSol Method of Rational Design of Protein Mutants with Enhanced Solubility, J. Mol. Biol., 427(2):478-90.

343.   Spires, T., Orne, J., SantaCruz, K., Pitstick, R., Carlson, G., Ashe, K., Hyman, B., 2006, Region-specific Dissociation of Neuronal Loss and Neurofibrillary Pathology in a Mouse Model of Tauopathy, Am J Pathol., 168(5);1598–1607.

344.   Stsiapura, V., Maskevich, A., Kuzmitsky, V., Turoverov, K., Kuznetsova, I., 2007, Computational Study of Thioflavin T Torsional Relaxation in the Excited State, J. Phys. Chem., 111, 22.

345.   Stsiapura, V., Maskevich, A., Kuzmitsky, V., Uversky, V., Kuznetsova, I., Turoverov, K., 2008, Thioflavin T as a molecular rotor: fluorescent properties of thioflavin T in solvents with different viscosity, J Phys Chem B., 112(49):15893-902.

346.   Studier, F., 2005, Protein production by auto-induction in high density shaking cultures. Protein Expr Purif.,41:207–234.

347.		Sugino, E., Nishiura, C., Minoura, K., In, Y., Sumida, M., Taniguchi, T., Tomoo, K., Ishida, T., 2009, Three-/four-repeat-dependent aggregation profile of Tau microtubule-binding domain clarified by dynamic light scattering analysis. Biochem. Biophys. Res. Commun. 385, 236–240.

348.		Sui, D., Liu, M., Kuo, M., 2015, In Vitro Aggregation Assays Using Hyperphosphorylated Tau Protein, J Vis Exp., 95;51537.

349.		Sultan, A., Nesslany, F., Violet, M., Bégard, S., Loyens, A., Talahari, S., Mansuroglu, Z., Marzin, D., Sergeant, N., Humez, S., et al., 2011, Nuclear tau, a key player in neuronal DNA protection. J. Biol. Chem., 286:4566–4575.

350.		Sunde, M., Serpell, L., Bartlam, M., Fraser, P., Pepys, M., Blake, C., 1997, Common core structure of amyloid fibrils by synchrotron X-ray diffraction, Volume 273, Issue 3, 31 October 1997, Pages 729-739.

351.		Suskiewicz, M., Sussman, J., Silman, I., Shaul, Y., 2011, Context-dependent resistance to proteolysis of intrinsically disordered proteins. Protein Sci., 20:1285–97.

352.		Takahashi, M., Miyata, H., Kametani, F., Nonaka, T., Akiyama, H., Hisanaga, S., Hasegawa, M., 2015, Extracellular association of APP and Tau fibrils induces intracellular aggregate formation of Tau, Acta Neuropathol., 129(6): 895–907.

353.		Taniguchi, S., Suzuki, N., Masuda, S., Hisanaga, S., Iwatsubo, T., et al., 2005, Inhibition of heparin-induced tau filament formation by phenothiazines, polyphenols, and porphyrins, J Biol Chem, 280;7614-7623.

354.		Taniguchi-Watanabe, S., Arai, T., Kametani, F., Nonaka, T., Masuda-Suzukake, M., Tarutani, A., Murayama, S., Saito, Y., Arima, K., Yoshida, M., Akiyama, H., Robinson, A., Mann, D., Iwatsubo, T., Hasegawa, M., 2016, Biochemical classification of Tauopathies by immunoblot, protein sequence and mass spectrometric analyses of sarkosyl-insoluble and trypsin-resistant Tau, Acta Neuropathol. 2016; 131: 267–280.

355.   Taylor, M., Moore, S., Mayes, J., Parkin, E., Beeg, M., Canovi, M., Gobbi, M., Mann, D.,
Allsop, D., 2010, Development of a proteolytically stable retro-inverso peptide inhibitor of β-
amyloid oligomerization as a potential novel treatment for Alzheimer's disease Biochemistry,
49;3261– 3272.

356.   Theunis, C., Crespo-Biel, N., Gafner, V., Pihlgren, M., Lopez-Deber, M., Reis, P., Hickman,
D., Adolfsson, O., Chuard, N., Ndao, D., Borghgraef, P., Devijver, H., Van Leuven, F., Pfeifer, A.,
Muhs, A., 2013, Efficacy and safety of a liposome-based vaccine against protein Tau, assessed in
Tau.P301L mice that model Tauopathy. PLoS One. 2013;8: e72301.

357.   Thies, W., and Bleiler, L., 2011, "2011 Alzheimer's disease facts and figures," Alzheimer's
and Dementia, 7(2);208–244.

358.   Thorn, D.C., Ecroyd, H., Sunde, M., Poon, S., Carver, J., 2008, Amyloid Fibril Formation by
Bovine Milk αs2-Casein Occurs under Physiological Conditions Yet Is Prevented by Its Natural
Counterpart, αs1-Casein, Biochemistry. 47(12):3926-3936.

359.   Thornhill IV, J., ed, 2012, NMS Psychiatry, 6th ed., Philadelphia, Lippincott Williams &
Wilkins.

360.   Totrov, M., Abagyan, R., 1997, Proteins 29(Suppl 1):215.

361.   Tsvetkov, P., Makarov, A., Malesinski, S., Peyrot, V., Devred, F., 2012, New insights into
tau–microtubules interaction revealed by isothermal titration calorimetry, Biochimie, 94(3);916-
919.

362.   Turrens J., 2003, Mitochondrial formation of reactive oxygen species, J. Physiol., 552(Pt
2):335–44.

363.   Twohig, D., and Nielsen, H., 2019, α-synuclein in the pathophysiology of Alzheimer's
disease, Molecular Neurodegeneration, 14(23);1-19.

364.   Uematsu, M., Nakamura, A., Ebashi, M., Hirokawa, K., Takahashi, R., Uchihara, T., 2017, Brainstem Tau pathology in Alzheimer's disease is characterized by increase of three repeat Tau and independent of amyloid β, Acta Neuropathologica Communications Neuroscience of Disease 20186:1.

365.   Usmani, S., Bedi, G., Samuel, J., Singh, S., Kalra, S., Kumar, P., Ahuja, A., Sharma, M., Gautam, A., Raghava, G., 2017, THPdb: Database of FDA-approved peptide and protein therapeutics, PLoS One., 12(7): e0181748.

366.   Uversky, V. and Lyubchenko, Y., 2013, Bio-nanoimaging: Protein Misfolding & Aggregation, San Diego, Academic Press.

367.   Uversky, V., 2019, Intrinsically Disordered Proteins and Their "Mysterious" (Meta)Physics, Front. Phys., 7:10.

368.   Uversky, V., Li, J., Fink, A., 2001, Evidence for a partially folded intermediate in α-synuclein fibril formation. J. Biol. Chem. 276, 10737–10744.

369.   Villegas-Llerena, C., Phillips, A., Garcia-Reitboeck, P., Hardy, J., Pocock, J., 2016, Microglial genes regulating neuroinflammation in the progression of Alzheimer's disease, Current Opinion in Neurobiology,36;74-81.

370.   Villemagne, V., Burnham, S., Bourgeat, P., Brown, B., Ellis, K., Salvado, O., Szoeke, C., Macaulay, S., Martins, R., Maruff, P., Ames, D., Rowe, C., Masters, C.; Australian Imaging Biomarkers and Lifestyle (AIBL) Research Group, 2013, Amyloid β deposition, neurodegeneration, and cognitive decline in sporadic Alzheimer's disease: A prospective cohort study. Lancet Neurol, 12(4):357–67.

371.   Vincent, A., TenBroeke, M., Maiese, K., 1999, Neuronal intracellular pH directly mediates nitric oxide-induced programmed cell death, J Neurobiol., 40(2):171-84.

372.   Von Bergen, M., Barghorn, S., Biernat, J., Mandelkow, E. M., Mandelkow, 2005, E. Tau Aggregation is Driven by a Transition from Random Coil to β-Sheet Structure. Biochim. Biophys. Acta, Mol. Basis Dis., 1739;158–166.

373.   Von Bergen, M., Barghorn, S., Li, L., Marx, A., Biernat, J., Mandelkow, E. M., and Mandelkow, E., 2001, Mutations of Tau protein in frontotemporal dementia promote aggregation of paired helical filaments by enhancing local β-structure. J. Biol. Chem. 276, 48165–48174.

374.   Von Bergen, M., Barghorn, S., Muller, S. A., Pickhardt, M., Biernat, J., Mandelkow, E. M., Davies, P., Aebi, U., Mandelkow, E, 2006, The Core of Tau-paired Helical Filaments Studied by Scanning Transmission Electron Microscopy and Limited Proteolysis. Biochemistry, 45;6446–6457.

375.   Von Bergen, M., Friedhoff, P., Biernat, J., Heberle, J., Mandelkow, E.M., Mandelkow, E., 2000, Assembly of tau protein into Alzheimer paired helical filaments depends on a local sequence motif ((306)VQIVYK(311)) forming beta structure, Proc Natl Acad Sci U S A., 9;97(10):5129-34.

376.   Voropai, E., Samtsov, M., Kaplevskii, K., Maskevich, A., Stepuro V., Povarova, I., Kuznetsova, M., Turoverov, K., Fink, A., Uverskii, V., 2003, Spectral Properties of Thioflavin T and Its Complexes with Amyloid Fibrils, Journal of Applied Spectroscopy, 70(6);868–874.

377.   Walker, S., Ullman, O., Stultz, C., 2012, Using Intramolecular Disulfide Bonds in Tau Protein to Deduce Structural Features of Aggregation-resistant Conformations, J Biol Chem. 2012 Mar 16; 287(12): 9591–9600.

378.   Wang, Y., Balaji, V., Kaniyappan, S., Krüger, L., Irsen, S., Tepper, K., Chandupatla, R., Maetzler, W., Schneider, A., Mandelkow, E., Mandelkow, E.M., 2017, The release and trans-synaptic transmission of tau via exosomes. Mol Neurodegener, 12(1):5.

379.   Ward, S., Himmelstein, D., Lancia, J., Fu, Y., Patterson, K., Binder, L., 2013, TOC1: Characterization of a Selective Oligomeric Tau Antibody. J. Alzheimer's Dis., 37, 593–602.

380.   Wegmann, S., Eftekharzadeh, B., Tepper, K., Zoltowska, K., Bennett, R., Dujardin, S.,
Laskowski, P., MacKenzie, D., Kamath, T., Commins, C., Vanderburg, C., Roe, A., Fan, Z., Molliex,
A., Hernandez-Vega, A., Muller, D., Hyman, A., Mandelkow, E., Taylor, P., Hyman, B., 2018, Tau
protein liquid–liquid phase separation can initiate Tau aggregation, The EMBO Journal, e98049

381.   Wei, Y., Thyparambil, A., Latour, R., 2014, Protein Helical Structure Determination Using
CD Spectroscopy for Solutions with Strong Background Absorbance from 190-230 nm, Biochimica
et Biophysica Acta (BBA) - Proteins & Proteomics 1844(12).

382.   West, T., Hu, Y., Verghese, P. B., Bateman, R. J., Braunstein, J. B., Fogelman, I., et al., 2017,
Preclinical and clinical development of ABBV-8E12, a humanized anti-tau antibody, for treatment
of alzheimer's disease and other tauopathies. J. Prev. Alzheimers Dis. 4, 236–241.

383.   Williams, 2006, Tauopathies: classification and clinical update on neurodegenerative
diseases associated with microtubule-associated protein Tau, Internal Medicine Journal, 36;652–
660.

384.   Wimo, A., Guerchet, M., Ali, G., Wu, Y., Prina, A., Winblad, B., Jönsson, L., Liu, Z., Prince,
M., 2017, The worldwide costs of dementia 2015 and comparisons with 2010, Alzheimer's &
Dementia, 13(1);1-7.

385.   Winblad, B., Graf, A., Riviere, M., Andreasen, N., Ryan, M.,2014, Active immunotherapy
options for Alzheimer's disease, Alzheimer's Research & Therapy, 6:7

386.   Wingfield, P., 2001, Protein Precipitation Using Ammonium Sulfate, Curr Protoc Protein
Sci, APPENDIX 3: Appendix–3F. doi:10.1002/0471140864.psa03fs13

387.   Winter, G., Griffiths, A., Hawkins, R., 1994, Hoogenboom HR. Making antibodies by phage
display technology. Annu RevImmunol, 12:433–55

388.   Wittmann, C., Wszolek, M., Shulman, J., Salvaterra, J., Lewis, J., Hutton, M., Feany, M., 2001, Tauopathy in Drosophila: neurodegeneration without neurofibrillary tangles, Science, 293;711-714.

389.   Wolfe, L., Calabrese, M., Nath, A., Blaho, D., Miranker, A., Xiong, Y., 2010, Protein-induced photophysical changes to the amyloid indicator dye thioflavin T, Proc Natl Acad Sci U S A., 28;107(39):16863-8.

390.   World Health Organisation, 2015, Dementia Fact sheet N°362, Retrieved October 02, 2015, from World Health Organisation: http://www.who.int/mediacentre/factsheets/fs362/en/

391.   Wu, C., Wang, Z., Lei, H., Duan, Y., Bowers, M., Shea, J., 2008, The Binding of Thioflavin T and Its Neutral Analog BTA-1to Protofibrils of the Alzheimer's Disease Aβ16–22Peptide Probed by Molecular Dynamics Simulations, J. Mol. Biol., 384, 718–729.

392.   Wu, J., Herman, M., Liu, L., Simoes, S., Acker, C., Figueroa, H., Steinberg, J., Margittai, M. et al., 2013, Small misfolded tau species are internalized via bulk endocytosis and anterogradely and retrogradely transported in neurons. J Biol Chem., 288:1856–1870.

393.   Xu, L., Zheng, J., Margittai, M., Nussinov, R., Ma, B., 2016, How Does Hyperphopsphorylation Promote Tau Aggregation and Modulate Filament Structure and Stability, ACS Chem. Neurosci. 2016, 7, 565–575.

394.   Xu, S., Brunden, K., Trojanowski, J., Lee, V., 2010, Characterization of Tau fibrillization *in vitro*, Alzheimer's Dement. 2010 March; 6(2): 110–117

395.   Xue, C., Lin, T., Chang, D., Guo, Z., 2017, Thioflavin T as an amyloid dye: fibril quantification, optimal concentration and effect on aggregation, R Soc Open Sci., Jan; 4(1): 160696.

396.   Yamashita, H., Kato, T., Oba, M., Misawa, T., Hattori, T., Ohoka, N., Tanaka, M., Naito, M., Kurihara, M., Demizu, Y., 2016, Development of a Cell-penetrating Peptide that Exhibits

Responsive Changes in its Secondary Structure in the Cellular Environment, Scientific Reports 6;33003.

397.   Yanamandra, K., Kfoury, N., Jiang, H., Mahan, T., Ma, S., Maloney, S., Wozniak, D., Diamond, M., Holtzman, D., 2013, Anti-Tau antibodies that block Tau aggregate seeding *in vitro* markedly decrease pathology and improve cognition *in vivo*, Neuron, 80;402–414.

398.   Yao, T., Tomoo, K., Ishida, T., Hasegawa, H., Sasaki, M., Taniguchi, T., 2003, Aggregation analysis of the microtubule binding domain in Tau protein by spectroscopic methods, J Biochem., 134(1):91-9.

399.   Yoshida, H., and Goedert, M., 2012, Phosphorylation of microtubule-associated protein Tau by AMPK-related kinases. J. Neurochem. 120, 165–176.

400.   Yu, W., Polepalli, J., Wagh, D., Rajadas, J., Malenka, R., and Lu, B., 2012, A critical role for the PAR-1/MARK-Tau axis in mediating the toxic effects of Aβ on synapses and dendritic spines. Hum. Mol. Genet. 21, 1384–1390.

401.   Zhang, W., Falcon, B., Murzin, A., Fan, J., Crowther, R., Goedert, M., Scheres, S., 2019, Heparin-induced tau filaments are polymorphic and differ from those in Alzheimer's and Pick's diseases, structural biology and molecular biophysics, eLifev.8; 2019, PMC6375701.

402.   Zheng, J., Liu, C., Sawaya, M., Vadla, B., Khan, S., Woods, J., Eisenberg, D., Goux, W., Nowick, J., 2011, Macrocyclic β-Sheet Peptides That Inhibit the Aggregation of a TauProtein-Derived Hexapeptide, J. Am. Chem. Soc. 2011, 133, 3144–3157.

403.   Zheng, W., Bastianetto, S., Mennicken, F., Ma, W., Kar, S., 2002, Amyloid l peptide induces Tau phosphorylation and loss of cholinergic neurons in rat primary septal cultures, Neuroscience, 115(1)201-211.

404.   Zhou, L., McInnes, J., Wierda, K., Holt, M., Herrmann, A., Jackson, R., Wang, Y., Swerts, J., Beyens, J., Miskiewicz, K., Vilain, S., Dewachter, I., Moechars, D., De Strooper, B., Spires-Jones, T.,

De Wit, J., Verstreken, P., 2017, Tau association with synaptic vesicles causes presynaptic dysfunction, Nature Communications, 8;15295.

405.   Zhu, H., Fernández, C., Fan, J., Shewmaker, F., Chen, J., Minton, A., Liang, Y., 2010, Quantitative Characterization of Heparin Binding to Tau Protein, J Biol Chem, 285(6); 3592–3599.

406.   Zhu, Y., Bu, Q., Liu, X., Hu, W,. Wang, Y., 2014, Neuroprotective effect of TAT-14-3-3ε fusion protein against cerebral ischemia/reperfusion injury in rats. PLoS One 9, e93334.

407.   Zilka, N., Filipcik, P., Koson, P., Fialova, L., Skrabana, R., Zilkova, M., Rolkova, G., Kontsekova, E., Novak, M., 2006, Truncated tau from sporadic Alzheimer's disease suffices to drive neurofibrillary degeneration in vivo. FEBS Lett 580:3582–3588.

408.   Zweckstetter, 2013, Alzforum, Does TauRx Drug Work by Oxidizing Tau, Available at <http://www.alzforum.org/news/research-news/does-Taurx-drug-work-oxidizing-Tau>, [Accessed 3rd June 2016]

APPENDICES

Appendix A: Current pipeline treatments in clinical development for AD associated with Aβ. 18 are active, 16 are completed, 25 are terminated (ClinicalTrials.gov, 2019 and Alzform, 2019).

	Drug	Company	Mechanism of Action	Indication	Clinical Phase	Clinical Trial Identifier	Status
1	**Vanutide cridificar (ACC-001)**	Janssen	Active Immunotherapy	Mild-Moderate AD	Phase 2	NCT00960531	Terminated
2	**Affitope AD02**	AFFiRiS AG	Active Immunotherapy	Mild-Moderate AD, Early AD	Phase 2	NCT01357629	Terminated
3	**CAD106**	Cystos/Novartis	Active Immunotherapy	Mild AD	Phase 2	NCT02565511	Active
4	**ACI-24**	AC Immune	Active Immunotherapy	Mild-Moderate AD; Down Syndrome	Phase 1	NCT02738450	Active
5	**UB-311**	United Biomedical	Active Immunotherapy	Mild AD	Phase 2	NCT03531710	Active
6	**LU AF20513**	Lundbeck/Otsuka	Active Immunotherapy	Mild AD	Phase 1	NCT02388152	Active
7	**Affitope AD02**	AFFiRiS AG	Active Immunotherapy	Mild-Moderate AD	Phase 2	NCT02008513	Terminated

8	ABvac 40	Araclon Biotech S.L.	Active Immunotherapy	MCI, Very Mild AD	Phase 2	NCT03461276	Active
9	AN-1792 (AIP 001)	Janssen/Pfizer	Active Immunotherapy	Mild-Moderate AD	Phase 2	NCT00021723	Terminated
10	Nasal Insulin (Detemir)		APP secretase inhibitor	AD	Phase 2	NCT02462161	Active
11	Verubecestat (MK-8931)	Merck & Co.	BACE inhibitor	Prodromal or Mild-Moderate AD	Phase 3	NCT01739348	Terminated
12	Lanabecestat (LY3314814)	AstraZeneca/Eli Lilly	BACE inhibitor	Earlyl-Mild AD	Phase 3	NCT02972658	Terminated
13	JNJ-54861911 (ALZ2002)	Janssen	BACE inhibitor	Early AD	Phase 2	NCT02406027	Terminated
14	AZD3293	AstraZeneca	BACE inhibitor	Mild-Moderate AD	Phase 1	NCT01795339	Completed
15	CNP520	Amgen, Inc., Novartis Pharmaceuticals	BACE inhibitor	Mild AD	Phase 2	NCT03131453	Active
16	Elenbecestat (E2609)	Eisai Inc.	BACE Inhibitor	Early AD	Phase 3	NCT02956486	Active
17	BI 1181181 (VTP 37948)	Boehringer Ingelheim, Vitae Pharmaceuticals	BACE Inhibitor	AD	Phase 1	NCT02254161	Terminated
18	LY2886721	Eli Lilly	BACE Inhibitor	MCI or Mild AD	Phase 1	NCT01561430	Terminated
19	LY3202626	Eli Lilly	BACE Inhibitor	Mild AD	Phase 2	NCT02791191	Terminated
20	Semagacestat (LY450139 Dihydrate)	Eli Lilly	BACE Inhibitor	AD	Phase 3	NCT00594568	Terminated

21	Verubecestat (MK-8931)	Merck Sharp & Dohme Corp.	BACE Inhibitor	Mild-Moderate AD	Phase 3	NCT01739348	Terminated
22	Tramiprosate (Alzhemed™)	Neurochem, Inc.	Dietary Supplement	Mild-Moderate AD	Phase 3	NCT00314912	Unknown
23	Epigallocatechin Gallate (EGCG)	Taiyo International	Dietary Supplement	Early AD	Phase 2	NCT00951834	Completed
24	Solanezumab (LY2062430)	Eli Lilly	Passive immunotherapy	Mild AD	Phase 3	NCT01900665	Terminated
25	Gantenerumab (RO4909832)	Roche/Genentech	Passive immunotherapy	Mild AD	Phase 3	NCT03443973	Active
26	Aducanumab (BIIB037)	Biogen Inc.	Passive Immunotherapy	MCI or Mild AD	Phase 3	NCT03639987	Terminated
27	Crenezumab (MABT5102A)	Roche/Genentech/ AC Immune	Passive Immunotherapy	Mild-Moderate AD	Phase 3	NCT03491150	Active
28	N3pG-Aβ (LY-3002813)	Eli Lilly	Passive Immunotherapy	Early AD	Phase 2	NCT03367403	Active
29	MEDI1814	AstraZeneca	Passive Immunotherapy	Mild-Moderate AD	Phase 1	NCT02036645	Completed
30	BAN2401	Eisai Inc.	Passive Immunotherapy	Mild AD	Phase 2	NCT02094729	Completed
31	Bexarotene	Biogen, Eisai Co., Ltd.	Passive Immunotherapy	Mild AD	Phase 2	NCT01782742	Completed
32	Etanercept (STEADI-09)	Amgen, Inc., Pfizer	Passive Immunotherapy	Mild-Moderate AD	Phase 2	NCT01716637	Completed
33	GSK933776	GlaxoSmithKline	Passive Immunotherapy	MCI or Mild AD	Phase 1	NCT01424436	Completed
34	Immune Globulin	Baxalta now part of Shire	Passive Immunotherapy	Mild-Moderate AD	Phase 3	NCT01736579	Terminated
35	Atabecestat (JNJ-54861911)	Janssen	Passive Immunotherapy	Early AD	Phase 2	NCT02569398	Active

36	Octagam®10%	Octapharma	Passive Immunotherapy	Mild-Moderate AD	Phase 2	NCT00812565	Completed
37	SAR228810	Sanofi	Passive Immunotherapy	Mild-Moderate AD	Phase 1	NCT01485302	Completed
38	AAB-003 (PF-05236812)	Pfizer/Janssen	Passive Immunotherapy	Mild-Moderate AD	Phase 1	NCT01369225	Terminated
39	Bapineuzumab (AAB-001)	Janssen	Passive Immunotherapy	Mild-Moderate AD	Phase 2	NCT00606476	Terminated
40	CAD106	Novartis	Passive Immunotherapy	MCI	Phase 2	NCT02565511	Active
41	LY2599666	Eli Lilly	Passive Immunotherapy	Mild-Moderate AD	Phase 1	NCT02614131	Terminated
42	LY3372993	Eli Lilly	Passive Immunotherapy	AD	Phase 1	NCT03720548	Active
43	Ponezumab (PF-04360365)	Pfizer	Passive Immunotherapy	Mild-Moderate AD	Phase 2	NCT01125631	Completed
44	Ibuprofen (ALZT-OP1)	AZTherapies, Inc.	Small Molecule	Early AD / Inflammation	Phase 3	NCT02547818	Active
45	Acitretin (RO 101670)	Actavis/Allergan plc	Small Molecule	Mild-Moderate AD	Phase 2	NCT01078168	Completed
46	Azeliragon	Neurochem, Inc.	Small Molecule	Mild AD	Phase 3	NCT02080364	Terminated
47	CHF 5074	CereSpir™ Incorporated, Chiesi Pharmaceuticals Inc.	Small Molecule	MCI	Phase 2	NCT01303744	Completed
48	Elayta (CT1812)	Cognition Therapeutics	Small Molecule	Mild-Moderate AD	Phase 2	NCT03507790	Active
49	EVP-0962	FORUM Pharmaceuticals Inc	Small Molecule	MCI or Early AD	Phase 2	NCT01661673	Completed

50	Pinitol (NIC5-15)	Humanetics Corporation	Small Molecule	AD	Phase 2	NCT00470418	Completed
51	PBT2	Prana Biotechnology Limited	Small Molecule	Early AD	Phase 2	NCT00471211	Completed
52	PF-06648671	Pfizer	Small Molecule	AD	Phase 1	NCT02407353	Terminated
53	PF-06751979	Pfizer	Small Molecule	AD	Phase 1	NCT02509117	Terminated
54	PQ912	Probiodrug AG	Small Molecule	Early AD	Phase 2	NCT02389413	Completed
55	Thalidomide	Banner Health	Small Molecule	AD	Phase 2	NCT01094340	Unknown
56	Levetiracetam (AGB101)	AgeneBio	Small Molecule	MCI	Phase 3	NCT01044758	Active
57	Avagacestat (BMS-708163)	Bristol-Myers Squibb	Small Molecule	Mild-Moderate AD	Phase 2	NCT00810147	Terminated
58	PBT1 (Clioquinol)	Prana Biotechnology Limited	Small Molecule	AD	Phase 2	N/A	Terminated
59	ELND005 (AZD-103)	Transition Therapeutics	Small Molecule	AD	Phase 2	NCT01766336	Terminated
60	Flurizan™ (MPC-7869)	Myrexis Inc.	Small Molecule	AD	Phase 3	NCT00380276	Terminated
61	RG7129 (RO5508887)	Roche	Small Molecule	AD	Phase 1	NCT01664143	Terminated

Appendix B: Current therapeutic strategies for AD (Anand et al., 2014).

- **Modulating neurotransmission**
  - Acetylcholinesterase inhibitors
  - NMDA receptor antagonists
  - GABAergic modulation
  - Serotonin receptor modulation
  - Histaminergic modulation
  - Adenosine receptor modulation
- **Tau based therapies**
  - Tau phosphorylation inhibition
  - Microtubule stabilization
  - Blocking Tau oligomerization
  - Enhancing Tau degradation
  - Tau based immunotherapy
- **Amyloid based strategies**
  - Secretase enzymes modulation
  - Amyloid transport
  - Preventing amyloid aggregation
  - Promoting amyloid clearance
  - Amyloid based immunotherapy
- **Oxidative stress reduction**
  - Exogenous antioxidant supplementation
  - Augmenting endogenous defence
- **Modulating intracellular signalling cascades**
- **Mitochondrial targeted therapy**
- **Modulation of cellular calcium homeostasis**
- **Anti-inflammatory therapy**
- **Others**
  - Gonadotropin supplementation
  - Lipid modifiers – Statins

- Growth factor supplementation
- Metal chelation
- Epigenetic modifiers
- Caspase inhibitors
- Nitric oxide synthase modulation
- Nucleic acid drugs
- Multi-target directed ligands
- Diabetes drugs - Liraglutide

Appendix C: Protein BLAST comparing human Tau$_{441}$ with *Drosophila* Tau$_{370}$

Max score	Total score	Query cover	E value	Ident
117	210	65%	1e-33	38%

Range 1: 193 to 384

Score	Expect	Method	Identities	Positives	Gaps
117 bits(293)	1e-33	Compositional matrix adjust.	82/214(38%)	121/214(56%)	29/214(13%)

```
Query  97   DRNGPNSPSSPVKTPTSTSSKPDK-SGTSRPPSATPSNKSAPKSRSASKNRLLLKTPEPE  155
            DR+G +SP SP  TP S S  P   +  +R P      ++ PKS S++K+RL
Sbjct  193  DRSGYSSPGSP-GTPGSRSRTPSLPTPPTREPKKVAVVRTPPKSPSSAKSRL--------  243

Query  156  PVKKVPMNKVQVGHAPSPNLKAVRSKIGSLDNATYKPGGGHVKIESKKIDIKAAPRIEAK  215
                        Q    P P+LK V+SKIGS +N  ++PGGG V+I +KK+D+    +++K
Sbjct  244  ----------QTAPVPMPDLKNVKSKIGSTENLKHQPGGGKVQIINKKLDLS---NVQSK  290

Query  216  -----NDKYMPKGGEKKIVTTKLQWN-AKSKIGSLENAAHKPGGGDKKIETLKMDFKDKA  269
                 N K++P GG +IV   +  +   SK GSL N  HKPGGG ++++ K+DFKD+
Sbjct  291  CGSKDNIKHVPGGGSVQIVYKPVDLSKVTSKCGSLGNIHHKPGGGQVEVKSEKLDFKDRV  350

Query  270  KPKVGSTANVKHQPGGGDIKIQTQKLEIKAQSKV  303
            + K+GS  N+ H PGGG+ KI+T KL  +  +K
Sbjct  351  QSKIGSLDNITHVPGGGNKKIETHKLTFRENAKA  384
```

Range 2: 255 to 355

Score	Expect	Method	Identities	Positives	Gaps
78.6 bits(192)	2e-20	Compositional matrix adjust.	44/102(43%)	64/102(62%)	3/102(2%)

```
Query  236  NAKSKIGSLENAAHKPGGGDKKIETLKMDFKDKAKPKVGSTANVKHQPGGGDIKIQTQKL  295
            N KSKIGS EN  H+PGGG +I   K+D  +  + K GS N+KH PGGG ++I   + +
Sbjct  255  NVKSKIGSTENLKHQPGGGKVQIINKKLDLSN-VQSKCGSKDNIKHVPGGGSVQIVYKPV  313

Query  296  EI-KAQSKVGSLDNVKHKPGGGEKKIFDDK-DYLKNVEHSVA  335
            ++ K  SK GSL N+ HKPGGG+ ++  +K D+   V+  +
Sbjct  314  DLSKVTSKCGSLGNIHHKPGGGQVEVKSEKLDFKDRVQSKIG  355
```

Appendix D: HPLC-MS data for AG01.
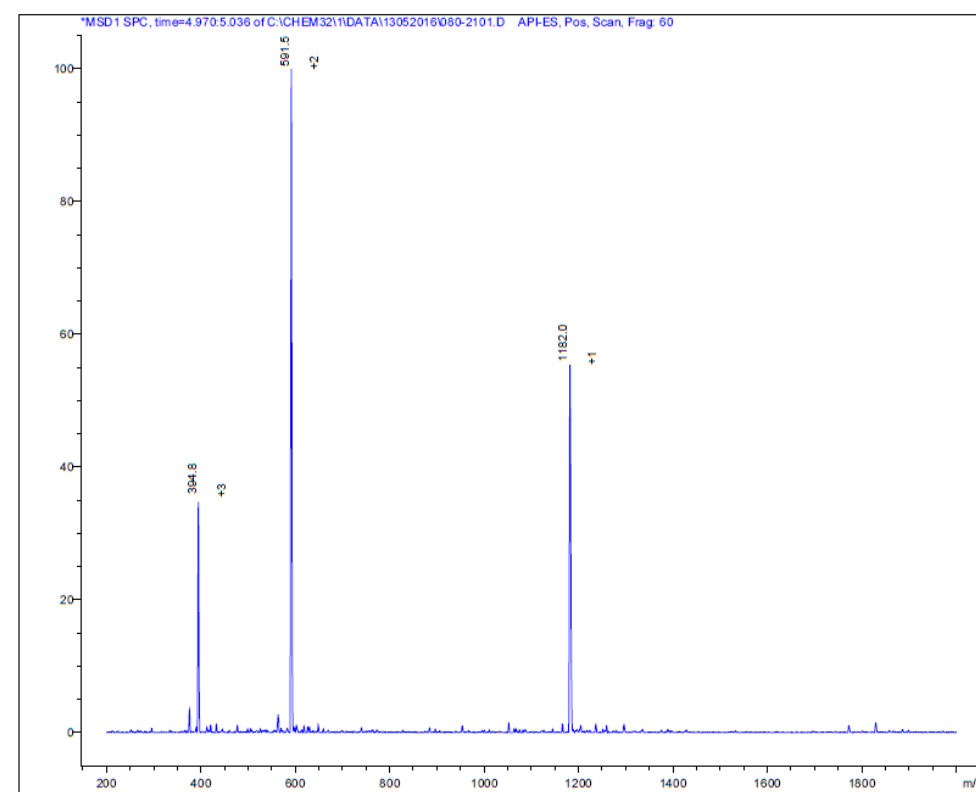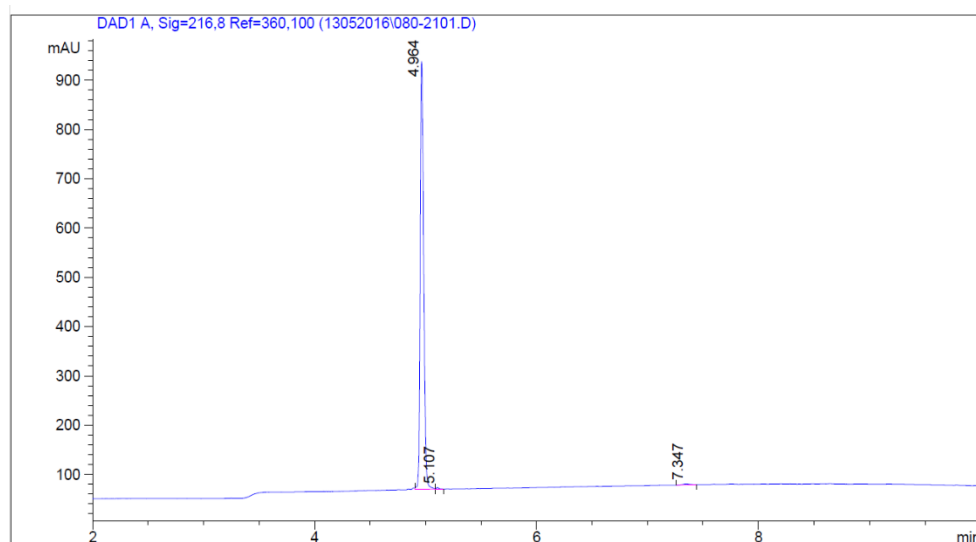
Appendix E: HPLC-MS data for AG02.
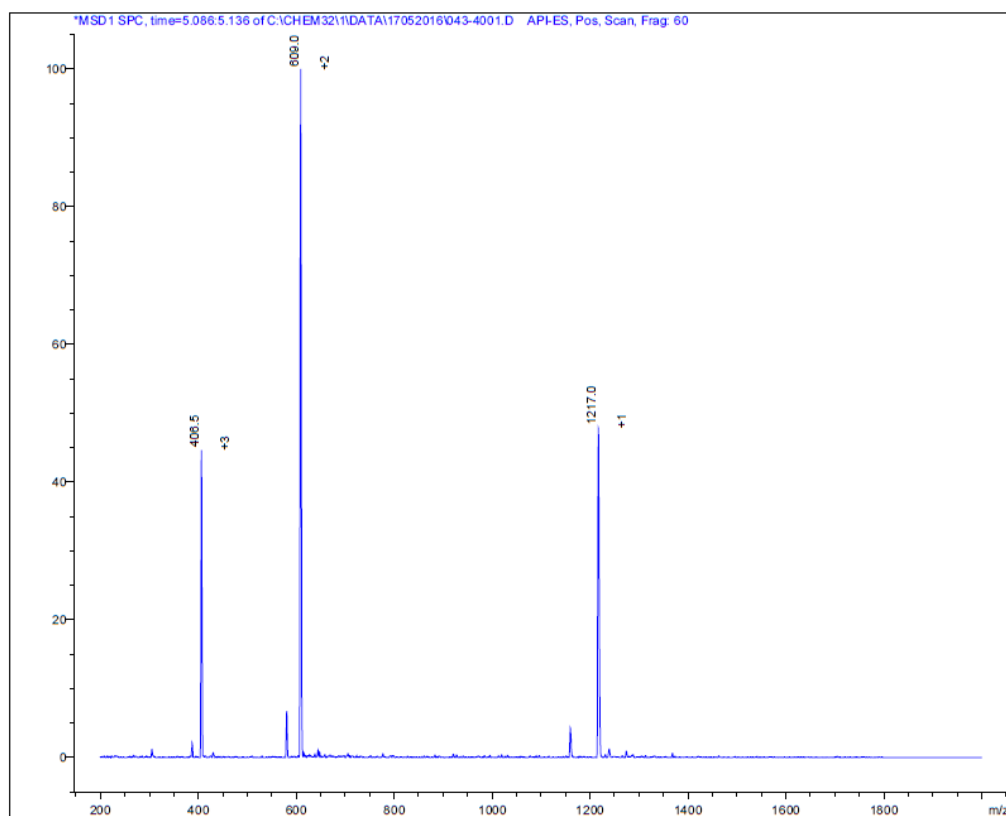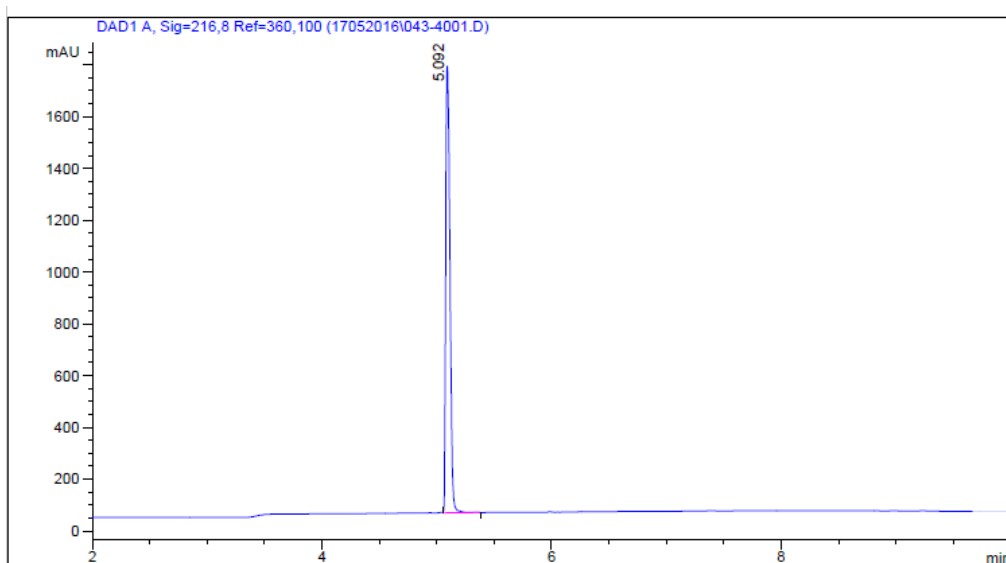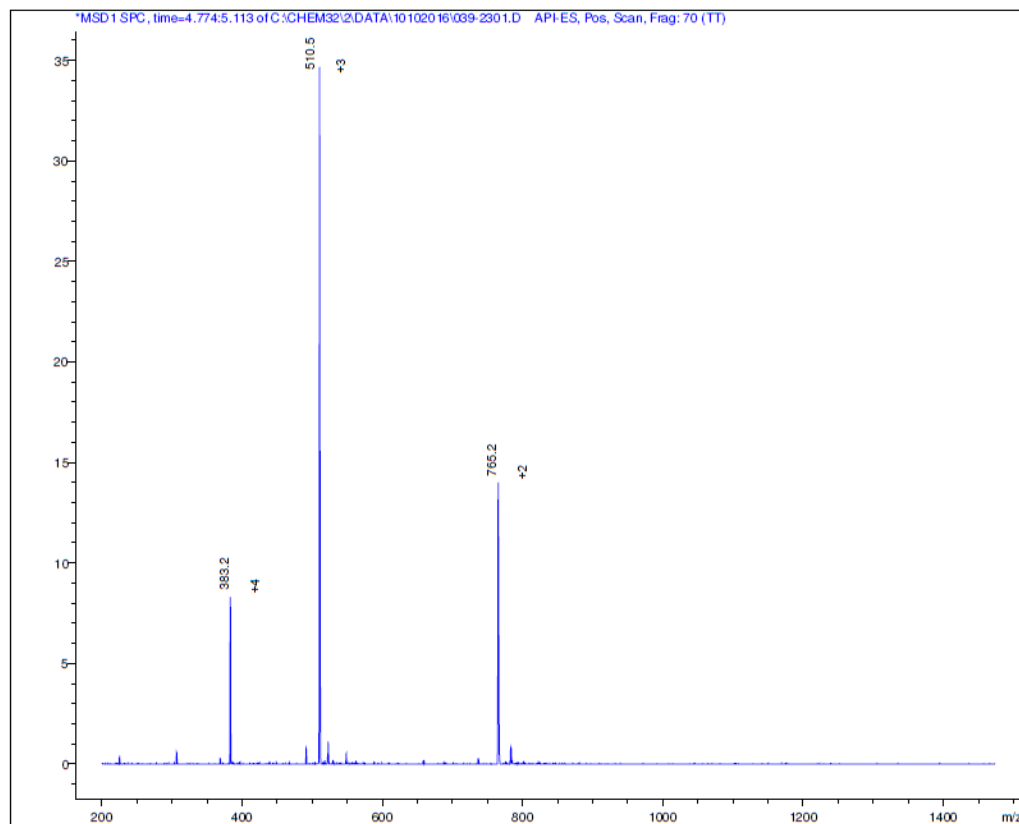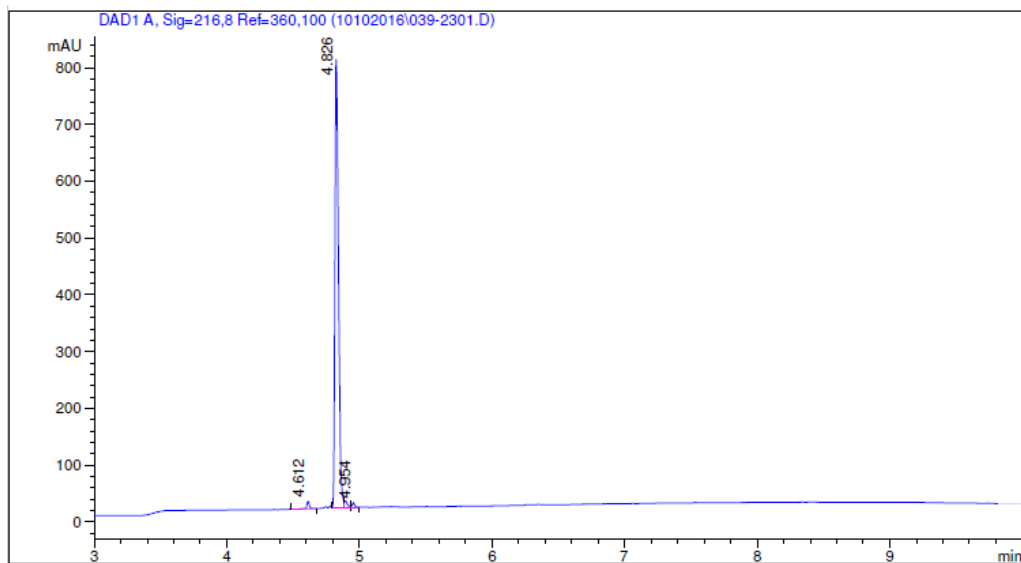
Appendix G: HPLC-MS data for AG02R5.
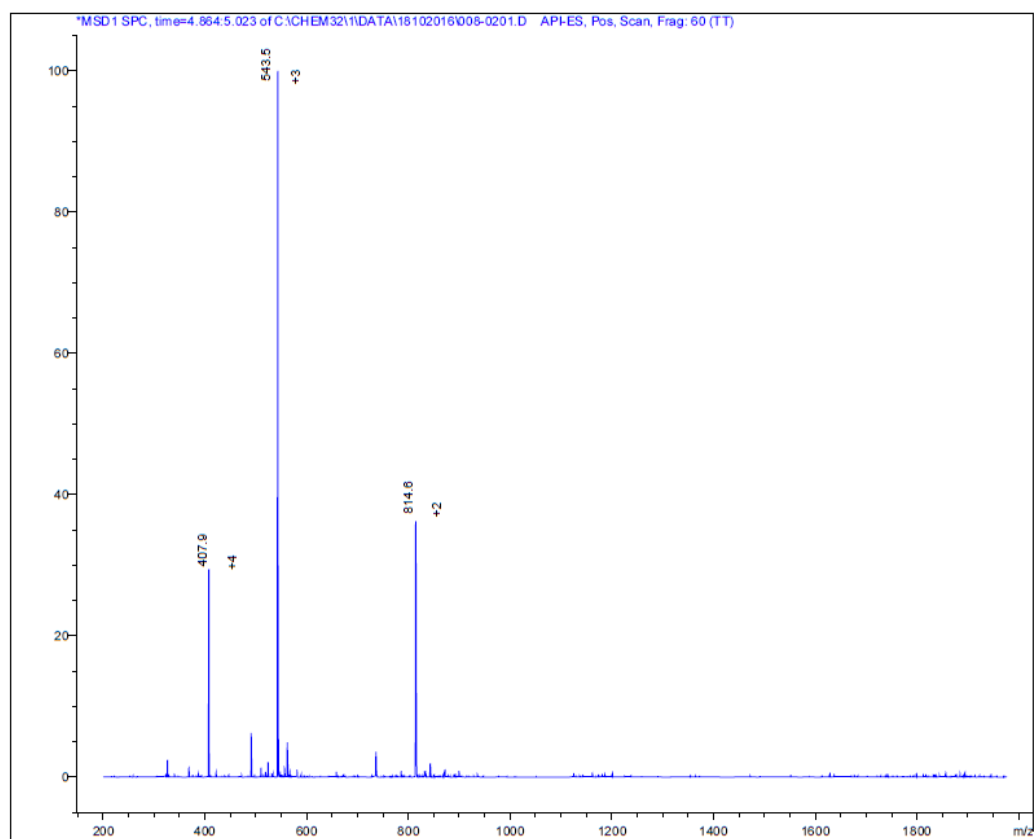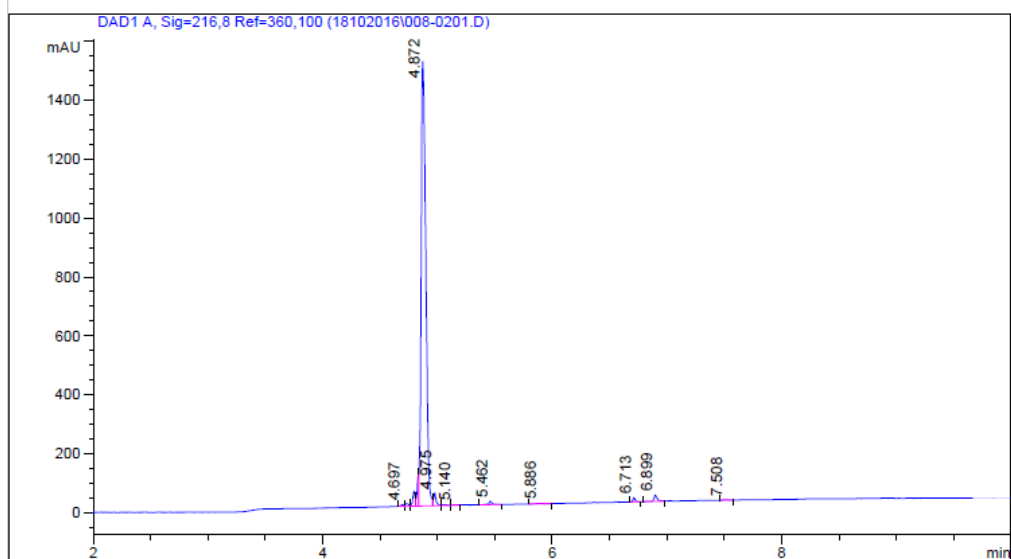
Appendix H: HPLC-MS data for AGR502.
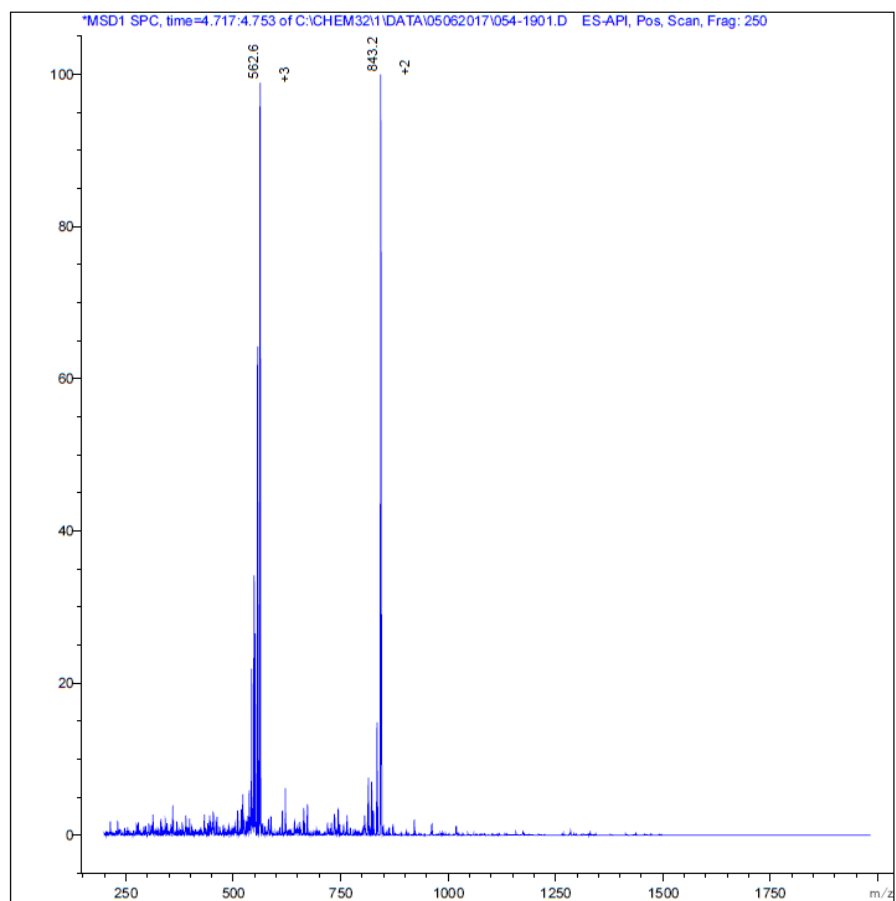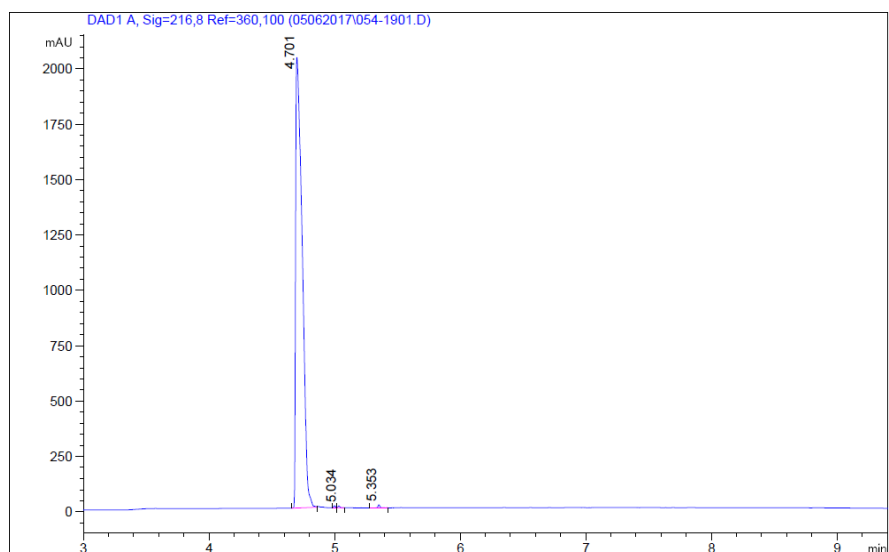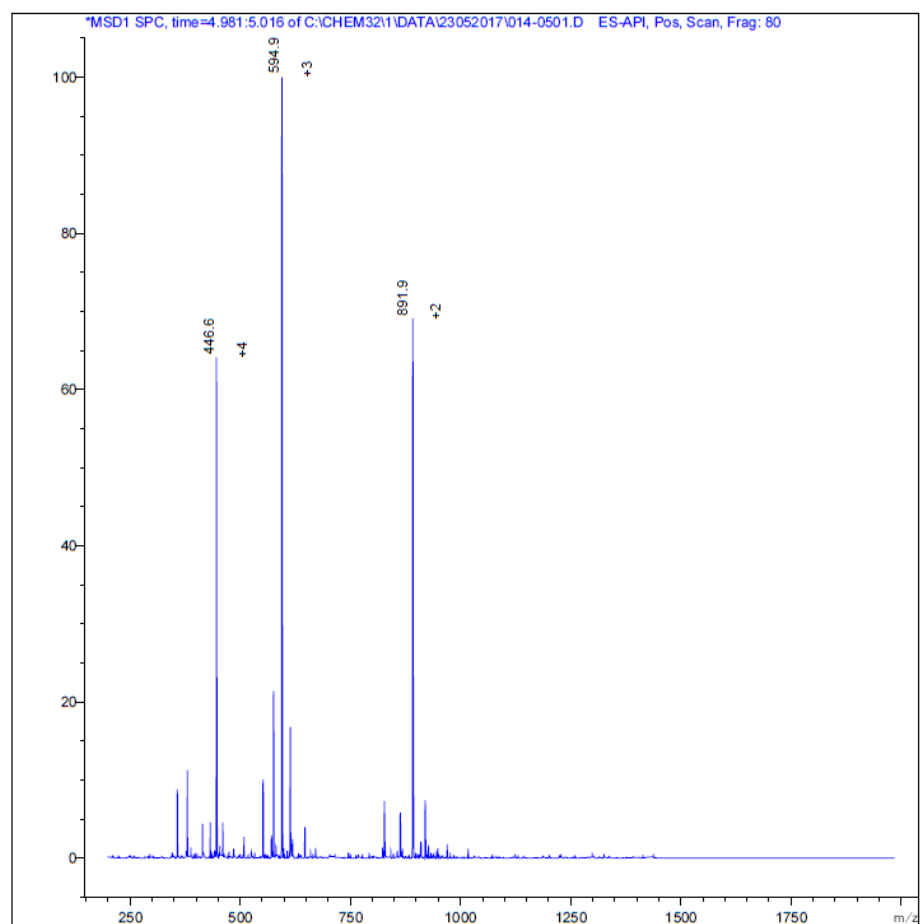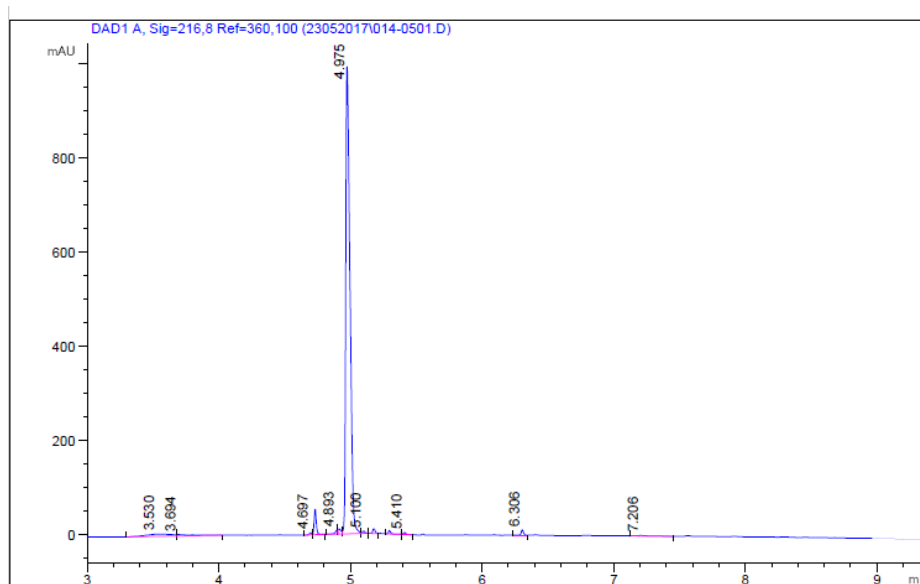
Appendix J: HPLC-MS data for AG02R6.
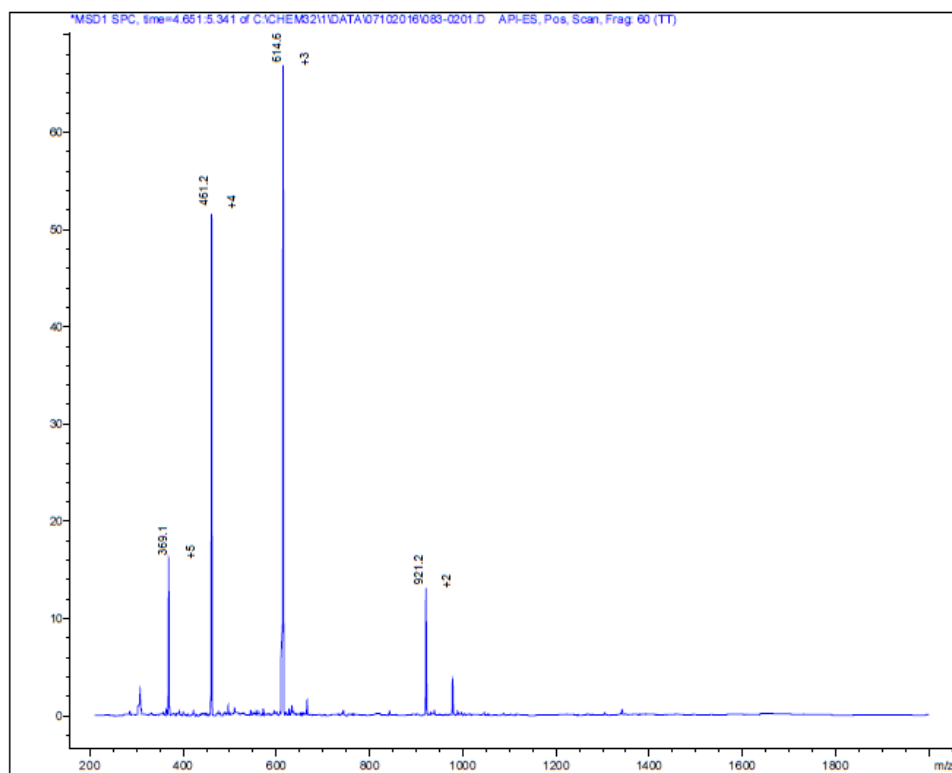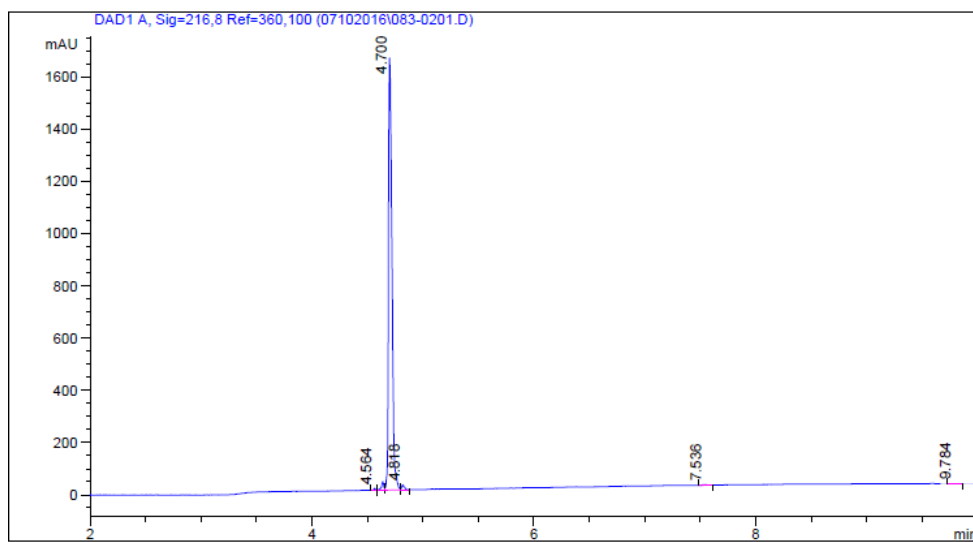
Appendix K: HPLC-MS data for AG02R9.
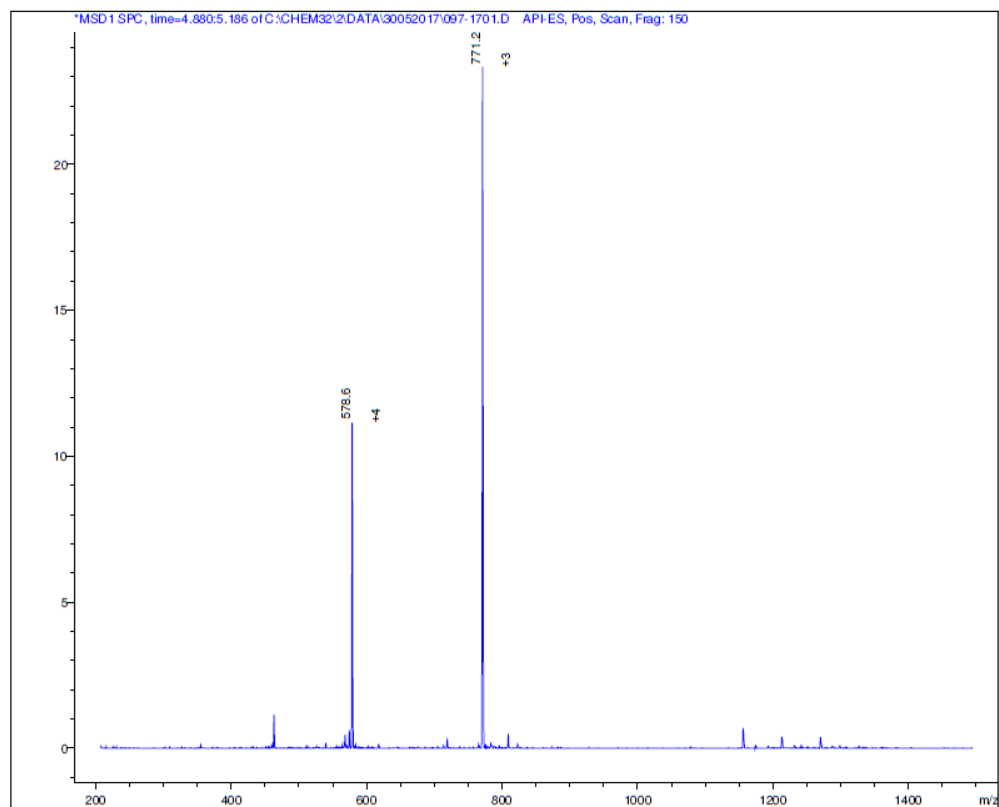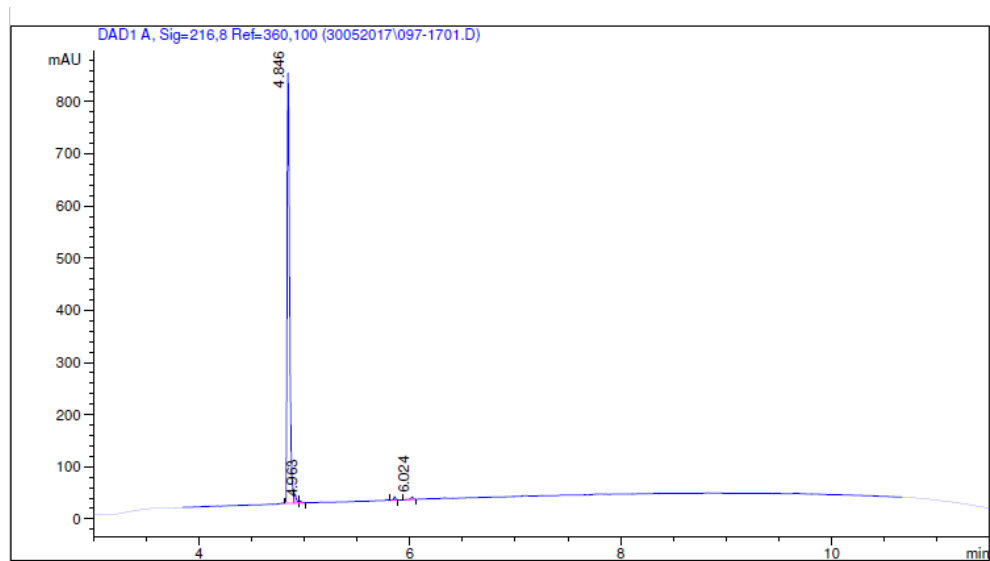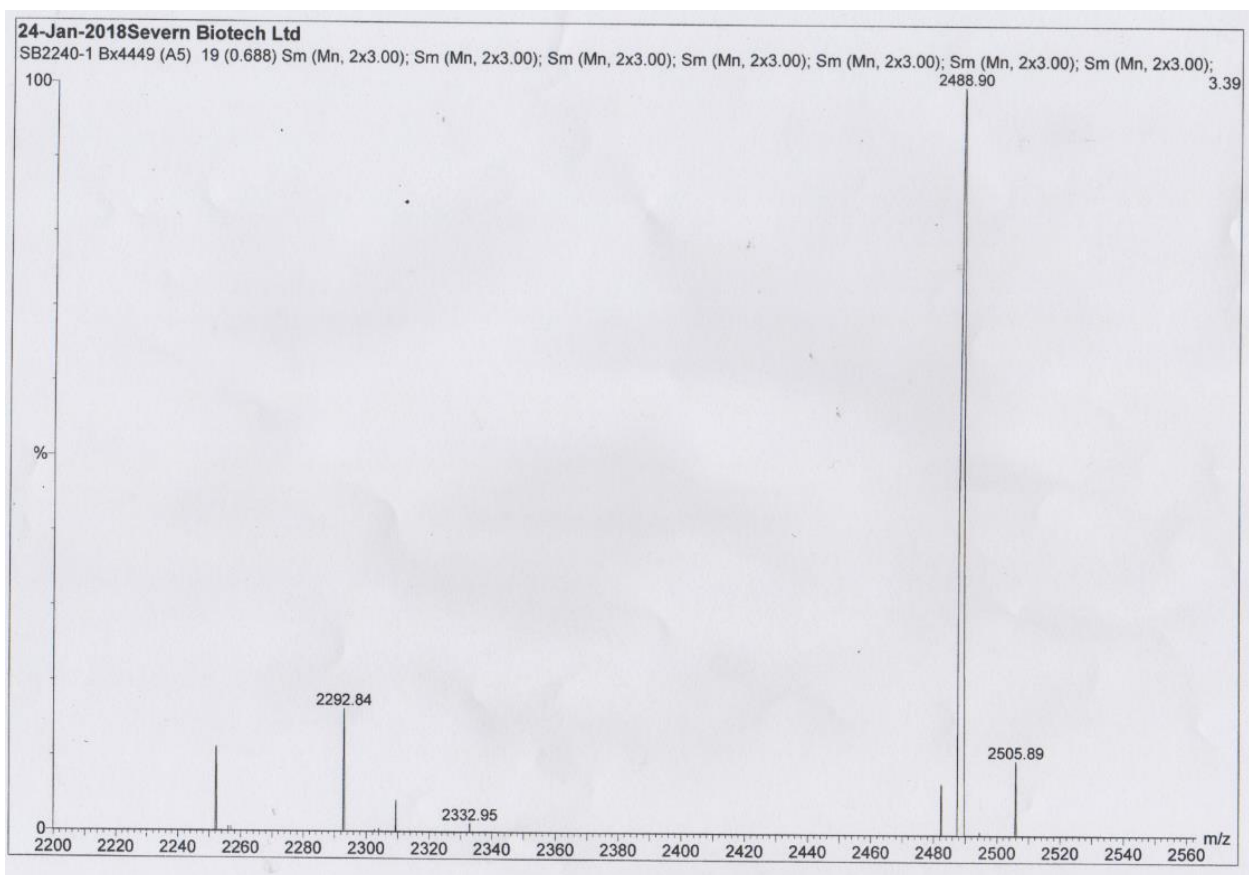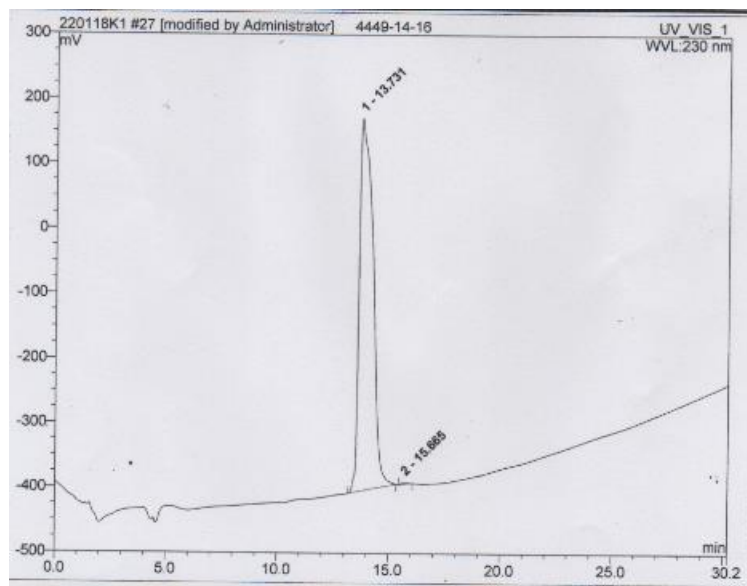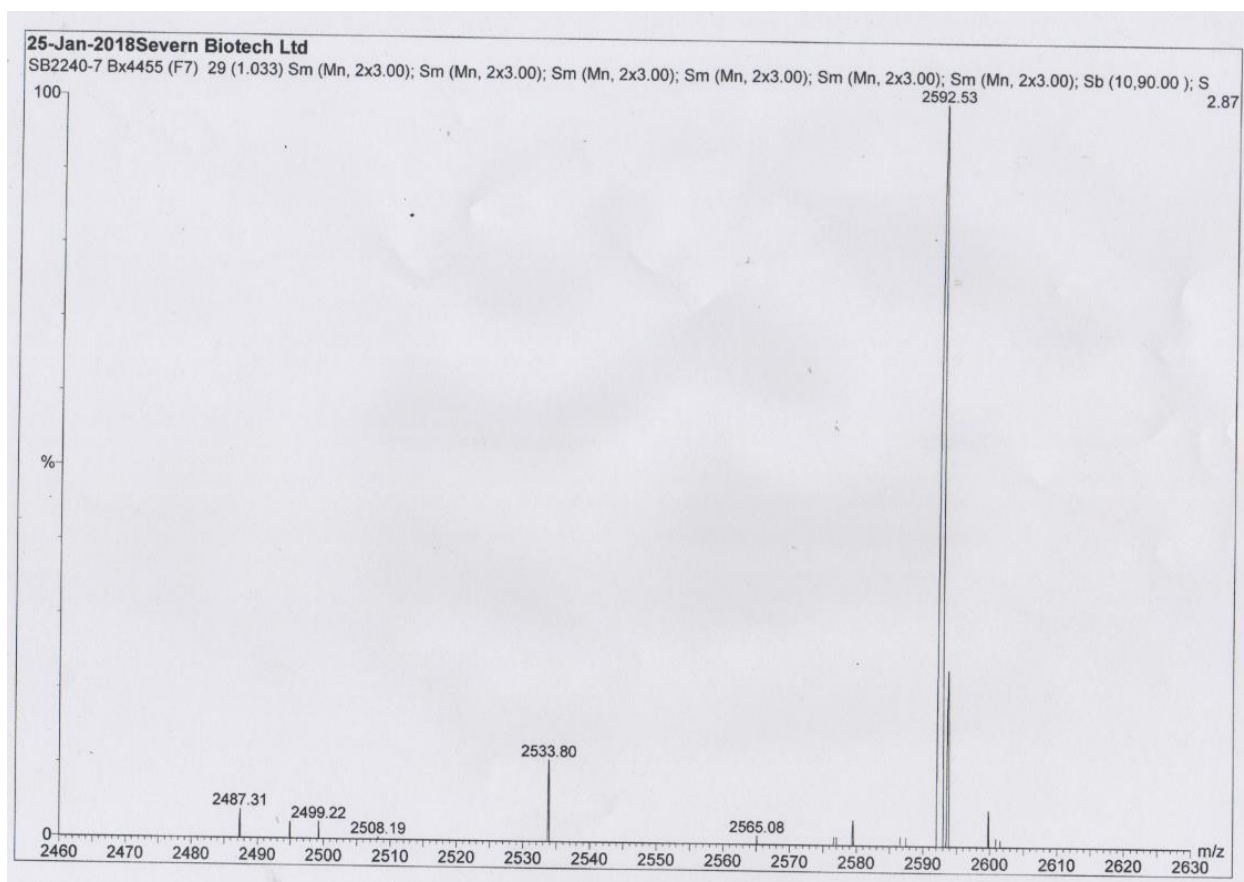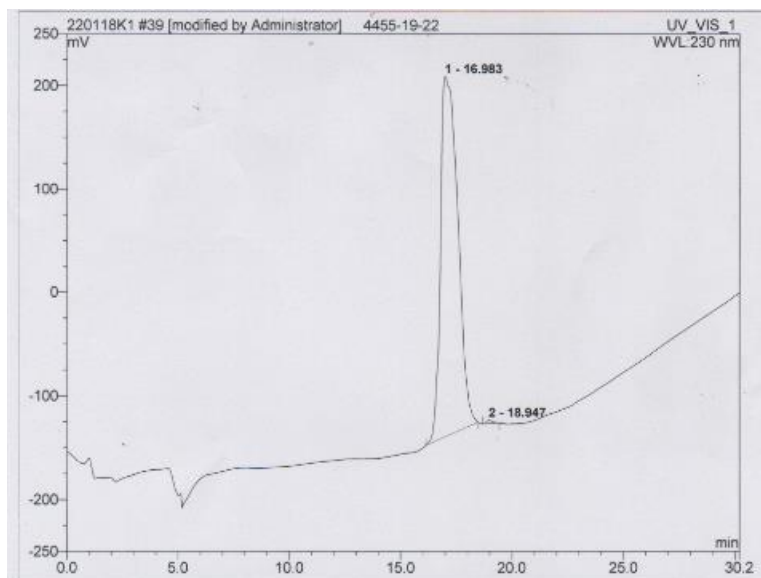
Appendix L: HPLC-MS data for AG02TAT.
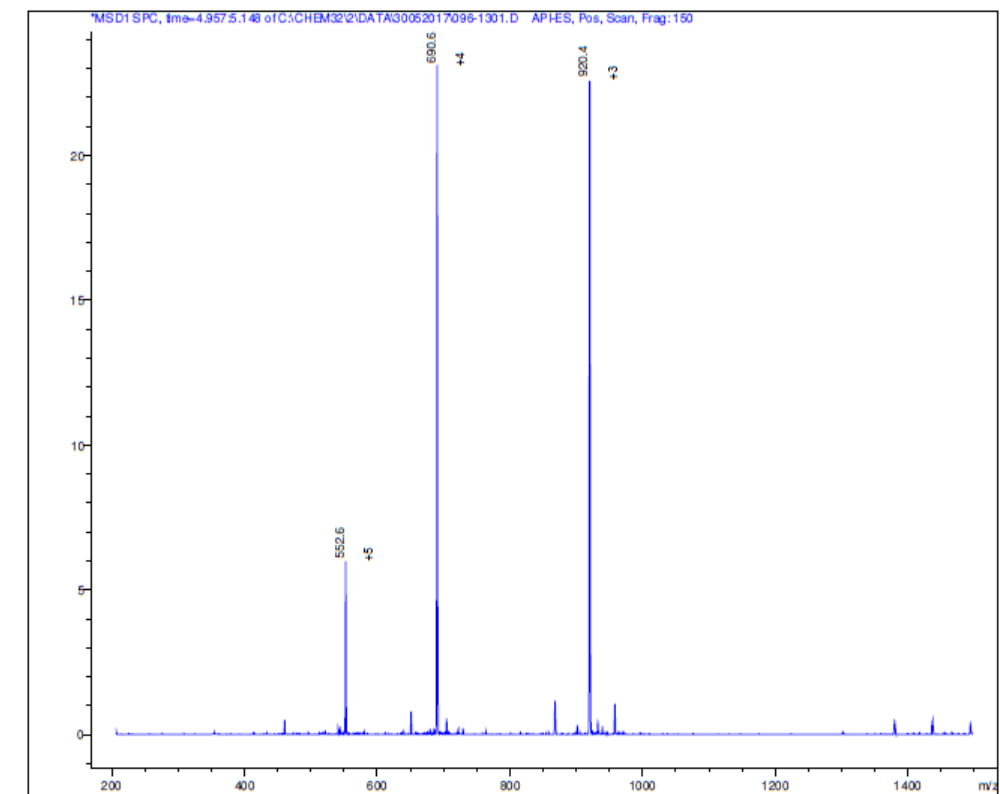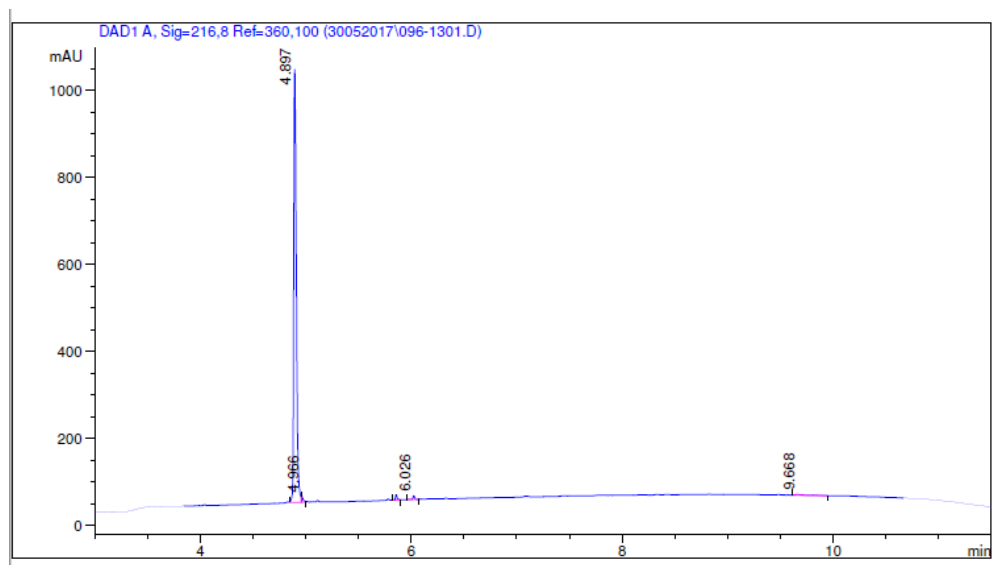
Appendix M: HPLC-MS data for AG02ΔI.
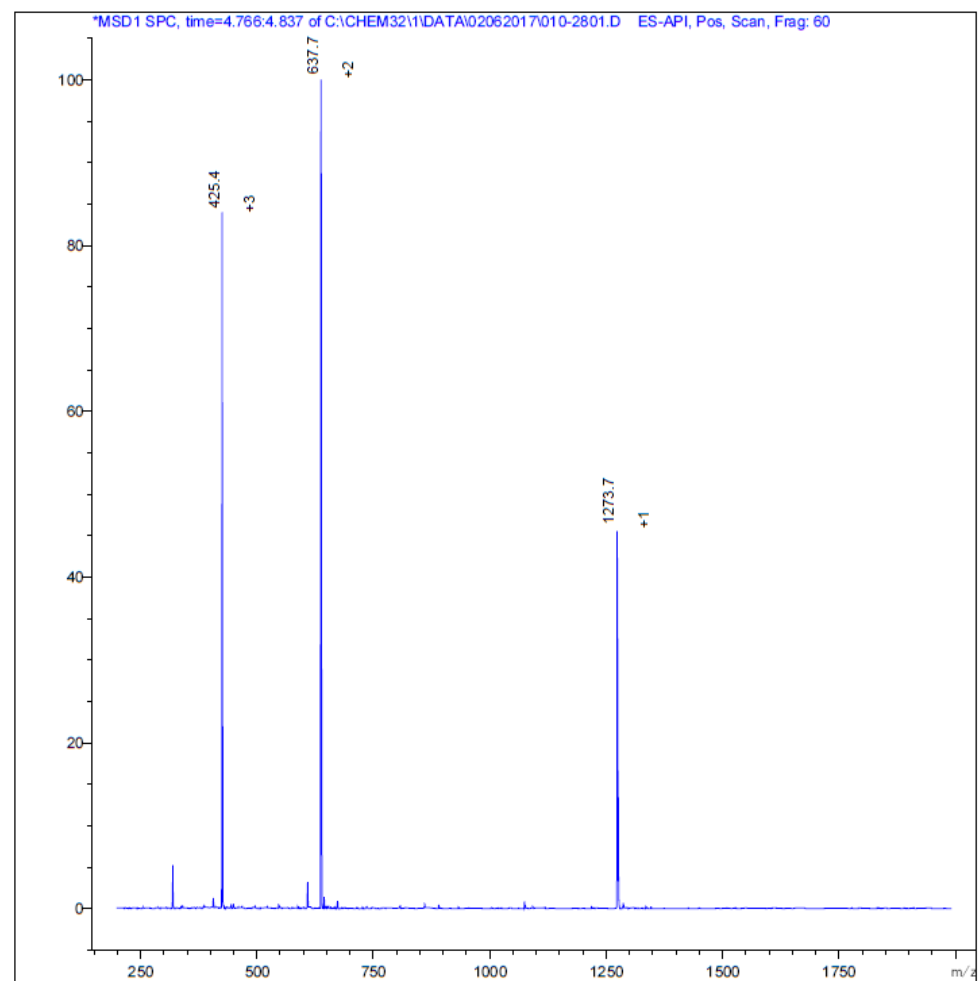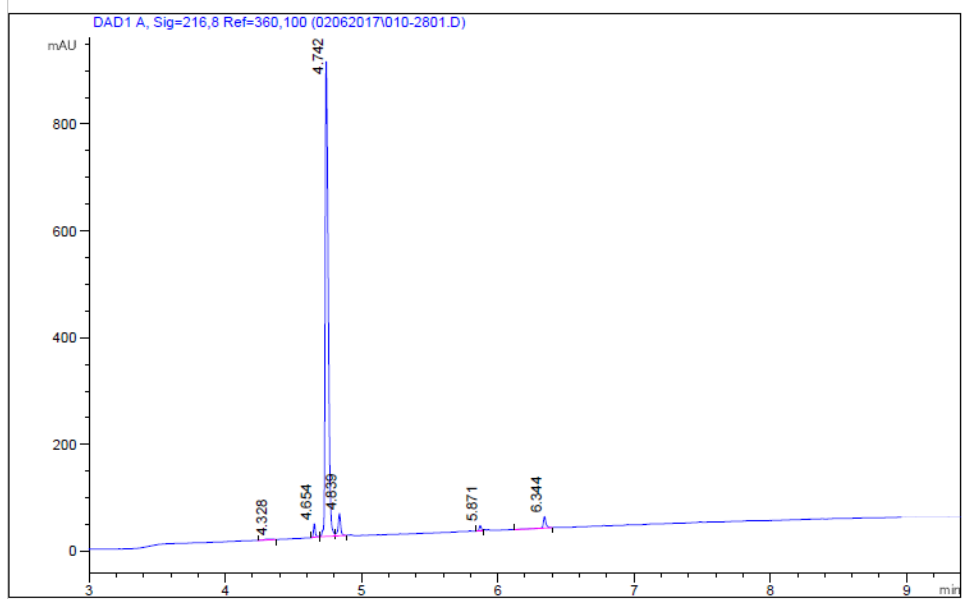
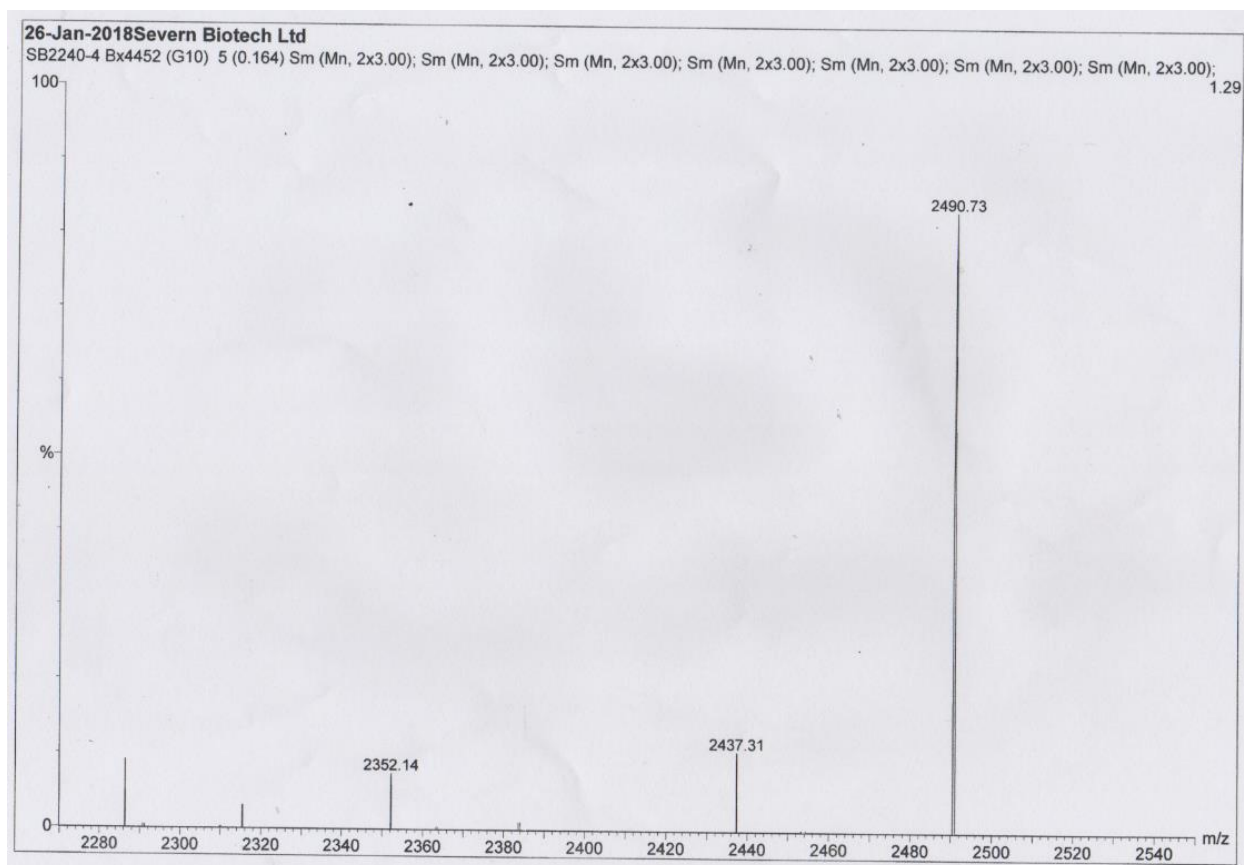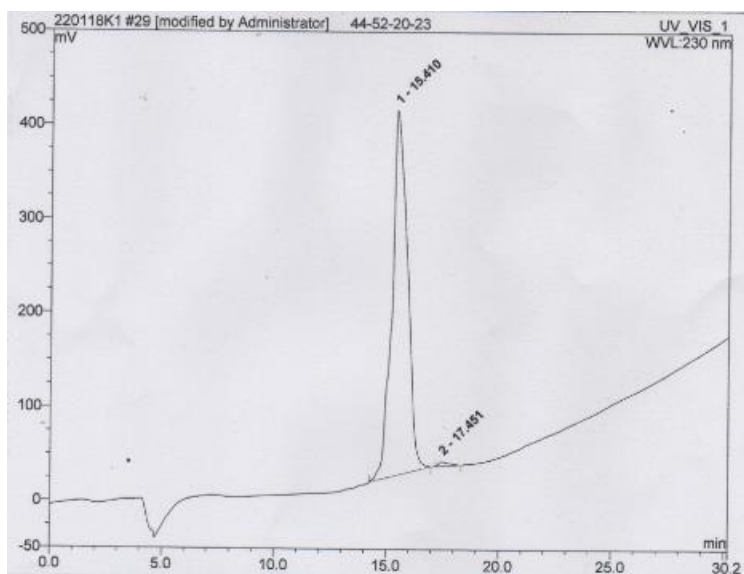**Appendix N**: HPLC-MS data for AG02ΔV.
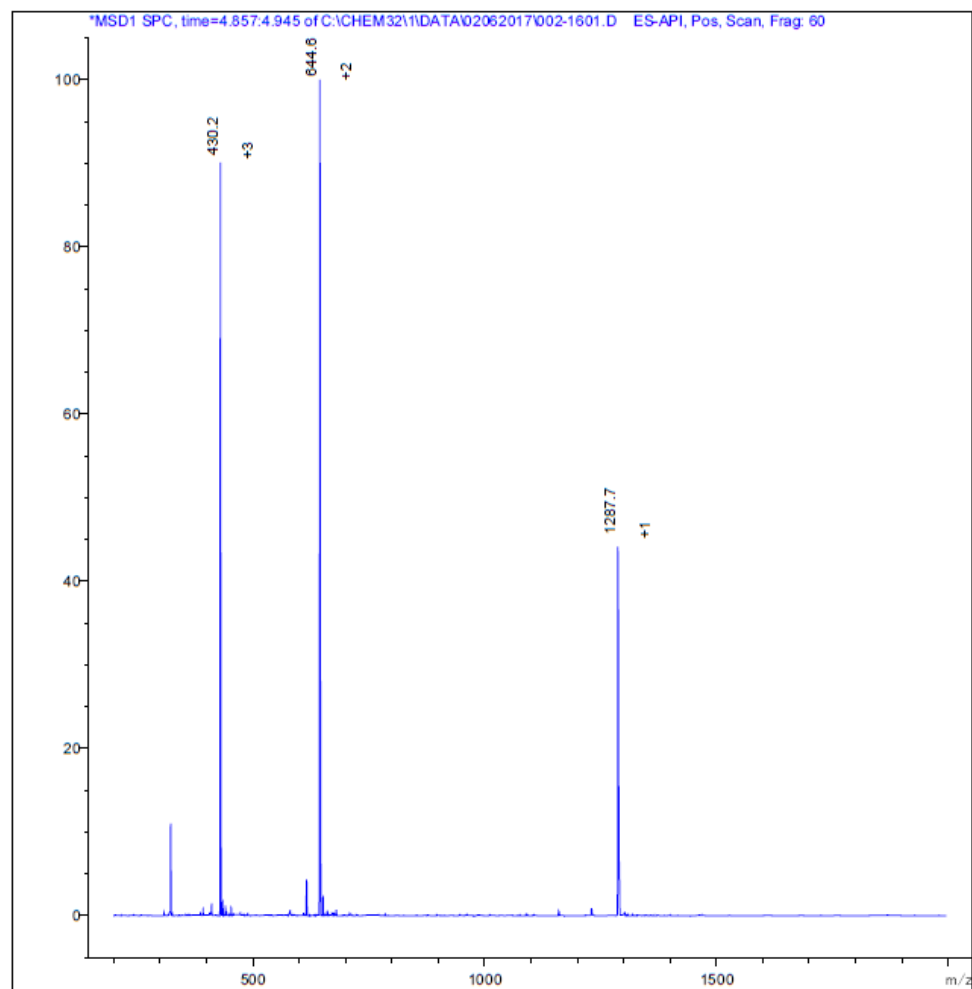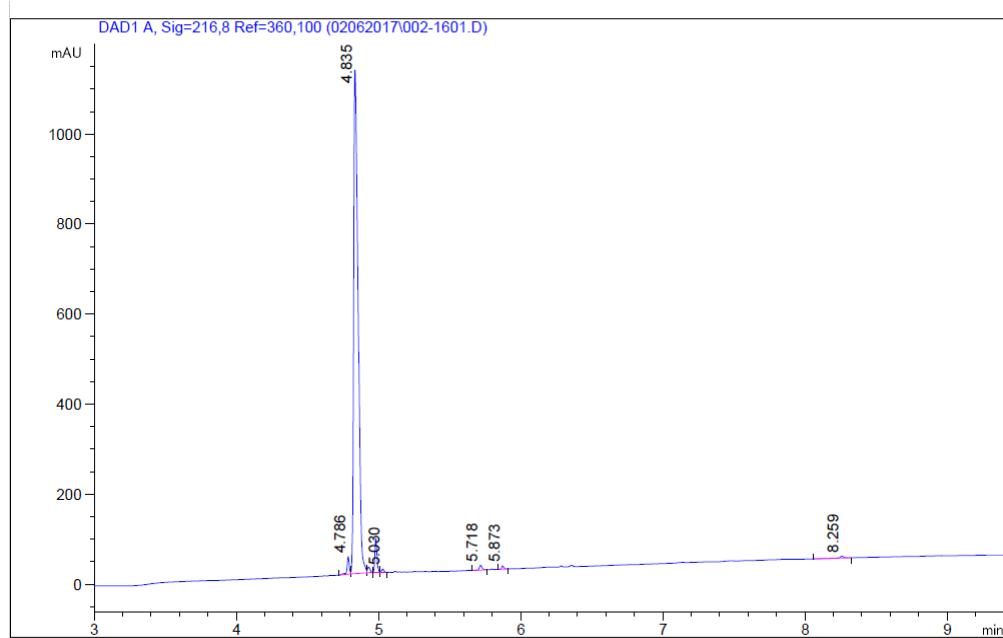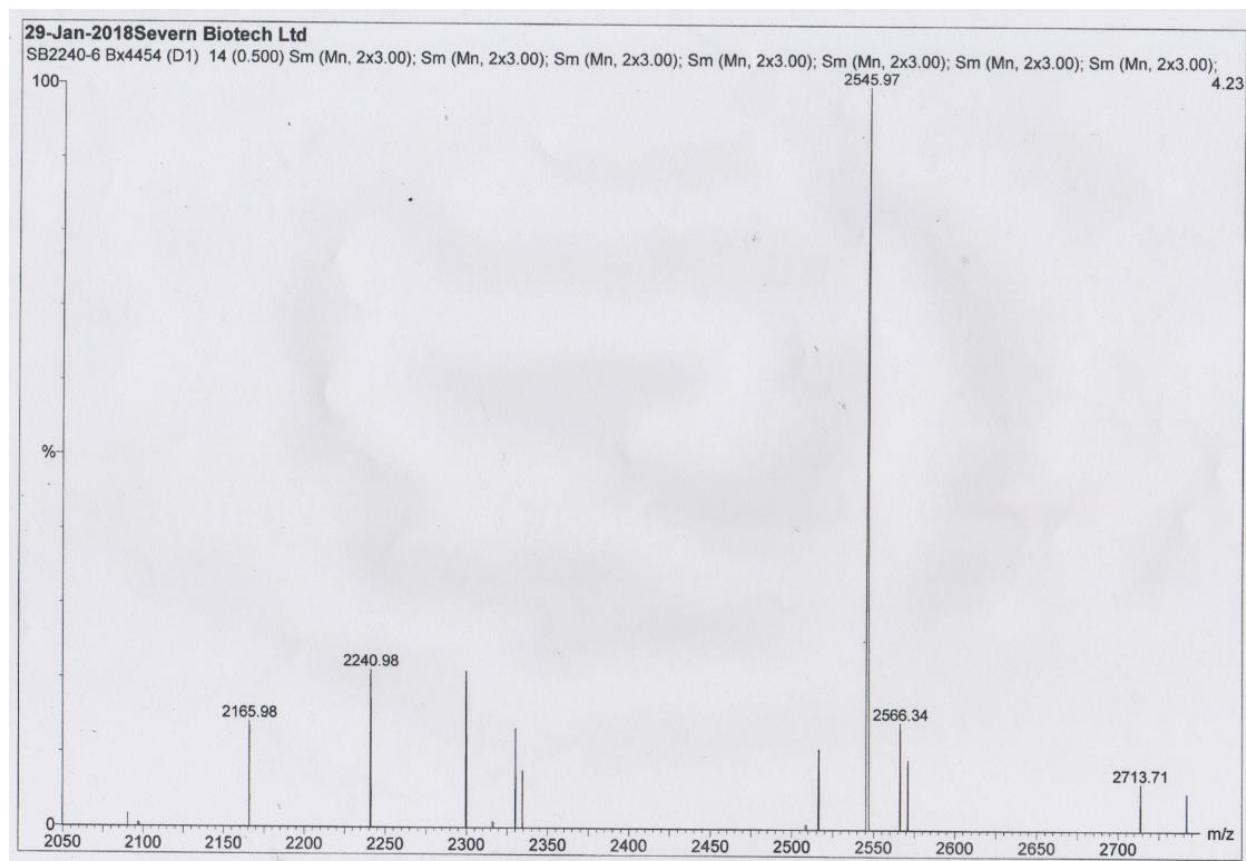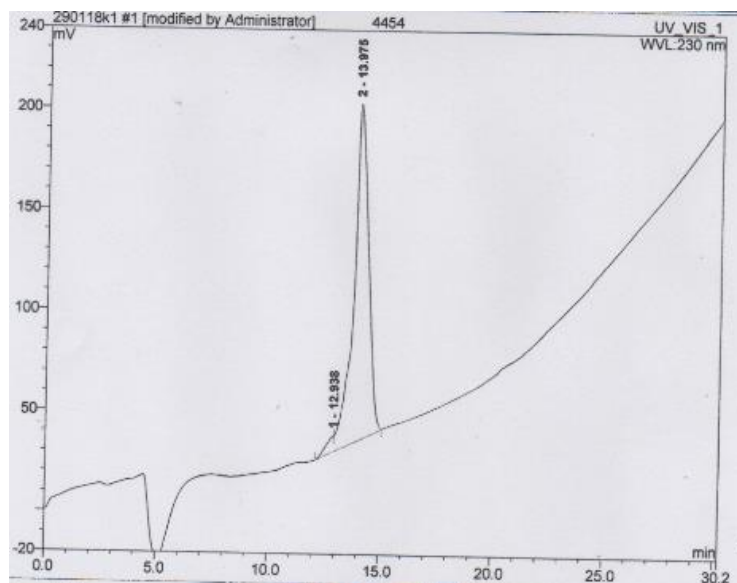
Appendix O: HPLC-MS data for AG03.
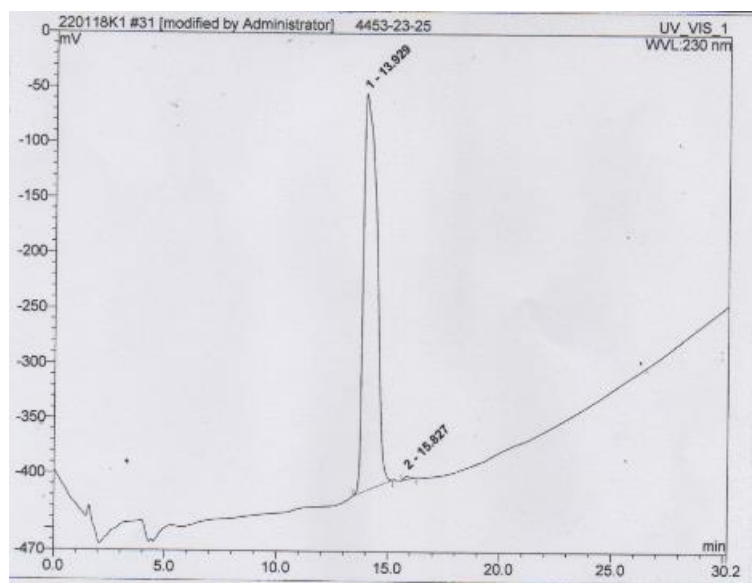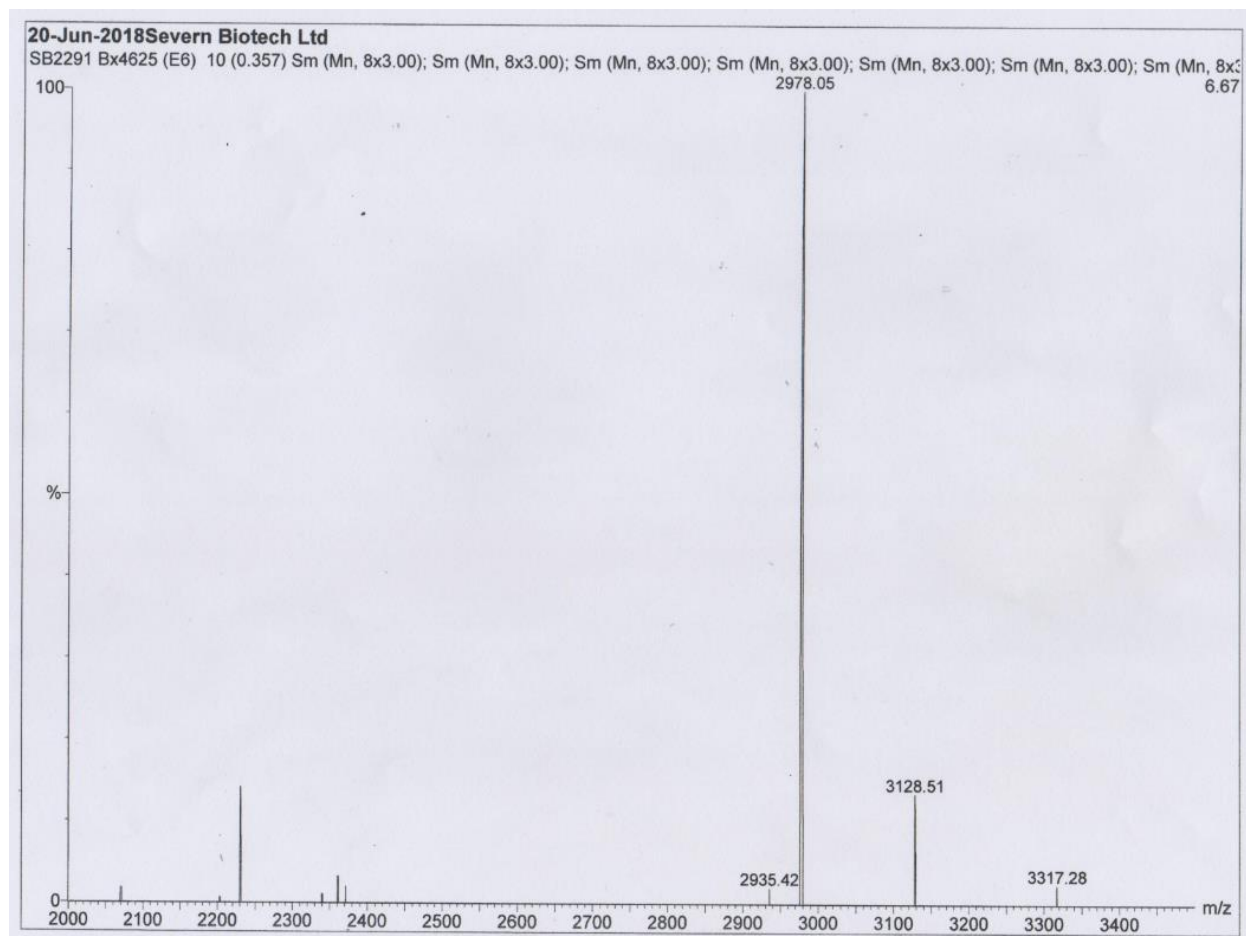
Appendix P: HPLC-MS data for AG03-Cys.
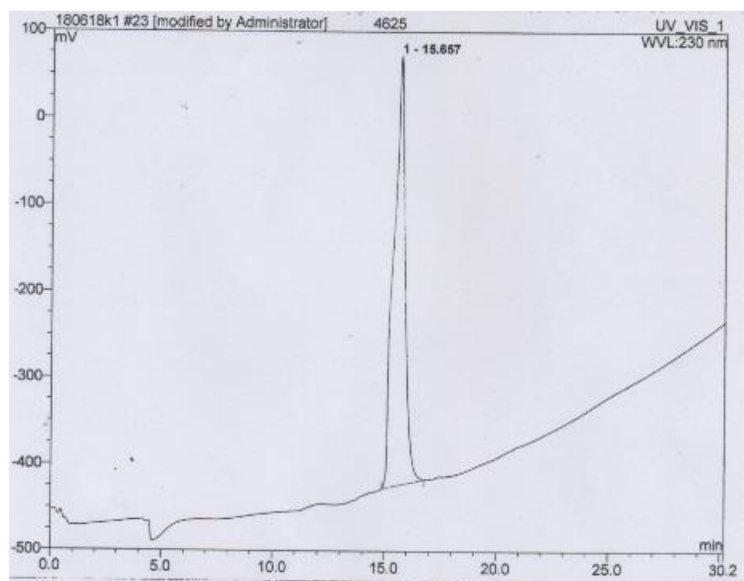
Appendix Q: HPLC-MS data for Scramble AG03.
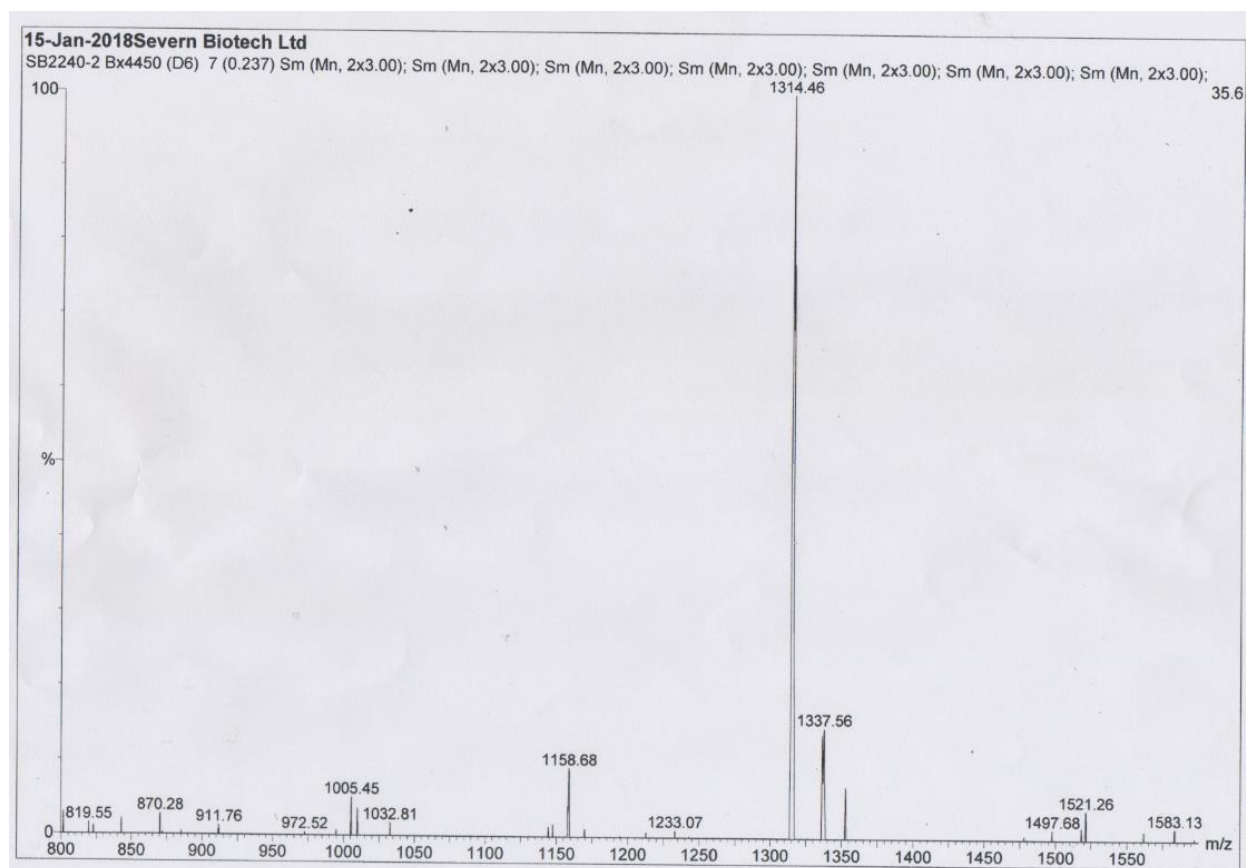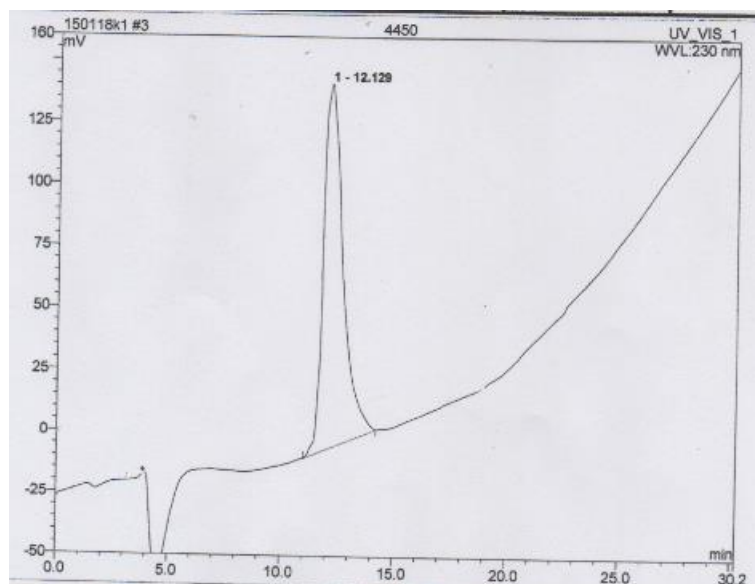
Appendix R: HPLC-MS data for AG03M.

Appendix S: HPLC-MS data for RI- AG03.
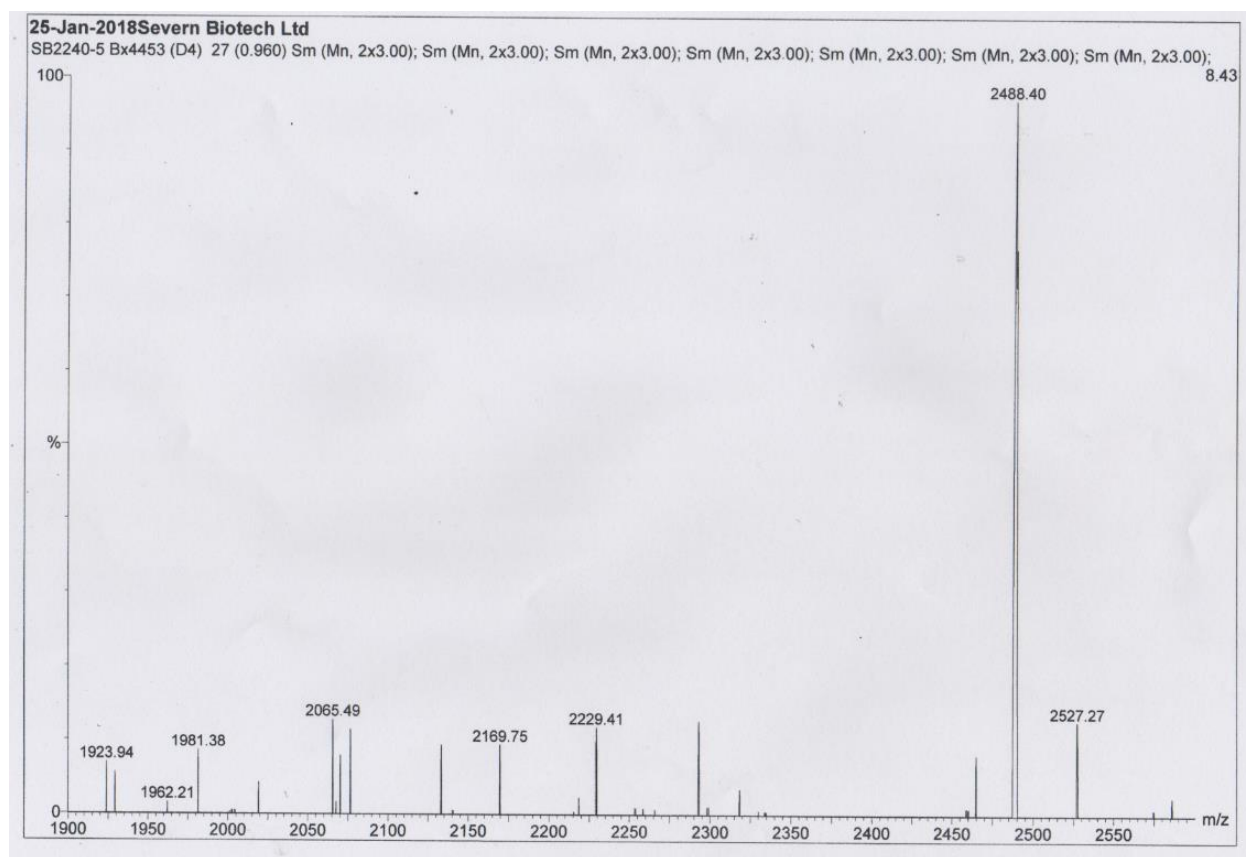
Appendix T: HPLC-MS data for FAM-RI-AG03.

Appendix U: HPLC-MS data for Poly-R.

275

Appendix V: HPLC-MS data for TAT.